MODELLING HORIZONTALLY LOADED PILES IN THE GEOTECHNICAL CENTRIFUGE

H. LOUW

MODELLING HORIZONTALLY LOADED PILES IN THE GEOTECHNICAL CENTRIFUGE

HENDRIK LOUW

A dissertation submitted in partial fulfilment of the requirements for the degree of

MASTER OF ENGINEERING (STRUCTURAL ENGINEERING)

in the

FACULTY OF ENGINEERING, BUILT-ENVIRONMENT AND INFORMATION TECHNOLOGY

UNIVERSITY OF PRETORIA

February 2020

DISSERTATION SUMMARY

MODELLING HORIZONTALLY LOADED PILES IN THE GEOTECHNICAL CENTRIFUGE

H. LOUW

Supervisor: Prof E.P. Kearsley

Co-Supervisor: Prof S.W. Jacobsz

Department: Civil Engineering

University: University of Pretoria

Degree: Master of Engineering (Structural Engineering)

Pile foundations are extensively used to support various structures that are constructed in soft/loose soils, where shallow foundations would be considered ineffective due to low bearing capacities and large settlements. The design of these structures to accommodate lateral applied loads in particular, usually imposed by winds, water and earth pressures, has gained popularity over the past few decades. The behaviour of horizontally loaded piled foundations is a complex soil-structure interaction problem and is usually concerned with the relative stiffness between the pile and the surrounding soil, where the relative stiffness is a function of both the stiffness and properties of the pile and the stiffness of the soil.

Many design assumptions and methods used for pile foundations are based on the principles observed from metal piles. This raises the question of the validity and accuracy of assumptions and methods for the use of analysing and designing reinforced concrete piles, that exhibits highly non-linear material behaviour and changing pile properties after cracking. Due to the elastic behaviour of metal sections, these methods typically only focus on the soil component of the soil-structure interaction problem, only allowing changes and non-linear behaviour of the soil surrounding the pile to take place upon load application, mostly disregarding the behaviour and response of the pile itself.

The main purpose and objective of the study was to determine whether aluminium sections in a centrifuge could be used to realistically and sufficiently accurately model the monotonic and cyclic response of reinforced concrete piles subjected to lateral loading. This was observed though a number of tests conducted in a geotechnical centrifuge on scaled aluminium and reinforced concrete piles, subjected to both monotonic and cyclic loading.

After conducting the tests on both the scaled aluminium and reinforced concrete piles in the centrifuge it was concluded that aluminium sections cannot be used to accurately model and predict the lateral behaviour of reinforced concrete piles. Both the scaled aluminium and reinforced concrete piles proved to model the concept of laterally loaded piles quite well regarding bending at low loads. However, even at low lateral loads, the observed response of the scaled reinforced concrete was significantly different than that observed from the scaled aluminium pile. Furthermore, as the magnitude of the applied load and bending increased, the scaled reinforced concrete pile cracked, resulting in non-linear behaviour of the section under loading, which was not the case for the scaled aluminium pile that remained uncracked. This contributed to the difference in behaviour between the piles studied, therefore, the true material behaviour and failure mechanisms involved with reinforced concrete piles were not replicated by using a scaled aluminium pile section. The non-linear behaviour of the scaled reinforced concrete pile after cracking affected both the behaviour of the pile, as well as the response of the soil surrounding the pile, in contrast with the behaviour observed from the scaled aluminium pile.

DECLARATION

I, the undersigned hereby declare that:

I understand what plagiarism is and I am aware of the University's policy in this regard;

The work contained in this project report is my own original work;

I did not refer to work of current or previous students, lecture notes, handbooks or any other study material without proper referencing;

I have not allowed anyone to copy any part of my project report;

I have not previously in its entirety or in part submitted this project report at any university for a degree.

_____

Hendrik Louw

14303737

7 February 2020

ACKNOWLEDGEMENTS

I wish to express my appreciation to the following organisations and persons who made this dissertation possible:

a) Professor E.P. Kearsley, my supervisor, for her guidance, optimism, patience and support for the duration of the dissertation and always keeping me on my toes. The magnitude of knowledge I gathered was irreplaceable and of enormous value.

b) Professor S.W. Jacobsz, my co-supervisor, for his contribution in the form of ideas and knowledge, and support for the duration of the dissertation.

c) To The Concrete Institute, the Concrete Society of Southern Africa and the WindAfrica project for their financial support during this project.

d) The following personnel from the University of Pretoria civil engineering laboratory for their practical advice and support:

- Mr Rikus Kock
- Mr Jurie van Staden
- Mr Jan Vermaak
- Mr Derick Mostert
- Mr Johan Scholtz
- Mr Jaco Botha
- Ms Vanessa Doman

e) My parents, Bertus and Malene Louw, for their endless love, encouragement and always believing in me and supporting me.

f) To my sister, Magdaleen Louw, for her moral support for the duration of the project, always believing in me, and reminding me that I am capable to do anything.

g) To my friends and family for their continued support and encouragement.

TABLE OF CONTENTS

PAGE

LIST OF TABLES

PAGE

LIST OF FIGURES

PAGE

LIST OF SYMBOLS

Symbol	Description	Units
A_m	Cross-sectional area of the model pile	L^2
A_p	Cross-sectional area of the prototype pile	L^2
c’	Cohesion of the soil	$M\ L^{-1}\ T^{-2}$
C_U	Coefficient of uniformity	-
D	Outside diameter of the prototype pile	L
D_m	Outside diameter of the model pile	L
D_r	Relative density	-
D_{10}	The size such that 10% of the particles are smaller than that size	L
D_{50}	Average or mean particle size	L
D_{60}	The size such that 60% of the particles are smaller than that size	L
E_m	Young’s modulus of the model pile	$M\ L^{-1}\ T^{-2}$
E_p	Young’s modulus of the prototype pile	$M\ L^{-1}\ T^{-2}$
E_s	Young’s modulus of the soil	$M\ L^{-1}\ T^{-2}$
E_{sec}	Secant modulus of the soil	$M\ L^{-1}\ T^{-2}$
E_0	Constraint modulus of the soil	$M\ L^{-1}\ T^{-2}$
e	Void ratio of the soil at its current state	-
e_L	Load eccentricity from soil surface	L
e_{max}	Void ratio of the densest possible soil packing state	-
e_{min}	Void ratio of the loosest possible soil packing state	-
G_s	Specific gravity	-
H	Lateral load	$M\ L\ T^{-2}$
H_{crack}	Cracking lateral load	$M\ L\ T^{-2}$
H_u	Ultimate lateral load	$M\ L\ T^{-2}$
I_m	Second moment of area of the model pile	L^4
I_p	Second moment of area of the prototype pile	L^4
k_h	Modulus of subgrade reaction	$M\ L^{-2}\ T^{-2}$
K_N	Absolute stiffness after N cycles	$M\ T^{-2}$
k_N	Secant stiffness after N cycles	$M\ T^{-2}$
K_a	Active earth pressure coefficient	-
K_p	Passive earth pressure coefficient	-
K_R	Pile-flexibility factor	-

L	Embedment length of the prototype pile	L
L_c	Critical length of the pile	L
L_m	Embedment length of the model pile	L
M	Bending moment	$M L^2 T^{-2}$
M_{crack}	Cracking bending moment of the pile	$M L^2 T^{-2}$
M_h	Bending moment at the soil surface	$M L^2 T^{-2}$
M_{hp}	Bending moment at the soil surface from the previous load cycle	$M L^2 T^{-2}$
M_{max}	Maximum bending moment	$M L^2 T^{-2}$
M_{per}	Permanent bending moment	$M L^2 T^{-2}$
M_{yield}	Yielding bending moment	$M L^2 T^{-2}$
N	Number of cycles	-
n	Centrifuge scaling factor	-
n_h	Coefficient of subgrade reaction	$M L^{-2} T^{-2}$
P	Axial force	$M L T^{-2}$
p	Lateral soil reaction	$M T^{-2}$
s’	Mean stress invariant	$M L^{-1} T^{-2}$
t’	Deviatoric stress invariant	$M L^{-1} T^{-2}$
t_m	Wall thickness of the model pile	L
x_d	Distance from fixity	L
y	Lateral soil displacement	L
y_h	Pile head displacement	L
y_{hper}	Permanent pile head displacement	L
y_{hpgain}	Permanent pile head displacement gain	L
y_p	Lateral pile displacement	L
y_s	Lateral surface displacement	L
z	Depth along the length of the pile	L
Z_m	Sectional modulus of the model pile	L^3
z_s	Depth below soil surface	L
γ	Unit weight of the soil	$M L^{-2} T^{-2}$
γ’	Effective unit weight of the soil	$M L^{-2} T^{-2}$
δ	Deflection	L
ε_a	Axial strain	-
ε_b	Bending strain	-
ε_1	Strain on the tension side of the model pile	-
ε_2	Strain on the compression side of the model pile	-
θ	Angle from the tangent line in the t’, s’- space	°

ρ	Density	$M\ L^{-3}$
ρ_{dmax}	Maximum dry density	$M\ L^{-3}$
ρ_{dmin}	Minimum dry density	$M\ L^{-3}$
ρ_w	Density of water	$M\ L^{-3}$
σ	Total stress	$M\ L^{-1}\ T^{-2}$
σ_a	Axial stress	$M\ L^{-1}\ T^{-2}$
σ_m	Total stress in the model pile	$M\ L^{-1}\ T^{-2}$
σ_1	Maximum principle stress	$M\ L^{-1}\ T^{-2}$
σ_3	Minimum principle stress	$M\ L^{-1}\ T^{-2}$
υ	Poisson's ratio of the soil	-
φ'	Friction angle of the soil	°

1 INTRODUCTION

1.1 BACKGROUND

Reinforced concrete is a strong, durable and versatile construction material that has been widely used in many types of structures for decades and is a composite of two vastly different materials, namely concrete and steel reinforcing. Due to its versatility, reinforced concrete can be formed into various shapes and sizes, ranging from a simple column, foundation or beam, to a slender plate or shell, subjected to a wide variety of load combinations. It is also a well-known assumption in reinforced concrete design that, due to the low tensile capacity of concrete, it is unable to resist significant forces or loads causing tensile stresses. For all design purposes, concrete is assumed to be cracked, affecting both the flexural stiffness and sectional properties of reinforced concrete members, resulting in a composite material that exhibits highly non-linear material behaviour.

Pile foundations are extensively used to support various structures that are constructed on soft/loose soils, where shallow foundations would be considered ineffective due to low bearing capacities and large settlements. Pile foundations are used to support vertical loads, but also lateral loads and in most cases a combination of vertical and lateral loads. The design of these structures to accommodate lateral applied loads, usually imposed by winds, water and earth pressures, has gained popularity over the past few decades. Typically, with these foundations, the lateral pile displacement depends on the soil reaction, and in turn, the soil reaction is influenced by the pile displacement, making analysis and design of these foundations difficult (Tomlinson, 1980). It is a complex soil-structure interaction problem that needs to be considered and is usually concerned with the relative stiffness between the pile and the surrounding soil, where the relative stiffness is a function of both the stiffness and properties of the pile and the stiffness of the soil.

Many design assumptions and methods used for pile foundations are based on the principles observed from metal piles (Reese *et al.*, 1974; Murchison & O'Neill, 1984). This raises the question of the validity and accuracy of these assumptions and methods for the use of analysing and designing reinforced concrete piles, that exhibits highly non-linear material behaviour and changing pile properties after cracking. Due to the elastic behaviour of metal sections, these methods typically only focus on the soil component of the soil-structure interaction problem, only allowing changes and non-linear behaviour of the soil surrounding the pile to take place upon load application, mostly disregarding the behaviour and response of the pile itself.

Numerous full-scale tests have been conducted in the past on laterally loaded steel and reinforced concrete piles. Due to the high cost associated with full-scale testing in the field, the use of physical scale models for modelling both structural and soil components, or even the interaction between the two, has become a popular tool, that provides fairly realistic results and behaviours of the full-scale problem at hand. The physical modelling of steel piles subjected to lateral loading have been investigated extensively by a number of researches using geotechnical centrifuge modelling. However, limited research has been conducted on the physical modelling of laterally loaded piles using reinforced concrete elements. The effect of the changing properties associated with concrete elements should be investigated.

The need thus arises to experimentally determine the effect of changing concrete properties on the relative stiffness of the soil-pile system, as well as establishing the response of laterally loaded reinforced concrete piles through the use of physical scale models in a centrifuge, which is the main focus of this dissertation.

1.2 OBJECTIVES

The primary focus of this dissertation was to investigate the response of single piles subjected to lateral loading. The response was investigated for both a scaled aluminium and reinforced concrete pile. The aluminium pile was used as a control test for the reinforced concrete pile, as aluminium is a medium that has been widely used and accepted to predict the behaviour of piles under lateral loading based on modelled piles in centrifuge experiments. Modelling a reinforced concrete pile allowed for the non-linear behaviour of concrete to be studied. This led to the formation of the research aim of whether scaled metal pile sections can be used to realistically and with sufficient accurately model the monotonic and cyclic response of reinforced concrete piles, subjected to lateral loading.

The main objectives of the study included the following:

- Comparing the behaviour of a scaled aluminium pile under monotonic horizontal loading to behaviour as predicted using published trends based on prototype site measurements.
- Comparing the behaviour of a scaled reinforced concrete pile to that of a scaled aluminium pile subjected to lateral loading to determine whether the behaviour is similar when the concrete pile is uncracked, and the soil has no load history (first load cycle).
- Determining the effect of cyclic loading on the soil-structure interaction for both aluminium and reinforced concrete scaled piles.

- Establishing whether concrete cracking has a significant effect on the behaviour of scaled piles.

1.3 SCOPE OF STUDY

Some restrictions and limitations were set when the study was done. The scope of the study was limited to the following aspects:

- The tests were laboratory-based, and all physical modelling was carried out using a geotechnical centrifuge at a constant acceleration (*g*-level).
- Only scaled cylindrical aluminium and reinforced concrete piles were investigated in this study.
- Piles were subjected to both monotonic and cyclic lateral loads in one direction.
- All tests were carried out in fine silica sand at a constant relative density, with the effect of soil density not forming part of the study.
- The effect of pile installation method, soil-pile interaction roughness, load eccentricity, pile length and pile diameter size did not form part of the study.
- Vertical loading and the effect it has on the lateral capacity of the piles was not considered in this dissertation.

1.4 METHODOLOGY

The methodology followed in the course of this project is described below.

- A literature review was conducted on the basic concepts of pile foundation design, as well as the common techniques used for analysing these structures under lateral loading, focusing on the interaction between the pile and the surrounding soil and the mechanisms governing their behaviour. Research specific to the physical modelling of laterally loaded piles under monotonic and cyclic lateral load conditions was investigated. Insight into the design and analysis of these structures raised a number of questions that aided in the design of the experimental work and the formulation of the research question.
- Careful design of the experimental work was required for testing in the centrifuge. Apart from the literature review, the design was based on a parametric study, conducting a multi-variable analysis based on literature, observing the response of the soil-pile system to

variations in pile and soil stiffnesses only, as these stiffnesses primarily govern the behaviour of the soil-pile system.

- All tests were carried out using fine silica sand, at a constant relative density. The experimental work conducted for this dissertation was as follows:
  - Selection and instrumentation of appropriate cross-sections and dimensions for the scaled aluminium and reinforced concrete piles for testing in the centrifuge.
  - Obtaining the properties of the scaled piles to aid in predicting the response of these piles under lateral loading.
  - Obtaining the properties of the fine silica sand through the use of standard testing procedures to quantify and predict the behaviour of the soil.
  - Building of soil models, ensuring that the relative density of the soil for each of the models are approximately the same and the installation and placement of all the piles are consistent.
- Tests were conducted in a geotechnical centrifuge at 30-*g*. The data was then analysed to determine the behaviour of the scaled aluminium and reinforced concrete piles, subjected to lateral loads, at a constant soil relative density.
- The behaviour of a scaled aluminium and reinforced concrete pile exposed to monotonic and cyclic lateral loading, in soil of constant relative density, was observed through monitoring strain and bending moment development, as well as lateral displacement of the pile at representative locations along the length of each of the piles.
- The lateral response of soil to a single pile subjected to monotonic and cyclic lateral loading was studied, using both scaled aluminium and reinforced concrete piles, also investigating the change in behaviour of the soil as a result of the applied lateral loads.
- The effect of a change in pile stiffness on the soil-pile system was studied.
- Experimental results were compared to theoretically and numerically predicted values, using a known software package, LPILE, and the finite difference method.
- Similarities and differences observed between the scaled aluminium and reinforced concrete pile were identified, in order to answer the research questions as indicated above.

1.5 ORGANISATION OF REPORT

The dissertation consists out of the following chapters:

- Chapter 1 serves as an introduction to the dissertation, describing the background, objectives, scope and methodology of the experimental work and dissertation.
- Chapter 2 contains a technical introduction based on a literature study. Applicable literature can be found in this chapter to support the experimental work and discussions.
- In Chapter 3 the parametric study that was conducted to determine the response of the soil-pile system to varying soil and pile properties is described, as the behaviour of piles under lateral loading is primarily governed by these properties. The aim of the parametric study is to aid in designing the experimental model.
- In Chapter 4 the experimental set-up and procedures undertaken during the study is described, presenting the experimental work conducted, also including the measuring equipment that was used during the tests in the centrifuge.
- In Chapter 5 the analysis and results obtained from the experimental observations is presented, followed by a discussion on these results.
- In Chapter 6 a comparison between the experimental observations is presented, discussing similarities and differences between the results presented in Chapter 5.
- Chapter 7 contains the conclusions and recommendations of the study.
- Chapter 8 provides the list of references.
- Appendix A contains information supporting the parametric study in Chapter 3.

2 LITERATURE REVIEW

2.1 INTRODUCTION

The behaviour of pile foundations under lateral loads is a complex soil-structure interaction problem that should be carefully investigated to ensure that the relevant aspects and mechanisms involved are accounted for. A large number of full-scale tests have been conducted in the past on the response of laterally loaded steel pile foundations, subjected to both monotonic and cyclic lateral loading (e.g. Reese *et al.*, 1974; Brown *et al., 1987;* Little & Briaud, 1988; Li *et al.*, 2015; Li *et al.*, 2017). All these studies included the observation and response of piles in terms of bending and displacement, as well as changing soil conditions as a result of the type and magnitude of the applied loads.

To better understand the observed full-scale behaviours in a more cost-effective way, many researchers have replicated and investigated the problem through the use of scale models in a geotechnical centrifuge. Many design methodologies are based on the observed responses from these full- and scaled tests on metal piles, raising concern regarding the validity and accuracy of these assumptions and methodologies for analysing and designing reinforced concrete piles, as the material behaviour is considerably different than that of metals.

Reinforced concrete is a versatile construction material that has been used in many structures for decades, consisting of a combination of concrete and steel reinforcing, where the concrete typically resists the compressive stresses and steel reinforcing the imposed tensile stresses. Due to the low tensile capacity of concrete (approximately ten per cent of its compressive strength), Mosley *et al.* (2012) mentioned that nearly all reinforced concrete structures are designed with the assumption that the concrete does not resist any tensile forces and thus structures are assumed to be cracked. This results in reinforced concrete members exhibiting highly non-linear material behaviour under loading. Typically, cracking does not affect the safety of the structure, provided that sufficient steel reinforcing is included in the section. Steel reinforcing primarily resists the tensile forces in the reinforced concrete members caused by applied loads, but also limits crack widths. Cracking does, however, cause a change in the cross-sectional properties of the section, reducing the flexural stiffness of a reinforced concrete member under bending. Elastic material properties can no longer be applied after this point had been reached, which results in a composite material that exhibits highly non-linear material behaviour - an aspect that cannot be overlooked and should be considered in the design of these structures.

Limited research on full-scale and scaled reinforced concrete piles has been published (e.g. Little & Briaud, 1988; Noor & Boswell, 1992; Ruesta & Townsend, 1997; Nip & Ng, 2005;

Jagodnik & Arbanas, 2015). All these researchers emphasised the importance of the effect of changing concrete properties after cracking on both the response of the pile, as well as the surrounding soil, under lateral loading.

The main aim of this literature review is to examine the mechanisms associated with analysing pile foundation structures, observing the various behavioural properties and responses, with the focus being on single piles subjected to lateral loads.

In the first section of the literature review, a brief background is given on the need and use of centrifuge modelling as a technique for modelling complex soil-structure interaction problems. The typical behaviour of single piles in a centrifuge, subjected to lateral loads, is discussed, focussing on pile response with regard to bending, shear, lateral deflection and soil reaction. Both monotonic and cyclic load effects were considered. Typical analysis methods for predicting the load-deflection response of laterally loaded single piles were discussed, also focusing on the soil-structure interaction, and in particular, the relative stiffness between the pile and the surrounding soil, as this largely influences the overall behaviour of the soil-pile system. The chapter concludes with a section that describes interpolation methods that have commonly been used to process experimental data and information for piles in practice, followed by a discussion on the non-linear response of concrete, an aspect that is generally overlooked and not considered, especially with focus on piles. Lastly, important scale and size effects that should be taken into account when modelling at small scales were also considered.

2.2 GEOTECHNICAL CENTRIFUGE MODELLING

2.2.1 Principles of centrifuge modelling

The use of small-scale models for solving complex engineering problems has been widely used in civil engineering. Full-scale testing in the field is very expensive, and sometimes even unfeasible. Thus, mainly due to its cost-effectiveness, small-scale modelling has become a tool to investigate realistic field behaviour. Structural engineers typically use scale models to determine the behaviour of complex structures subjected to a number of different loading conditions (wind, water, vibrations, etc). On the other hand, apart from modelling the behaviour of complex structures, geotechnical engineers typically use small-scale models for testing in the laboratory especially when they are dealing with unknown soil stress-strain behaviour (Madabhushi, 2015).

Typically, when dealing with soils, the use of small-scale models is more complex, and not as simple as dividing by the scale factor, as in the case for structural models. Due to the non-linear stress-strain behaviour of soils, it is not conservative, for geotechnical problems, to predict the

response of a full-scale prototype problem by testing small-scale models in a laboratory at 1-*g*, where g refers to the earth's gravitational acceleration. A 1/*n* scale model will essentially only give a 1/*n* fraction of the true stresses and strains actually experienced by the prototype. The use of centrifuge modelling accommodates for this, creating stresses and strains experienced by the prototype at model scale to capture the true behaviour of the problem at hand (Knappett *et al.*, 2011). Thus, by combining both small-scale structural and soil modelling in a centrifuge, complex soil-structure interaction problems can be investigated.

The basic principle of centrifuge modelling can be explained in **Figure 2-1**, as indicated by Schofield (1980). A 1/*n* scale model of a full-scale prototype model is tested in the enhanced gravity field created by the geotechnical centrifuge to accommodate for the non-linear stress-strain behaviour of soils. Furthermore, Schofield (1980) indicated that the effect of gravity is increased by the same geometric factor, n, relative to the normal earth's gravity field (1-*g*). However, to achieve a correct gravity field, the relationship between the scale factor, *n*, the angular velocity, ω, and the centrifugal acceleration at any radius, *r*, should be correct. **Equation 2-1** indicates the relationships between the abovementioned variables, which is also indicated in **Figure 2-1**.

$$r\omega^2 = ng \qquad \textbf{Equation 2-1}$$

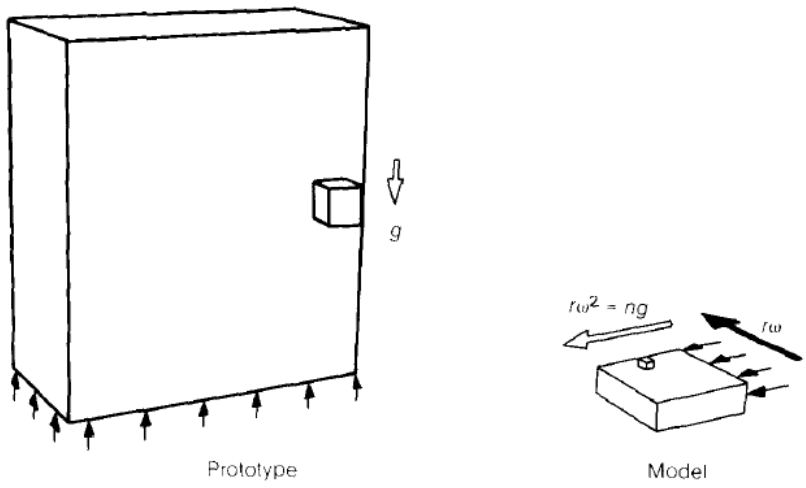

Figure 2-1: Principle of centrifuge modelling (Schofield, 1980)

2.2.2 Scaling laws

As seen in **Figure 2-1**, the use of centrifuge modelling introduces the concept of scaling laws. To realistically model non-linear stress-strain behaviour of soils in a centrifuge, as well as soil-

structure interaction problems, the appropriate scaling laws need to be applied. Scaling laws are relationships that relate the behaviour of the centrifuge model to the prototype (Madabhushi, 2015). By using these laws, the observed behaviour of the scale model in the centrifuge can be used to predict the behaviour of the prototype. In turn, the predicted behaviour of the prototype can infer the response of the actual field structure, assuming that the prototype and field structure are closely related, and the important features of the field structure are present in the prototype. **Table 2-1** indicates the various scaling laws that are typically applicable to centrifuge testing.

Table 2-1: Scaling laws (derived from Schofield, 1980)

Parameter at prototype scale	Scaling law for centrifuge acceleration, ***n.g***
Acceleration/acceleration due to gravity, seepage velocity, frequency	n
Mass density, stress, strain, velocity	1
Length, displacement, time (dynamic)	$1/n$
Area, force, time (consolidation)	$1/n^2$
Volume, mass, bending moment, work, energy	$1/n^3$

Madabhushi (2015) mentioned that there are a few limitations involved with centrifuge modelling that should be considered. He indicated that it is important to understand these limitations to ensure that the problem being investigated is not adversely affected. He indicated that the following errors and limitations should be taken into account:

- Variation in gravity field
- Radial gravity field
- Particle size effects
- Strain rate effects
- Coriolis accelerations

Typically for centrifuge modelling, depending on the problem to be investigated, either the flexural rigidity, E_pI_p, or the axial rigidity, E_pA_p, of the section is scaled, taking into account both the stiffness of the material, as well as the dimensional properties of the section. For the purpose of this dissertation, that is concerned with the physical modelling of laterally loaded piles, both the E_pI_p and E_pA_p should be scaled appropriately, as indicated by Madabhushi (2015), which cannot be done simultaneously. As observed from many researchers that conducted centrifuge tests on laterally loaded piles in the past, only the E_pI_p is typically scaled correctly, as the pile is primarily exposed to forces causing bending in the pile (Swain, 1979; Georgiadis

et al., 1992; Yan & Byrne, 1992; Dyson & Randolph, 2001; Li *et al.*, 2010; Leblanc *et al.*, 2010; Abadie & Byrne, 2014; Kirkwood & Haigh, 2014; Zhu *et al.*, 2016).

2.3 MONOTONIC RESPONSE OF SINGLE PILES SUBJECTED TO LATERAL LOADS

As one of the most efficient foundations to resist lateral loading, pile foundations have been widely used for many civil engineering applications, especially in the offshore gas and oil industry (Li *et al.*, 2017). As mentioned in Chapter 1, the dissertation is focused on both the monotonic and cyclic behaviour of laterally loaded single piles. However, before considering the behaviour of a single pile due to cyclic lateral loading, it is important to first look at the behaviour under monotonic or static loading conditions. By doing so, the change in behaviour between monotonic and cyclic laterally loaded piles can be quantified and any differences and uncertainties explained.

The following subsections focuses on the load-deflection response of single piles subjected to monotonic lateral loading, followed by the bending moment and soil reaction behaviour, respectively.

2.3.1 Load-deflection response to monotonic loading

Zhu *et al*. (2016) conducted a number of centrifuge tests on a 30 mm hollow aluminium model pile, with an embedment length of 600 mm, observing the monotonic and cyclic response of a single pile subjected to lateral loads at different *g*-levels. They plotted the normalised load against the normalised pile head horizontal displacement, as indicated in **Figure 2-2**. D refers to the diameter of the pile and γ' to the effective unit weight of the soil. It can be seen that as the lateral load increased, the horizontal pile head deflection also increased.

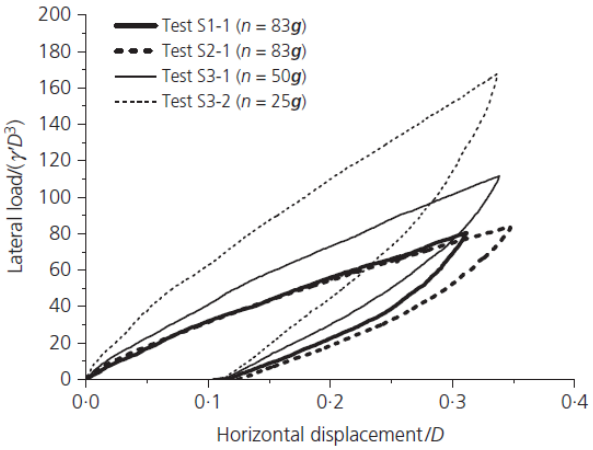

Figure 2-2: Load-deflection curves for monotonic lateral load application (Zhu *et al.*, 2016)

It is interesting to note that the slope of the load-deflection curves was larger at lower *g*-levels than at higher *g*-levels, decreasing as the magnitude of the applied load increased. Zhu *et al*. (2016) mentioned that the difference in the observed slope at higher *g*-levels was due to the confinement that is more, resulting in a stiffer response from the soil-pile system. It should also be noted that the curves did not create a plateau at large lateral loads, indicating that the ultimate failure capacity of the soil was not reached (Li *et al.*, 2017). A plateau normally refers to an increase in the lateral deflection of a pile at a constant load, something that is typically not observed during serviceability conditions. Furthermore, it can be seen in **Figure 2-2** that, upon load removal, the pile had suffered permanent displacements.

Similar to Zhu *et al*. (2016), Russo (2016) indicated that, based on results from Brown *et al.* (1987), the relationship between the applied load and the resulting lateral deflection is highly non-linear, even at low load levels, as shown in **Figure 2-3**. Brown *et al.* (1987) based their findings on the instrumentation of nine full-scale hollow steel piles, with an outside diameter of 273 mm and an embedment length of about 3 m, that was loaded laterally. The solid line refers to the measured data, with the dashed line representing the initial tangent of the curve. He indicated that the non-linear behaviour of both the soil and the pile contributed to the non-linear behaviour that was observed with the load-deflection curve. From **Figure 2-2** and **Figure 2-3** it is interesting to note that the initial portion of the load-displacement response of the pile, at loads corresponding to less than 10% of the ultimate capacity of the soil, the behaviour of the soil seemed fairly linear.

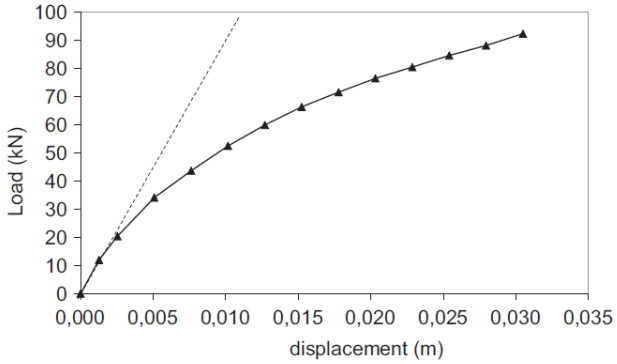

Figure 2-3: Load-displacement relationship (Russo, 2016, adapted from Brown *et al.*, 1987)

2.3.2 Bending, shear and deflection response to monotonic loading

To understand the overall behaviour of a single pile subjected to lateral loads, the bending moment, shear force and deflected shapes should be considered, along with the transverse soil

reaction that occurs in front of the pile upon load application. Firstly, the bending moment development in a pile, as a result of monotonic lateral loading is considered. Georgiadis *et al.* (1992) conducted a number of centrifuge tests at 50-*g* on scaled single aluminium model piles, with diameters ranging between 20 and 25 mm with an embedment length of 181 mm. They examined the bending moment, shear force, soil reaction and corresponding deflection response of a pile due to monotonic lateral loading. **Figure 2-4** indicates the bending moment diagram along the length of the pile, observed by Georgiadis *et al.* (1992), for various load magnitudes at prototype scale, applying the correct scaling factors to the scaled model pile results. The pile for test P_{1A} had a prototype *EI* of 3878.5 MNm^2, and P_{2A}, a prototype *EI* of 2495.0 MNm^2. As expected, the bending moment increased with an increase in the magnitude of the applied lateral load. It can also be seen that the shape of the bending moment diagram corresponded to that typically observed for a short pile, where the whole length of the pile is affected by the applied load, and failure of the soil-pile system is commonly caused by rotation of the pile.

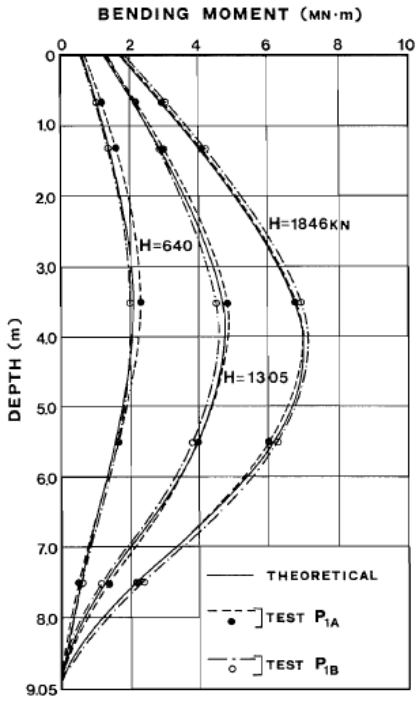

Figure 2-4: Bending moment distribution (Georgiadis *et al.*, 1992)

Similarly, Lin *et al.* (2015) and Zhu *et al.* (2016) observed this behaviour from centrifuge model tests on aluminium piles under monotonic lateral loading. However, the shape of the bending moment diagram obtained by Zhu *et al.* (2016) corresponded to that typically observed for a long pile, as seen in **Figure 2-5**, also at prototype scale, applying the correct scaling factors to the scaled model pile results. They investigated the response of a 30 mm aluminium model pile at 83-*g*. For a long pile, the top two-thirds of the pile is largely affected by the applied load, and

failure is typically caused by yielding of the pile. Classification between a short and long pile is discussed in more detail later in this chapter and is generally a function of both the stiffness and dimensions of the pile and the stiffness of the soil. Lastly, from **Figure 2-4** and **Figure 2-5** it seemed that, at lower applied loads, the maximum bending moment experienced by the pile also increased approximately linearly with an increase in the magnitude of the applied load, similar to what was observed from the load-displacement response.

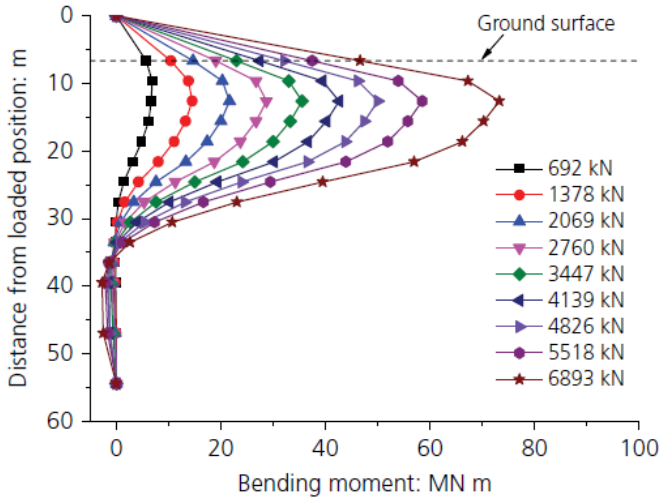

Figure 2-5: Bending moment distribution (Zhu *et al.*, 2016)

Furthermore, Russo (2016) mentioned that the relationship between the applied load and the maximum moment experienced by a pile is nearly linear, as can be seen in **Figure 2-6**, similar to what was observed from Georgiadis *et al.* (1992) and Zhu *et al.* (2016) at lower applied loads. He concluded this based on results obtained by Brown *et al.* (1987), for the same full-scale tests on steel piles mentioned earlier. The solid line refers to the measured data, with the dashed line representing the initial tangent of the curve. One can argue that the difference between the dashed and soil line at larger applied loads, as observed in **Figure 2-6,** can only be due to the change in the properties of the soil (becoming non-linear), as tests were conducted on steel pile sections that did not reach yielding strains. This raises the question of whether the behaviour of soil at small lateral loads can be considered as linear.

Apart from the magnitude of the lateral load, Poulos (1982) mentioned that the bending moment behaviour of a pile is largely influenced by the relative soil-pile stiffness, and explains the behaviour observed in **Figure 2-6**. The concept of relative soil-pile stiffness is discussed later.

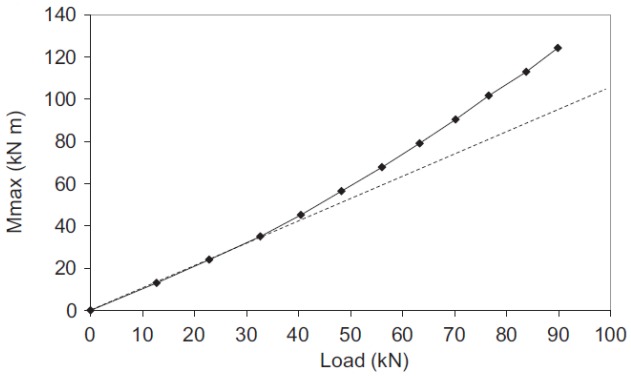

Figure 2-6: Load-maximum bending moment relationship (Russo, 2016, adapted from Brown *et al.*, 1987)

Georgiadis *et al.* (1992) indicated that the corresponding soil reaction, shear force and lateral deflection of the pile can be obtained through methods of differentiation and integration (discussed in Section 2.6). **Figure 2-7** indicates the typical shape for the soil reaction **(a)** and shear force **(b)** experienced by the pile, obtained from **Figure 2-4**, at prototype scale. It can be seen that both the soil reaction and shear force increased with an increase in the magnitude of the applied load, as expected. Similar to the bending moment results in **Figure 2-4**, the soil reaction and shear force also seemed to increase almost linearly with an increase in the magnitude of the applied load, with the soil reaction increasing proportionally with depth for the first four meters. However, when considering the lateral displacement of the pile with increasing lateral load, the lateral displacement did increase, but not linearly (see **Figure 2-8**).

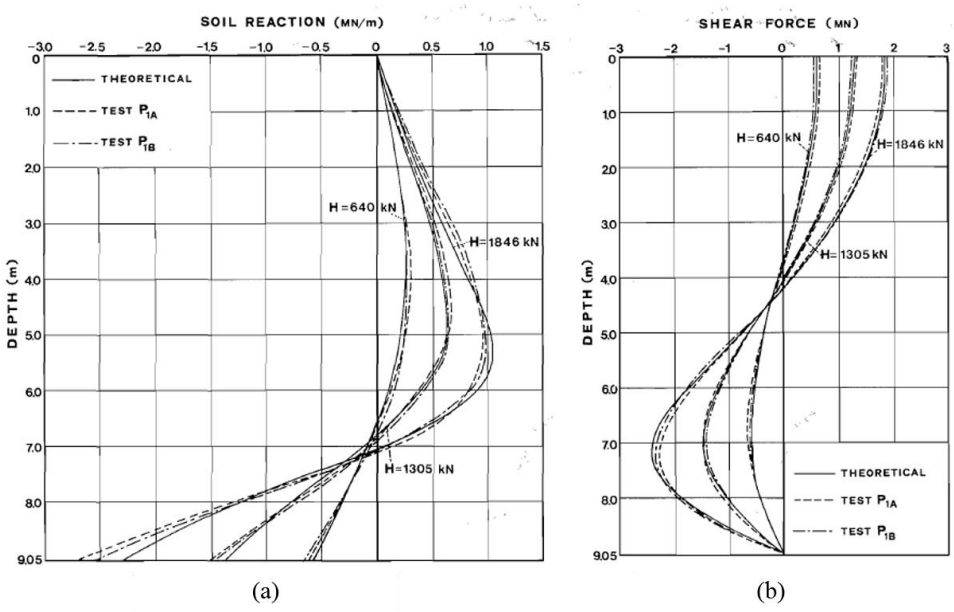

Figure 2-7: Distribution along the length of the pile: (a) soil reaction, (b) shear force (Georgiadis *et al.*, 1992)

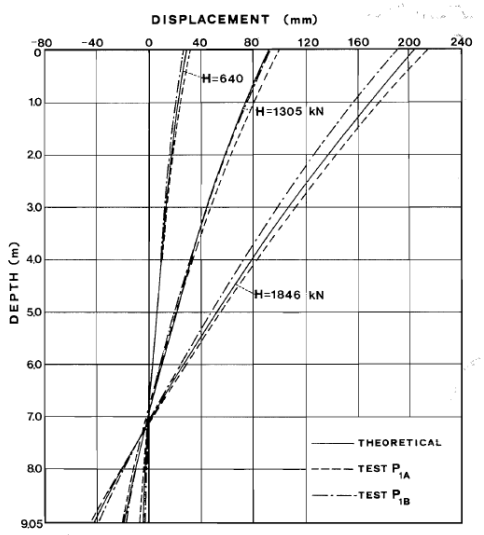

Figure 2-8: Lateral displacement of the pile (Georgiadis *et al.*, 1992)

Furthermore, with regard to the lateral displacement of the pile, Swain (1979) conducted a number of monotonic centrifuge tests on an 8 mm laterally loaded piles at 100-*g*. The scaled piles extended into dense sands and stiff clays, and was constructed from Dural, which is the common name used for one of the earliest types of age-hardenable aluminium alloys. He measured the lateral displacement with depth and plotted it for various horizontal load magnitudes, as indicated in **Figure 2-9**. Swain (1979) mentioned that insignificant movement of the pile happened beyond a depth of 60 mm (6 m deep at prototype scale) for a long pile. This depth is normally termed the effective length of the pile and determines the fixity of the pile.

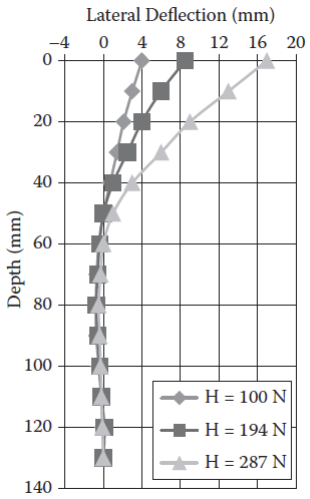

Figure 2-9: Lateral deflection of pile (Madabhushi, 2015, adapted from Swain, 1979)

Similar behaviour was observed more recently by Zhu *et al.* (2016), with minimal movement of the pile at the pile tip and larger movements towards the top of the pile where the horizontal load was applied. As mentioned previously, this is typical behaviour for a long pile and differs from the deflected shape observed for a short pile (Georgiadis *et al.*, 1992).

2.3.3 Soil reaction response to monotonic loading in the form of *p-y* curves

It is common in pile foundation design to plot *p-y* curves. These curves give an indication of the interaction between the pile and the surrounding soil at various depths, where *p* refers to the lateral soil reaction [M T^{-2}] and *y* to the lateral soil deflection [L]. The main idea behind these curves is to calculate the ultimate soil resistance with depth and can be plotted for both monotonic and cyclic load tests. The evolution of *p-y* curves is discussed later. Verdure *et al.* (2003) conducted a series of centrifuge tests at 40-*g* in sand, observing the influence of monotonic and cyclic loading on the soil-pile interaction, pile head displacement and bending moment response, for different cyclic loading types and cyclic loading magnitudes. Tests were conducted on a hollow aluminium pile, with an outer diameter of 18 mm, and embedded length of 300 mm, at model scale. The study was limited to the comparison between monotonic and cyclic lateral loading of piles, with the monotonic behaviour discussed here, followed by the discussion of cyclic loads in the next section. With regard to the *p-y* response of the piles in the centrifuge, Verdure *et al.* (2003), similarly to Georgiadis *et al.* (1992), obtained this response by fitting a function through the bending moment data and differentiating it twice to get the soil reaction (*p*) and integrating it twice to get the lateral deflection (*y*). **Figure 2-10** indicates the *p-y* curves for the monotonic loading of the pile at different depths as observed by Verdure *et al.* (2003), where C1 and C2 in the legend refers to the container number and 40, 60 and 80 to the relative amplitude of the cycles ($\Delta H/H_{max}$) expressed in percentage.

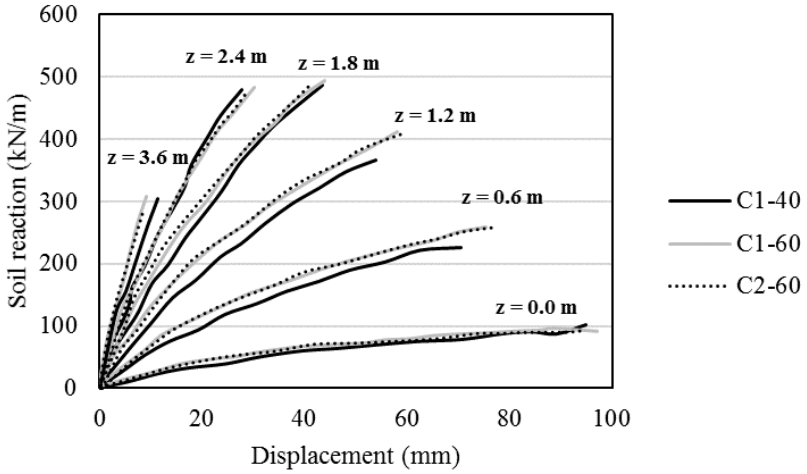

Figure 2-10: Comparison of monotonic *p-y* curves (adapted from Verdure *et al.*, 2003)

As expected, the soil reaction increased with an increase in lateral displacement of the pile, which is linked to the magnitude of the applied load. It can also be seen that there was a rapid increase in the stiffness with depth for the first three meters, with soil reaction stabilizing at larger depths (Verdure *et al.*, 2003). This increase in stiffness of the soil with depth was also mentioned by Barton (1982), Dyson & Randolph (2001) and Zhu *et al.* (2016), with the *p-y* curves at shallow depths being softer and becoming stiffer with increasing depths. Lastly, it should also be noted that for these tests at small displacements (low loads), the reaction of the soil seemed fairly linear. This confirms the behaviour observed earlier with the linear increase in the bending moment, shear force and soil reaction with increasing applied load at small loads. However, the significant soil reaction at the surface (z = 0 m), as indicated in **Figure 2-10**, raised some concern, as the reaction of the soil at the soil surface is typically accepted to be zero for sands.

2.4 CYCLIC RESPONSE OF SINGLE PILES SUBJECTED TO LATERAL LOADS

The application of monotonic loading is rarely encountered in practice but should still be mentioned. However, the effect of cyclic lateral loading on single piles is an aspect that should be considered and investigated and is more representative of real-life problems due to the occurrence of cyclic lateral loading in nature, such as wind, water and earth pressures. Typically, the methods used for analysing the effects of cyclic lateral loading on a single pile are limited, and only take into account the effects through the application of degradation factors (Little & Briaud, 1988). Additionally, many researchers have indicated that, under long-term cyclic loading, the behaviour of the soil-pile system shows a different response, due to the soil around the pile densifying rather than degrading.

Long & Vanneste (1994) conducted extensive research in the past to determine the effect of cyclic lateral loading on the behaviour of pile foundations. Their findings were based on 34 full-scale cyclic lateral load tests from various researchers, comprising out of steel, timber and reinforced concrete piles. These piles had different diameters and embedded lengths in soils ranging from loose to dense sand. The focus was on model parameters that were important to the behaviour and response of piles subjected to repetitive lateral loading. These parameters included pile and soil properties, as well as the number of load cycles. It is important to mention that majority of these tests were carried out for less than 100 load cycles on each of the piles, with only three of the piles being exposed to a maximum of 500 load cycles. This, however, raises a question about how representative these results are in terms of the long-term cyclic loading effects of piles. The observed effects are nevertheless discussed.

Long & Vanneste (1994) indicated that the behaviour of a cyclic laterally loaded pile depends on various characteristics. These characteristics were as follows, all of which is explained in the remainder of this section:

- Magnitude and direction of the lateral load.
- The initial geometrical and structural properties of the pile.
- Initial properties of the soil in which the pile is embedded.
- Change in the properties of the soil and pile as the pile is being loaded cyclically.

Regarding the direction of the lateral load mentioned above, Long & Vanneste (1994) indicated that applying a load in one direction, instead of two directions, has a greater effect on the cumulative deformation taking place, inducing more permanent strains in both the pile and the surrounding soil. Furthermore, they mentioned that the geometrical and structural properties of the pile were influenced as the pile was being loaded. Moments generated within the pile caused the pile to bend, mobilising the tension and compression capacity of the pile section. Typically, with steel cross-sections, the pile remains elastic, with the flexural stiffness (E_pI_p) being unaffected by any number of cycles or magnitude of the load. However, due to the low tensile capacity of reinforced concrete, the flexural stiffness decreases with increasing moments and number of load cycles. This is due to the progressive cracking of the cross-section. Lastly, Long & Vanneste (1994) indicated that since the deflection of a pile is influenced by changes in the flexural stiffness, the influence of these changes should be incorporated into design considerations. This is usually neglected due to the minimal effect it has on the pile performance at working loads, as only a small portion of the pile experiences large bending moments that can cause a change in the flexural rigidity. Long & Vanneste (1994) concluded that the effect of cycle number on the pile head displacement and bending moment response greatly depends on the changes in the mechanical properties of the pile, such as the strength and modulus of elasticity, as well as the accumulation of permanent strains in the soil. Later, Lin & Liao (1999), similarly to Long & Vanneste (1994), indicated that the most important parameters influencing the behaviour of a pile under cyclic loading are the cyclic loading type, type of pile installation, soil properties, pile embedment length and the soil-pile relative stiffness ratio.

The following subsections focused on the load-deflection response of piles subjected to cyclic lateral loading, followed by the secant stiffness behaviour of the soil-pile system, as well as the bending moment and soil reaction response to the number of load cycles, respectively.

2.4.1 Load-deflection response to cyclic loading

Li *et al.* (2010) conducted a series of cyclic lateral load tests in sand on a 1/100 scale stainless steel monopile, with an outer diameter of 50 mm, in a centrifuge, investigating the axial and

lateral response of the monopile under one-way force-controlled lateral loads. They indicated that limited research was available on the influence of cycle numbers on pile deflection, accumulated permanent displacement and the secant stiffness of the pile, and that many of the analysis procedures (discussed later) did not take into account the effects of number of load cycles and the permanent deformation that accumulates with the increasing number of load cycles. Typically, the behaviour of laterally loaded pile foundations is based on the recommendations from static lateral load tests, with the only difference being the application of a degradation factor to incorporate the effects of cycles.

Considering the lateral load applied as a function of lateral pile head displacement under one-way cyclic lateral loading, Li *et al.* (2010) observed that an increase in load amplitude resulted in an increase in pile head displacement, similar to the monotonic load behaviour, as indicated in **Figure 2-11**. They also mentioned that, when considering the first load cycle at the first lateral load amplitude (206 N), it is evident that the reaction of the soil is non-linear, with the gradient of the load-displacement curve decreasing with increasing lateral displacement, which was also observed under monotonic loading (first load cycle).

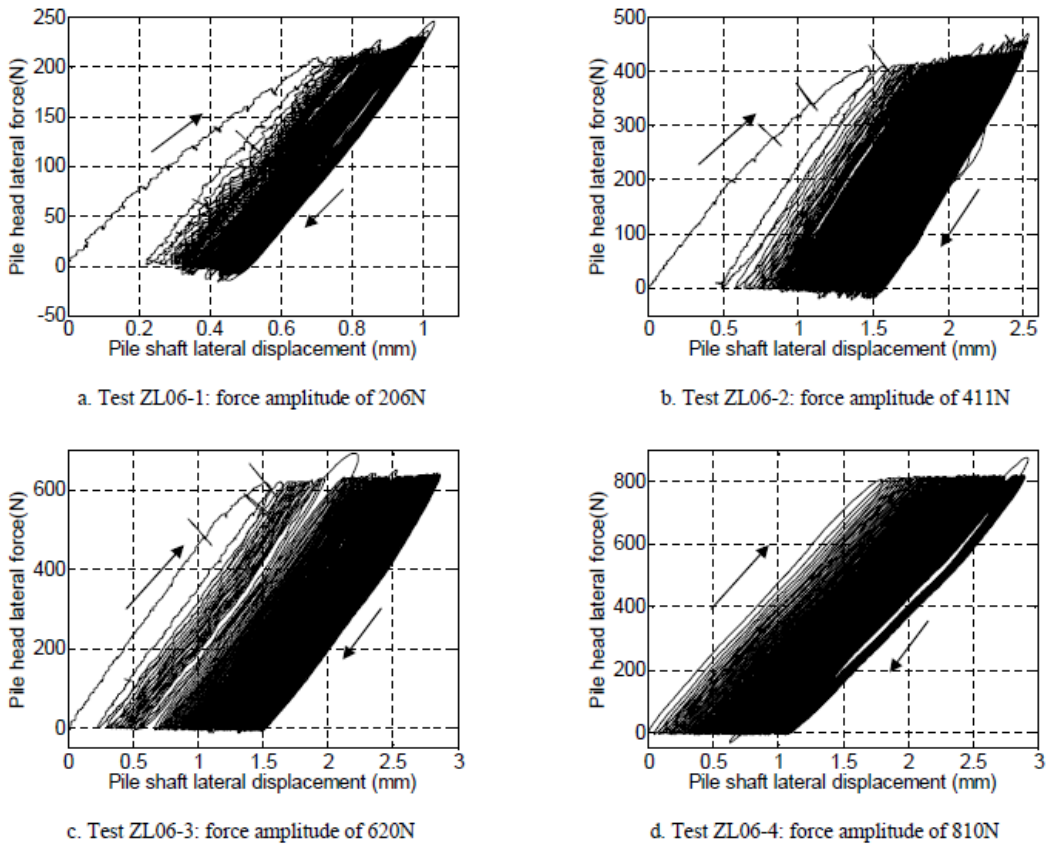

Figure 2-11: Load-displacement curves for various load amplitudes (Li *et al.*, 2010)

For the load cycles to follow, the gradient of the loading and unloading curves were fairly linear and stiffer than the first cycle. Each time the magnitude of the lateral load was increased the same phenomenon occurred for the first cycle at that load.

Long & Vanneste (1994) also mentioned that the effect of cyclic loading on the deformation of laterally loaded piles were the greatest for the first load cycle, after which the effect diminished as cycling continued, which is similar to what Li *et al.* (2010) observed. Leblanc *et al.* (2010) also observed this phenomenon regarding the increase in stiffness of the soil-pile system with number of load cycles. They indicated that this contrasts the methodology where static load-displacement curves are degraded to account for cyclic loading. Their findings were based on a number of laboratory tests that were conducted on a small-scale 80 mm stiff copper pile, in drained sand, subjected to between 8000 and 60000 load cycles at 1-*g*. They indicated that the long-term loading of a foundation would most likely change the stiffness of the soil surrounding the pile and influence the behaviour of the foundation. Thus, it is important to assess the concepts of stiffness and strength changes during long-term cyclic loading (Leblanc *et al.*, 2010).

Figure 2-12 shows that, for different load amplitudes, the maximum displacement of the pile increased logarithmically with an increase in the number of load cycles (Li *et al.*, 2010), with the rate of increase also being higher at larger load magnitudes. This is indicative of significant permanent deformation of the soil developing around the pile shaft.

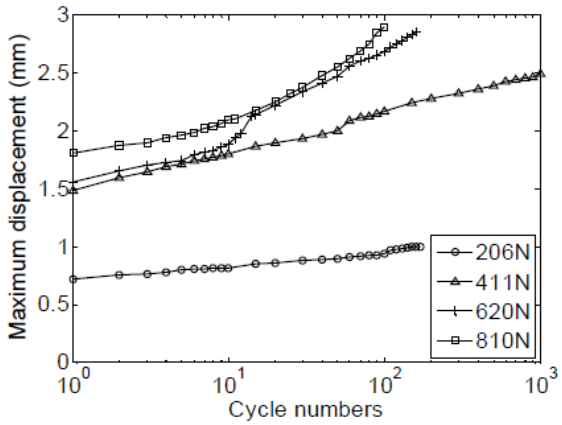

Figure 2-12: Maximum pile displacement (Li *et al.*, 2010)

Due to one-way cyclic shearing, the induced lateral soil stress state was high at maximum displacement and small at the end of the return leg. This led to the densification of the sand in front of the pile, changing the soil stiffness, creating progressive pile lateral permanent displacement (Li *et al.*, 2010). However, as the magnitude of the applied load reached a certain

point the relationship between the maximum lateral displacement and the number of load cycles did not increase logarithmically anymore, resulting in excessive lateral displacements to take place. At larger loads, soil typically have a higher tendency to behave plastically, resulting in progressive increments of permanent displacements to take place.

Verdure *et al.* (2003) indicated that, regardless of the magnitude of the lateral load, the pile deflection is depended on the nature of the soil (sand or clay) as well as the soil properties (relative density and shear strength), which justifies the behaviour observed by Li *et al.* (2010) at higher loads, as the properties of the soil changed.

2.4.2 Absolute and secant stiffness of the soil-pile system

When considering the perceived increase in stiffness of the soil-pile system, Abadie & Byrne (2014) indicated that, for analysis of cyclic phenomenon, the term for stiffness should be carefully defined. They classified stiffness in one of two ways. The first is defined as the absolute stiffness (K_N), which relates the soil state at cycle N to the initial state. It describes the evolution of the interaction between the pile and the surrounding soil and is defined as the ratio between the applied load and the absolute deflection of the pile. The second is defined as the cyclic secant stiffness (k_N), which characterises the state of the soil-pile interaction after N cycles. The evolution in stiffness is critical and it is indicative of the change in natural frequency of the structure with cycle number. The definition for both the absolute and cyclic secant stiffness can be seen in **Figure 2-13**, where K_0 and k_0 refers to the absolute and secant stiffness for the first load cycle, respectively, followed by K_N and k_N which represents that absolute and secant stiffness after N cycles.

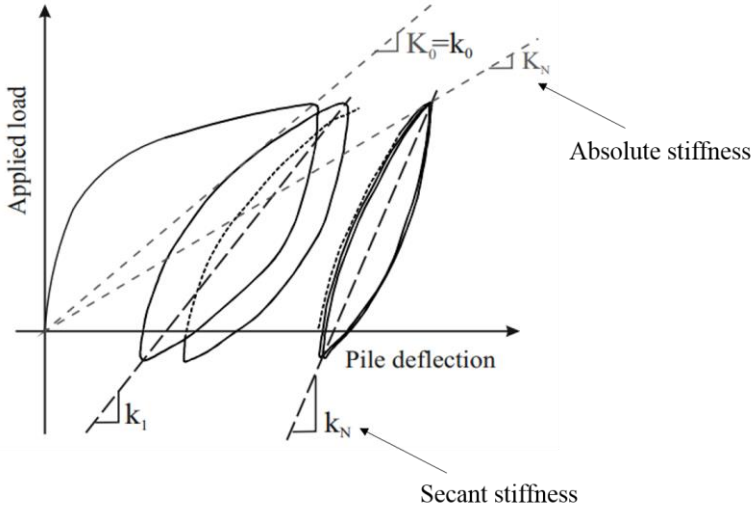

Figure 2-13: Definition of absolute and cyclic secant stiffness (adapted from Abadie & Byrne, 2014)

With an increasing number of load cycles, the absolute stiffness of a pile would decrease, due to increased permanent deformation of the pile taking place, while the secant stiffness would increase as a result of the soil densification under repeated load cycles.

Verdure *et al.* (2003) indicated that to better visualise the effect of load cycles on the stiffness behaviour of the soil-pile system, the cyclic stiffnesses should be plotted as a function of the number of load cycles. They only considered the secant stiffness during their investigating, referring to it as the global stiffness. Verdure and his co-workers mentioned that the calculation of the secant stiffness typically uses pile deflection at the location of load application. However, if the pile deflection was taken at other locations along the length of the pile, such as the soil surface, the stiffness would be different. They mentioned that the analysis of cyclic load effect is not typically done on the magnitude of the global stiffness (secant stiffness), but on its change during cyclic loading, thus the magnitude is of lesser importance.

Verdure *et al.* (2003) normalised the stiffness data with the global stiffness (secant stiffness) obtained from the first (monotonic) cycle (k_0). This was to eliminate the initial state of the soil (stiffness), making it possible to only focus on the change in the behaviour of the soil-pile system as a result of the load cycles. The normalised stiffness data is indicated in **Figure 2-14**. It can be seen that after the first load cycle, the global stiffness (secant stiffness) varied little with number of cycles, which is indicative that the first load cycle on the pile, at any given load magnitude, influenced the soil the most.

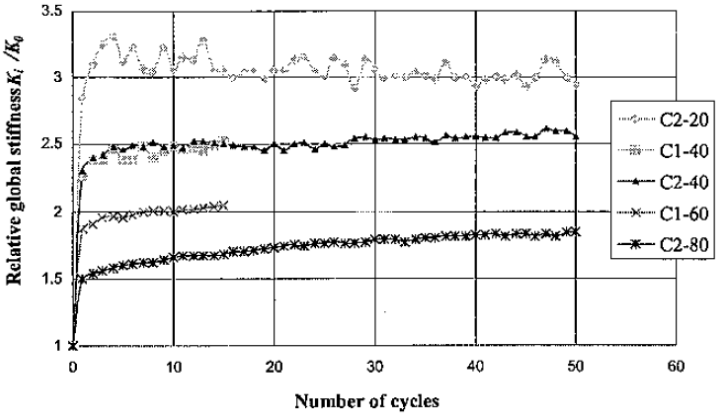

Figure 2-14: Relative secant stiffness versus number of load cycles (Verdure *et al.*, 2003)

Furthermore, Verdure *et al.* (2003) mentioned that to better understand the effects of cycle number on pile response, and to eliminate the effect of the non-linearity of the soil at the first cycle, the secant stiffness should rather be compared to that of the second load cycle as shown in **Figure 2-15**. It should be mentioned that the tendencies observed in **Figure 2-14** can also be seen here with minimal changes to number of load cycles. Furthermore, they indicated that,

depending on the magnitude of the load, the secant stiffness can increase to between 1.3 and 1.8 times the initial secant stiffness, indicating hardening behaviour of the soil. This behaviour was also observed by Little & Briaud (1988) with regard to the increase in secant stiffness.

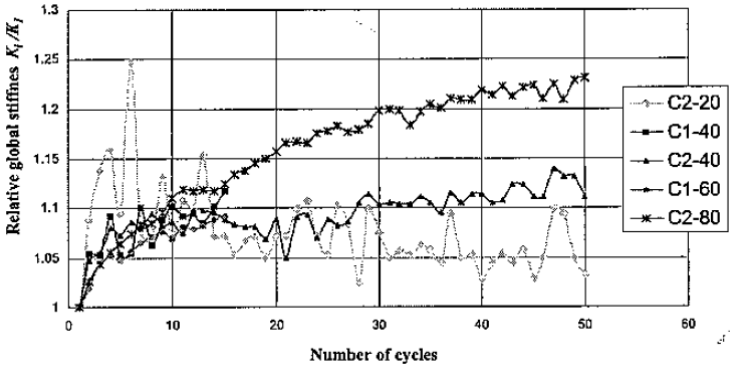

Figure 2-15: Relative secant stiffness versus number of cycles from the second load cycle (Verdure *et al.*, 2003)

Similar to Verdure *et al.* (2003), Li *et al.* (2010) plotted the secant stiffness for their results presented in **Figure 2-11**. They mentioned that the pile secant stiffness increased with an increase in the number of load cycles (see **Figure 2-16**). They also indicated that the increase in the pile secant stiffness with an increase in number of load cycles increased at a reducing rate.

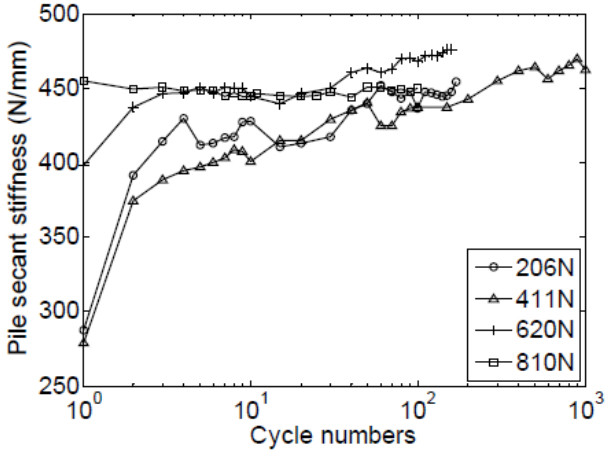

Figure 2-16: Pile secant lateral stiffness (Li *et al.*, 2010)

The minimal increase in the pile secant stiffness for the 620 N and 810 N load cases was due to the stress history induced in the preceding tests at lower loads. At lower loads, the smaller secant stiffness was as a result of the non-linearity of the initial virgin soil. By considering **Figure 2-16**, Li *et al.* (2010) indicated that the local densification of the soil from the cyclic

lateral loads, as mentioned previously, might have raised the shear modulus of the sand around the pile and led to the pile secant stiffness increasing with an increase in the number of load cycles applied.

This was also mentioned by Long & Vanneste (1994), observing that a volume change in the soil may occur from the repetitive lateral loading, depending on the initial stress state and density of the soil. This was later justified by Li *et al.* (2015), indicating that the previous loading history of the soil had a significant effect on the response of a pile. They illustrated that, for lateral loads below the previous maximum load, the load-displacement response increased in stiffness, as the load was increased. However, if the applied load exceeded the previous applied maximum load, the stiffness reduced, similar to what Li *et al.* (2010) observed. Furthermore, Li *et al.* (2015) suggested that this increase in stiffness caused by cyclic loading is related to particles and principle stress re-orientation to withstand the applied stresses. Zhu *et al.* (2016) mentioned that the secant stiffness for a single pile typically increases between 50-150% in the first 1000 cycles at high cyclic loading frequencies. This indicated that the use of a degradation factor to incorporate cyclic effects into pile behaviour should be considered with care.

With regard to the absolute stiffness, Little & Briaud (1988) indicated that the absolute stiffness decreased with increase in number of load cycles. They based their observations on full-scale cyclic loading of reinforced concrete and steel pile foundations, respectively. This behaviour was due to the increasing permanent deformation and displacement of the pile taking place with load cycles. They also indicated that an instantaneous reduction in the absolute stiffness occurred, in the case of reinforced concrete piles. They argued that it was indicative of a crack that had formed in the concrete section, which was not present and observed with the steel piles which showed a gradual reduction.

Werkmeister *et al.* (2001) investigated the effect of cyclic loading on the performance of unbound granular materials for the use in pavements using cyclic triaxial tests. They referred to the concept, caused by the repetitive loading, as shakedown, as was originally proposed by Johnson (1986). The idea behind this concept is to investigate the permanent deformation that occurs under pavement structures due to trafficking. Similarly, this can be applied to the response of a pile subjected to cyclic loading. **Figure 2-17** indicates the idealised behaviour of granular materials under repeated cyclic loads. Werkmeister *et al.* (2001) indicated that the shakedown concept and permanent strain accumulation can be described by three ranges, with range one referred to as the plastic shakedown (A), range two, the intermediate response-plastic creep (B), and range three, the incremental collapse (C), depending on the stress applied to the

soil. Werkmeister *et al.* (2004) mentioned that these ranges and deformation behaviour can be described by two different methods. The two methods are as follows:

- Macro-mechanical method – describing the deformation behaviour on the basis of the friction between the grains of soil, particle shape and density.
- Micro-mechanical method – describing the behaviour of the grain assembly under cyclic loading as a consequence of the compaction, consolidation and the distortion processes in the material.

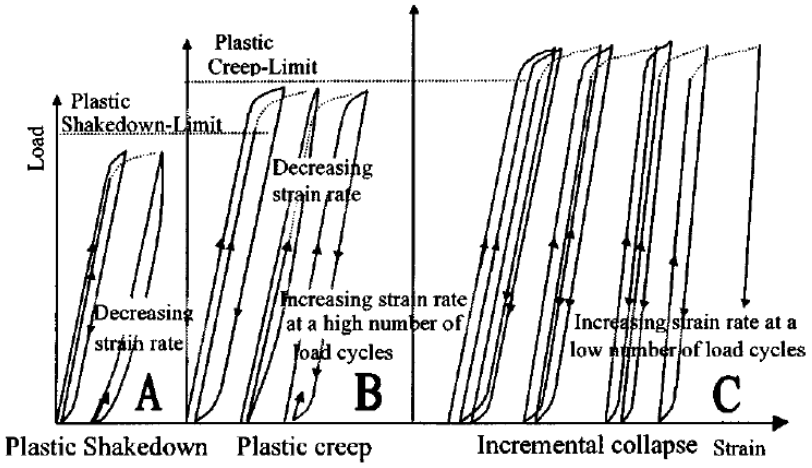

Figure 2-17: Idealised behaviour of granular materials under cyclic loads (Werkmeister *et al.*, 2001)

Range A and C showed the most interesting information. They indicated that range A is typical for low applied stresses to the soil. The response is plastic for a finite number of load applications and becomes entirely resilient after the post-compaction period, with no further permanent strains occurring after that. Werkmeister *et al.* (2004) indicated that the accumulated strains obtained in this range depend on the load level. Furthermore, they mentioned that for range C, a continuing incremental plastic deformation was observed for each additional load cycle. Thus, at higher load levels the response was always plastic, and each load application resulted in a progressive increment of permanent strain at the same load level.

2.4.3 Bending response to cyclic loading

Another important parameter to consider is bending moments that are developing within the pile due to the cyclic lateral loads. Verdure *et al.* (2003) plotted the bending moment versus depth along the length of a pile for the tests they conducted on a scaled aluminium pile in the centrifuge, as shown by **Figure 2-18**. They indicated that load cycles had two main effects on the behaviour of the pile under bending (see **Figure 2-18**):

- The maximum bending moment increased with the number of load cycles.
- The depth of the maximum bending moment increased with the number of cycles (stabilising at a depth of five times the diameter of the pile).

Previously, Poulos (1982) also mentioned the increase in the maximum moment and the change in the distribution of the bending moments with an increase in the number of load cycles. He indicated that the maximum moment typically occurred at larger depths than under static load conditions due to the number of cycles at any given maximum load level.

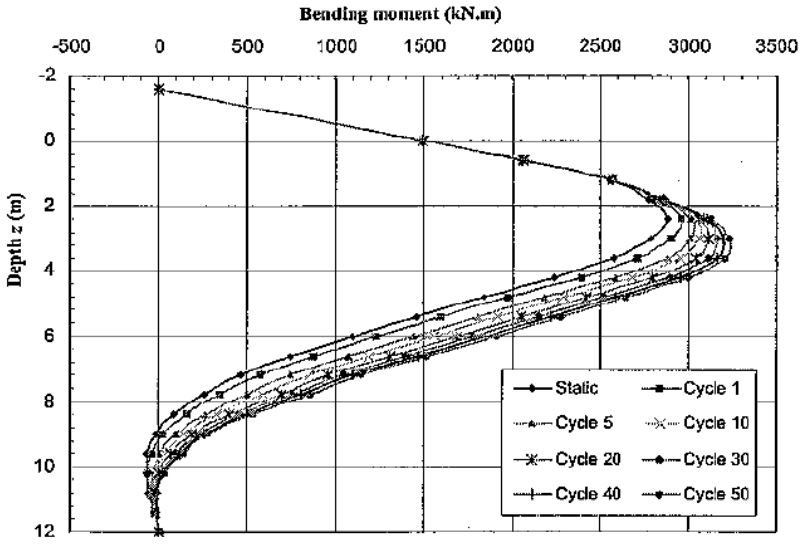

Figure 2-18: Bending moment versus depth for different number of cycles (Verdure *et al.*, 2003)

Kirkwood & Haigh (2014) indicated that the effect of cyclic loading on the foundation stiffness could also be observed when considering the bending moments experienced by the pile. This was observed from a series of centrifuge tests on an aluminium pile, with a diameter of 45 mm, at 100-*g*. The aim of the tests was to determine the development of soil stresses around a pile subjected to various loading regimes. They plotted the normalised bending moments with depth for different load cycles (see **Figure 2-19**) and mentioned that, at the maximum load applied in each load cycle, the bending moment remained relatively constant for the first 1000 load cycles. Li *et al.* (2015) and Zhu *et al.* (2016) also mentioned this behaviour. Zhu *et al.* (2016) however observed an increase in the maximum bending moment for the first 500 cycles, with a decrease in maximum bending moment after that, which was possibly due to the shallow sand that weakened around the pile and densified after a number of load cycles. In **Figure 2-19**, M refers to the bending moment experienced by the pile, where M_h is the moment applied to the pile head on the same load cycle. The normalised bending moments were plotted for different cyclic loading ratios (ζ_c) where the cyclic loading ratio is defined as the ratio between the minimum

and maximum lateral applied load, with a value of 0 corresponding to one-way lateral loading and -1 to two-way lateral loading, respectively (Leblanc *et al.*, 2010).

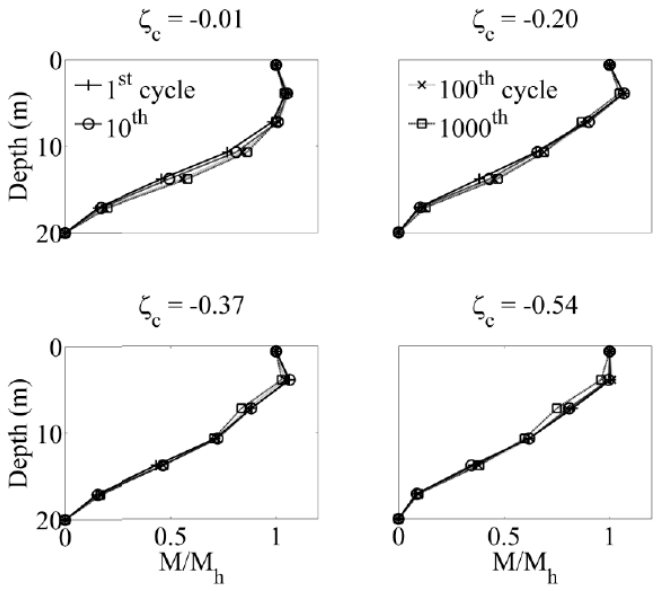

Figure 2-19: Bending moment profile along the length of the pile at maximum load application (Kirkwood & Haigh, 2014)

Kirkwood & Haigh (2014) indicated that the bending moments observed in the pile, at the point of zero lateral load for various cyclic loading ratios contrasted the behaviour of the pile at maximum load application, as indicated by **Figure 2-20**, and should be investigated.

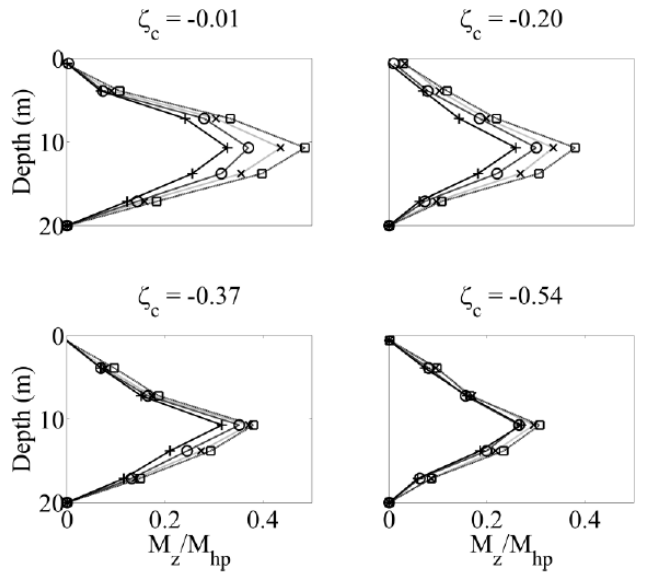

Figure 2-20: Bending moment profile along the length of the pile at zero lateral load application (Kirkwood & Haigh, 2014)

M_z refers to the bending moment in the pile at zero lateral load and M_{hp} refers to the maximum moment applied to the pile head during the previous load cycle. It can be seen that the largest effect of cyclic loading was when ζ_c = -0.01, justifying what Long & Vanneste (1994) mentioned that one-way lateral loading had a larger effect on the pile behaviour than two-way lateral loading. It should also be mentioned that an increase in the number of load cycles resulted in an increase in the permanent (non-zero) bending moments experienced by the pile. Lastly, by considering **Figure 2-19** and **Figure 2-20**, the maximum bending moment upon load application did not correspond with the maximum permanent bending moment upon load removal, indicating a change in the condition of the soil.

This difference in permanent bending moments with an increase in the number of load cycles (see **Figure 2-20**) can better be described by **Figure 2-21**. Kirkwood & Haigh (2014) plotted the normalised permanent bending moments against the number of load cycles, for a prototype depth of 10.7 m (107 mm at model scale). They referred to these permanent bending moments, at no applied load applications, as locked-in moments, caused by soil stresses which developed in response to the applied cyclic lateral loads. Kirkwood & Haigh (2014) also indicated that these locked-in moments increased logarithmically with the number of load cycles, showing an increase in the foundation stiffness (secant modulus).

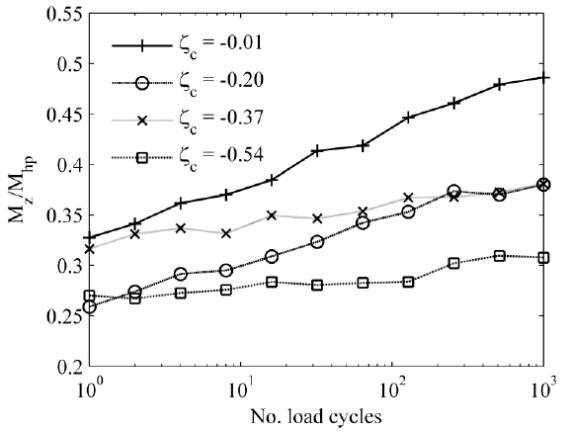

Figure 2-21: Normalised locked-in bending moment for number of load cycles (Kirkwood & Haigh, 2014)

2.4.4 Soil reaction response to cyclic loading in the form of *p-y* curves

When considering the *p-y* response of a pile subjected to horizontal load cycles, Verdure *et al.* (2003) followed the same procedure as with the monotonic load test. **Figure 2-22** indicates the full-scale *p-y* curves for the cyclic load tests near the soil surface, after applying the correct scaling factors to the results of the scaled test. They observed that significant hysteresis occurred initially, with a continuous reduction of the soil reaction and hysteresis with the

number of load cycles. Zhu *et al.* (2016) also indicated that the hysteresis loops of *p-y* curves at shallower depths were larger than those at deeper depths, as shown in **Figure 2-23**, where D refers to the diameter of the pile of 30 mm, with tests conducted at 83-*g*. The results presented are results scaled to full-scale values using the correct scale factors. It can also be seen that the pile shaft had a continuous accumulation of residual horizontal displacements, and did not return to the initial position, which they argued was due to the fact that sand particles filled the gap between the pile and the soil at the side opposite to the one-way loading direction.

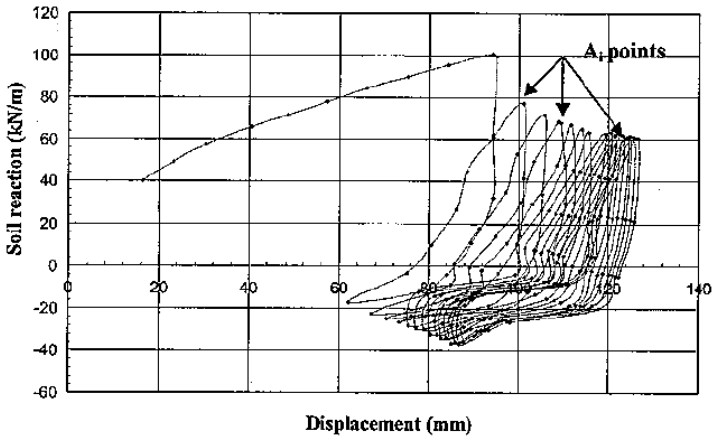

Figure 2-22: Cyclic *p-y* response (Verdure *et al.*, 2003)

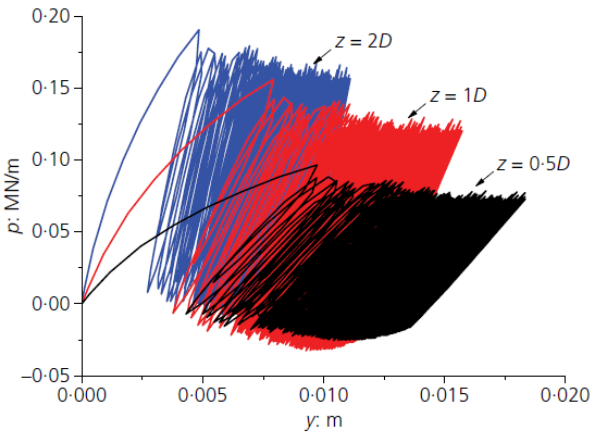

Figure 2-23: Cyclic *p-y* curves at different depths (Zhu *et al.*, 2016)

Verdure *et al.* (2003) plotted the peak points (A_i points) for each cycle in **Figure 2-22** as shown in **Figure 2-24**. At depths of between 0 and 2.4 m, they indicated that the soil reaction decreased with number of load cycles, while the pile displacement increased. Furthermore, they indicated the soil exhibited some degradation perhaps because of the yield limit of the soil had been reached. At larger depths, Verdure *et al.* (2003) mentioned that both the pile displacement and soil reaction increased with increase in the number of load cycles, and the *p-y* response was

similar to that observed for the monotonic load test (see **Figure 2-10**), as the yield limit of the soil was not exceeded. Thus, cyclic loading had minimal effect on the behaviour of the soil and the pile at depths exceeding 2.4 m below the ground level. They also added that to balance the reduction in soil reaction observed at smaller depths, increased soil reaction had to be mobilised at larger depths (the influence sphere increased downwards). Similar to the monotonic test from Verdure *et al.* (2003), the soil reaction at the surface (z = 0 m) for the cyclic load test in **Figure 2-24**, raised some concern, as the soil reaction at the soil surface is typically accepted to be zero for sands.

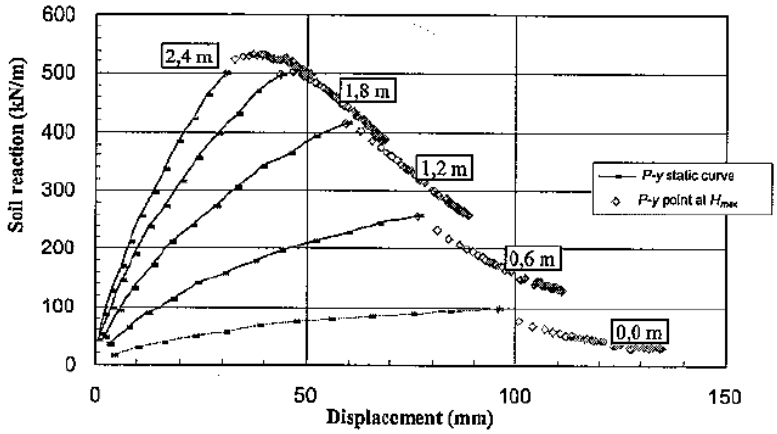

Figure 2-24: Evolution of A_i points (p-y relationship under H_{max}) at different depths (Verdure *et al.*, 2003)

2.5 SINGLE PILE BEHAVIOUR (ANALYSIS MECHANISMS REVIEWED)

The design and analysis of laterally loaded pile foundations are primarily based on either the ultimate lateral resistance of the pile or the soil or the load-deflection response of the soil-pile system. The load capacity (resistance) of the piles is dependent on not only the ultimate resistance of the soil but also the strength of the pile, thus taking into account the interaction between the pile and the soil. However, more often than not, the strength or properties of the pile are neglected and only the behaviour of the soil is considered in the design and analysis of these structures.

In many instances, such as retaining walls and wind turbine foundations, the ultimate load resistance is only reached at very large deflections, resulting in the serviceability limit of both the pile and the soil being exceeded. Thus, the design of laterally loaded pile foundations is typically governed by the maximum allowable lateral displacement (load-deflection response), rather than the ultimate load capacity. Design practice in the past used empirical information to predict the lateral behaviour of pile foundations, based on full-scale lateral load tests. Due to changing soil conditions (non-linearity), obtaining an exact solution for the lateral behaviour of

piles is complex. However, over the past few decades, a theoretical approach for designing laterally loaded pile foundations and predicting their load-deflection response have been developed.

Poulos & Davis (1980) indicated that the two approaches that have generally been employed were as follows:

- Subgrade reaction approach
- Elastic approach

They indicated that the subgrade reaction approach, based on the Winkler model, assumes that the soil is not continuous and that the reaction of the pile at a point, subjected to a lateral load, is related to the displacement at that point. On the other hand, the elastic approach assumes the soil to be an elastic continuum.

The interaction between a pile and the surrounding soil still remains a complex soil-structure interaction problem that requires careful attention when designing, taking into account all the limitations associated with the different analysis procedures. However, more recently, pile and soil material models have been researched, implemented and tested to compensate for both the non-linear behaviour of soil, as well as that of concrete, to predict more realistic behaviour of the complex soil-structure interaction problem.

This dissertation focuses on predicting the load-deflection response of piles, and not on the ultimate load capacity. However, to better understand and visualise the overall load-deflection response of piles, it was important to first consider the basic failure modes of laterally loaded piles at ultimate capacity. In the following subsections, these basic principles are discussed, followed by the various analysis approaches used to determine and predict the load-deflection response of a single pile.

2.5.1 Lateral capacity of piles – failure modes

Even though the ultimate resistance or capacity of the soil-pile system did not form part of this study, it is necessary to consider the basic failure modes of laterally loaded piles to better describe the load-deflection response of a pile. Fleming *et al.* (2008) indicated that if a pile is loaded laterally, normal stresses in the soil in front of the pile would increase, resulting in decreasing stresses in the soil behind the pile. They also mentioned that displacements in the soil would tend to be radially away from the pile in the front of the pile, and radially towards the pile behind it. As illustrated by **Figure 2-25**, it can be seen that at some stage, near the ground surface, a gap would form between the pile and the soil behind the pile, with the soil in front of the pile forming a wedge, resulting in failure of the soil. To determine the distribution

of limiting pressures on the pile, various mechanisms have to be taken into account, which fall outside the scope of this dissertation and is thus not discussed.

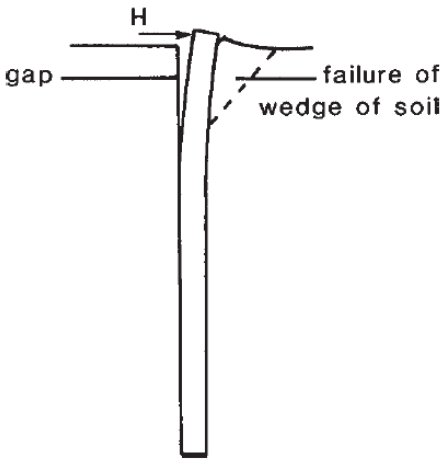

Figure 2-25: Deformation of pile under lateral load (Fleming *et al.*, 2008)

Broms (1964b), Poulos & Davis (1980) and Fleming *et al.* (2008) mentioned that the collapse of a soil-pile system at ultimate capacity, subjected to lateral loading (H_u), can occur in either one of two modes. **Figure 2-26** indicates both these failure modes for a free-headed pile. The first mode describes the soil-pile system as rigid (short) and the second mode as flexible (long). The typical shape of the soil reaction (resistance) and bending moment diagrams for both these modes are also shown for ultimate soil conditions. For a free-headed short pile, ultimate failure is as a result of the rotation or translation of the pile (soil failure) rather than the yielding of the pile. The maximum moment experienced by the pile is smaller than the yielding moment, which is typical behaviour for a pile that has a large yielding (plastic) moment. However, in the case with a free-headed long pile, ultimate failure is as a result of the yielding of the pile at the location where the maximum moment occurs (pile failure), with the formation of a plastic hinge, resulting in an increase in lateral deflection above the plastic hinge. The maximum moment experienced by the pile is thus larger than the yielding of the pile. The basic mechanisms of pile rotation and pile yielding proposed for the free-headed piles are also valid for fixed-headed piles.

Broms (1964b) indicated that in the case of short (rigid) piles, an increase in the embedment length resulted in a decrease in deflections at the ground surface, while for long (flexible) piles, the lateral deflections at ground level were unaffected by a change in the embedment length. Furthermore, he indicated that an increase in the flexural rigidity, E_pI_p, of the pile section would result in a decrease in lateral deflection for long piles (pile yields) but is not the case for short

piles (pile rotates and does not yield). Classification of piles, on whether a pile can be considered to be rigid or flexible, is discussed later.

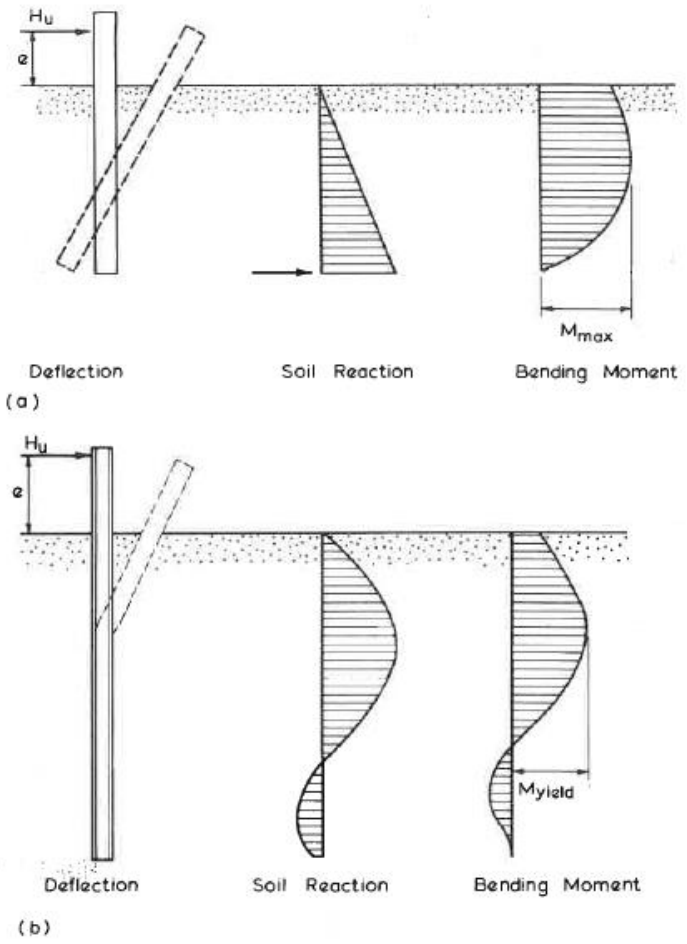

Figure 2-26: Free-head piles in a cohesionless soil: (a) short, (b) long (Poulos & Davis, 1980, adapted from Broms, 1964b)

2.5.2 Subgrade reaction analysis approach

The subgrade reaction approach for a single pile is based on the principles of the Winkler model, which simplifies the pile as an elastic beam and represents the soil as a series of unconnected linear-elastic springs, with deflection occurring only at the location of the springs, disregarding the influence of adjacent springs and deflections on the movement at that point, assuming no continuity. Poulos & Davis (1980) indicated that one of the obvious disadvantages of this method is the lack of continuity of the soil, as real soil is at least to some extent continuous, with the displacement at a point being influenced by the forces and stresses at other locations within the soil. They also indicated that a spring modulus, which have units of force per unit

length, has to be used, which is dependent on the size of the foundation, and typically a parameter that is difficult to obtain.

Besides the drawbacks indicated, the subgrade reaction approach has been widely used in foundations practices, not only due to its simplicity regarding computation but also due to the ability to incorporate nonlinearity of the soil (Section 2.5.4), changes in soil stiffness with depth, as well as the layering of the soil profile.

The Winkler model assumes that the relationship between the pressure, *p*, at a point and the deflection, *y*, at that same point are proportional and depends on the stiffness of the spring. By applying this principle to laterally loaded piles, the stiffness of the spring is represented by the modulus of subgrade reaction, also referred to as the coefficient of subgrade reaction, as indicated by **Equation 2-2**, and have units of pressure per unit length. It should be mentioned that a relationship exists between the modulus of subgrade reaction and the spring modulus, with the only difference being that the spring modulus takes into account the diameter of the pile.

$$p = k_h y \qquad \textbf{Equation 2-2}$$

where,

p = lateral soil reaction [M T^{-2}]

k_h = modulus of subgrade reaction [M L^{-2} T^{-2}]

y = lateral soil displacement [L]

Assuming elastic beam theory, the pile can be simplified as a thin strip, whose behaviour is described by the beam equation (see **Equation 2-3**).

$$E_p I_p \frac{d^4 y}{dz^4} = -pD \qquad \textbf{Equation 2-3}$$

where,

E_p = modulus of elasticity of the pile [M L^{-1} T^{-2}]

I_p = second moment of area of the pile [L^4]

z = depth below the soil surface [L]

D = diameter of the pile [L]

Based on the assumed elastic beam theory, axial effects on the pile was ignored. Solutions for the equation can be obtained numerically (finite difference method) or analytically (closed-form solution), depending on the assumption made regarding the modulus of subgrade reaction of the soil, i.e. whether it is constant with depth or varies along the length of the pile, the former typically being solved analytically and the latter using the finite difference method. From these solutions of the deflections with depth, the corresponding soil reaction, shear force and bending moment along the length of the pile can be determined. However, Duncan *et al.* (1994) and Long & Vanneste (1994) indicated the contribution of both bending moments and shear forces to the deflection behaviour of laterally loaded piles, contradicting the assumption that axial effects could be ignored. Shear capacity of any beam section is typically dependent on the size of the cross-sectional area, which in turn also affects the axial capacity of that section. This questions the validity of the assumption that axial and shear effects can just be ignored, as piles with the same flexural rigidity, E_pI_p, might not have the same axial rigidity, E_pA_p.

Poulos & Davis (1974) indicated that movements and rotations of a single pile was influenced mainly by two factors, besides the applied loads, moments and soil conditions. These factors greatly affect the response of the pile and can be incorporated into the equation above by means of boundary conditions as was also indicated by Yan & Byrne (1992), Dyson & Randolph (2001) and Zhu *et al.* (2016). These two factors were:

- A free-head pile, having free rotation at the top
- A fixed-head pile having no rotation at the top of the pile

The modulus of subgrade reaction, as mentioned, is a constant that relates deflection of soil to soil reaction or pressure and is dependent on the relative density of the soil (Li *et al.*, 2017). The distribution of this coefficient along the length of the pile depends on the type of soil. Typically, this modulus is taken to be constant along the length of a pile in clays ($n = 0$), wherein sands it is assumed to vary linearly with depth ($n = 1$), as indicated by **Equation 2-4** (Palmer & Thompson, 1948). Lin & Liao (2006) indicated that this assumption regarding sands are generally only true for uniform sands, whereby Li *et al.* (2017) mentioned that this assumption is not true for over-consolidated dense sand deposits.

$$k_h = k_L\left(\frac{z}{L}\right)^n \qquad \textbf{Equation 2-4}$$

where,

k_L = modulus of subgrade reaction, k_h, at the pile tip (z = L) [M L^{-2} T^{-2}]

L = embedded length of the pile [L]

n = an empirical index equal to or greater than zero [-]

Terzaghi (1955), Broms (1964b) and Poulos & Davis (1980) indicated that it is convenient to re-express **Equation 2-4** for sands (see **Equation 2-5**), based on the assumption that, for sands, the coefficient of subgrade reaction increases linearly with depth. It can be seen from this equation, as indicated by Broms (1964b), that the coefficient is independent of the stiffness and length of the pile.

$$k_h = n_h(\frac{z}{D}) \qquad \textbf{Equation 2-5}$$

where,

n_h = coefficient of subgrade reaction [M L^{-2} T^{-2}]

The coefficient of subgrade reaction is generally determined by one of the following methods:

- Full-scale lateral load test on a pile
- Plate-loading tests
- Empirical correlations with other soil properties

By using full-scale lateral load tests, the coefficient is determined by instrumenting the pile to measure pile deflection and soil pressure. However, this method is time-consuming and expensive. The use of plate-loading tests has been initiated by Terzaghi (1955) and Broms (1964b), with one of the main limitations being to correlate the derived values on a plate to that on a pile, assuming that the distribution of load is constant along the width of the pile (see **Figure 2-27),** which is not true.

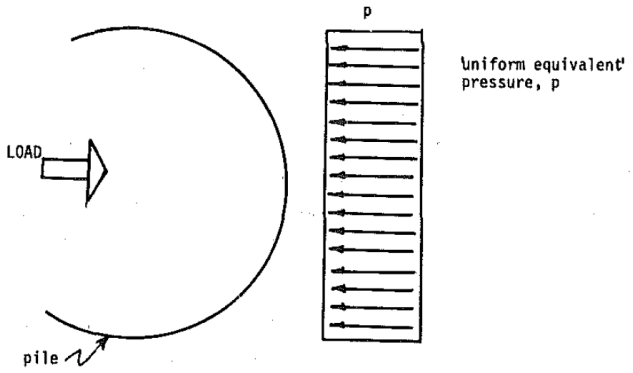

Figure 2-27: Simplified modulus pressure distribution along width of pile (Smith, 1987)

Figure 2-28 indicates the distribution of pressure along the width of the pile, as proposed by Smith (1987), which indicates that significant side shear and front pressures are mobilised to

resist the translating pile. For the rest of the dissertation, the distribution of pressure along the width of the pile will be taken as constant, as it is not the focus of this research.

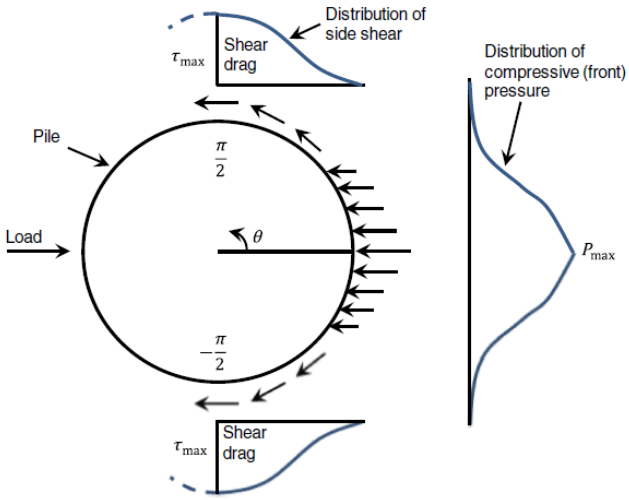

Figure 2-28: Pressure distribution along width of pile (Lin *et al.*, 2015, adapted from Smith, 1987)

Typical values for the coefficient of subgrade reaction of sand, as proposed by Terzaghi (1955), is indicated in **Table 2-2**, depending primarily on the relative density of the sand, and whether the sand is dry, moist or submerged.

Table 2-2: Values of n_h for sand (Poulos & Davis, 1980, adapted from Terzaghi, 1955)

Relative density	Loose	Medium	Dense
n_h, dry or moist sand (MN/m^3)	2.2	6.6	17.6
n_h, submerged sand (MN/m^3)	1.4	4.9	11.8

Broms (1964b) concluded that, based on a series of full-scale tests on free-headed and restraint (fixed) piles, the used of these coefficients tend to overestimate the deflections at working loads, yielding results which were conservative. Furthermore, Reese *et al.* (1974) mentioned that these coefficients were very low, and proposed different coefficients, which is shown later.

As it is however known that the relationship between deflection and soil pressure is nonlinear, the soil pressure would reach a limiting value at large displacements (Poulos & Davis, 1980). Thus, when applying linear theory, care should be taken when selecting the appropriate coefficient of subgrade modulus. Reese & Matlock (1956) argued that assuming a linear increase in the modulus of subgrade, for sands, allows for some soil yielding and nonlinearity.

They indicated that this can be said due to the secant modulus towards the top of the pile would tend to be small, increasing with depth due to higher soil strength and lower levels of deflection.

When applying the effect of cyclic loading on the subgrade reaction, care should also be taken when selecting a value for the coefficient. Broms (1964b) and Poulos & Davis (1980) indicated that cyclic loading causes deterioration of the soil resistance, thus reducing the value of k_h or n_h to 30% of the value applicable to the initial loading. Furthermore, Broms (1964b) indicated that the effect of cyclic loading had a larger effect on soils at lower relative densities than soils at higher relative densities. Lastly, it is also worthwhile mentioning, besides the effect of cyclic loading, that the overall modulus of subgrade reaction depends on the lateral displacement of the soil, and the magnitude of the load being applied.

2.5.3 Elastic analysis approach

Modelling any problem in engineering by assuming elastic material properties simplifies all calculations. Many researchers have investigated the analysis of laterally loaded piles, assuming the soil to be an elastic continuum. Poulos & Davis (1980) indicated that, for the elastic analysis approach on single piles, presenting the soil as an elastic continuum is more satisfactory, as it accounts for the continuous nature of the soil. They indicated that the use of this approach works well for predicting the vertical settlement of piles and pile groups subjected to axial loading and could be modified to allow for yielding of soil. Apart from that, the use of the elastic analysis could also incorporate the effect of group action of piles under lateral loads. One of the largest drawbacks of this analysis method, as indicated by Poulos & Davis (1980), is the difficulty in determining the correct soil modulus. Nevertheless, many researchers have investigated the incorporation of a changing soil modulus to consider yielding of soil when using this approach.

Similar to the subgrade reaction analysis (see **Figure 2-27**), the elastic analysis approach simplifies the pile as a thin rectangular strip with width corresponding to the diameter of the pile, flexural rigidity, E_pI_p, the same as that of the pile and length corresponding to the embedment depth of the pile. It is also assumed that the material of the pile is homogeneous, isotropic and elastic-perfectly plastic.

The following assumptions are typically made regarding the distribution of stresses and properties of the soil:

- The horizontal stress distribution on the strip is constant over the width.
- The soil is assumed to be a semi-infinite material that is homogeneous, isotropic and elastic-perfectly plastic.

- The soil has a uniform modulus of elasticity, E_s, and Poisson's ratio, υ_s under elastic conditions.
- Soil at the back of the pile, near the surface, adheres to the pile.

However, varying E_s with depth along the pile can also be incorporated in the analysis. It is also important to mention that it is not strictly true that the soil sticks to the back of the pile, as shown by **Figure 2-29**. As mentioned in Section 2.5.1, near the surface, the soil in front of the pile moves in an upward direction (wedge), whereas the soil located behind the pile moves downward and fill the void created by the lateral deflection of the pile, forming a gap.

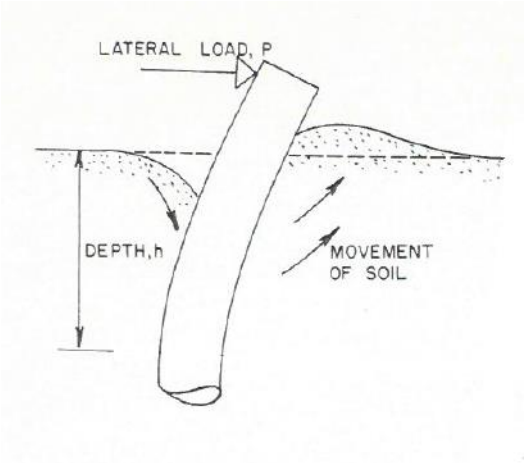

Figure 2-29: Soil movement at surface due to lateral loading (adapted from Broms, 1964b)

With the elastic analysis approach, the concept of relative stiffness of a soil-pile system came about. Although not accurate, due to the behaviour of soil being highly nonlinear, this concept gives a good indication in predicting the typical behaviour of a soil-pile system at low loads, where soil is still within its elastic state.

The behaviour of any soil-structure interaction problems in civil engineering can typically be predicted by considering the concept of relative stiffness. The relative stiffness is usually defined as the stiffness and properties of the structure, relative to the stiffness and properties of the soil, and it is generally applicable when a purely elastic analysis is used. Westergaard (1926) indicated that the behaviour of slab on subgrade can be predicted by considering the radius of relative stiffness, which is a function of the modulus of elasticity, poisons ratio and thickness of the slab, as well as the stiffness modulus of the subgrade. For pipelines subjected to tunnelling, Klar *et al.* (2005) showed that a pipe-soil system can be described as flexible or rigid, depending on its relative rigidity. They defined that the relative rigidity is a function of the pipe bending stiffness, the Young's modulus of the soil, radius of the pipeline, as well as the inflection point of the greenfield soil settlement curve.

With regard to pile foundations, Poulos & Davis (1980) indicated that the behaviour of a pile foundation can also be predicted by the relative stiffness concept, referred to as the pile-flexibility factor, as indicated by **Equation 2-6**:

$$K_R = \frac{E_p I_p}{E_s L^4} \qquad \textbf{Equation 2-6}$$

where,

$E_p I_p$ = flexural stiffness of the pile [M L^3 T^{-2}]

E_s = Young's modulus of the soil [M L^{-1} T^{-2}]

L = embedment length of the pile (below the soil surface) [L]

They showed that K_R is a dimensionless measure of the flexibility of the pile relative to that of the soil, predicting the behaviour of the soil-pile system. K_R has limiting values of ∞ for an infinitely rigid (short) pile and zero for an infinitely long pile, with the differences between a short and long pile mentioned in Section 2.5.1. Poulos (1982) indicated that a pile can be considered stiff if $K_R > 0.1$, whereas a $K_R < 10^{-5}$ is considered to be flexible. As soil is a non-linear material, K_R is usually derived using the secant values of E_s, but should however still be regarded as an approximate, as the theory is based on a purely linear elastic analysis.

The concept of relative stiffness of the soil-pile system is also not unknown to structural engineers. According to the BS EN 1992-1-1:2004+A1:2014, when designing soil-structure interaction of pile foundations the same equation is used, as indicated by Poulos & Davis (1980), to determine the rigidity of the structural system. Typically, a relative stiffness higher than 0.5 is indicative of a rigid structural system.

Later, based on more recent research, Poulos & Hull (1989) indicated that the difference between flexible and rigid piles can also be calculated by looking at the critical length (L_c) of the pile and comparing it to the embedment length (L) of the pile. They calculated the critical length by using **Equation 2-7**:

$$L_c = 4.44 \left(\frac{E_p I_p}{E_s}\right)^{\frac{1}{4}} \qquad \textbf{Equation 2-7}$$

They indicated that if $L > L_c$, the pile is considered to be flexible, whereas if $L < L_c$ the pile is considered to be rigid.

Based on the literature regarding the densification of the sand surrounding the pile due to cyclic loading, it is interesting to consider the effect it might have on the overall behaviour and response of the soil-pile system. An increase in the stiffness of the soil would reduce the pile flexibility factor, resulting in the behaviour of a pile to possibly change from a short pile to a long pile. A similar argument could also be raised with respect to the change in the flexural rigidity of a reinforced concrete pile after cracking, and how this might affect the outcome of the soil-pile response.

Comparisons between the elastic and subgrade reaction approaches have shown that they are in reasonable agreement with each other for stiffer piles, while the subgrade reaction approach overestimates the bending moments for flexible piles as indicated in **Figure 2-30**, and underestimates the bending moments for fixed-headed rigid piles. It should be noted that this behaviour was observed for a ratio between the embedment length of the pile (L) and the diameter of the pile (d) of 25 and might have been different for other length-diameter ratios.

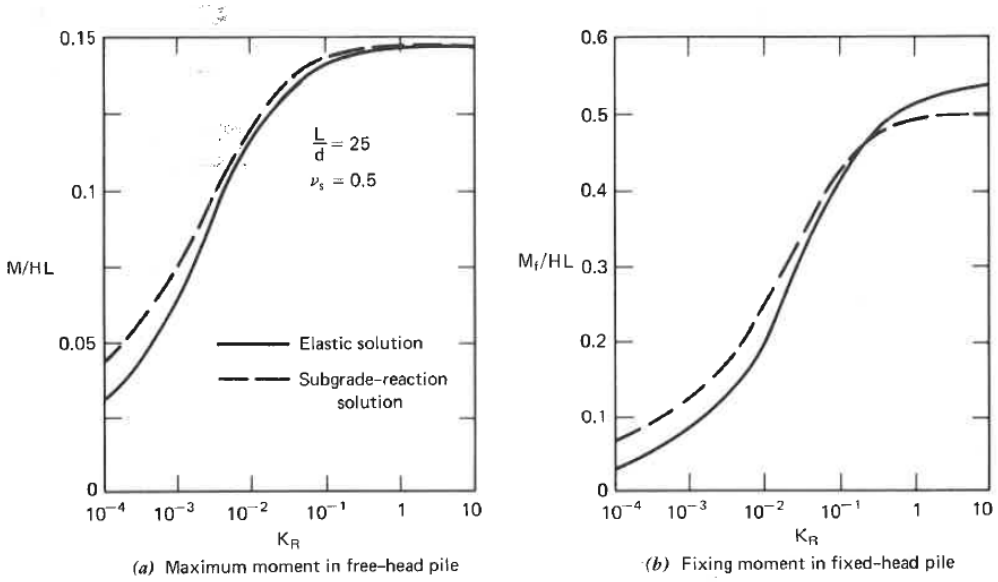

Figure 2-30: Comparison of elastic and subgrade reaction solutions for moment, constant E_s (Poulos & Davis, 1980)

2.5.4 Non-linear soil analysis

Due to the nature of soil, the relationship between the lateral deflection of the soil (or pile) and the corresponding soil reaction is nonlinear. To account for these effects, a number of nonlinear soil models have been developed and implemented over recent years by many researchers, allowing for the degradation of soil stiffness with increased strain and displacement experienced by the soil. The most commonly referred to procedure, as proposed by McClelland

& Focht (1958), based on the concept of *p-y* curves, is still widely used for designing pile foundations, mainly due to its simplicity. As indicated earlier, *p* refers to the soil lateral reaction (usually in force per unit length), where the *y* refers to the soil lateral displacement or pile deflection at a point of interest along the length of the pile. The concept of *p-y* curves can be explained by considering **Figure 2-31**, where a cylindrical pile has been subjected to a lateral deflection (y_i) caused by a laterally applied load. Before the load is applied, the unit stress distribution from the soil surrounding the pile is considered to be uniform, with the stresses being normal to the surface of the pile. However, when the pile is subjected to a lateral load, deflection of the pile occurs, resulting in the stresses decreasing on the back side of the pile and increase on the front side of the pile (in the direction of pile movement). Integration of these unit stresses results in the lateral soil resistance, p_i, acting in the opposite direction than y_i.

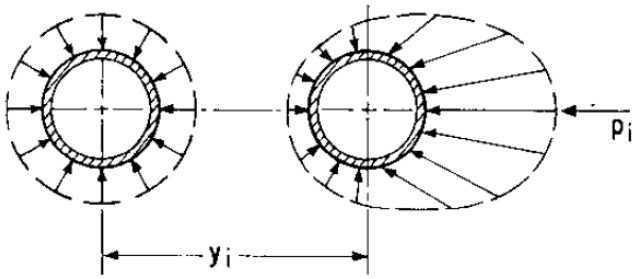

Figure 2-31: Concept of *p-y* curves (Reese *et al.*, 1974)

The interaction between the pile and the surrounding soil is difficult to quantify, as the deflection of a pile at any point below the soil surface depends on the soil response, and the soil response, in turn, depends on the deflection of the pile. The *p-y* curve represents the total soil resistance at a particular depth as a function of the lateral displacement of a horizontally loaded pile and this correlation is typically expressed by tangent hyperbolic functions (O'Neill & Murchison, 1983; Pinto *et al.*, 1999).

The load transfer curves can be generated taking into account the non-linear behaviour of the soil, by specifying the soil type, strength and deformability properties, as well as the geometry of the pile and loading conditions. It is assumed that the properties of the pile remain constant. Similar to the subgrade reaction method, mentioned previously, the principles of the *p-y* curve approach also uses the beam theory equation, as indicated by **Equation 2-3**, representing the soil as a series of unconnected springs. However, this equation can be written in a more generalized form by incorporating variation in pile stiffness and soil stiffness along the length of the pile (see **Equation 2-8**), while neglecting the effects of axial loading.

$$E_p I_p \frac{d^4 y}{dz^4} + E_s y = 0 \qquad \textbf{Equation 2-8}$$

where,

y = lateral deflection of the pile [L]

$E_p I_p$ = flexural stiffness of the pile [M L^3 T^{-2}]

z = depth along the length of the pile [L]

E_s = Young's modulus of the soil [M L^{-1} T^{-2}]

As with the subgrade reaction approach, the nonlinear analysis (*p*-*y* curve analysis) approach also models the behaviour of the soil at a depth to be independent from the behaviour at other locations (series of springs), with the soil pressure uniformly distributed over the width of the pile (see **Figure 2-27**), disregarding the side shear and front pressures mentioned previously. Reese (1977) indicated that, even though this assumption is not correct, it is sufficient for practical purposes.

As seen in **Equation 2-8**, a secant modulus is required to obtain a solution to the finite difference equation. This value typically varies with depth below the soil surface, becoming larger towards the bottom for the pile, as indicated by **Figure 2-32**.

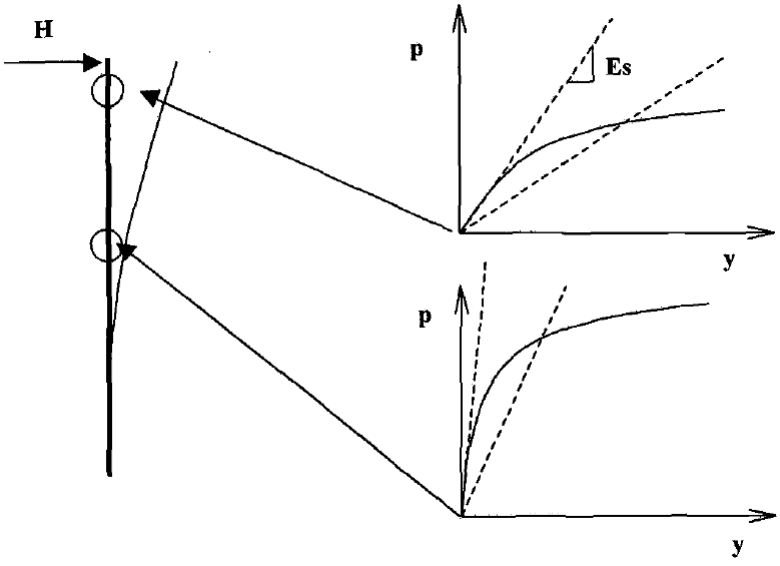

Figure 2-32: Evolution of secant modulus with depth (Pinto *et al.*, 1999)

Reese & Matlock (1956) indicated that for a uniform sands, the initial stiffness of the *p-y* curve, represented by slope of the *p-y* curve, as shown in **Figure 2-32,** increases linear with depth, and is expressed by **Equation 2-9**, as mentioned previously.

$$E_s = k_h z$$ **Equation 2-9**

where,

k_h = modulus of subgrade reaction (similar to the subgrade reaction approach) [M L^{-2} T^{-2}]

z = depth along the length of the pile [L]

However, to account for the non-linear behaviour of soil, Matlock & Reese (1961) argued that the response of the soil-pile system can be determined through an iterative process, changing the variation of E_s with depth in accordance with the calculated deflection. As the pile is loaded and deformation of the pile and the surrounding soil occurs, the secant modulus of the *p-y* curve would no longer have a linear variation (changing stiffness) with depth. **Figure 2-33** indicates the non-linear idealisation of soil springs, each having a stiffness that is related to the soil modulus. These values for the soil moduli are calculated from the *p-y* curves at various levels below the soil surface as indicated by Reese *et al.* (1974) and Smith (1987), with the values primarily influenced by critical depth effects (depth below the soil surface), load level, as well as the pile deflection profile.

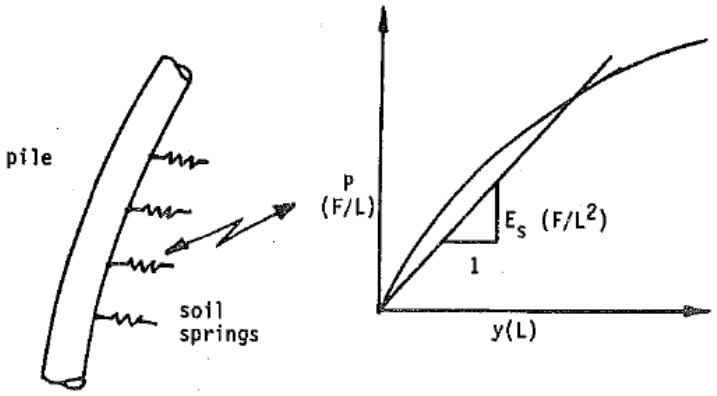

Figure 2-33: Nonlinear idealisation of a soil spring (Smith, 1987)

Procedures for constructing these *p-y* curves had been developed for different kinds of soils, such as clays (Reese & Welch, 1975; Reese *et al.*, 1975) and sands (Reese *et al.*, 1974), for both short-term static and long-term cyclic lateral loading. These procedures were based on experiments conducted on well-instrumented full-scale steel piles carried out in the presence of

free water (submerged), assuming the properties of the pile will remain unchanged. A number of modifications had been proposed by many researchers (Scott, 1980; Bogard & Matlock, 1980; O'Neill & Murchison, 1983). The dissertation only focused on the application of the procedures proposed by Reese *et al.* (1974) for sands.

For the nonlinear analysis, as indicated by Reese *et al.* (1974), at small movements, the stress-strain relationship of the soil is required. However, as the movements become larger, the use of soil parameters at ultimate failure is required, such as φ, where φ is the friction angle of the soil. The equation used to produce the *p-y* curves for sand is as indicated in **Equation 2-10**:

$$K_a = tan^2\,(45° - \frac{\varphi'}{2}) \qquad \textbf{Equation 2-10}$$

where,

K_a = active earth pressure coefficient [-]

K_0 = earth pressure at rest coefficient (= 0.4) [-]

α = $\varphi'/2$ [˚]

β = 45˚ + $\varphi'/2$ [˚]

Reese *et al.* (1974) suggested that the initial k_h-values, as listed in **Table 2-3**, should be used for the soil, depending on the relative density for dry, moist and submerged sands. Murchison & O'Neill (1984) recommended that k_h should be corrected based on the relative density of the soil, as indicated by **Figure 2-34**.

Table 2-3: Values of k_h for sands (Reese *et al.*, 1974)

Relative density	Loose	Medium	Dense
k_h, dry or moist sand (MN/m^3)	6.8	24.4	61.0
k_h, submerged sand (MN/m^3)	5.4	16.3	33.9

The ultimate resistance of the soil can be calculated using **Equation 2-11** and **Equation 2-12**, taking the minimum of the values obtained. This value is then used, along with factors incorporating static or cyclic loading, to compose a series of *p-y* curves at various depths below the soil surface, as indicated in **Figure 2-35**. p_m is a certain percentage of p_u, while y_m and y_u are ratios of the pile diameter. It should also be pointed out the diameter of the pile is referred to as b in **Equation 2-11**, **Equation 2-12** and **Figure 2-35**.

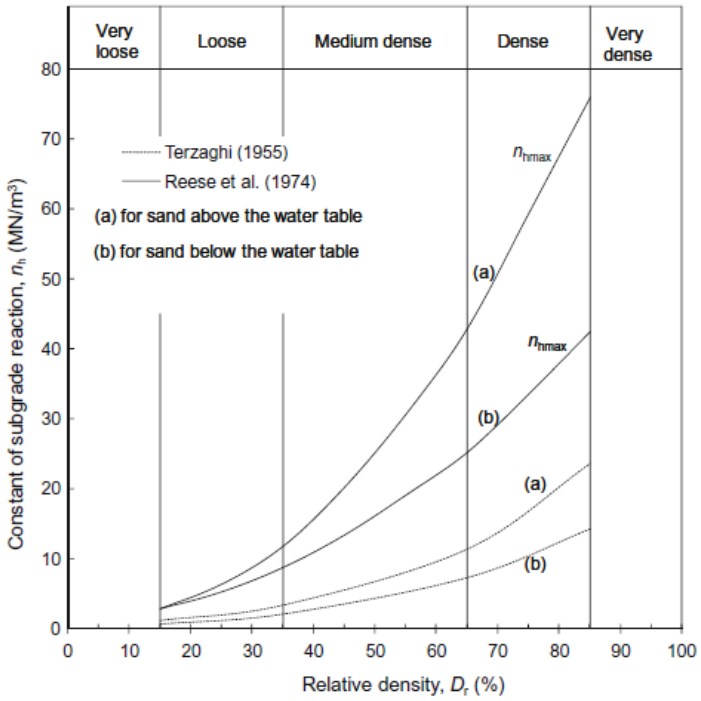

Figure 2-34: Coefficient of subgrade reaction, n_h versus relative density, D_r (Zhang, 2009, adapted from Murchison & O'Neill, 1984)

Lastly, the coordinate point (y_k, p_k) is determined from an empirical relationship involving y_m, y_u, p_m and p_u. X_1 to X_4 refers to the different depths below the soil surface, with X_1 typically being the closest to the soil surface and X_4 near, if not at, the bottom of the pile.

$$p_{ct} = \gamma H_z \left[\frac{K_0 H_z \tan\varphi' \sin\beta}{\tan(\beta-\varphi')\cos\alpha} + \frac{\tan\beta}{\tan(\beta-\varphi')}(b + H_z \tan\beta \tan\alpha) + K_0 H_z \tan\beta (\tan\varphi' \sin\beta - \tan\alpha) - K_a b\right] \quad \textbf{Equation 2-11}$$

$$p_{cd} = K_a b \gamma H_z (\tan^8\beta - 1) + K_0 b \gamma H_z \tan\varphi' \tan^4\beta \quad \textbf{Equation 2-12}$$

where,

γ = unit weight of the soil [M L^{-2} T^{-2}]

b = diameter of the pile [L]

H_z = depth factor, depending on the ratio between the depth below the soil surface and the diameter of the pile (z/b) [-]

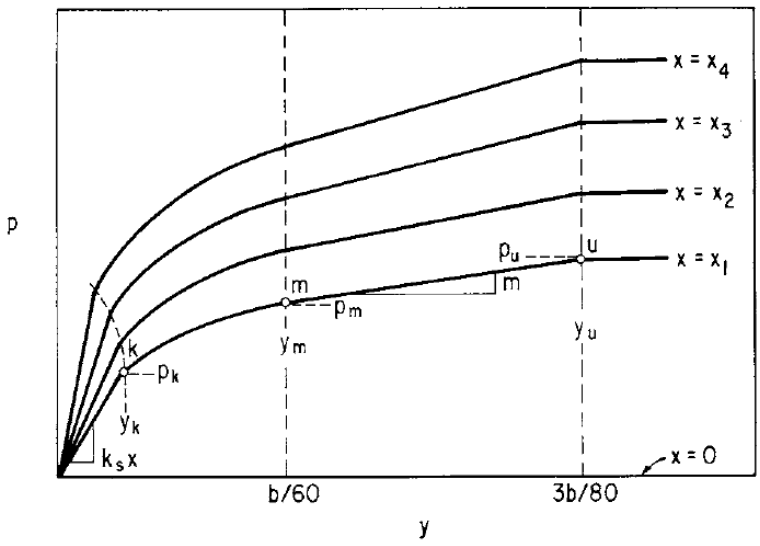

Figure 2-35: Typical proposed *p-y* curves (Reese *et al.*, 1974)

Limitations and assumptions for the nonlinear analysis method in sands, as indicated by Reese *et al*. (1974), were as follows:

- The soil was assumed to be a cohesionless sand.
- The pile was assumed to have been driven, resulting in the sand to be densified, rather than loosened during installation.
- The procedure assumed the pile to be essentially vertical.

From these solutions for the deflections with depth, the corresponding soil reaction, shear force and bending moment along the length of the pile can be determined.

The main advantage of this analysis method is the ability to simulate the non-linearity and non-homogeneity of the soil surrounding the pile. One of the major disadvantages of this method, however, is that the continuous nature of the soil is ignored. Software programs, such as COM622 (Reese, 1977), COM624 (Reese *et al.*, 1984) and LPILE (Reese, 1985) have been developed to incorporate these aspects into pile design and predicting behaviour based on the nonlinear effects of soil.

Duncan *et al.* (1994) indicated that the use of this non-linear analysis had proven to be in good agreement with field measurements. They also indicated that two factors contribute to the non-linear response of a pile subjected to lateral loads:

- The load-deflection behaviour of the soil around the pile is non-linear. As the load transferred from the pile to the soil increases by a fraction of its value, the deflection increases by a greater fraction, as indicated by the tangent hyperbolic function. The

behaviour of the soil-pile system remains non-linear even if the behaviour of the pile continues to be linear.

- As the strength of the soil around the top part of the pile becomes mobilised, additional loads must be transferred to greater depths, to areas where the strength of the soil has not yet been mobilised. To transfer the loads to greater depths, the pile, in effect, must span a greater distance, resulting in the moments increasing in the top of the pile, as was mentioned by Verdure *et al.* (2003) earlier.

Furthermore, Georgiadis *et al.* (1992) plotted the pile bending moment diagram with depth and compared it to the methods typically used to predict the behaviour of piles subjected to lateral loads, as indicated by **Figure 2-36**. Both the methods proposed by Reese *et al.* (1974) and Murchison & O'Neill (1984) underestimated the bending behaviour of the pile. They indicated that these differences are partly due to the higher initial stiffnesses recommended for these methods. This differences could be seen when considering **Figure 2-37**, where they plotted the lateral load as a function of the pile head displacement (*p-y* curves).

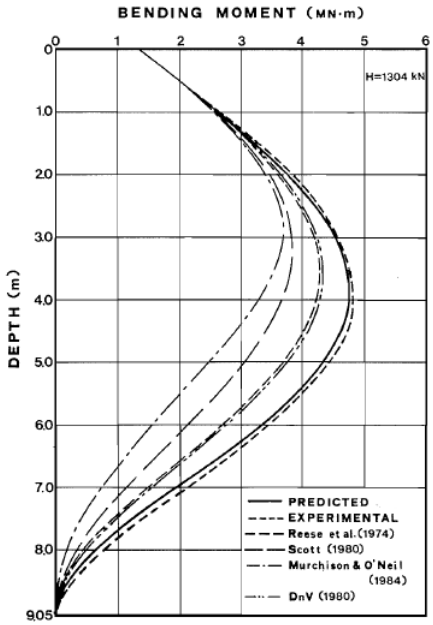

Figure 2-36: Comparison between predicted and measured bending moment distributions (adapted from Georgiadis *et al.*, 1992)

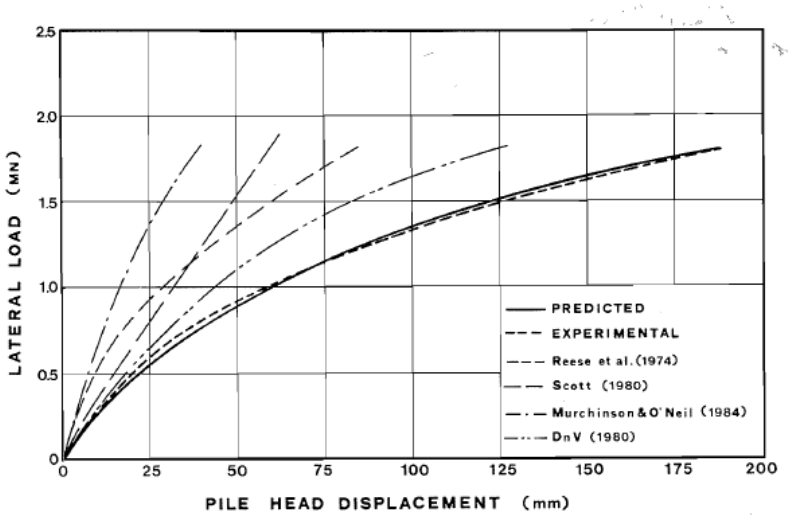

Figure 2-37: Comparison between predicted and measured *p-y* curves (adapted from Georgiadis *et al.*, 1992)

2.6 INTERPRETATION METHODS FOR DETERMINING PILE BEHAVIOUR

As mentioned previously, a conventional method to derive the *p-y* curves from a fully instrumented test pile is through the use of mathematical functions, usually an n^{th} order polynomial or spline, fitted through the measured bending moment or curvature data points (Georgiadis *et al.*, 1992; Yan & Byrne, 1992; Pinto *et al.*, 1999; Dyson & Randolph, 2001; Verdure *et al.*, 2003; Tak Kim *et al.*, 2004; Nip & Ng, 2005; Zhu *et al.*, 2016). By fitting the bending moment-curvature function, based on the strain gauge data, the deflected profile can be obtained by back-calculation using double integration with respect to depth as indicated by **Equation 2-13**:

$$y = \int (\int \frac{M}{EI}\, dz)\, dz \qquad \textbf{Equation 2-13}$$

The first and second derivative of the fitted moment-curvature function can then be used to derive the shear force and soil reaction profiles, respectively (**Equation 2-14** and **Equation 2-15**). The relationship between the derived soil reaction, shear force, deflection and the bending moment data can be expressed as indicated in **Figure 2-38**.

$$Q = \frac{dM}{dz} \qquad \textbf{Equation 2-14}$$

$$p = \frac{d^2M}{dz^2} \qquad \textbf{Equation 2-15}$$

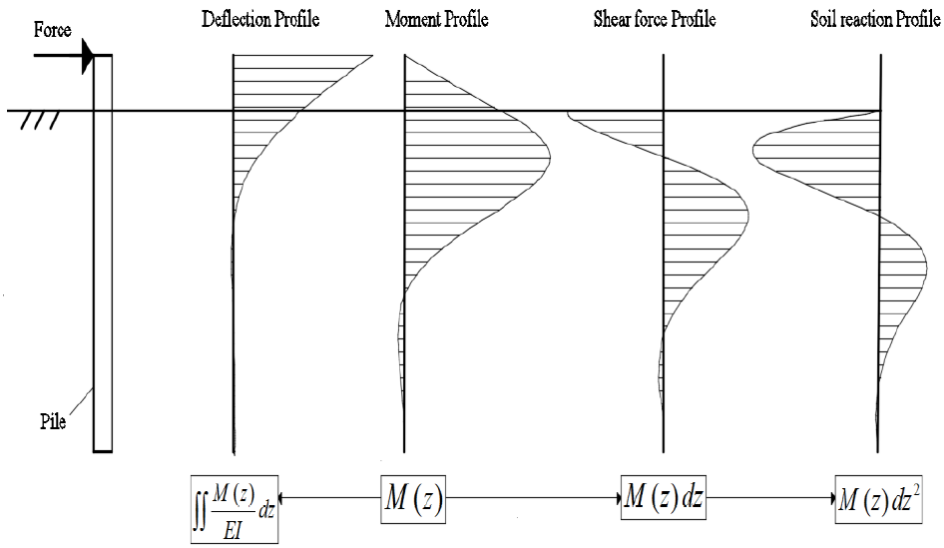

Figure 2-38: Pile lateral response from mathematically fitted curves (EI Naggar & Heidari, 2018)

As indicated by many researchers, direct differentiation of the moment profile could however lead to the amplification of measurement errors, resulting in inaccurate shear force and soil reaction profiles. Thus, the quality of the fitted curve through the measured data points drastically influences the behaviour (Verdure *et al.*, 2003).

Verdure *et al.* (2003) and Zhu *et al.* (2016) fitted a 7th order polynomial through the bending moment data obtained from their centrifuge tests. Tak Kim *et al.* (2004) proposed the use of a 4th order polynomial. Lastly, Georgiadis *et al.* (1992), Yan & Byrne (1992) and Dyson & Randolph (2001) fitted 4th order splines and cubic splines through their bending moment data points, respectively, and found it to be in good agreement with the experimental curves obtained from their tests, as indicated by **Figure 2-39** from Dyson & Randolph (2001).

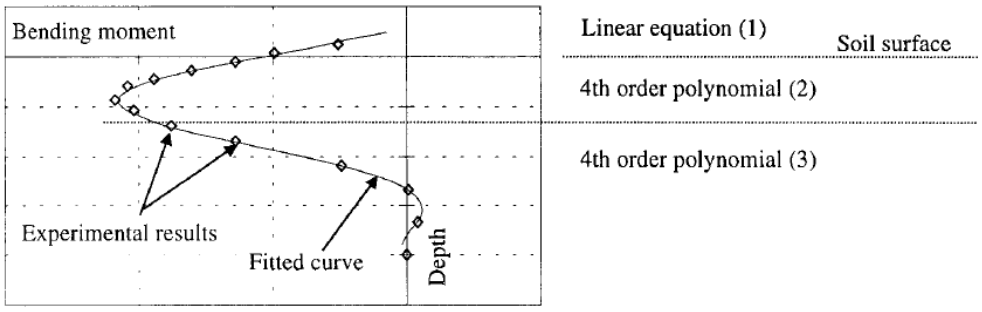

Figure 2-39: Equations fitted through the bending moment data points (Dyson & Randolph, 2001)

Uncertainty still exists around the accuracy of these interpolation functions. Yuan *et al.* (2016) conducted an evaluation on four data interpolation methods and compared it to the values obtained from LPILE, the software used for predicting the non-linear response of laterally loaded piles, as indicated previously. Bending moment curves were fitted through data using four interpolation methods, followed by a process of differentiation and integration to get the corresponding soil reaction and deflection, respectively, to construct the corresponding *p-y* curves. The following four interpolation methods were proposed and investigate:

- Polynomial interpolation method (PIM)
- Moving cubic polynomial curve-fitting method (MCP)
- Difference method (DM)
- Cubic spline (CSM)

Yuan *et al*. (2016) concluded the following for each of the interpolation methods:

- The PIM method yielded unreasonable soil resistance versus depth curves. They indicated that this method is limited in application because the bending moment function must satisfy several constraints and is only reliable for a large number of data points.
- The MCP method is a local curve-fitting technique, which avoids the global trend of scattered data. The results obtained from this method was in reasonable agreement with the values obtained from LPILE. The method resulted in smaller errors but becomes complex with a larger number of data points.
- The soil resistance calculated from the DM method closely approximated the "true" soil response, yielding the smallest sum of error squares (SSE_{norm}) value overall (see **Figure 2-40**). However, the soil resistance calculated at the soil surface was very large.

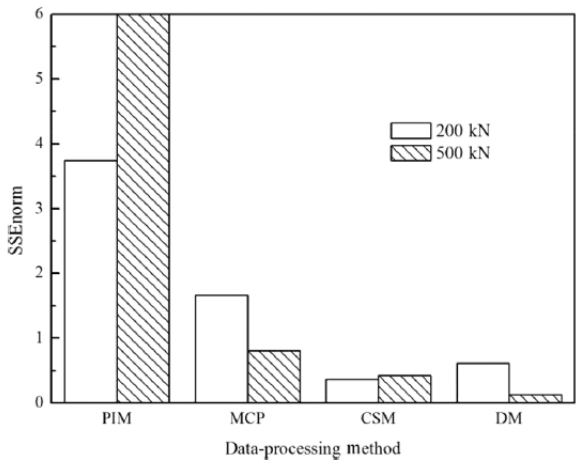

Figure 2-40: SSE_{norm} values for the different interpolation functions (Yuan *et al.*, 2016)

- Lastly, the CSM method resulted in the smallest difference between the calculated curves and the "true" *p-y* soil response. It yielded the second smallest SSE_{norm} (see **Figure 2-40**). They indicated that CSM is considered to be the most effective method for describing *p-y* curves in layered soils.

2.7 NON-LINEAR BEHAVIOUR AND FATIGUE LIFE OF CONCRETE

The response of laterally loaded pile foundations is a complex soil-structure interaction problem. Lin & Liao (2006) indicated that, in the case of concrete piles, the problem becomes more difficult due to the non-linear behaviour of concrete. Failure of the soil-pile system, using steel piles, typically occurs as a result of the soil failing and not the pile yielding, which is not the case with concrete, where the pile would crack before the soil fails. This phenomenon is generally overlooked and neglected.

Duncan *et al.* (1994) and Long & Vanneste (1994) mentioned that, especially in the case of reinforced concrete piles, the flexural stiffness should be reduced when tensile stresses in the piles exceeded the tensile capacity of the concrete. They indicated that the moment of inertia of a cracked concrete section can reduce to about 40-50% of the full uncracked section. Furthermore, Pinto *et al.* (1999) and Nip & Ng (2005) indicated that it is crucial to characterise the non-linear behaviour of a concrete pile. They indicated that as the curvature (bending moment) of the pile increases, past the cracking moment, there is a reduction in the flexural rigidity of the pile section, as seen in **Figure 2-41**, which is expected from all reinforced concrete members after cracking.

Ashour & Norris (2000) and Lin & Liao (2006) also indicated that depending on whether the concrete section is cracked or uncracked, the appropriate moment of inertia should be used for the section, seeing that the moment of inertia reduces as the pile cracks.

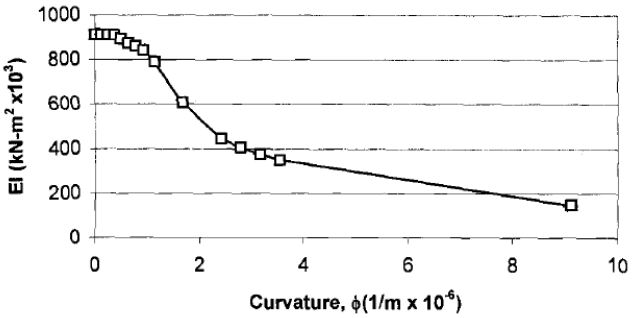

Figure 2-41: Graphical representation of non-linear variation of flexural rigidity with curvature (Pinto *et al.*, 1999)

Lin & Liao (2006) conducted a full-scale lateral load test on a single bored and single precast concrete pile during a High-Speed Rail Project in Taiwan. As seen in **Figure 2-42** and **Figure 2-43**, by plotting the lateral load versus pile head deflection for the bored and precast pile respectively, assuming that the flexural rigidity (E_pI_p) of a pile foundation remained constant with an increase in load, the capacity of the pile is overestimated. The flexural rigidity of concrete piles reduced with the increased load, resulting in larger deflections at lower lateral loads, as indicated.

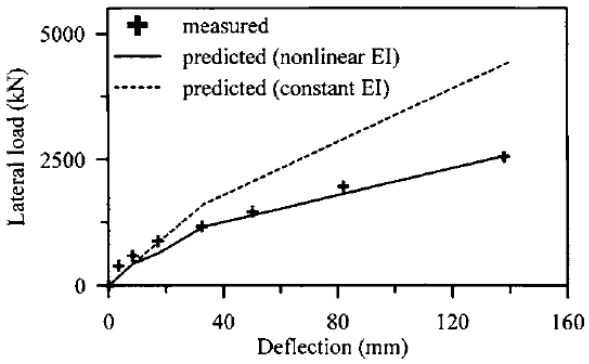

Figure 2-42: Lateral load versus pile head deflection - single bored pile (Lin & Liao, 2006)

Apart from the non-linear behaviour of concrete caused by exceeding its tensile capacity, concrete subjected to cyclic loading has a significant trend that should be considered and explained that also can lead to its non-linear behaviour. This is different from steel, largely due to the nonhomogeneous nature of concrete against the fairly homogenous nature of steel. Domone & Illston (2010) indicated that successive loading and unloading cycles of concrete, below the ultimate stress levels (tensile capacity), causes substantial, but diminishing hysteresis loops, as well as residual or permanent strains at zero load, as shown by **Figure 2-44**.

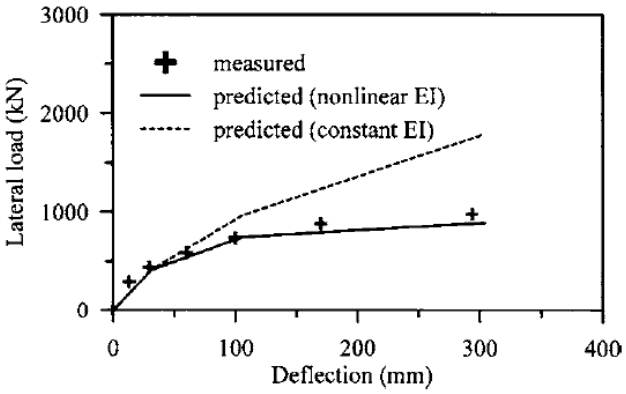

Figure 2-43: Lateral load versus pile head deflection - single precast pile (Lin & Liao, 2006)

They indicated that the behaviour can be explained by considering the contribution of microcracking to the overall concrete strain. Microcracks typically form at the transition zone between the aggregate and surrounding mortar, as this is a region of relative weakness, with the number and width of these depending on the properties of the concrete. Depending on the stress level, these cracks might increase in size and numbers, making a progressively increasing contribution to the strain that develops in the concrete, resulting in non-linear behaviour below its ultimate stress levels.

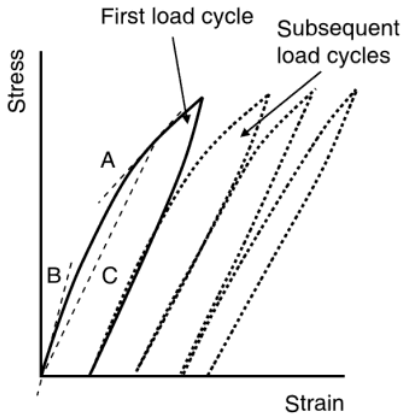

Figure 2-44: Behaviour of concrete under cyclic loading (Domone & Illston, 2010)

The successive loading and unloading cycles of a material up to failure, at any given stress state below the ultimate stress levels, is termed the fatigue life of that material and is typically defined by S/N curves which can be used to estimate the cumulative fatigue damage (Soutsos & Domone, 2018). The cumulative fatigue damage of the material is usually determined by applying Miner's rule. This rule states that the portion of the fatigue life that is used up by a number of successive stress cycles at a particular stress state is proportional to the total number of cycles in the fatigue life, for the only stress level applied to the material. This indicates that more load cycles are required at a lower stress state to cause fatigue failure, while fewer load cycles would cause failure at a higher stress. The fatigue life of a material is governed by the prior load history of the material. **Figure 2-45** indicates a typical S/N curve for plain concrete, presented by Lee & Barr (2004), based on results from other researchers. It can be seen that 10^5 load cycles at 70% stress level will cause fatigue failure of the concrete, in comparison to the 10^1 load cycles at 95% stress level. Cyclic horizontal loading of concrete piles could thus result in fatigue failure at loads significantly lower than the static failure load.

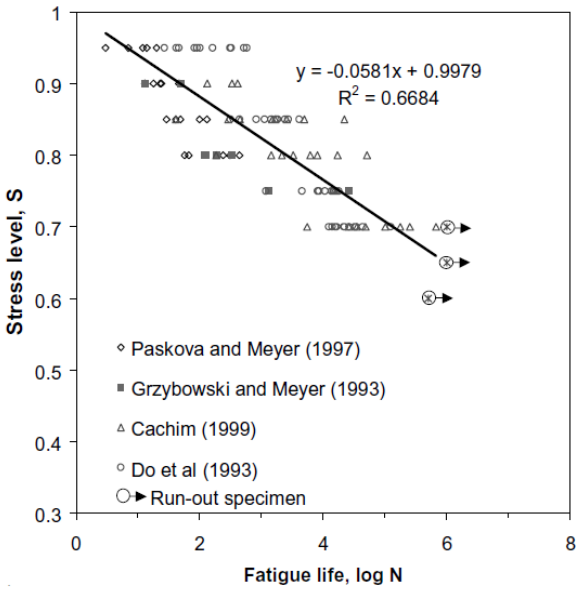

Figure 2-45: S/N curve for plain concrete (Lee & Barr, 2004)

2.8 SCALE AND SIZE EFFECTS OF REINFORCED CONCRETE MEMBERS

With regard to scaled modelling in the centrifuge, as mentioned previously, a number of factors have to be taken into account to ensure realistic behaviour is modelled and observed for the problem at hand. Madabhushi (2015) mentioned that, for centrifuge modelling, aluminium alloys are typically used to model structural components such as retaining walls and foundations, due to the ease of machining and fabricating elements. This was observed for all the research mentioned in the literature above. Madabhushi (2015) indicated that the axial and bending behaviour of structural components are normally captured, but not the failure mechanism, due to the difference in yield stress between the prototype material and the scale model material, for example, concrete members. Thus, the need arises to use appropriate materials to not only model the concept (axial and bending) but also to model the correct failure behaviour of the structural member to make it possible to study the correct soil-structure interaction problem. To do so, in the case of concrete members, both the stiffness, as well as the strength of the scaled concrete should be representative of that at prototype scale. However, the use of concrete as the scale model material, introduces a number of aspects that cannot be avoided and is more complex than the use of aluminium for modelling structural behaviour.

Noor & Boswell (1992) indicated that no particular problems are likely to occur for scaled reinforced concrete elements for a scale ratio of up to 1:4. They also mentioned that for technical reasons, it becomes necessary to reduce the scale of the concrete even more, possibly up to 1:8, by using fine-grained concrete and small diameter reinforcing bars without producing size effects, ensuring that the bond between the concrete and the reinforcing bars is reproduced

at model scale. However, Knappett *et al.* (2011) mentioned that geotechnical models in a centrifuge typically necessitates large scale factors between 1:20 and 1:100, which is significantly larger than the conventional small-scale structural modelling mentioned previously.

Research has been conducted into the choice of suitable model materials. Noor & Boswell (1992) mentioned that the use of fine-aggregate mortars as concrete and steel wires as reinforcing has proven to produce reinforced concrete characteristics. They indicated that the following requirements should be considered:

- Geometric similitude is essential.
- The stress-strain curves for the model and prototype materials should be similar both in tension and compression.
- The strains in the model and prototype at failure should be identical.

Noor & Boswell (1992) indicated that the size effects should also be considered. They indicated that size effects could occur for all scales when the smallest model dimension were of the same magnitude as the largest aggregate. This is contrary to the fundamental principles of mechanics of similarity which demand that the material structure must always be small in comparison to the smallest model dimension. Thus, Noor & Boswell (1992) mentioned that, in the case of cement-based concrete models, the behaviour of thin members will be greatly influenced.

As mentioned, size effects have a significant influence on the physical properties of cement-based concrete (Sabnis *et al.*, 1983). Sabnis *et al*. (1983) observed a change in the nominal strength of the concrete with a change in specimen size, resulting in cracking and failure of the member to occur at slightly higher loads. Noor & Boswell (1992) mentioned that this is typically the behaviour for scaled concrete due to the heterogeneity of the material. Later, Knappett *et al.* (2011) also indicated that the significant overstrength that resulted from the reduced-scale model was due to the quasi-brittle nature of the concrete. They indicated that the strength of the reinforced concrete elements typically involves the fracture of the concrete, with the fracture being linked to the number and size of flaws within the concrete. Furthermore, they mentioned that these flaws were linked to the size of the aggregate. Thus, as the size of the aggregate was decreased, the number of flaws also decreased, resulting in an increase in strength.

Sabnis *et al.* (1983) indicated that variations in the strength of scaled concrete specimens of different sizes, but similar shape, could be as a result of one or more of the following factors:

- Density, compaction and loss of water

- Aggregate grading, curing and age
- Drying and water gain
- Stress and strain rates
- End conditions
- Testing machines

More recently, a number of researchers have investigated the use of small-scale reinforced concrete structural elements for the use in a geotechnical centrifuge (Knappett *et al.*, 2010; Knappett *et al.*, 2011; Knappett *et al.*, 2018). Knappett *et al.* (2011) developed a new model concrete consisting of plaster (Gypsum-based), water and fine sand, based on work conducted by Sabnis *et al.* (1983). Knappett *et al.* (2011) conducted a number of three- and four-point bending tests on a number of model beams containing different amounts of main reinforcing bars, with and without shear reinforcing. The beams without shear reinforcing showed the typical shear flexural failure, however, the ultimate shear capacities at prototype scale was underpredicted. The beams with shear reinforcing represented the equivalent full-scale section bending moments well, as indicated in **Figure 2-46**. However, failure mechanisms of beams under these loads were not necessarily representative of a flexural beam failure.

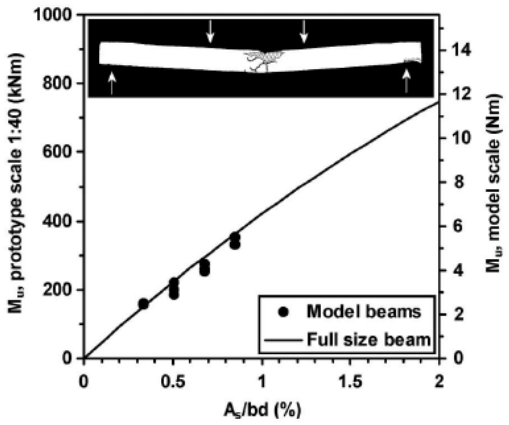

Figure 2-46: Ultimate moment capacity of model beams (Knappett *et al.*, 2011)

Sabnis *et al.* (1983) indicated that the use of a Gypsum-based mortar, as a substitute for cement-based mortar, had been considered by many researches due to two main advantages it has over cement-based mortar, as seen with Knappett *et al.* (2011). The first main advantage, as mentioned, is that cement-based concrete models tend to have an excessive tensile strength compared to the prototype concrete, which is not a problem with Gypsum-based mortars. Secondly, cement-based concrete requires a longer curing period to develop the appropriate strength level. On the other hand, Sabnis *et al.* (1983) mentioned that one of the main disadvantages of Gypsum-based mortars is the strong influence of moisture content of the

mechanical properties of the model concrete. Thus, care should be taken during curing procedures.

As indicated earlier, to accurately model concrete, both the strength and stiffness characteristics of the prototype concrete should match and be representative. Typically, model concrete constructed with only hardened concrete pastes (HCP), such as Gypsum-based mortars, does not include the use of aggregate in their composition. As can be seen from **Figure 2-47** the stiffness behaviour is low in comparison to that of concrete with the presence of aggregate. The inclusion of aggregate in the concrete matrix is thus important to accurately model the stiffness behaviour of the model concrete.

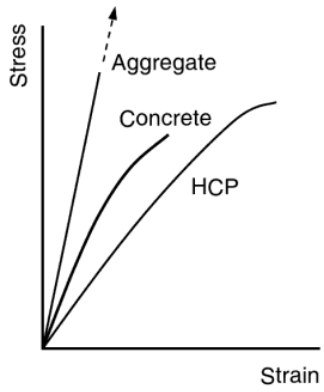

Figure 2-47: Behaviour of aggregate, concrete and HCP (Domone & Illston, 2010)

The effect of the percentage aggregates on the stiffness of the concrete can be seen in **Figure 2-48**. As the percentage aggregate increases, the stiffness of the concrete increases fairly linearly. Domone & Illston (2010) indicated that the volume concentration of aggregate for normal concrete mixes is in the ranges of between 50-80%.

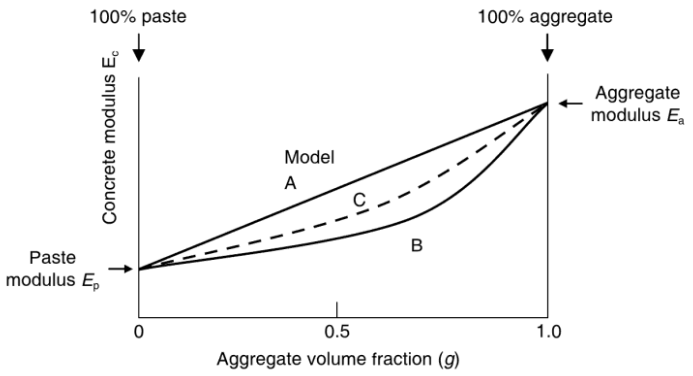

Figure 2-48: The effect of volume concentration of aggregate on the stiffness of concrete (Domone & Illston, 2010)

Limited research has been conducted on the use of cement-based model concrete for centrifuge application. Care should be taken when considering the use of only Gypsum-based mortars to model concrete. The strength of the concrete might be modelled accurately, however, due to the absence of aggregate, the stiffness will not be scaled appropriately. The aim of the research is to implement the use of conventional cement-based model concrete for the use in geotechnical centrifuge modelling of soil-structure interaction problems, using commercially available materials and technologies. This will add to current research and development in this field of study.

2.9 SUMMARY

Various aspects regarding piles subjected to both monotonic and cyclic loading were discussed, mainly focussing on pile and soil response and the factors governing their behaviour. Based on the observed bending moments, shear forces and soil reactions from a number of experiments on piles under both monotonic and cyclic lateral loading, it seemed that, for applied loads below about 10% of the ultimate capacity of the soil, the soil had a tendency to still respond within its linear region, with the bending moment, shear force and soil reaction increasing linearly with increase in applied load. Thus, due to the fact that the design of laterally loaded pile foundations is typically governed by the load-deflection response and not the ultimate capacity of the soil, the question is raised whether soil can be assumed to respond linearly or not at small loads.

Literature indicate that the interaction between the pile and the surrounding soil are largely influenced by both the stiffness and dimensional properties of the pile and the stiffness of the soil (relative flexibility factor). However, even though this factor is based on purely elastic conditions, changes in the properties of the soil occur (densification from repetitive loading), as well as the reduction of the flexural rigidity of piles (reinforced concrete piles after cracking). This might affect the response of the soil-pile system, as this factor continuously changes.

Characteristics regarding the use of centrifuge modelling for modelling this soil-pile interaction problem were also discussed, as well as the problems typically encountered with centrifuge modelling, which aided in the correct design of the models for testing. The literature review concluded with a discussion on the interpretation and interpolation of experimentally measured data for piles. Emphasis was also given to the non-linear behaviour of reinforced concrete and the effect thereof on the overall behaviour of concrete after cracking. This highlighted the importance of investigating the non-linear behaviour of concrete on the response of piles.

A number of aspects and properties observed in literature were considered in the designing of the experimental work and is discussed in Chapter 4. Some of the properties included the stiffness of the soil and pile as they are important properties contributing to pile response. The

subsequent chapters include a parametric study investigating the change in behaviour of the soil-pile system to changing pile and soil conditions based on the literature, followed by the experimental procedures and set-up.

3 PARAMETRIC STUDY (MULTI-VARIABLE ANALYSIS)

3.1 INTRODUCTION

As mentioned in the literature, the response of piles to lateral loads is a complex soil-structure interaction problem, that is influenced by both the properties of the soil, as well as the properties of the pile. Thus, to better understand the response of the soil-pile system, and to aid in the experimental design of the centrifuge tests, a parametric study was conducted to determine the influence of these properties on the soil-pile response. The parametric study was carried out by using the subgrade reaction approach, based on the principles of the Winkler model assuming that the soil remains linear, as well as the non-linear soil analysis approach, originally proposed by McClelland & Focht (1958) and modified by Reese *et al.* (1974) for sands. Both these procedures are discussed in Chapter 2.

Even though this dissertation is concerned with the physical modelling of laterally loaded piles, the parametric study was conducted on a full-scale reinforced concrete pile. Byrne & Berry (2008) indicated that the typical diameters of reinforced concrete piles range between 300 mm and 2000 mm depending on the problem to be addressed. For these analyses, a 600 mm diameter pile was chosen. Even though the diameter of the pile has an influence on the response of the soil-pile system, the main focus of the parametric study was on the relative stiffness between the pile and the surrounding soil, as this primarily governs the response. The diameter and second moment of area of the pile as well as the embedded length of 10 m were kept constant while the stiffness of the soil and the pile were varied.

Winterkorn & Fang (1975) suggested that, for a free-headed concrete pile with a diameter of 600 mm, the safe allowable lateral load is about 100 kN. For both the subgrade reaction approach and the non-linear soil analysis approach, the same monotonic lateral load of 100 kN was applied to the top of the pile, at the soil surface. A bending moment might also exist at the soil surface. This is due to eccentricity of the applied lateral load and is highly variable depending on the application for which the pile is used. Thus, for the principle of applying a bending moment at the soil surface, it was decided that the lateral load should act at an eccentricity of 1 m above the surface of the soil, resulting in a 100 kNm bending moment at the soil surface. The aim of the parametric study was to determine the changes in the response of the soil-pile system as a consequence of changing soil and pile properties. The magnitude of the applied load was kept constant at 100 kN, applied 1 m from the soil surface, and thus bending moment was not of importance.

3.2 SUBGRADE REACTION ANALYSIS

A finite-difference program was written in Microsoft Excel Visual Basic for Application (VBA). The program was based on the Winkler model, as discussed in the previous chapter using the beam equation, assuming that the soil comprises out of a series of unconnected linear-elastic springs. The stiffness of the springs is related to the coefficient of subgrade reaction, n_h, assuming that the coefficient varies linearly with depth (for sands). The appropriate boundary conditions for a free-headed pile was also taken into account in the program.

A multi-variable analysis was carried out to determine the relationship and response of the soil-pile system to variations in the properties of the pile and the properties of the soil surrounding the pile. **Table 3-1** indicates the properties of the pile and the soil that was used in the multi-variable analysis. For each of the pile stiffnesses shown the response of the pile was determined for all of the indicated coefficients of subgrade reaction. The response of the pile was observed in terms of the bending moment, shear force, soil reaction and lateral displacement. As mentioned, the pile had a diameter of 600 mm and an embedded length of 10 m that was kept constant during the analyses.

The coefficient of subgrade reaction, referred to as the soil stiffness for the rest of this chapter, was in accordance to the values proposed by Terzaghi (1955) for a loose, medium and dense sand. Values lower and higher than those proposed by Terzaghi (1955) were selected to consider extreme cases.

Table 3-1: Pile and soil properties – subgrade reaction analysis

Youngs's modulus of the pile, E_p (GPa)	**Coefficient of subgrade reaction, n_h (MN/m^3)**
10	1.0
25	2.2
50	6.6
100	17.6
150	25.0
200	50.0

Figure 3-1 and **Figure 3-2** indicates the bending moment, shear force, soil reaction and lateral pile displacement response of a pile, subjected to the same monotonic lateral load and moment at the soil surface, varying the properties of the pile and the surrounding soil, as indicated in **Table 3-1**. As mentioned previously, the magnitude of the lateral load and bending moment applied at the soil surface was not important, as the aim of the parametric study was to determine the response of the soil-pile system to changing soil and pile properties. Only the results for a pile Young's modulus of 25 GPa (concrete) and 200 GPa (steel), respectively, and coefficients of subgrade reaction (soil stiffness) of 2.2 MN/m^3 and 17.6 MN/m^3 are indicated

and discussed. The coefficient of subgrade reaction of 2.2 MN/m^3 and 17.6 MN/m^3 corresponds to a loose and dense sand, respectively (Terzaghi, 1955). The results of the full analysis conducted on all the combinations of pile and soil stiffnesses are presented in Appendix A. From **Figure 3-1** and **Figure 3-2**, the following main conclusions could be drawn in terms of the effect of the stiffness of the pile and the soil.

With regard to the pile stiffness:

- By increasing the stiffness of the pile, an increase in the bending moment occurred. Changes in the shapes of the shear force and soil reaction distributions were observed.
- The lateral displacement of the pile decreased with an increase in the stiffness of the pile, for both the soil stiffnesses.
- As the stiffness of the pile increased, the pile behaved as a short pile, with the effect being greater at a lower soil stiffness.
- The pile behaved as a long pile for lower pile stiffnesses, with the effect being greater for a higher soil stiffness.

With regard to the soil stiffness:

- By increasing the stiffness of the soil, the bending moment in the pile decreased. Changes in the shapes of the shear force and soil reaction distributions were also observed.
- The lateral displacement of the pile decreased with an increase in the stiffness of the soil, for both the pile stiffnesses.
- As the stiffness of the soil increased, the pile behaved as a long pile, with the effect being greater at a lower pile stiffness.
- The pile behaved as a short pile at lower soil stiffnesses, with the effect being greater for a higher pile stiffness.

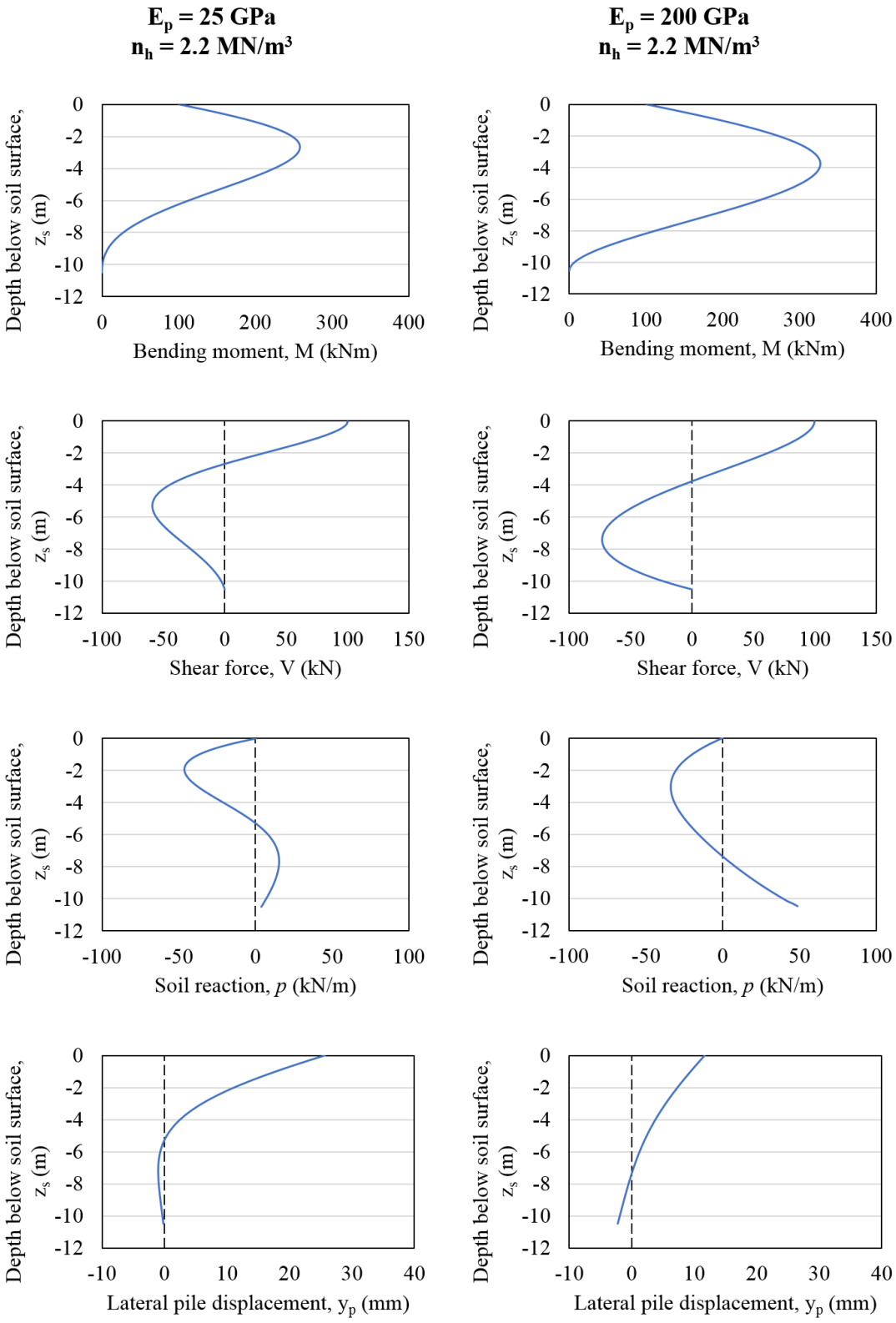

Figure 3-1: Soil-pile response (subgrade reaction analysis) - 2.2 MN/m³

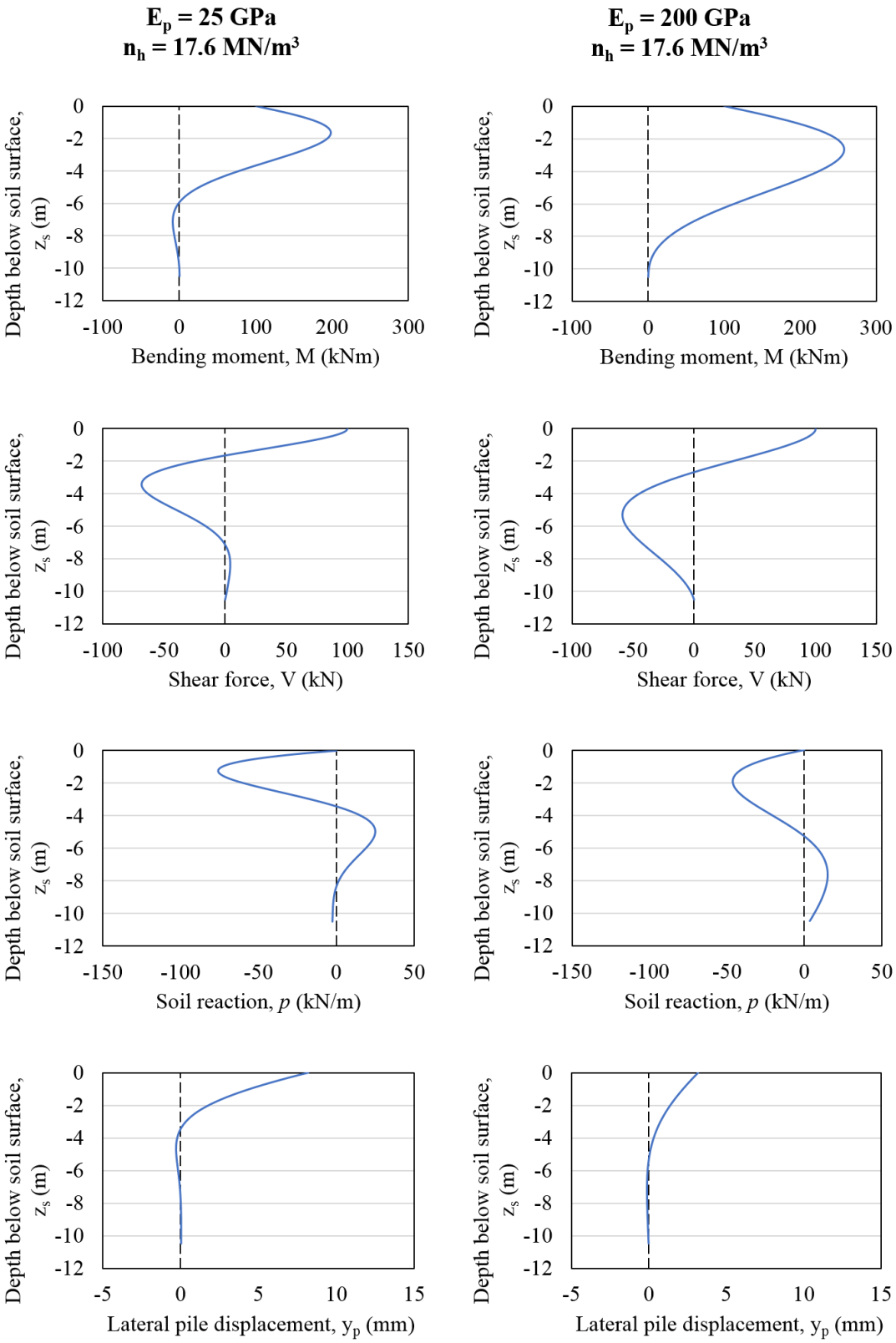

Figure 3-2: Soil-pile response (subgrade reaction analysis) - 17.6 MN/m³

3.3 NON-LINEAR SOIL ANALYSIS

Due to the fact that soil is a highly non-linear material, the analysis conducted on the full-scale pile using the subgrade reaction analysis was repeated to incorporate the non-linear effects of soils. The non-linear soil analysis was conducted using the LPILE student version program, originally developed by Reese (1985). The same procedure, in terms of varying the stiffness of both the pile and the soil, was followed for the non-linear soil analysis. The 600 mm diameter reinforced concrete pile was used, with an embedded depth of 10 m, a laterally applied load of 100 kN and a moment of 100 kNm to the top of the pile at the soil surface. Not all the variations in pile and soil stiffnesses were conducted using LPILE. Only those presented in the previous section were considered during this analysis as indicated in **Table 3-2**, with the stiffness of the soil corresponding to that of loose and dense sand according to Terzaghi (1955).

Table 3-2: Pile and soil properties – non-linear soil analysis

Young's modulus of the pile, E_p (GPa)	Coefficient of subgrade reaction, n_h (MN/m^3)
25	2.2
200	17.6

The LPILE program required the following parameters as input:

- Analysis type
- Pile properties
- Loading type
- Pile head boundary conditions and loading
- Soil layers and types

A basic modelling analysis was conducted on the LPILE software, computing the response of the pile using elastic pile stiffness, similarly to the subgrade reaction analysis. The only difference between the subgrade reaction analysis and this analysis was the non-linear behaviour of the soil that was included. Properties of the pile that had to be specified included, the length of the pile, number of increments in which the pile length should be subdivided, the diameter, cross-section, moment of inertia as well as the modulus of elasticity of the pile. LPILE also required that it should be specified whether static or cyclic loading is used. Static loading was selected for this analysis, as the pile was only loaded once, similar to the subgrade reaction analysis. A free headed pile was chosen for the boundary condition of the pile head, with a lateral load and bending moment applied to the top of the pile at the soil surface. Lastly, for the soil type, the *p-y* curve model proposed by Reese *et al.* (1974) was used. In addition to the coefficient of subgrade reaction, the non-linear analysis method and LPILE also required the

specification of a friction angle and unit weight of the soil. Winterkorn & Fang (1975) indicated that, based on Peck *et al.* (1974), the friction angle for loose and dense sand are as indicated in **Table 3-3**. Regarding the unit weight of the sand, Byrne & Berry (2008) indicated that the unit weight of loose and dense sand can be approximated as indicated in **Table 3-4**. These values were all used to accompany the respective coefficients of subgrade reaction and pile stiffnesses, mentioned previously, during each analysis.

Table 3-3: Friction angle for loose and dense sand (adapted from Winterkorn & Fang, 1975, from Peck *et al.*, 1974)

Type of soil	Friction angle (˚)
Loose sand	30
Dense sand	38

Table 3-4: Unit weight for loose and dense sand (Byrne & Berry, 2008)

Type of soil	Unit weight, γ (kN/m^3)
Loose sand	16
Dense sand	19

Figure 3-3 and **Figure 3-4** indicates the bending moment, shear force, soil reaction and lateral pile displacement response of a pile, subjected to the same lateral load and moment at the soil surface, varying the properties of the pile and the surrounding soil, as indicated by **Table 3-2**, **Table 3-3** and **Table 3-4** for the non-linear soil analysis. As mentioned previously, the magnitude of the lateral load and bending moment applied at the soil surface was not deemed to be important, as the aim of the parametric study was to determine the response of the soil-pile system to changing soil and pile properties. From **Figure 3-3** and **Figure 3-4** similar conclusions could be drawn with regard to the change in stiffness of the pile and the stiffness of the soil. It is worthwhile mentioning that no noticeable difference was observed between the graphs obtained from the non-linear soil analysis and the subgrade reaction analysis. This was due to the soil still mostly behaving within the elastic region, with the specified properties as used for the soil, the pile, and the magnitude of the applied loads. This raises the question of whether it can be assumed that the soil acts linearly, for piles under allowable lateral loads, as the design of laterally loaded piles is governed by the maximum allowable lateral displacement, rather than the ultimate capacity of the soil. Apart from the behaviour of the soil, the analyses were conducted assuming the flexural stiffness of the pile remained constant and was unaffected by the magnitude of the load. This is not strictly true in the case of the reinforced concrete pile which could crack, resulting in the flexural stiffness of the pile decreasing after cracking.

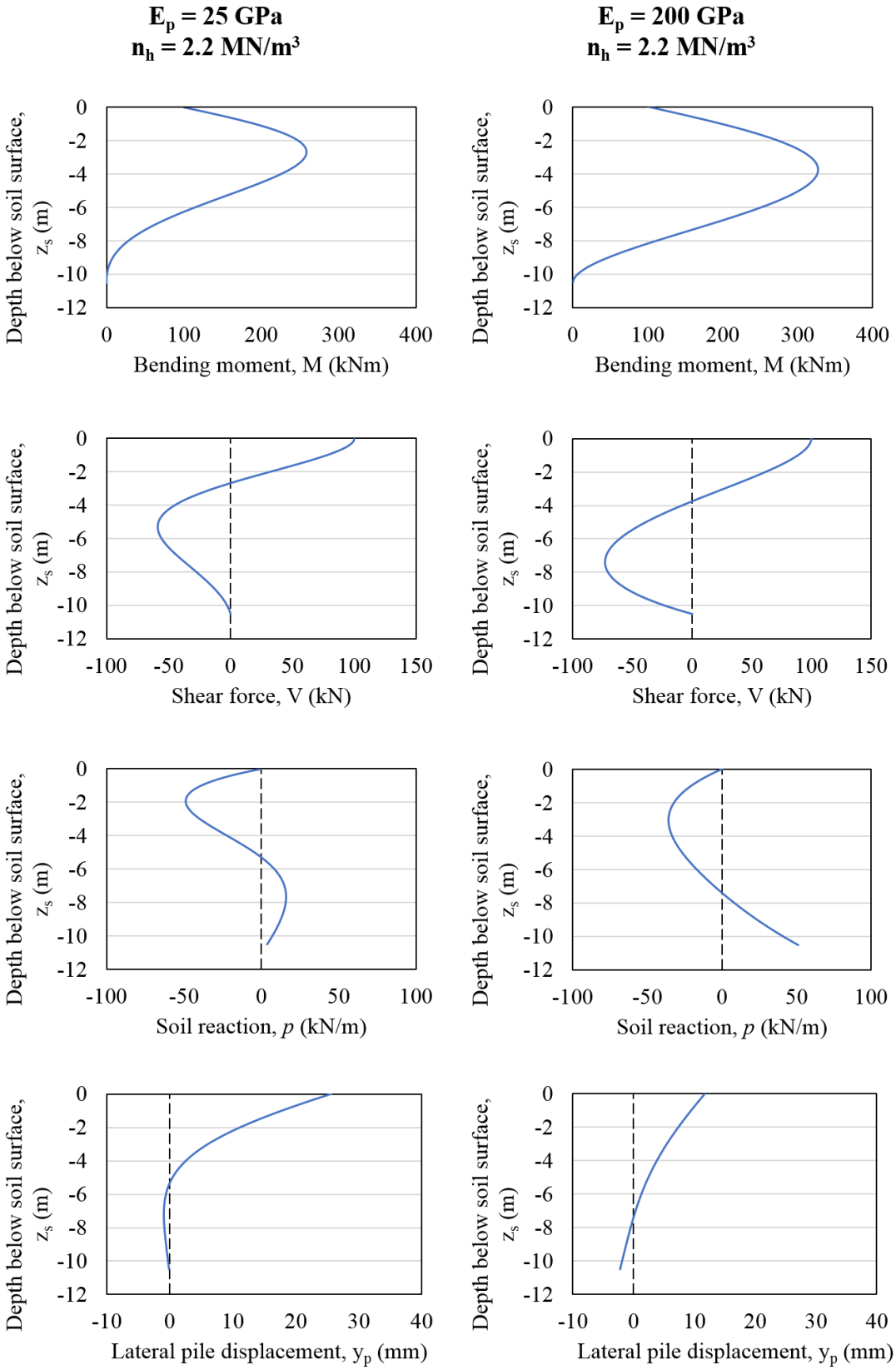

Figure 3-3: Soil-pile response (non-linear soil analysis) - 2.2 MN/m³

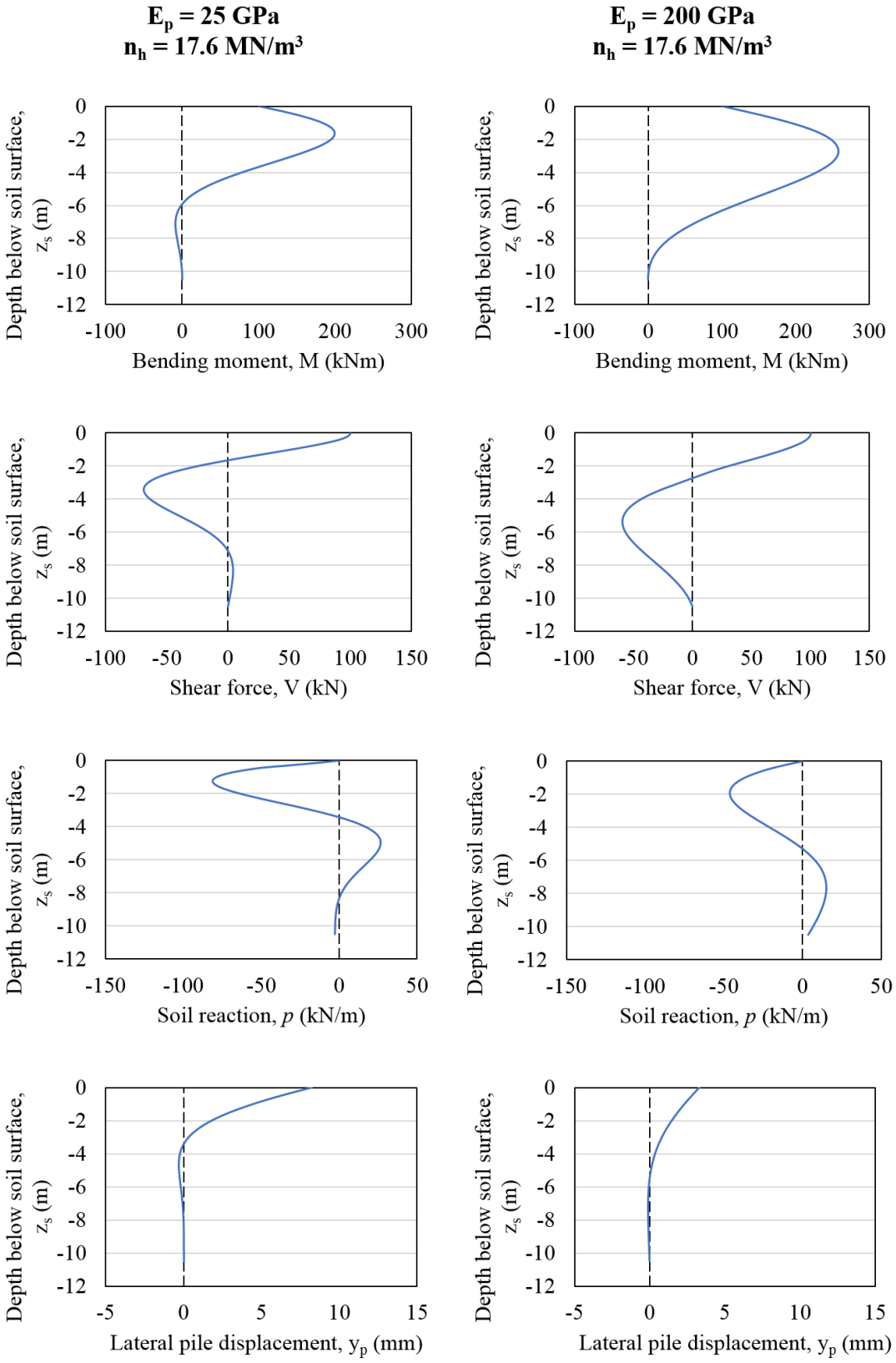

Figure 3-4: Soil-pile response (non-linear soil analysis) - 17.6 MN/m³

3.4 COMPARISON BETWEEN SUBGRADE REACTION AND NON-LINEAR SOIL ANALYSIS

The subgrade reaction analysis results were compared to that obtained for the non-linear soil analysis for both monotonic and cyclic load conditions. It is important to note that the subgrade reaction method cannot account for cyclic load conditions, as it is only a linear soil model. To incorporate cyclic effects into the subgrade analysis method, consideration should be given to changing soil conditions (non-linear behaviour) and the selection of the correct coefficient of subgrade reaction to incorporate these effects. The non-linear soil analysis can accommodate for this. **Figure 3-5** indicates the relationship between the lateral displacement and the applied lateral load at the soil surface for dense sand (n_h = 17.6 MN/m^3) using the different analysis approaches. The idea behind this was to indicate the change in behaviour from linear to non-linear soil conditions after the pile has reached a specific load. The properties of the soil and the pile is indicated in **Table 3-5**. A pile with a stiffness of 30 GPa was selected, as this realistically represents the stiffness of full-scale concrete piles in practice. The cyclic response of the pile also depends on the number of times a specific load is being applied. To test the concept, 1000 load cycles were applied to the pile for each load magnitude.

Table 3-5: Properties - comparison between analysis types (n_h = 17.6 kN/m^3)

Property	Value
Pile Young's modulus, E_p (GPa)	30
Coefficient of subgrade reaction, n_h (MN/m^3)	17.6
Unit weight, γ (kN/m^3)	19
Friction angle (˚)	38

It can be seen from **Figure 3-5** that, at small applied loads, the soil behaviour can be assume to be linear, with no noticeable differences occurring between the observed displacements. However, with an increase in the magnitude of the applied load, at about 100 kN for the non-linear monotonic analysis, and 50 kN for the non-linear cyclic analysis, the behaviour of the soil-pile system changed from linear to non-linear, as indicated by the displacement values. It should be mentioned that the cyclic behaviour is as a result of 1000 cycles only, with the response being potentially different for a different number of cycles applied.

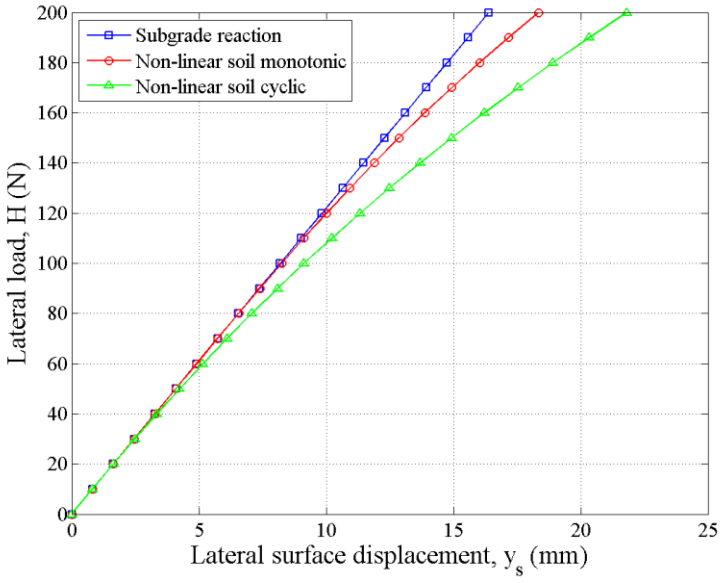

Figure 3-5: Comparison between analysis types (n_h = 17.6 MN/m^3)

3.5 SUMMARY

A parametric study was carried out using both the subgrade reaction analysis approach and non-linear soil analysis approach under monotonic loading conditions. The aim of the study was to determine the response of the soil-pile system due to the variation in properties of the pile and the soil surrounding the pile, as these primarily govern the behaviour of the pile under lateral loads. Changes in the stiffness of the soil and the pile had a significant influence on the bending moment and lateral displacement response of the pile caused by horizontal loading. Thus, any changes that might occur will have a significant effect on the overall response of the soil-pile system. A change in the behaviour of the soil-pile system (linear to non-linear) was also observed raising the question of whether soil can be assumed to react linear, neglecting non-linear soil behaviour, under allowable lateral loads. The importance of taking into account the changing stiffness of reinforced concrete pile as a result of cracking was also emphasised. The chapter concluded with a section discussing the change in behaviour between the subgrade reaction approach and the non-linear soil approach, also considering cyclic lateral loading. The results obtained from this study was utilised in the design of the experimental set-up and procedures for testing in the centrifuge as discussed further in Chapter 4.

4 EXPERIMENTAL SET-UP

4.1 INTRODUCTION

The aim of this investigation was to establish whether and to what extent results obtained from horizontally loaded scaled aluminium piles are valid and accurate for predicting the behaviour of full-scale reinforced concrete piles. From the parametric study conducted in the previous chapter, the interaction between a 600 mm diameter pile and the surrounding soil was studied, focussing on the stiffness of the pile as well as the surrounding soil and how they influence each other. In order to investigate the aim, centrifuge models were designed and constructed, using both a scaled aluminium pile and reinforced concrete pile, respectively, applying a lateral load to the top of each of the piles. This allowed for the behaviour of the two piles to be observed and compared. Both monotonic and cyclic behaviour was studied, taking into account the effect of an uncracked and cracked reinforced concrete pile in dry sand.

In this chapter, the preparational and experimental procedures followed prior to and during the tests in the centrifuge are explained and discussed. The main focus is on centrifuge modelling, including the design procedures of the model piles, pile instrumentation and calibration, as well as soil classification. Section 4.2 covers all the aspects associated with the centrifuge test model design, as well as the selection of the appropriate dimensions for the piles. Furthermore, Section 4.3 and Section 4.4 contains the instrumentation and calibration of the two piles, followed by the classification of the soil in Section 4.5, focussing on determining the properties of the soil through particle size distribution, density calculations, oedometer tests and triaxial tests. The chapter concludes with Section 4.7 and Section 4.8 discussing the model preparation and test set-up, followed by the various testing equipment and logging systems that were used.

4.2 CENTRIFUGE TEST MODEL DESIGN

Centrifuge testing was chosen as the method for all experimental work. The first part of this section comprises of a description of the centrifuge that was used, followed by the necessary scaling laws that was applied to the model. A brief overview of the model container is given, followed by a discussion on the procedures for selecting and designing the scaled aluminium and reinforced concrete piles.

4.2.1 Geotechnical centrifuge facility

All models were tested using a geotechnical centrifuge. Due to the non-linear stress-strain behaviour of soils, a geotechnical centrifuge was required to accelerate small scaled-down soil

models to a high acceleration, in order to produce realistic strains – something that cannot be achieved at 1-*g*. The University of Pretoria commissioned a geotechnical centrifuge in 2012 with a capacity of 150 *g*-ton. Characteristics and specifications of the centrifuge can be seen in **Table 4-1**. **Figure 4-1** shows the centrifuge that was used for testing.

Table 4-1: Specifications of the geotechnical centrifuge (Jacobsz *et al.*, 2014)

Specification	Description
Model name and type	Actidyn C67-4
Capacity	150 *g*-ton
Rated payload	1500 kg to 100-*g*
Maximum rotational speed	208 RPM
Radius	3 m
Model platform dimensions	0.8 m x 1.0 m

Figure 4-1: Geotechnical centrifuge of the University of Pretoria

4.2.2 Scaling laws

As mentioned in Chapter 2, the use of centrifuge modelling introduces the concept of scaling laws. To realistically model non-linear stress-strain behaviour of soils in a centrifuge, the appropriate scaling laws need to be applied. Scaling laws are relationships that relate the behaviour of the centrifuge model to the prototype (Madabhushi, 2015).

Table 4-2 indicates the various scaling laws that are applicable to the design of the centrifuge tests that were conducted for this dissertation, based on **Table 2-1** in Chapter 2. These laws were also applied to the results obtained from each test to aid in comparison and analysis in Chapter 5.

Table 4-2: Scaling laws – centrifuge model

Parameter at prototype scale	Scaling law for centrifuge acceleration, *n.g*
E_p, E_s, E_{sec}, ε, σ	1
D	$1/n$
A_p, H	$1/n^2$
M	$1/n^3$
I_p	$1/n^4$

Descriptions of the symbols used are as follows, but can also be found under the list of symbols at the beginning of the dissertation:

E_p = Young's modulus of the prototype pile [M L^{-1} T^{-2}]

E_s = Young's modulus of the soil [M L^{-1} T^{-2}]

E_{sec} = secant modulus of the soil [M L^{-1} T^{-2}]

ε = strain [-]

σ = stress [M L^{-1} T^{-2}]

D = outside diameter of the prototype pile [L]

A_p = cross-sectional area of the prototype pile [L^2]

H = lateral load [M L T^{-2}]

M = bending moment [M L^2 T^{-2}]

I_p = second moment of area of the prototype pile [L^4]

4.2.3 Model container – strongbox

The model container (strongbox) that was used for all the tests in the centrifuge was one of the standard containers at the centrifuge facility. **Figure 4-2** shows the model container that was used. The container box was manufactured from aluminium, with a wall thickness of 50 mm. The inside dimensions of the box are also indicated in **Figure 4-2**. Boundary effects play a significant role in the behaviour of models in a centrifuge. Thus, based on the scaling factors, and the size of the piles, it was decided to use this box to minimise the effects caused by boundaries. A brief discussion on the measuring equipment that was attached to the strongbox is included in the subsequent sections.

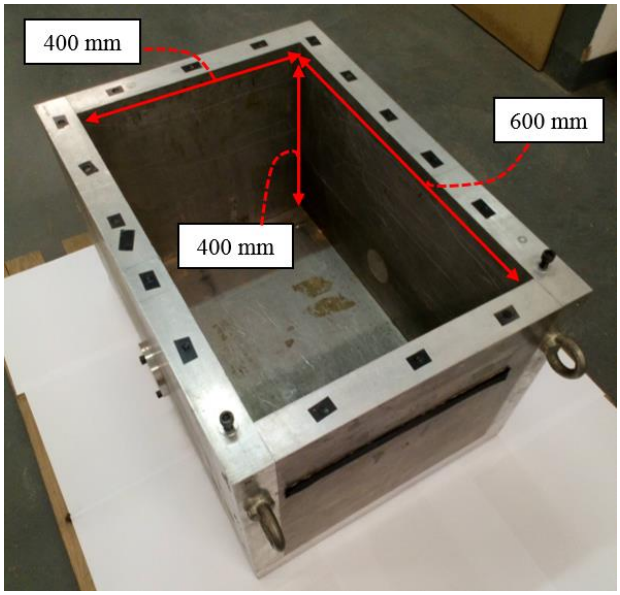

Figure 4-2: Model container – strongbox

4.2.4 Model piles and properties

To determine the dimensions of the model piles, it was important to first consider the size of the full-scale pile that needed to be modelled. Based on the full-scale parametric study conducted in Chapter 3, the research aim, and the size of the available model container, it was decided to scale down a pile, with a diameter of 600 mm and an embedment length of approximately 10 m. Assuming that a full-scale reinforced concrete pile will be used, Byrne & Berry (2008) indicated that, as a guideline for a 600 mm pile, 6 x Y20 main reinforcing bars should be used. Since the focus of the research was to determine and compare the response of both a scaled aluminium and reinforced concrete pile to lateral loads, the scaling laws (Section 4.2.2) along with **Equation 4-1** were used to determine the appropriate dimensions of the scaled model piles. As the primary problem concerned bending of the pile, the flexural rigidity (E_mI_m) for both the scaled aluminium and reinforced concrete piles were scaled accordingly, ensuring that both piles had the same flexural rigidity. It was assumed, for calculation purposes, that the full-scale reinforced concrete pile would have a compressive cube strength of 25 MPa and a modulus of elasticity of 30 GPa. These values were utilised in **Equation 4-1** to determine the size of the scaled model piles. Tests on the scaled piles were conducted at 30-*g* (n = 30).

$$\frac{E_pI_p}{E_mI_m} = n^4 \qquad \textbf{Equation 4-1}$$

where,

E_pI_p = flexural rigidity of the prototype pile [M L^3 T^{-2}]

E_mI_m = flexural rigidity of the model pile [M L^3 T^{-2}]

For the scaled aluminium model pile, a standard size hollow aluminium pipe was used, where the outer diameter was 19.2 mm with a wall thickness of 1.3 mm. It was decided that the aluminium model pile would have a total length of 400 mm, with 350 mm embedded in the soil, corresponding to a 10.5 m embedment depth at full-scale.

For the scaled reinforced concrete pile, a pile was cast using a typical 25 MPa characteristic compressive strength concrete mix design that was scaled down. The mix composition of the scaled concrete is indicated in **Table 4-3**. A CEM V / A (S-V) 42.5N cement was used as the binder for the scaled concrete. Dolomite crusher sand, passing the 1 mm sieve size, was selected for both the fine and coarse aggregate, which is representative of a typical 26 mm dolomite stone that had been scaled down. The superplasticiser comprised of a mixture of 50% Chryso Optima 100 and 50% Chryso Premia 100. The addition of the superplasticiser to the mix composition was to increase the workability of the mix for pouring and casting such small piles.

Table 4-3: Scaled concrete mix composition

Material	Relative density (RD)	kg/m^3
Cement	2.78	300
Water	1.00	250
Dolomite crusher sand	2.85	1870
Superplasticiser	1.06	21

The process for casting the scaled reinforced concrete pile was as follows:

- A trial mix was conducted on the scaled concrete mix design to determine the approximate strength and stiffness of the concrete. This was used as an initial indication for determining the size of the pile that needed to be cast to adhere to the scaling laws mentioned previously. Based on the trial mix results, a pile was cast using a 21 mm inside diameter PVC pipe as a mould.
- The full-scale main reinforcing bars (6 x Y20s) were modelled using 6 x 0.60 mm stainless steel wires. A reinforcing steel cage was constructed around a 17 mm outside diameter PVC pipe. The 17 mm diameter pipe was chosen to allow for enough concrete cover over the steel when the scaled concrete pile was cast (Mosley *et al.*, 2012). Placement of the main reinforcing steel wires (0.60 mm), around the circumference of the 17 mm pipe, is indicated in **Figure 4-3**, with equal spacing between the main bars. To keep the steel reinforcing in place, 0.21 mm stainless steel wire was spiralled at a pitch of approximately 10 mm around the cage and fixed to the main steel. The spiral reinforcing and pitch were similar to what is normally used in full-scale reinforced concrete piles. To ensure sufficient bond between

the steel wire and the concrete, all steel wires were soaked in hydrochloric acid for an hour prior to cage construction. **Figure 4-4** shows the completed steel reinforcing cage.

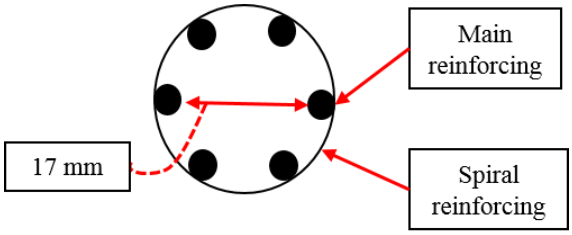

Figure 4-3: Schematic of scaled reinforcing steel cage cross-section

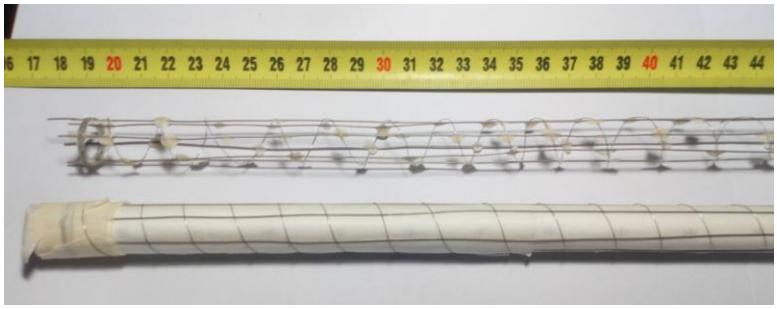

Figure 4-4: Complete scaled reinforcing cage

- The reinforcing steel cage was then placed in the 21 mm diameter PVC pipe mould after which the scaled concrete was mixed and cast. **Figure 4-5** indicates the cross-section of the cast pile, followed by **Figure 4-6** showing the completed cast pile.

Figure 4-5: Model reinforced concrete pile cross-section

Figure 4-6: Completed model reinforced concrete pile

Similar to the scaled aluminium pile, the scaled reinforced concrete pile was trimmed to have a total length of 400 mm, with 350 mm being embedded in the soil, which corresponded to an embedment depth of 10.5 m at full-scale. The strengths of the steel reinforcing wire and scaled concrete from the final concrete mix used to cast the pile were measured using standard testing methods and is presented below.

The tensile capacity of the stainless steel wires, used as main reinforcing in the scaled reinforced concrete piles was determined from tensile tests on three specimens. The stress-strain diagrams obtained from the tensile tests on the three specimens are shown in **Figure 4-7**. It can be seen from the graph, based on an average between the three specimens, that the yield strength of the 0.60 mm stainless steel wire was approximately 330 MPa, with a modulus of elasticity of 101 GPa (E_m), indicating that the wire should behave linearly elastic up to around 3000 micro-strain. The ultimate tensile strength was 692 MPa.

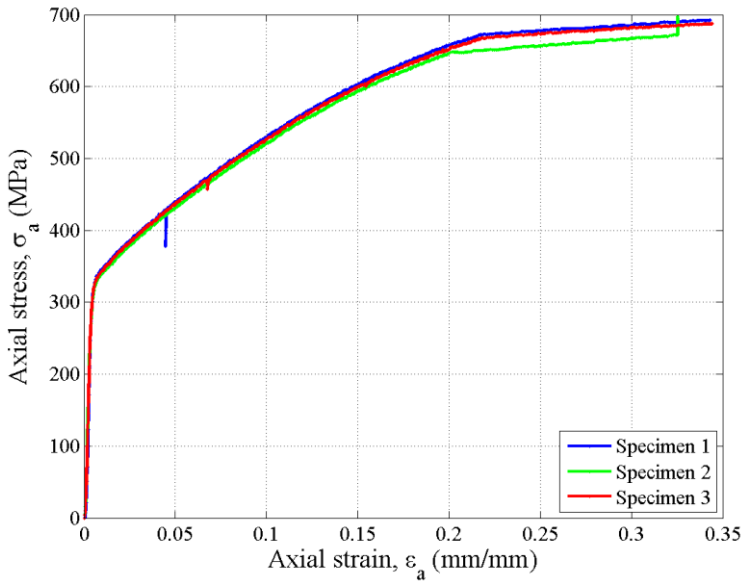

Figure 4-7: Stress-strain diagram – stainless-steel wires

All concrete material properties, such as the compressive strength and indirect tensile strength as well as the modulus of elasticity were measured after 28 days and are reported as the average of a set of three measured values. The strength testing was in accordance with BS EN 12390-3:2009, BS EN 12390-6:2000 and BS EN 12390-13:2013. Small test specimens were cast to ensure that the strength of the scaled concrete is representative (Noor & Boswell, 1992). **Figure 4-8** indicates the respective test specimens that were cast to obtain the material properties mentioned above.

Figure 4-8: Cubes and cylinders used to obtain material strengths

The indirect tensile capacity of the scaled concrete was obtained from splitting cylinder tests on 50 mm diameter cylinders, and the compressive strengths from 50 mm cubes. For obtaining the secant modulus of elasticity of the scaled concrete, a 100 mm long, 50 mm diameter cylinder, was loaded to 40% of its compressive strength, measuring the deformation in the cylinder using a standard collar over the central 50 mm of the cylinder. All cubes and cylinders for the respective material tests were demoulded four days after casting and placed in the same room as the cast pile to ensure that the properties measured from the cubes and cylinders were representative of the pile. Three of the six cubes were cured in water at 25 ˚C as a standard concrete compression strength testing procedure to obtain the characteristic compressive strength of the concrete mix. All procedures regarding the preparation and curing of the concrete test specimens were in accordance with ASTM Standard C192/C192M – 18 and C511 – 19. These average strengths are presented in **Table 4-4**. The density of the scaled concrete was determined as 2382 kg/m^3.

It can be seen that the compression and tensile strength values represent typical strengths that would be expected for a full-scale concrete pile.

Table 4-4: Scaled concrete strengths and modulus of elasticity

Property	28-day
Compression strength (MPa)	35.8
Compression strength – 25 ˚C water cured (MPa)	34.2
Splitting cylinder strength (MPa)	2.8
Secant modulus of elasticity (GPa)	20.5

4.3 PILE INSTRUMENTATION

After determining the size and properties of the piles based on full-scale dimensions and properties, focus shifted to the physical scale model and monitoring of the behaviour of the piles during the tests. To measure the strain development in the piles in response to the laterally applied load, the two model piles were instrumented with a series of strain gauges. As indicated in the previous section, the first model foundation consisted of aluminium, where the second was scaled concrete with the appropriate steel reinforcing, both having an embedment depth of 350 mm, as indicated in **Figure 4-9**, resulting in an L_m/D_m ratio of 18.2 for the aluminium pile and 16.6 for the reinforced concrete pile. L_m refers to the embedded length of the model pile and D_m to the outside diameter of the model pile. It can also be seen in **Figure 4-9** that the horizontal load was applied to the top of the pile at a distance of 37.5 mm above the surface of the soil, allowing for a bending moment to be created at the surface of the soil. This height corresponded to the height to the centre of the linear actuator and load cell that was fixed to the strongbox. This height was kept constant for all the centrifuge tests as load eccentricity did not form part of the dissertation.

To measure the strain development in the pile as a result of the lateral loads, strain gauges were attached to both sides of the pile. Both the scaled aluminium and reinforced concrete piles were instrumented in the same way, using twelve precision resistance strain gauges on each. These strain gauges were placed on the sides of the piles, connected to form 12 quarter- Wheatstone Bridges, six on the tension and six on the compression side of each of the piles. These locations corresponded to the expected location of maximum tension and compression stresses in the pile. Due to the maximum bending moment expected to occur between four and five pile diameters below the surface of the soil, as indicated by literature (see Section 2.3.2), the entire length of the pile was not instrumented. Placement of the stain gauges is indicated schematically in **Figure 4-9**, with the top-most strain gauge at the surface of the centrifuge soil model and the bottom-most strain gauge 200 mm below the surface of the soil. It was also assumed that the was unrestricted at the head/pile cap, with rotation allowed at the pile cap.

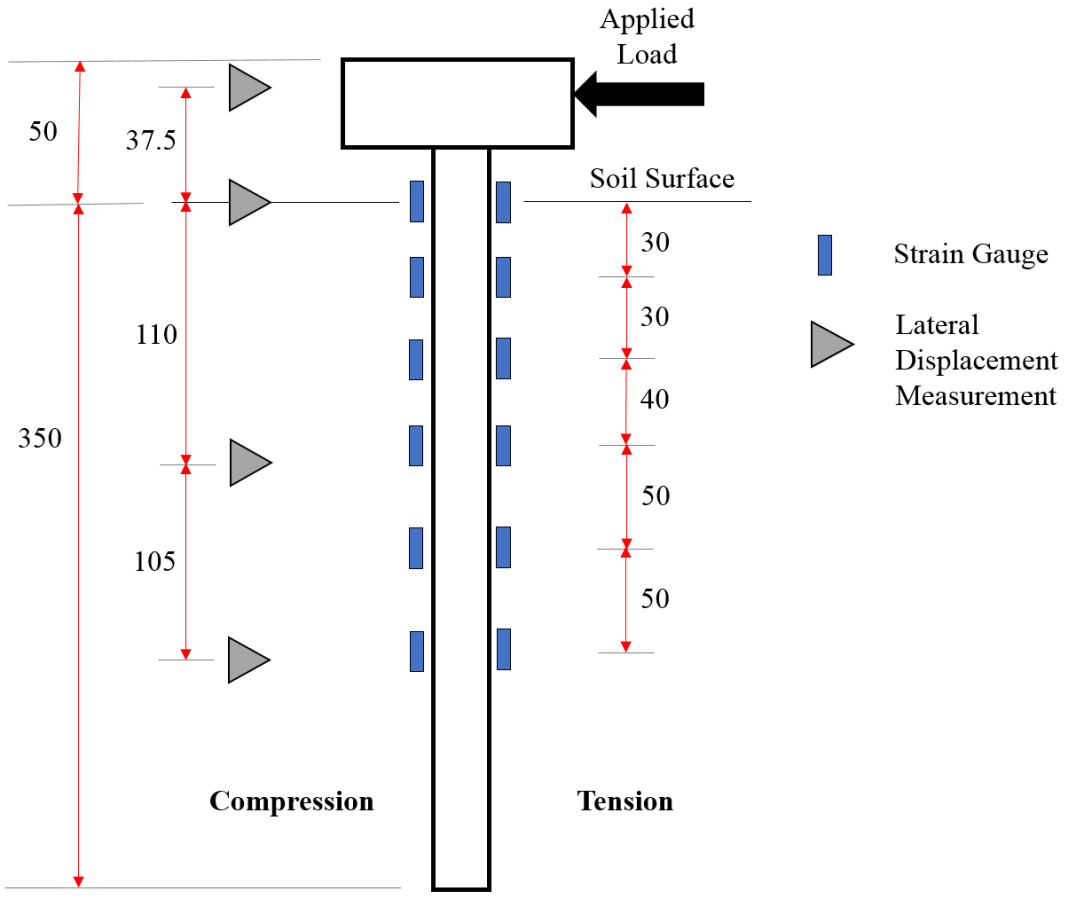

Figure 4-9: Strain gauge and lateral displacement measurement placement

Due to the size of the model piles, a strain gauge with a small gauge length had to be used to ensure a localised strain measurement instead of an average strain measurement over a significant length. A strain gauge with a 2 mm gauge length was selected for both the scaled aluminium and reinforced concrete piles. For the aluminium pile strain gauges for use on aluminium were used, where strain gauges for use on ceramic were used for the scaled reinforced concrete pile. Characteristics of both the aluminium and ceramic precision resistance strain gauges are presented in **Table 4-5** and **Table 4-6**, respectively.

Table 4-5: Strain gauge specifications – aluminium

Specification	Description
Manufacturer	Tokyo Sokki Kenkyujo Co., Ltd.
Model name and type	FLA-2-23-3LJC
Gauge factor	2.16 ± 1%
Gauge length	2 mm
Gauge resistance	118.5 ± 0.5 Ω
Thermal coefficient	23 x 10^{-6} /°C

Table 4-6: Strain gauge specifications – ceramic

Specification	Description
Manufacturer	Tokyo Sokki Kenkyujo Co., Ltd.
Model name and type	FLA-2-8-3LJC
Gauge factor	2.10 ± 1%
Gauge length	2 mm
Gauge resistance	118.7 ± 0.5 Ω
Thermal coefficient	8 x 10^{-6} /°C

In order to obtain the bending moments experienced by the pile, the measured strain data had to be converted to bending moments using the appropriate formulas. By measuring the strain using quarter-bridges, comparison between the bending and axial strain development in the pile could be monitored separately by using **Equation 4-2**.

$$\sigma_m = \frac{P}{A_m} \pm \frac{M}{Z_m} \qquad \textbf{Equation 4-2}$$

where,

σ_m = total stress in the model pile [M L^{-1} T^{-2}]

P = axial force experienced by the pile [M L T^{-2}]

A_m = cross-sectional area of the model pile [L^2]

M = bending moment experienced by the pile [M L^2 T^{-2}]

Z_m = sectional modulus of the model pile ($I_p/(D_m/2)$) [L^3]

D_m = outside diameter of the model pile [L]

To calculate the axial force and bending moment components from **Equation 4-2**, **Equation 4-3** and **Equation 4-4** were used. It should be mentioned that these equations are only valid for linear elastic material properties. Once the material has yielded, these equations cannot be used anymore.

$$P = \frac{(\varepsilon_1 + \varepsilon_2) E_m A_m}{2} \qquad \textbf{Equation 4-3}$$

$$M = \frac{(\varepsilon_1 - \varepsilon_2) E_m Z_m}{2} \qquad \textbf{Equation 4-4}$$

where,

E_m = Young's modulus of the model pile [M L^{-1} T^{-2}]

ε_1, ε_2 = strain measured on the side of the pile experiencing maximum tension and compression, respectively [-]

Figure 4-10 shows the instrumented scaled aluminium pile, followed by the instrumented scaled reinforced concrete pile in **Figure 4-11**.

Lateral displacement of the pile was measured at four locations along the length of the pile, the first 37.5 mm above the soil surface (where the load was applied) using an LVDT, the second at the soil surface, also using an LVDT, and at two locations below the surface of the soil. For measuring the lateral displacement of the pile below the soil surface, mini-extensometers were fixed to the side of the pile at two locations on the section of the pile that was embedded in the soil. The equipment used for measuring the lateral displacements is presented in Section 4.7.2. All the locations where the lateral displacement of the pile was measured are indicated in **Figure 4-9**.

Taylor (1995) indicated, based on research conducted by Lyndon & Pearson (1988), that surface roughness of a pile had a large effect on both the load-deflection curve and bending moment distribution of a laterally loaded pile and this should be considered when designing centrifuge experiments. Thus, to increase the friction and interaction between the pile and surrounding soil, and to ensure that both piles had the same soil-pile interaction properties and surface roughness, fine silica sand was glued to the outside surface of both the piles for the entire embedded length. **Figure 4-12** and **Figure 4-13** indicates the instrumented scaled aluminium and reinforced concrete piles covered in this fine silica sand.

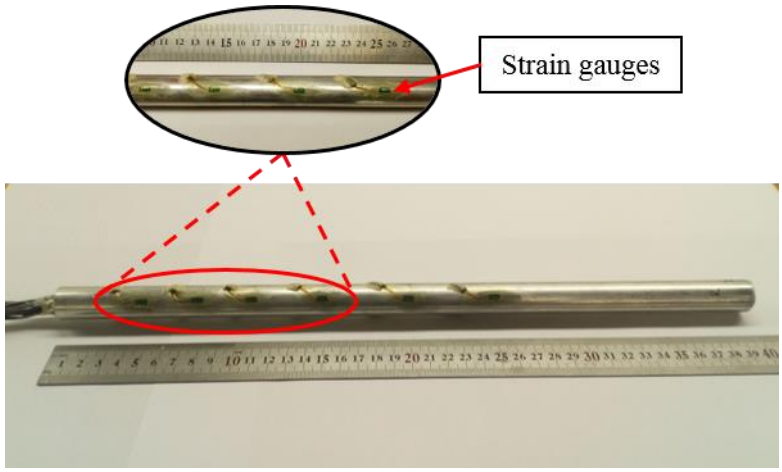

Figure 4-10: Instrumented scaled aluminium pile – without silica sand

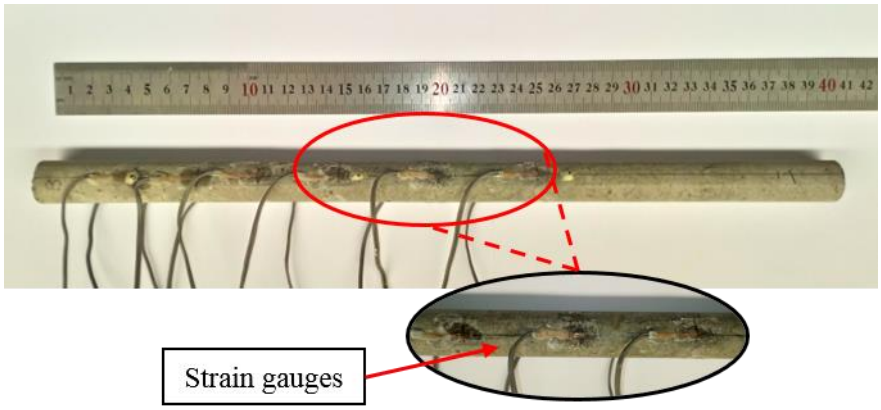

Figure 4-11: Instrumented scaled reinforced concrete pile – without silica sand

Figure 4-12: Instrumented scaled aluminium pile – with silica sand

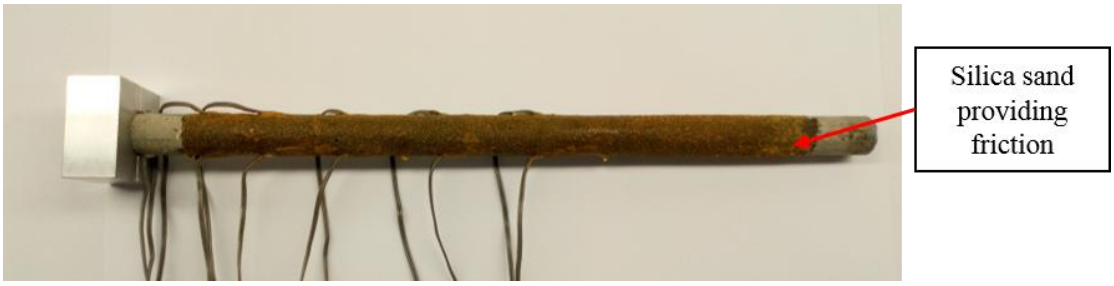

Figure 4-13: Instrumented scaled reinforced concrete pile – with silica sand

Based on literature, it was decided to a apply a one-way (compressive) lateral load only to the piles. The one-way lateral load was applied to the pile through an aluminium pile cap that was fixed to the top of each of the scaled aluminium and reinforced concrete piles. **Figure 4-14** indicates the dimensions of the pile cap that was used.

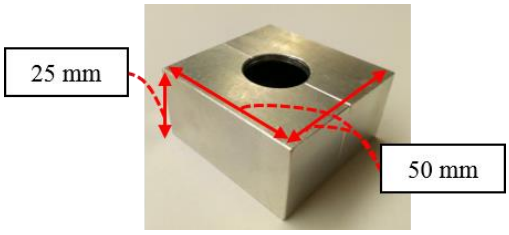

Figure 4-14: Pile cap

4.4 PILE CALIBRATION

In order to obtain the actual Young's modulus of the scaled aluminium and reinforced concrete piles, both instrumented piles had to be calibrated prior to testing in the centrifuge. The Young's modulus was obtained by conducting a simple bending test on the two piles, whereby the piles were placed horizontally and fixed on one end and loaded with a point load on the other end, thus forming a cantilever beam. For the scaled aluminium pile, weights of different magnitudes, ranging between 8 and 26 N were suspended from the pile. The corresponding bending moment within the pile was calculated from the strain measured using the strain gauges that were attached to the pile. Linear variable differential transformers (LVDTs) were used to measure downward deflection of the pile as a result of the applied load. Similar procedures were followed for the scaled reinforced concrete pile. However, weights on this pile ranged between 1 and 3 N to ensure that the pile did not crack prior to testing in the centrifuge so that it remained within its uncracked elastic strain region. It should also be mentioned that, due to the variability of the properties of the scaled concrete it was necessary to calibrate the concrete pile that was used for the centrifuge test to ensure that the true material behaviour was captured.

The measured bending moments and deflections for both these piles were then compared to theoretically predicted values to determine the Young's modulus of the pile by finding the least error between the measured and the theoretical values. **Figure 4-15** indicates the deflection, δ, and bending moment, M, with distance from fixity, x_d, for an applied load of 26.4 N for the scaled aluminium pile. **Figure 4-16** indicates the same plots regarding deflection and bending moment, but for the scaled reinforced concrete pile for an applied load of 2.9 N.

The Young's modulus of the scaled aluminium pile was determined to be approximately 66 GPa (E_m) and the Young's modulus of the scaled reinforced concrete pile as 31 GPa (E_m). The errors between the measured and theoretical values were within 5%.

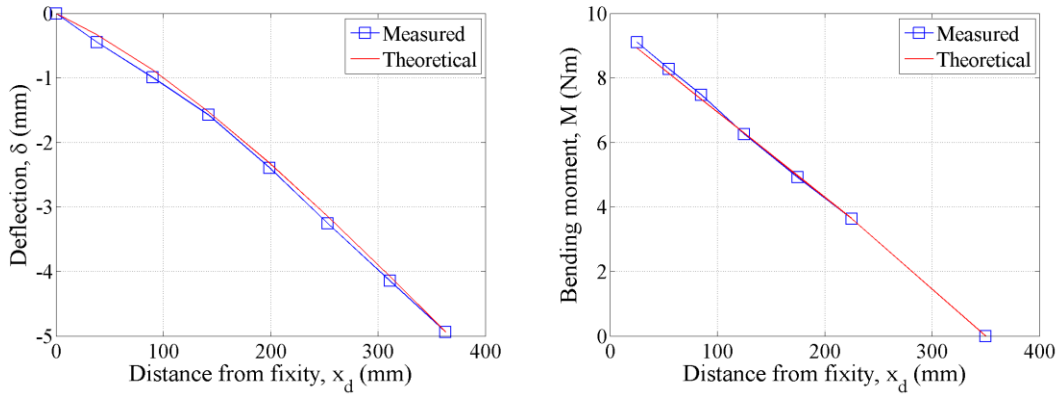

Figure 4-15: Scaled aluminium pile calibration (26.4 N) – Young's modulus

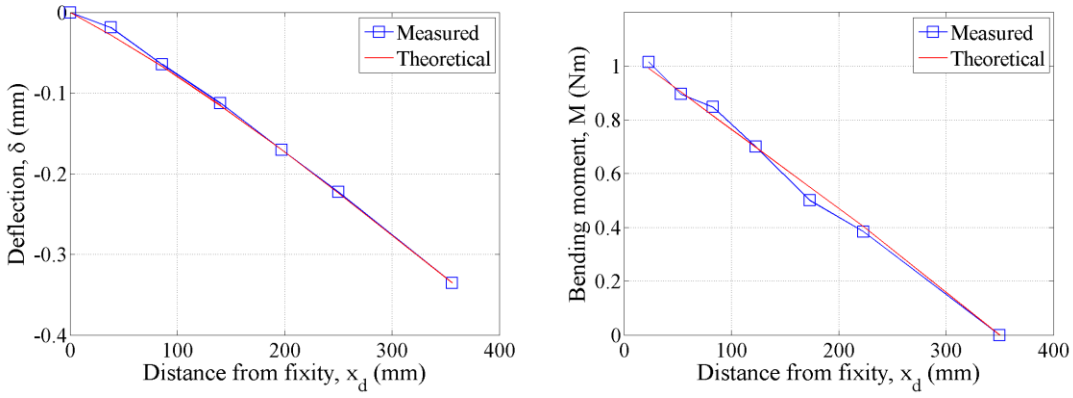

Figure 4-16: Scaled reinforced concrete pile calibration (2.9 N) – Young's modulus

After determining the Young's modulus of the two piles, the sectional properties of the piles could be determined (E_mI_m and E_mA_m), as indicated in **Table 4-7**. Knappett *et al.* (2011) mentioned that the strength of centrifuge models, especially in the case of scaled concrete, is important, and that the cracked value of E_mI_m for scaled reinforced concrete section is a more appropriate measure of the structural stiffness for replicating displacements. Based on this, the cracked properties of both sections are also included, assuming that the aluminium pile cannot crack. The indicated A_m and I_m values are for the aluminium and the uncracked reinforced concrete sections. From **Table 4-7** it can be seen that the flexural stiffness (E_mI_m) of the scaled reinforced concrete pile had a significantly higher value than anticipated based on the preliminary results from the concrete trial mix design (higher E_m). In contrast, the measured Young's modulus of the aluminium pile was less than the expected value (66 GPa in comparison with 69-70 GPa) (Gere & Goodno, 2013). This indicates the importance of calibration and how essential it is to obtain the correct material properties. Thus, based on the flexural stiffnesses, a direct comparison of the results from the scaled aluminium and reinforced concrete piles were not possible, but behavioural trends could still be investigated and compared. It is interesting to note that, even though the centrifuge model represents primarily a problem concerned with bending, the axial rigidity (E_mA_m) of the scaled reinforced concrete pile was significantly larger than that of the scaled aluminium pile. This is due to the small area of the hollow aluminium section opposed to the solid section of the reinforced concrete. Lastly, it is worthwhile mentioning that the flexural and axial stiffness of the scaled reinforced concrete pile is larger than that of the aluminium pile when the concrete section is still uncracked. This is however not the case once the scaled reinforced concrete pile section cracks, resulting in both the flexural and axial stiffnesses to decrease to values below that of the aluminium pile.

Table 4-7: Scaled aluminium and reinforced concrete piles dimensions

Pile type	D_m (mm)	t_m (mm)	A_m (mm^2)	I_m (mm^4)	Uncracked		Cracked	
					E_mA_m (MN)	E_mI_m (MNmm^2)	E_mA_m (MN)	E_mI_m (Nmm^2)
Aluminium	19.2	1.3	73.1	2943.4	4.8	194.3	-	-
Reinforced concrete	21.1	-	352.9	10036.0	11.1	316.1	1.2	18.0

4.5 PILE CAPACITIES

From the pile calibration in the previous section, the bending moment capacity (yielding moment) of the scaled aluminium and reinforced concrete pile can be calculated. For the scaled aluminium pile, the yielding moment (M_{yield}) can be calculated using the flexural (bending) stress formula (My/I), assuming that the yield stress of the aluminium is 270 MPa (Gere & Goodno, 2013). The calculated yield moment is indicated in **Table 4-8**.

For the reinforced concrete pile, both the cracking moment (M_{crack}) and yielding moment (M_{yield}) should be calculated. The reinforced concrete pile was under-reinforced, which will result in the reinforcing steel to yield before the concrete crushes once the yielding moment in the section has been reached. For the cracking moment calculated (see **Table 4-8**), the flexural stress formula was used, assuming that the concrete would crack at a tensile stress of 2.8 MPa.

Table 4-8: Aluminium and reinforced concrete pile bending capacities

Pile type	M_{crack} (Nm)	M_{yield} (Nm)
Aluminium	-	82.8
Reinforced concrete	2.7	4.9

Calculating the yielding moment for the reinforced concrete pile is however more complicated. In order to incorporate the formation of a crack into behaviour of the scaled concrete pile, and determine the yielding moment of the section, it was necessary to plot the flexural rigidity, E_mI_m, of the concrete section against the bending moment for different conditions of the concrete. These conditions usually include the uncracked, partially cracked and fully cracked sections. **Figure 4-17** illustrates the flexural rigidity of the pile against the bending moment for the scaled reinforced concrete pile, showing the variation of the flexural rigidity with bending moment. This diagram was established from the requirements of strain compatibility and equilibrium of forces. The flexural rigidity of the scaled concrete section reduced instantaneously after an approximate bending moment of 2.7 Nm (see **Figure 4-17**). The values obtained from this diagram were utilised for ultimate limit state conditions in determining the bending moment experienced by the pile after the formation of the crack in Chapter 5. The calculated yielding moment for the scale reinforced concrete pile is also indicated in **Table 4-8**.

Furthermore, it should be mentioned that even though the uncracked reinforced concrete pile had a higher flexural rigidity than the aluminium pile, the yielding moment of the aluminium is significantly larger than the reinforced concrete pile, due to the higher yield stress of the aluminium pile.

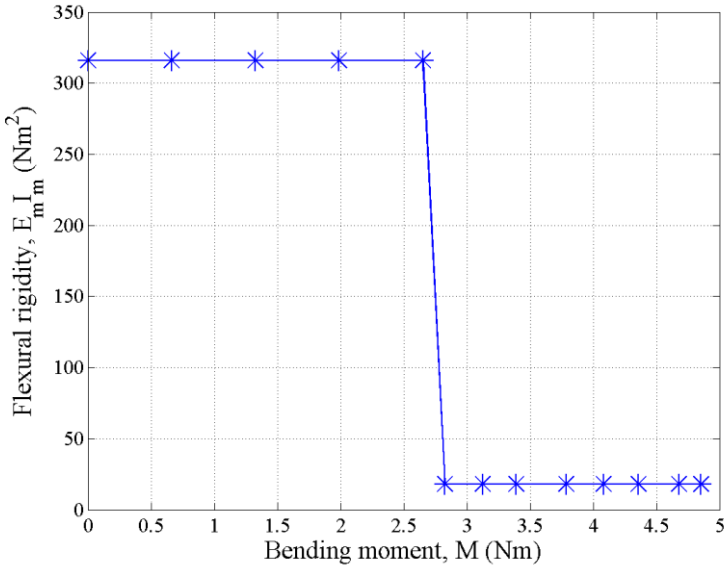

Figure 4-17: Computed relationship between the flexural rigidity of the pile and the bending moment

4.6 SOIL CLASSIFICATION AND PROPERTIES

Air pluviation is a well-known technique used to ensure not only uniform relative density throughout the entire soil model, but also repeatability in preparing sand for centrifuge modelling, when a number of tests have to be conducted at the same relative density (Madabhushi, 2015). Typically, uniformly graded silica sands are used to minimise compaction and settlement during centrifuge spin-up. During the process of air pluviation, sand is placed in a hopper, or pluviator, suspended over the model container at a specific drop height, after which sand is allowed to drop from this height, through a nozzle into the model container at a constant flow rate. During this process, the drop height is controlled, ensuring that a constant height is kept as the level of the sand in the model container increases. The specific drop height is usually determined by creating calibration charts, varying the height of the hopper and determining the corresponding relative density of the sand model from that height.

This technique was followed for preparing all the sand models for testing in the centrifuge. Based on the availability of sand, and the need for the maximum possible packing density according to Fuller's grading curve theory, two silica sands, with different gradings, were

mixed in a 1:1 ratio. The two sands, referred to as Sand 1 and Sand 2 in the remainder of the dissertation, were combined using a riffler, or sample splitter, to ensure uniform mixing of the two sands. The 1:1 ratio sand mixture, which was used for all the tests, is referred to as the Centrifuge Sand Mix in the remainder of the report.

The packing density of the Centrifuge Sand Mix was obtained from creating a calibration chart, varying the drop height of the hopper and measuring the corresponding relative density of the sand model, keeping the flow rate of the sand constant. **Figure 4-18** shows the hopper, or pluviator that was used. A 1200 mm long corrugated flexible hose was attached to the bottom of the hopper outlet to aid in placement of the sand within the model. A drop height of 1600 mm (1200 mm inside a corrugated pipe and 400 mm freefall) was selected as the optimal height to obtain the highest packing density for the sand and was used for preparing all the sand models in the model container.

Figure 4-18: Sand pluviator

The following subsections describe the various tests conducted on the sand and the results obtained, which were used for the classification of the Centrifuge Sand Mix.

4.6.1 Particle size distribution

The British Soil Classification System classifies soils into groups, known as Basic Soil Types, depending on their particle sizes. Soils can be classified per **Table 4-9**.

Table 4-9: Particle size ranges (adapted from Knappett & Craig, 2012)

Clay	Silt			Sand			Gravel		
	Fine	Medium	Coarse	Fine	Medium	Coarse	Fine	Medium	Coarse
Dimensions – mm									
< 0.002	0.002 – 0.006	0.006 – 0.02	0.02 – 0.06	0.06 – 0.2	0.2 – 0.6	0.6 – 2	2 – 6	6 – 20	20 – 60

The particle size distributions for both Sand 1 and Sand 2 were determined, separately, as well as for the Centrifuge Sand Mix. The particle size distributions were measured using a Malvern Instruments Mastersizer 2000 (Hydro 2000MU) apparatus. The particle size distribution for Sand 1, Sand 2 and Centrifuge Sand Mix is shown in **Figure 4-19**.

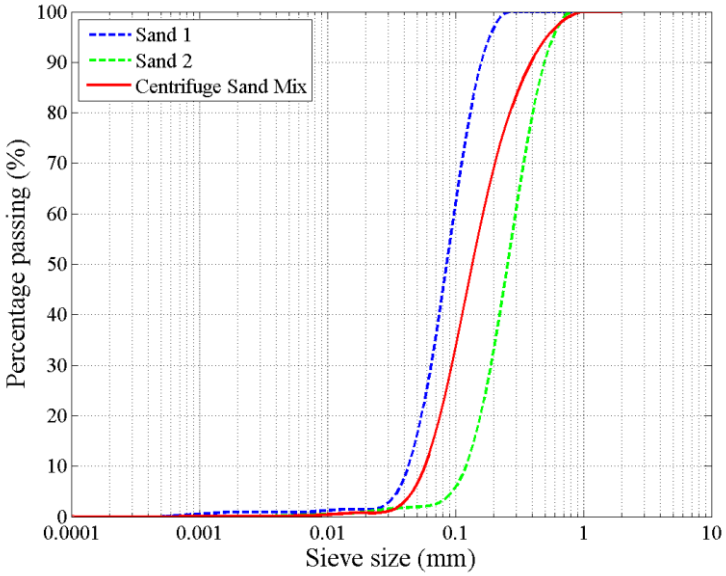

Figure 4-19: Particle size distribution

Based on **Figure 4-19**, it can be seen that the sand particles lie primarily between the ranges of 0.06 mm and 2 mm, classifying as a sand according to the British Soil Classification System, with parts also falling within the silt category. According to the Unified Soil Classification System (ASTM Standard D2487-11), the soil is classified as a silty sand (SM), with more than 12% fines, a coefficient of uniformity of less than 6, and practically no gravel particles.

According to Smith (2014), the general shape and slope of a distribution curve are best described by the coefficient of uniformity (C_U), as indicated by **Equation 4-5**.

$$C_U = \frac{D_{60}}{D_{10}} \qquad \textbf{Equation 4-5}$$

where,

D_{10} = the size such that 10% of the particles are smaller than that size [L]

D_{60} = the size such that 60% of the particles are smaller than that size [L]

He indicated that for a coefficient of uniformity of smaller than 4, the grading of the soil can be considered uniform, and if it is larger than 4, the soil is either well-graded or gap graded. From the Malvern Mastersizer test data above, the C_U was calculated as 2.97. Based on this information, the C_U for the Centrifuge Sand Mix, used for all centrifuge tests, is smaller than 4, indicating that the silty sand is uniformly graded. Thus, the change in density during centrifuge spin-up could be considered negligible. It can also be seen from the particle size distribution curve that the D_{50}, which is the average or mean particle size, is 138 µm.

Madabhushi (2015) indicated that an important aspect to consider when scaling down models for testing in a centrifuge is the ratio between the particle size of the soil and the dimensions of the model. He suggested that in order to avoid particle size scale effects with regard to piles, the ratio between the diameter of the pile and the typical particle size (mean particle size) should at least be 25. Ovesen (1979) also indicated similar restrictions on the ratio between the pile diameter and particle size to minimise scale effects. From the particle size distribution, the ratio between the diameters of the two scaled piles and the mean particle size was determined. For the scaled aluminium pile, the ratio was calculated as 139, and for the scaled reinforced concrete pile, as 153. Both these ratios satisfied the criteria specified by Madabhushi (2015), thus particle size scale effects in terms of pile behaviour should be negligible for these centrifuge tests.

4.6.2 Specific gravity

Specific gravity refers to the density of the solid particles of a soil. The specific gravity, G_S, of the Centrifuge Sand Mix was obtained using the AccuPyc II 1340 Series Pycnometer.

Tests were conducted on soil specimens from the Centrifuge Sand Mix, taking the average of three particle densities. The average value for the particle density of the Centrifuge Sand Mix was 2.689 g/cm^3.

4.6.3 Sand density

The ASTM defines relative density (D_r) as the state of compactness of soil with respect to the loosest and densest states at which it can be placed. It is expressed as the ratio of the difference between the void ratio of a cohesionless soil in the loosest state and any given void ratio, to the difference between its void ratios in the loosest and densest state. e_{min} and e_{max} represents the

densest and loosest possible soil packing states that can occur, respectively. Relative density is defined as indicated by **Equation 4-6**.

$$D_r = \frac{e_{max} - e}{e_{max} - e_{min}} \qquad \textbf{Equation 4-6}$$

where,

e = void ratio of the soil at its current state [-]

In order to determine the relative density at which the Centrifuge Sand Mix is for all the respective centrifuge tests, the maximum (ρ_{dmax}) and minimum (ρ_{dmin}) dry density of the soil, as well as the corresponding void ratios, were determined. The ASTM Standard D4253-16 and D4254-16 were used to determine the maximum and minimum dry density, respectively. Three tests were conducted for each of the two test methods mentioned, taking the average values for the minimum and maximum dry densities.

Table 4-10 indicates the average results for the minimum and maximum dry densities, as well as the corresponding maximum and minimum void ratios, which were calculated using **Equation 4-7** and **Equation 4-8**, respectively. All tests were conducted at a similar relative density. These calculated values are indicated in Chapter 5 for each of the tests conducted.

$$e_{max} = \left(\frac{\rho_w G_s}{\rho_{dmin}}\right) - 1 \qquad \textbf{Equation 4-7}$$

$$e_{min} = \left(\frac{\rho_w G_s}{\rho_{dmax}}\right) - 1 \qquad \textbf{Equation 4-8}$$

where,

ρ_w = density of water at 20˚C (≈ 1000 kg/m^3) [M L^{-3}]

G_s = specific gravity (as per Section 4.6.2) [-]

Table 4-10: Minimum and maximum density test results

Parameter	Value
Maximum dry density (kg/m³)	1754
Minimum dry density (kg/m³)	1505
Maximum void ratio (e_{max})	0.79
Minimum void ratio (e_{min})	0.53

4.6.4 Oedometer test results

In an elastic material the strain or deformation, due to imposed stress, is a function of the magnitude of the stress, with the effect being fully reversible. If over a certain range, the relationship between stress and strain is linear, Hooke's Law can be applied. However, the stress-strain relationship of soil is far from linear.

Due to the non-linear stress-strain behaviour of soils, estimating an appropriate soil stiffness, i.e. Young's modulus, is one of the more difficult soil parameters to obtain. For experimental and numerical work, the stiffness values of the soil obtained in this section were utilised.

Both a one-dimensional oedometer test and triaxial compression tests were conducted on the soil to determine the confined and unconfined stiffness. In this section, the one-dimensional oedometer test results are presented. Procedures for the one-dimensional oedometer test were based on ASTM Standard D4546-14e1.

A soil sample was prepared in the confining ring and cylinder of an oedometer. The relative density of the soil specimen within the confining ring was approximately 0.80, which corresponded to the relative density of the sand, obtained from the process of pluviation. The relative density was then calculated using the values for the maximum and minimum dry densities mentioned in Section 4.6.3. The prepared specimen was placed into the oedometer and a seating pressure of 1 kPa was applied to the sample. As mentioned, the test was used to determine the Young's modulus of the dry sand and not the swelling or collapsing of the soil, thus no water was added to the sample during the test. The specimen was then loaded, in equal increments, to a stress point corresponding to the equivalent soil stress at the bottom of the model container in the centrifuge at 30-*g*, as tests were carried out at this *g*-level. This covered the entire range of vertical pressures in the centrifuge soil model. The specimen was then unloaded, in the same increments, to an applied pressure of 1 kPa, followed by reloading of the specimen to twice the equivalent stress at the bottom of the model container at 30-*g*. An LVDT was used to measure the changed in the thickness of the original specimen. The corresponding strain was calculated, taking into account the initial zero reading and the original specimen height.

Figure 4-20 shows the stress-strain diagram of the one-dimensional oedometer test that was conducted on the Centrifuge Sand Mix, where σ_a refers to the axial stress and ε_a to the axial strain.

The approximate constraint modulus (E_0) of the soil was calculated by fitting a linear trendline to the 200% loading curve (twice the equivalent stress) and obtaining the gradient of that line.

It can be seen that the constraint modulus of the Centrifuge Sand Mix was 34.7 MPa. To obtain the corresponding Young's modulus of the soil (E_s), **Equation 4-9** should be used.

$$E_0 = \frac{E_s\,(1-\upsilon)}{(1+\upsilon)(1-2\upsilon)} \qquad \textbf{Equation 4-9}$$

where,

υ = Poisson's ratio of the sand [-]

Winterkorn & Fang (1975) indicated that the Poisson's ratio of sand is approximately 0.3. Using this Poisson's ratio, the Young's modulus of the soil was calculated from the constraint modulus as 46.7 MPa, taken as 47 MPa for all future calculations.

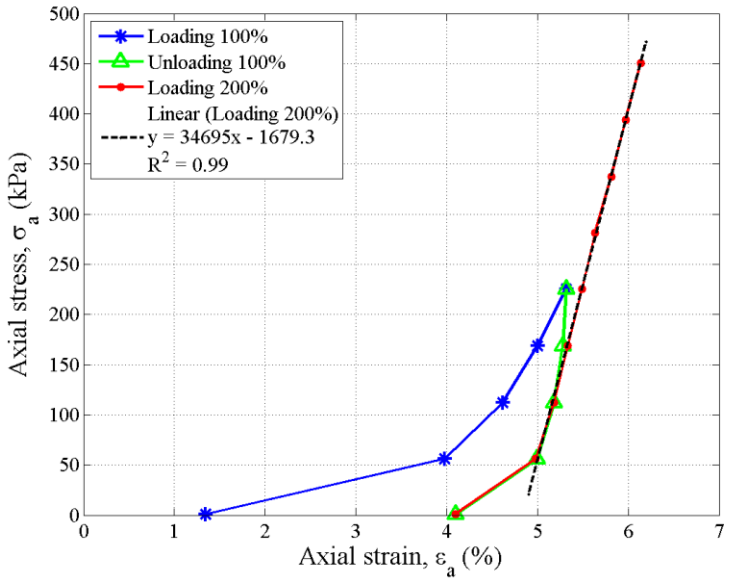

Figure 4-20: Oedometer test results

4.6.5 Triaxial test results

To determine the strength characteristic of the Centrifuge Sand Mix, triaxial tests were also conducted on the sand.

Three triaxial tests were conducted on the Centrifuge Sand Mix at 25 kPa, 150 kPa and 300 kPa confining pressures (σ_3'), with the specimens all having approximately the same relative density (≈ 0.80). The 300 kPa maximum confining pressure was chosen as it corresponds to the confining pressure at the bottom of the centrifuge soil model at 30-*g*, similar to the oedometer test. All the soil test specimens were dry and were kept dry for the duration of the test. In this section, the results obtained from the three dry triaxial compression tests are presented. These

results include the initial conditions of each specimen, the shear strength results (i.e. φ', c') as well as the local strain measurement results (E_{sec}). Procedures for the drained triaxial compression test was based on ASTM Standard D7181-11.

4.6.5.1 Initial conditions

The initial conditions for each of the triaxial tests are listed in **Table 4-11**. Soil specimens were prepared in the triaxial mould and membrane at a relative density corresponding to the maximum packing density obtained from air pluviation. The relative density was calculated using the values for the maximum and minimum dry densities mentioned in Section 4.6.3. As mentioned, triaxial tests were conducted on dry soil specimens, thus the moisture content was assumed to be 0% for all the tests.

Table 4-11: Triaxial tests – initial conditions

Initial condition parameter	Triaxial 1 (σ_3' = 25 kPa)	Triaxial 2 (σ_3' = 150 kPa)	Triaxial 3 (σ_3' = 300 kPa)
Moisture content (%)	0	0	0
Dry density (kg/m^3)	1700	1692	1703
Void ratio (G_s = 2.689 g/cm^3)	0.59	0.60	0.58
Relative density	0.78	0.75	0.80

4.6.5.2 Shear strength results

The shear strength parameters, i.e. the angle of friction (φ') and cohesion (c'), of the Centrifuge Sand Mix were determined by plotting the deviatoric stress invariant, t', against the mean stress invariant, s', which represents the maximum shear and normal effective stress values, respectively. Values for t' and s' were calculated using **Equation 4-10** and **Equation 4-11**, respectively. **Figure 4-21** indicates the stress paths for the results obtained from the triaxial tests on the Centrifuge Sand Mix in the t', s'- space, at different confining pressures. The relative density for each test was approximately 0.80, as indicated in Section 4.6.5.1.

$$t' = \frac{1}{2}(\sigma_1' - \sigma_3') \qquad \textbf{Equation 4-10}$$

$$s' = \frac{1}{2}(\sigma_1' + \sigma_3') \qquad \textbf{Equation 4-11}$$

where,

σ_1' = maximum principal stress [M L^{-1} T^{-2}]

σ_3' = minimum principal stress (confining pressure) [M L^{-1} T^{-2}]

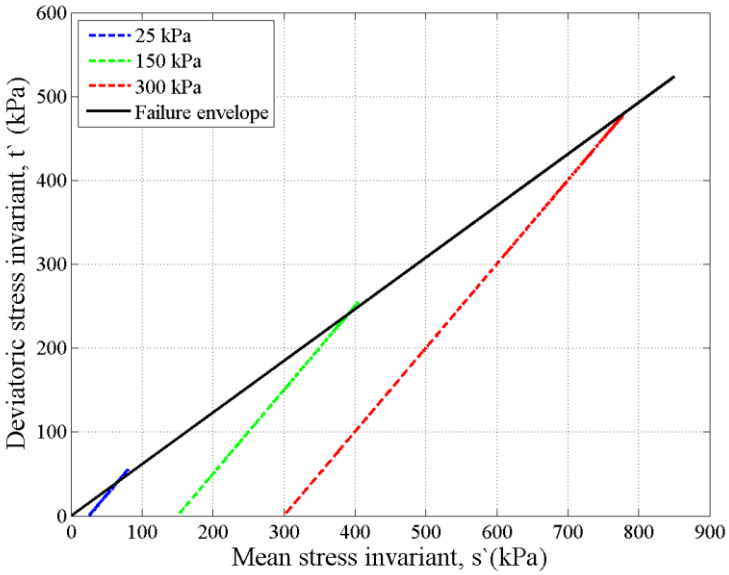

Figure 4-21: Stress path results – 80% RD

The failure envelope was drawn on the stress paths graphs in **Figure 4-21**, which connects the top of each stress path, forming a tangent line. By drawing this failure line in the *t'*, *s'*- space, the friction angle of the Centrifuge Sand Mix could be determined by using **Equation 4-12**. Values for the calculated friction angle are presented in **Table 4-12**, as well as the cohesion. Due to the fact that the Centrifuge Sand Mix was dry, the cohesion was not calculated but assumed to be 0 kPa.

$$tan\,\theta = sin\,\varphi' \qquad \textbf{Equation 4-12}$$

where,

θ = angle from the tangent line in the *t'*, *s'*- space [˚]

Table 4-12: Shear strength parameters – triaxial tests

Friction angle, φ' (˚)	Cohesion, c' (kPa)
32	0

4.6.5.3 Local strain measurement results – secant modulus

As mentioned previously, due to the non-linear stress-strain behaviour of soils, estimating a representative soil stiffness is one of the more difficult soil parameters to obtain. A value for

the soil stiffness, i.e. Young's modulus, can be derived in several ways from a non-linear stress-strain relationship obtained from a test conducted on a soil specimen.

From the triaxial test results for each of the respective confining pressures, the maximum principle stress (σ_1') or axial stress was plotted as a function of the axial strain. Axial strains were measured using linear variable differential transformers (LVDTs) that were mounted to the side of the soil specimen in the triaxial during the tests. The secant modulus was then calculated and plotted against the axial strain. Secant modulus is defined as the slope of a line drawn from the origin of a stress-strain diagram to any point of interest along the stress-strain curve. These values indicate the stiffness of the soil at both small-strains, as well as large working strains. The secant modulus can be determined using **Equation 4-13**.

$$E_{sec} = \frac{\sigma_a}{\varepsilon_a} \qquad \textbf{Equation 4-13}$$

where,

σ_a = axial stress [M L^{-1} T^{-2}]

ε_a = axial strain [-]

Figure 4-22 indicates the secant modulus as a function of axial strain. Initially, at small-strains, the secant modulus is high, ranging between 300 and 600 MPa. However, with an increase in axial strain, the secant modulus decreased to a value of less than 100 MPa above an axial strain of 0.1%.

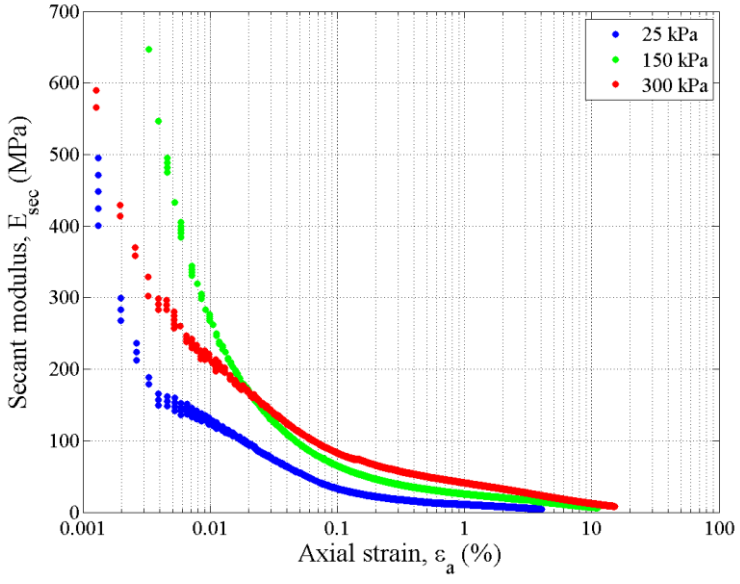

Figure 4-22: Secant modulus – 80% RD

4.6.6 Ultimate pile capacity

From the measured properties of the pile and the soil above, the ultimate pile capacity can be calculated. This is based on the methods presented by Poulos & Davis (1980), originally proposed by Broms (1964b), taking into account the properties of both the pile and the surrounding soil. The ultimate lateral load (H_u) and maximum bending moment (M_{max}) in the pile can be calculated by using **Equation 4-14** and **Equation 4-15**, respectively.

$$H_u = \frac{0.5\,\gamma\,D\,L^3\,K_p}{e_L + L} \qquad \textbf{Equation 4-14}$$

$$M_{max} = H_u[e_L + \frac{2}{3}(0.82)\sqrt{\frac{H_u}{DK_p\gamma}}] \qquad \textbf{Equation 4-15}$$

where,

γ = unit weight of the soil [M L^{-2} T^{-2}]

D = diameter of the pile [L]

L = embedment length of the pile [L]

K_p = passive earth pressure coefficient [-]

e_L = load eccentricity from soil surface [L]

The ultimate lateral load and maximum bending moment in the pile at model scale were calculated as indicated in **Table 4-13**. Calculations predicted that the scaled aluminium and reinforced concrete piles should yield before the soil fails, indicating that both piles can be considered as long piles. Thus, the maximum bending moment indicated in **Table 4-13** corresponds to the yielding moment of the pile and not the moment required to cause soil failure. Even though not shown in **Table 4-13**, the reinforced concrete pile would crack at a lateral load (H_{crack} = 46.1 N) smaller than the ultimate load, at a bending moment of approximately 2.7 Nm. It is interesting to note that even though the reinforced concrete pile had a higher flexural rigidity, the ultimate lateral load and maximum moment for the reinforced concrete pile was significantly smaller than that of the aluminium pile. Although both scaled piles were supposed to model a full-scale reinforced concrete pile with a diameter of approximately 600 mm, the use of aluminium for modelling full-scale reinforced concrete piles should be questioned due to the ultimate capacity that is significantly larger than that typically expected for a reinforced concrete pile. As indicated in the literature, the majority of tests on

scaled metal piles in the past were carried out at very high loads due to their application in offshore structures, which would probably not be representative for reinforced concrete piles. The horizontal loads applied in this experiment were limited to loads causing moments:

- Smaller than the cracking moment of the reinforced concrete pile.
- Between the cracking and yield moment of the pile – which would typically be service conditions for reinforced concrete.
- Exceeding the yielding moment of the reinforced concrete pile.

Table 4-13: Ultimate capacities of the piles

Pile type	γ (kN/m^3)	D (mm)	e_L (mm)	φ' (˚)	H_u (N)	M_{max} (Nm)
Aluminium	16.7	19.2	37.5	32	695.1	82.8
Reinforced concrete	16.7	21.1	37.5	32	76.6	4.9

4.7 MEASURING EQUIPMENT

This section describes the equipment, apart from the strain gauges, that was used for measuring the behaviour and response of the piles in the centrifuge. This included equipment for measuring the lateral displacement of the pile above and below the soil surface, as well as the load being applied to the pile.

Placement of all of the strain gauges were discussed in Section 4.3. The rest of the measuring equipment can be seen in this section, as well as in Section 4.8, showing the full model set-up.

4.7.1 Linear Variable Differential Transformer (LVDT)

Lateral displacement of the pile at both the pile cap and the soil surface were measured using linear variable differential transformers (LVDTs). Displacement at the pile cap and soil surface were measured using a 10 mm HBM LVDT (WI/10mm-T) and 5 mm HBM LVDT (WI/5mm-T), respectively. Rotation of the pile cap was measured using two additional 5 mm HBM LVDTs (WI/5mm-T). **Figure 4-23** indicates the 10 mm and 5 mm HBM LVDTs that were used for measuring lateral displacements and pile cap rotation during the centrifuge tests.

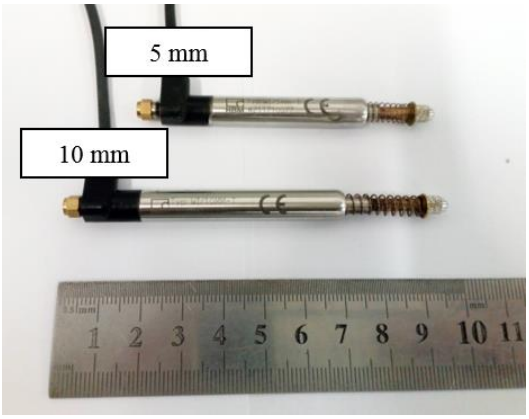

Figure 4-23: Linear variable differential transformer (LVDT) – centrifuge model

4.7.2 Mini-extensometer measurement system

The lateral displacement of the pile below the surface of the soil could not be measured using linear variable differential transformers (LVDTs). To accommodate measurement of sub-surface pile displacements, a measurement system was placed inside the strongbox. The measurement system consisted of metal strips that had been instrumented with 120 Ω precision resistance strain gauges, clamped to an aluminium block. The strain gauges were connected to form half- Wheatstone Bridges. A hypodermic needle, fixed to the side of the pile at specific locations (Section 4.3), extended through the soil to the instrumented metal strips that was preloaded. The hypodermic needle was placed inside a sheath to limit the effect of soil friction. As the pile was loaded laterally, movement of the pile below the soil surface was transferred via the needles to the metal strips, causing the metal strips to deflect, creating lateral mini-extensometers. The metal strips were preloaded to ensure continuous contact between the needles and the metal strips for the duration of the test. During model preparation soil was placed with caution around these needles, ensuring that the density, or particle packing, is the same as with the rest of the soil model. Confining pressures of the soil prevented the thin slender needles to buckle and deflect vertically. **Figure 4-24** shows a schematic of the centrifuge model cross-section, focusing on the mini-extensometer measuring system, as explained above, and its placement in the centrifuge strongbox. The front and back view of the mini-extensometer measurement system is indicated in **Figure 4-25**.

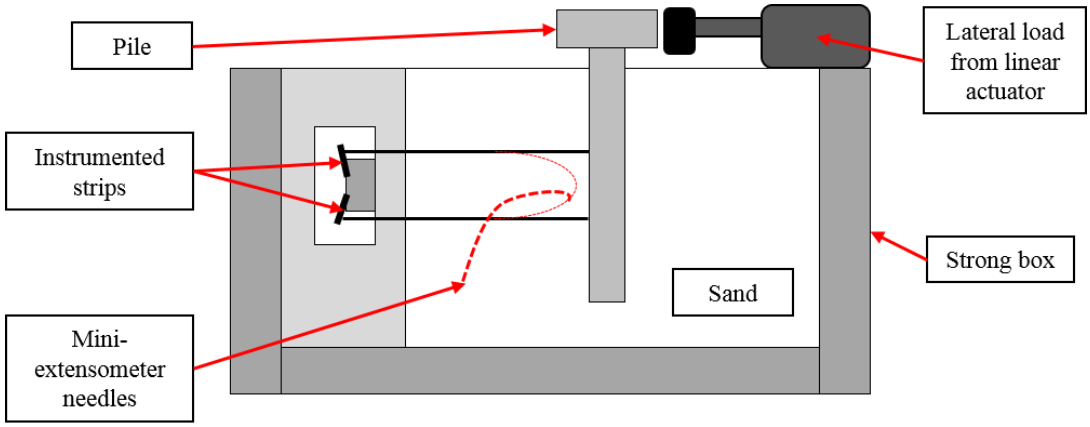

Figure 4-24: Centrifuge model cross-section – mini-extensometer

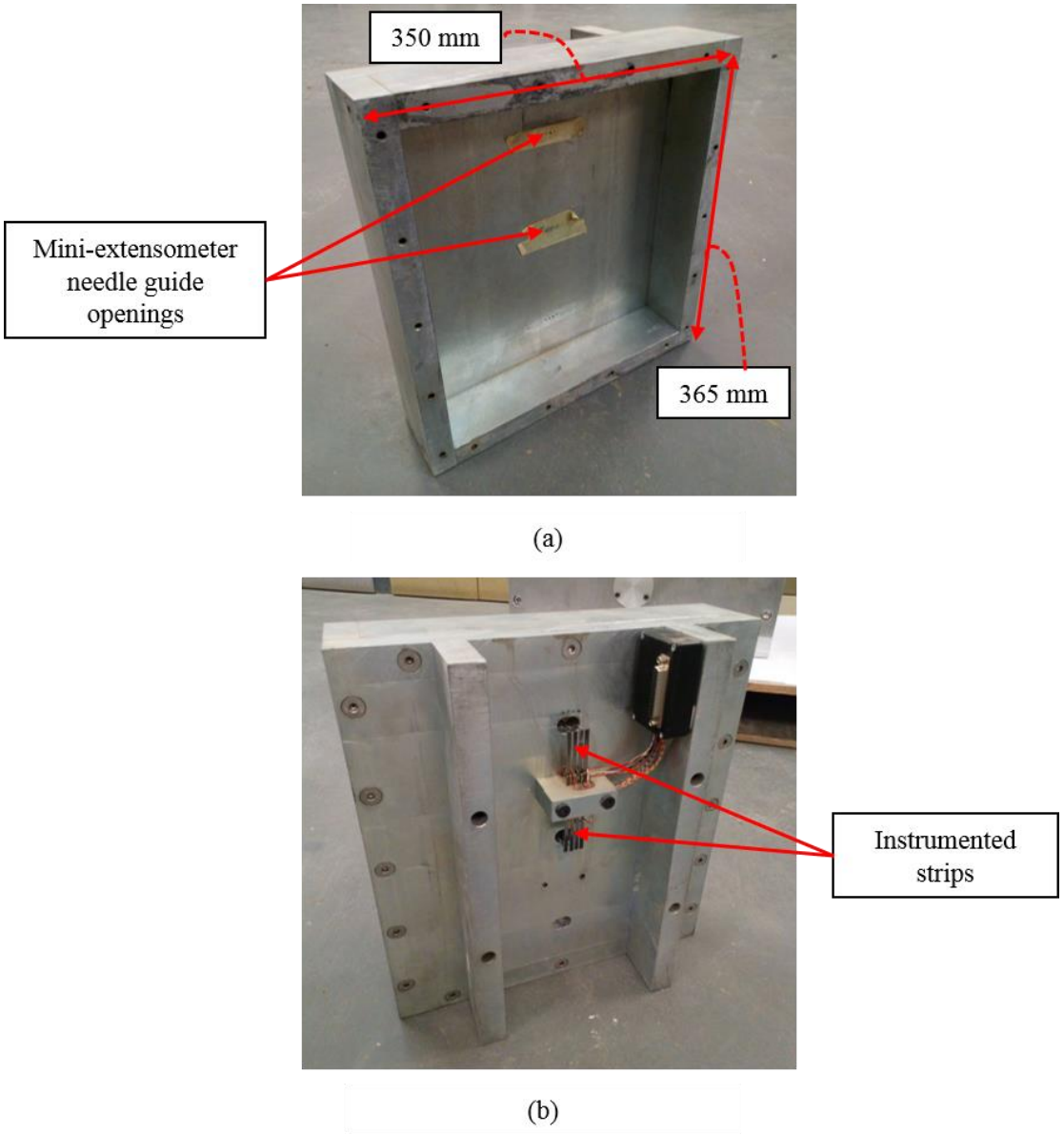

Figure 4-25: Mini-extensometer measurement system: (a) front view, (b) back view

4.7.3 Linear actuator and load cell

A one-way (compressive) lateral load was applied to the pile at 37.5 mm above the surface of the soil and was kept constant for all the tests in the centrifuge, as this dissertation is not concerned with the effect of load eccentricity on the behaviour of laterally loaded piles. The one-way lateral load applied to the pile cap was exerted using a 500 N SKF linear actuator (CAHB-10-B3A-050213-ACCAPD-000). Based on literature it was decided to use a one-way lateral load, due to the fact that it should have the largest influence on the behaviour of the pile and the surrounding soil. A 500 N HBM button load cell (C9C 0.5kN 1mV/V) was attached to the front of the linear actuator shaft to measure the magnitude of the corresponding load that was applied to the pile cap. **Figure 4-26** indicates the linear actuator, as well as the button load cell used for all the centrifuge tests.

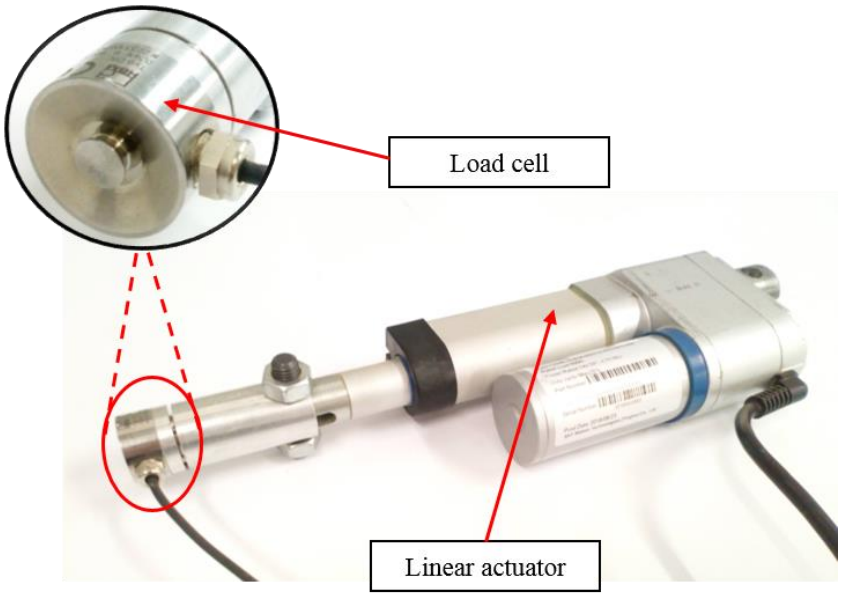

Figure 4-26: Linear actuator and load cell

4.8 MODEL SET-UP AND TESTING PROCEDURE

This section provides information on the procedures followed to prepare and set-up the various soil-pile models. The focus of the study is to determine the behaviour of a scaled aluminium and reinforced concrete piles, subjected to lateral loading, to establish whether hollow aluminium sections can be used to accurately model the monotonic and cyclic response of reinforced concrete sections. A total of three tests were conducted in the centrifuge, two on the aluminium pile and one on the scaled reinforced concrete pile. The first test on the scaled aluminium pile was a monotonic lateral load test, followed by a second test on the same scaled aluminium pile, where the pile was exposed to cyclic loading and the behaviour was observed.

The test on the scaled reinforced concrete pile consisted of a cyclic load test only. Both the scaled aluminium and reinforced concrete piles were instrumented in the same way, allowing for comparisons to be drawn.

A brief description of the model preparation and testing procedures is as follows:

- The scaled aluminium or reinforced concrete pile was placed in the centre of the strongbox (model container), at the correct height, ensuring a 350 mm embedment length in the soil. As indicated in Section 4.2.3, the inside depth of the strongbox was 400 mm, allowing for a 50 mm space (≈ two times the pile diameter) between the pile tip and the bottom of the strongbox. Georgiadis *et al.* (1992) indicated that to minimise the influence of the base of the box, two or more pile diameters should be sufficient. Upon pile placement, prior to sand pluviation, the instrumented strips for the mini-extensometer system were preloaded by the hypodermic needles attached to the pile to ensure continuous contact.
- The sand was pluviated into the strongbox from a height of 1600 mm. Care was taken near the mini-extensometer needles, and around the pile diameter to ensure sufficient contact between the pile and surrounding soil.
- The sand was pluviated up to the top of the centrifuge strongbox, 400 mm above the base of the box.
- The same procedure was followed with regard to the placement of the sand in the strongbox for all three tests, ensuring a constant relative density.
- After pluviation, the surface was scraped to a level surface.

The test models were loaded onto the centrifuge platform, where after all the electronic measuring equipment was connected, and the tests conducted. Apart from the mini-extensometers measuring lateral displacement of the pile below the soil surface, the LVDTs measuring the lateral displacement of the pile at the pile cap and soil surface, as well as the rotation of the pile cap, were fixed to an aluminium bracket that spanned over the length of the strongbox. The linear actuator and load cell were fixed to the side of the strongbox at a height that corresponded to the centre of the pile cap. CATMAN software was used to log the displacement, load and strain data, respectively. **Figure 4-27** contains a schematic of the full centrifuge model cross-section, showing all the measuring equipment.

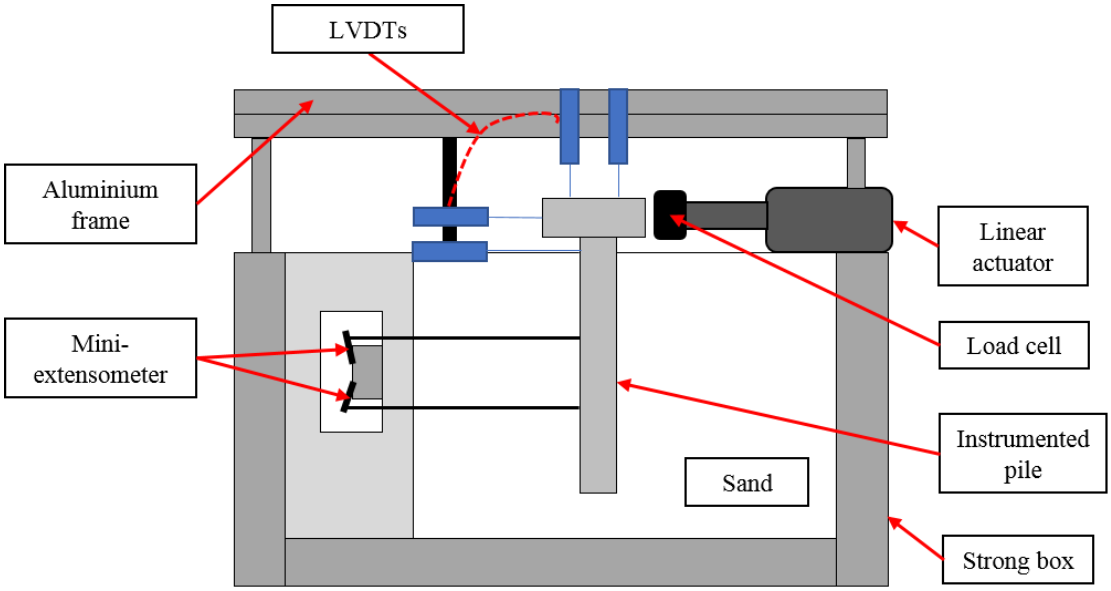

Figure 4-27: Centrifuge model cross-section – whole model

Strain gauges were attached to the side of the pile, as indicated previously, but is not indicated. **Figure 4-28** indicates the typical model set-up for both the aluminium and scaled reinforced concrete pile tests, excluding the aluminium bracket and measuring equipment, with **Figure 4-29** showing the complete model set-up.

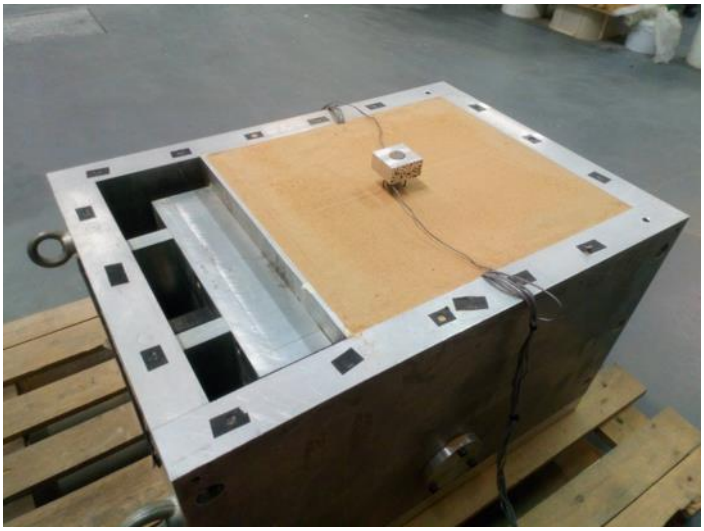

Figure 4-28: Typical model set-up

The approximate density, and corresponding relative density, of each of the centrifuge test models were recorded after model preparation and air pluviation. All tests on the models were carried out at 30-*g*. After conducting the three tests, the observed and measured data was prepared and analysed. The results are presented and discussed in Chapter 5.

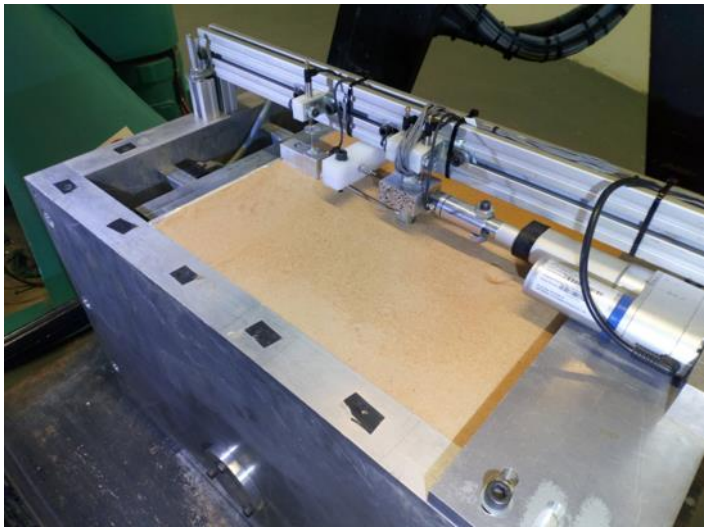

Figure 4-29: Complete model set-up

5 RESULTS AND DISCUSSIONS: CENTRIFUGE TESTS

5.1 INTRODUCTION

In this chapter, the results obtained from the centrifuge tests are discussed. As mentioned previously, a total of three tests were conducted at 30-*g*, the first being a monotonic lateral loading test on the scaled aluminium pile, followed by a cyclic lateral load test on the same scaled aluminium pile and lastly a cyclic lateral load test on the scaled reinforced concrete pile. The monotonic and cyclic load tests on the aluminium pile allowed for differentiation between the behaviour of the same pile under monotonic and cyclic conditions. The cyclic loading tests on both the scaled aluminium pile and reinforced concrete pile allowed for comparisons to be drawn between the two piles.

The first part of this chapter comprises of the measured densities of the soil models tested in the centrifuge. These densities were used to determine and check the necessary properties of the soil in Chapter 4. These properties were then used to predict the pile-flexibility factor, indicating whether the pile can be considered as short or long.

The rest of the chapter contains the results from each of the tests mentioned above, observing and comparing their behaviour under monotonic and cyclic lateral loading conditions, indicating the mechanisms that possibly give reason for their behaviour. Furthermore, each section of the results on the three tests concludes with a comparison of the measured data in the centrifuge to numerically and theoretically predicted values, using the LPILE student version program, similar to what was used during the parametric study. This aided in determining the validity of the experimentally measured results.

5.2 CENTRIFUGE TESTS SOIL DENSITIES

The densities of the soil models for all the centrifuge tests were measured after model preparation before testing in the centrifuge. This was to ensure that the density of the soil for all the soil models after pluviation were within a narrow range in order to make it possible to compare results. This was also to verify whether the tests conducted for classifying the soil in Chapter 4 were correct. A summary of the densities and the corresponding relative density obtained from each soil model is tabulated in **Table 5-1**.

Table 5-1: Densities of soil models

Test name	Density (kg/m^3)	Relative density, D_r
Monotonic scaled aluminium pile	1680	0.70
Cyclic scaled aluminium pile	1685	0.72
Cyclic scaled reinforced concrete	1691	0.75

5.3 SOIL-PILE FLEXIBILITY FACTOR

Apart from the fact that soil is highly non-linear, the relative stiffness, or pile-flexibility factor, of the soil-pile system can give a good indication of the typical behaviour of the pile, whether it can be considered as a short or a long pile. Besides the Young's modulus of the soil and flexural rigidity of the pile, the embedment length of the pile is also important for determining the pile-flexibility factor. As indicated in Chapter 4, both the scaled aluminium and reinforced concrete piles had an embedded length of 350 mm ($L_m/D_m \approx 17.5$), with 50 mm extending above the soil surface.

After considering the various parameters mentioned above, the pile-flexibility factor could be calculated. By applying the formulas set up by Poulos & Davis (1980) and Poulos & Hull (1989), the pile flexibility factor (K_R) and critical length (L_c) could be calculated, as is indicated in **Table 5-2**, assuming the scaled reinforced concrete section was still uncracked. It should be emphasised that, as mentioned previously, the relative stiffness theory is based on purely linear elastic analysis, assuming that the Young's modulus of the soil and the flexural stiffness of the pile remains constant. However, soil is a highly non-linear material, with a Young's modulus that changes as the strains within the soil increases. Reinforced concrete also exhibits highly non-linear material behaviour after cracking. The rigidity factor would be sensitive to both these changes and this could affect the overall response of the soil-pile system. Thus, for discussion purposes, the pile-flexibility factor and critical length was also determined for the cracked reinforced concrete section, assuming that the Young's modulus of the soil remains constant for simplicity. However, changes in the Young's modulus of the soil will have an effect on the relative rigidity of the soil-pile system.

Based on the information provided in **Table 5-2**, and the ranges specified by Poulos & Davis (1980) and Poulos & Hull (1989), an interesting observation was made. Based on the results from the critical length (Poulos & Hull, 1989), both the scaled aluminium and reinforced concrete piles could be considered long. However, when considering the pile-flexibility factor (Poulos & Davis, 1980) calculated for both the scaled aluminium and reinforced concrete piles, both factors fell between the ranges specified for a short and long pile, with the pile not behaving completely as a short pile or a long pile. The pile-flexibility factor for the reinforced

concrete pile was also higher than that of the aluminium pile while the reinforced concrete pile was still uncracked. However, as the reinforced concrete section cracked, and the flexural rigidity of the pile changed, the flexibility factor decreased significantly, with the pile response leaning more towards the behaviour of a long pile, which was not the case with the aluminium pile with an unchanged flexural stiffness. In addition, literature indicated a densification of the soil that would take place due to cyclic loading. With the Young's modulus of the soil that is difficult to quantify, in theory, densification of the soil will result in the Young's modulus increasing which will decrease the flexibility factors of both piles. This will result in both piles behaving as long piles.

Table 5-2: Pile-flexibility factor calculations

Pile type	Flexural rigidity, E_mI_m (MNmm^2)	Soil Young's modulus, E_s (MPa)	Embedded length, L_m (mm)	Pile-flexibility factor, K_R	Critical length, L_c (mm)
Scaled aluminium	194.3	47	350	0.28×10^{-3}	200
Scaled uncracked reinforced concrete	316.1	47	350	0.45×10^{-3}	226
Scaled cracked reinforced concrete	18.0	47	350	0.026×10^{-3}	110

5.4 MONOTONIC RESPONSE OF THE SCALED ALUMINIUM PILE

Before considering the cyclic response of the scaled aluminium and reinforced concrete piles, analysis and discussions first focus on the response of the scaled aluminium pile to monotonic loading, modelling the short-term behaviour of the pile to loading. For the monotonic test on the scaled aluminium pile, a lateral load was applied to the top of the pile in one direction in order to observe the response of both the soil and the pile to the applied load. During this test the pile was loaded horizontally to a load of 100 N at model scale, which corresponded to the safe allowable lateral load for a 600 mm free-headed concrete pile at full-scale, as suggested by Winterkorn & Fang (1975). The horizontal load of 100 N corresponds to 15% of the ultimate capacity of the aluminium pile of 695 N. For the monotonic load test on the scaled aluminium pile, the focus was on the lateral load-displacement and bending moment response of the pile to an increase in load magnitude, which showed similar results to that observed in literature.

5.4.1 Load-displacement response

Figure 5-1 shows the load-displacement response of the scaled aluminium pile for the entire monotonic test. It can be seen that, as the lateral load (H) increased up to 100N (full-scale load

of 90 kN), the displacement of the pile head (y_h) also increased in the horizontal direction, as expected. A permanent pile head displacement of about 0.25 mm was observed after unloading the pile. It should also be noted that the lateral displacement of the pile head did not reach a plateau at applied loads, indicating that the ultimate failure of the soil was not reached during this test.

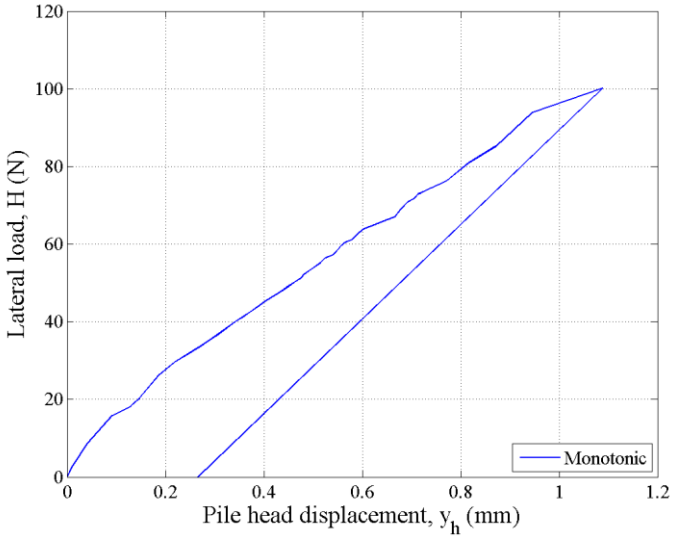

Figure 5-1: Load-displacement response – monotonic aluminium test

5.4.2 Bending moment and lateral pile displacement response

In order to determine the influence of the magnitude of the lateral load on the response of the pile, in particular, both the bending moment and lateral displacement of the pile were observed.

From the equations in Chapter 4, the bending moments could be calculated and plotted from the strain measured in the pile. **Figure 5-2** presents the bending moment (M) experienced along the length of the pile for various load magnitudes during the monotonic test up until 200 mm below the surface of the soil where the strain was measured. The bending moments were plotted against the depth below the soil surface (z_s) to better visualise the response in terms of depth into the soil. Positive values on the y-axis of the figure referred to the position above the soil surface and negative below the soil surface. It was assumed that the bending moment at the point of load application (z_s = 37.5 mm) was zero. As illustrated in **Figure 5-2**, an increase in the magnitude of the lateral load resulted in an increase in the bending moment experienced by the pile, which was expected. For a load magnitude of 25 N, the maximum measured bending moment occurred at 60 mm below the soil surface, and at 100 mm below the soil surface for the higher loads indicated, which corresponded to approximately three and five pile diameters, respectively. It should also be mentioned that with an increase in the magnitude of the applied

load, a linear increase in the maximum bending moment was observed, similar to what was seen in literature for low loads.

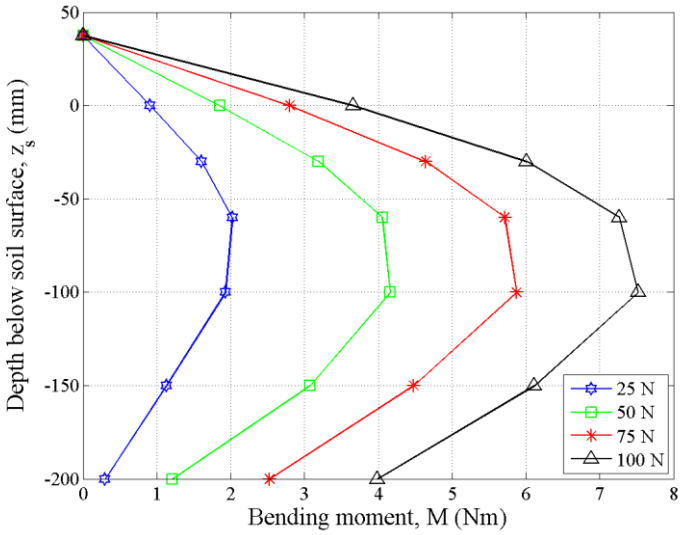

Figure 5-2: Bending moment with depth – monotonic aluminium test

The lateral displacement of the pile (y_p) was plotted along the length of the pile, as indicated in **Figure 5-3**, for the same load magnitudes as with the bending moments during the monotonic test. The lateral displacement was only plotted up to 215 mm below the surface of the soil where the lateral displacement was measured. These values were measured using the equipment described in Section 4.7.

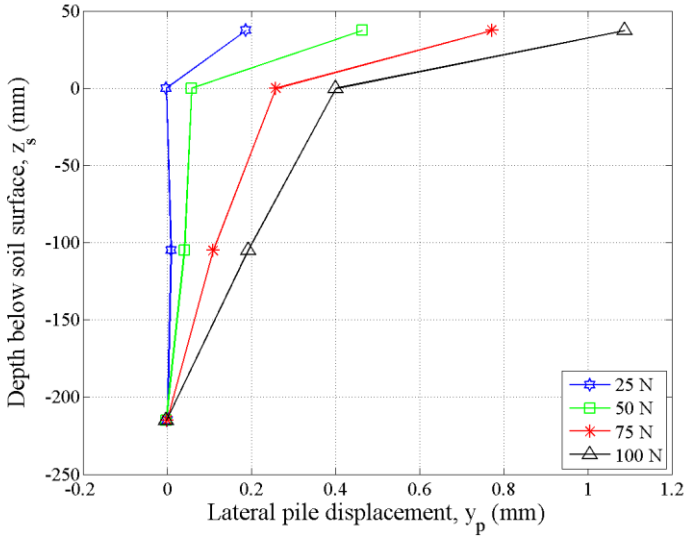

Figure 5-3: Lateral pile displacement with depth – monotonic aluminium test

The lateral pile displacements were plotted against the depth below the soil surface (z_s). As expected for all the load magnitudes, the maximum lateral movement of the pile occurred at the position of load application (z_s = 37.5 mm), with the magnitude of displacements reducing with an increase in depth below the soil surface. At low loads, the majority of the movement of the pile was concentrated at the pile head, with minimal movement occurring below the soil surface. However, as the horizontal load magnitude increased, more of the soil surrounding the pile was disturbed, resulting in the pile experiencing movement below the soil surface.

5.4.3 Comparison to load-displacement techniques

In order to determine the validity of the results obtained from the monotonic test on the scaled aluminium pile in the centrifuge, the results were compared to that predicted by the LPILE student version program. The LPILE program was used during the parametric study in Chapter 3, observing the behaviour between the pile and the surrounding soil while allowing for non-linear soil behaviour to be incorporated. Similar procedures were followed during this analysis, conducting the analysis on a full-scale pile in sand. However, for this analysis the actual pile dimensions and properties were used, as well as the measured soil properties, assuming that the sectional properties of the pile remained constant. Based on the observed behaviour from Georgiadis *et al.* (1992) regarding the stiffnesses of the soil proposed by Reese *et al.* (1974) and Murchison & O'Neill (1984) which underestimated the bending behaviour of the pile, the stiffness of the soil was not assumed but determined through an iterative process to obtain the best fit. A coefficient of subgrade reaction of 2.4 MN/m^3 was selected for the sand used in all the centrifuge models.

Furthermore, to aid in comparing the predicted values to the measured values, the results from the centrifuge scale model had to be converted to full-scale values by applying the appropriate scaling laws. **Figure 5-4** indicates the comparison between the measured and predicted bending moments and lateral displacements of the pile. **Figure 5-4 (a)** and **(b)** indicate the measured bending moment and lateral displacement results from the centrifuge test at full-scale, as well as the predicated results using the LPILE program, for a monotonic load of 50 N and 100 N, respectively. It can be seen that the selected coefficient of subgrade reaction resulted in a good approximation of the measured bending moment and lateral displacement results of the pile. However, the measured lateral displacement at the soil surface did not seem to be in agreement with the predicted shape and seems to be incorrect.

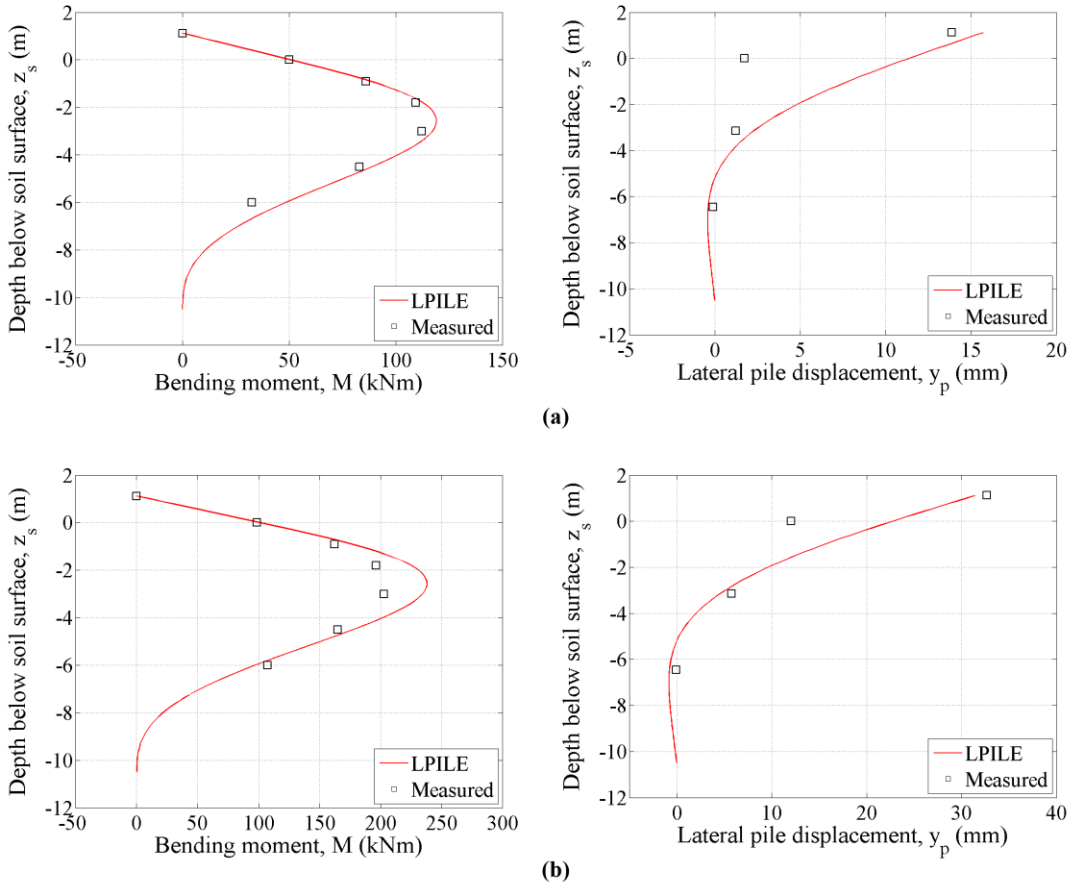

Figure 5-4: LPILE comparison with bending moment and lateral pile displacement results at full-scale from monotonic test: (a) 50 N, (b) 100 N – aluminium

5.4.4 Summary

Results observed for the scaled aluminium pile under monotonic loading conditions include the following:

- As the magnitude of the applied load increased the bending moment and the lateral displacement of the pile also increased.
- Permanent displacement of the pile occurred after load removal.
- At low load magnitudes, the maximum measured bending moment occurred three pile diameters below the surface of the soil, increasing to five pile diameters at higher load magnitudes.
- The maximum displacement of the pile occurred above the soil surface, at the location of load application.
- At low load magnitudes, the lateral movement of the pile primarily occurred above the surface of the soil. However, as the magnitude of the applied load increased, more soil

surrounding the pile was disturbed, resulting in the rest of the pile below the soil surface to experience movement.

- The measured bending moment and lateral displacement results from the centrifuge test were in good agreement with the predicted values from the LPILE software package.

5.5 FIRST LOAD CYCLES

In line with the soil-pile flexibility factor, before considering the behaviour of both the scaled aluminium and reinforced concrete pile under cyclic loading conditions, the first load cycle for both the cyclic load tests on the scaled aluminium and reinforced concrete piles were investigated. This allowed for comparison between the two piles, at low loads under the condition that both piles were responding within their elastic region (uncracked in the case of the reinforced concrete pile) and the surrounding soil had no prior load history. For the first load cycle on the scaled aluminium pile, the pile was loaded to about 40 N, whereas for the scaled reinforced concrete pile, the pile was loaded to 30 N. **Figure 5-5** indicates the load-displacement response of the scaled aluminium and reinforced concrete for these first load cycles. As the lateral load (*H*) increased, the displacement of the pile also increased. The response of the scaled reinforced concrete pile was stiffer than that of the scaled aluminium pile, which was expected based on the flexural rigidity for each of the piles indicated. Due to the higher flexural stiffness, the scaled reinforced concrete pile experienced less permanent displacement than that of the scaled aluminium pile, regardless of the magnitude of the applied load.

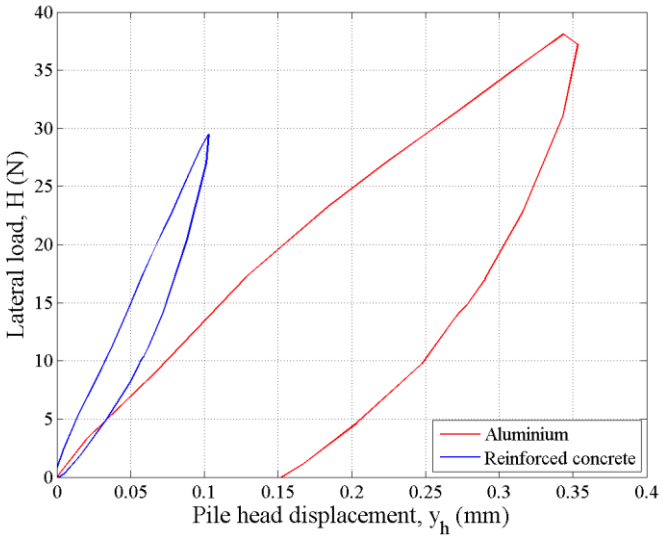

Figure 5-5: Load-displacement results - first load cycle

To justify the assumption that both the scaled aluminium and reinforced concrete piles exhibited material behaviour that can be assumed to be elastic under these loads, the bending strain (ε_b) along the length of the pile was plotted for both the tension (T) and compression (C) side of the pile (see **Figure 5-6**). **Figure 5-6 (a)** and **(b)** indicate the strain response of the scaled aluminium and reinforced concrete piles, respectively for an applied load of 10 N and 30 N. From **Figure 5-6** it can be seen no cracking or yielding had occurred for both the scaled aluminium and reinforced concrete piles (elastic material behaviour), with the response of the pile being almost symmetrical on both the tension and compression side of each of the piles.

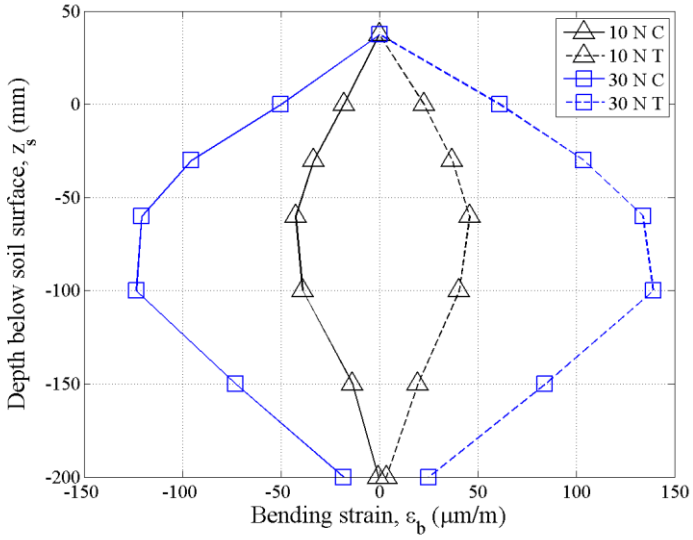

(a)

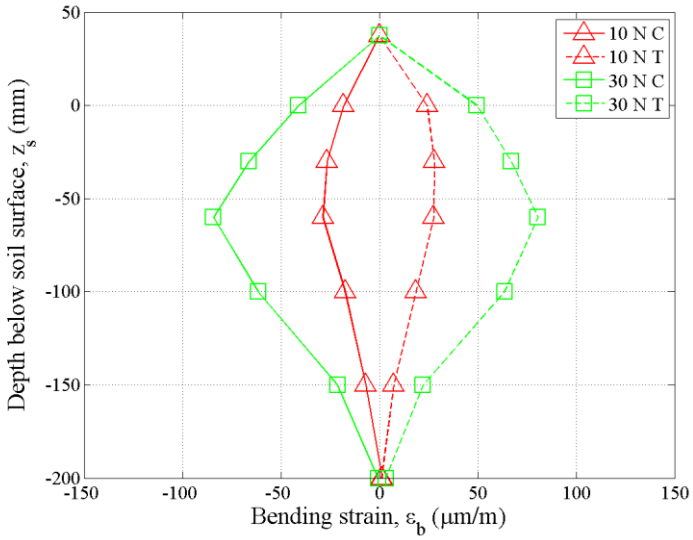

(b)

Figure 5-6: Strain development: (a) aluminium, (b) reinforced concrete first load cycle

Furthermore, by converting the strain results above, using the appropriate material properties, the bending moment experienced by the pile could be determined, as indicated in **Figure 5-7** for both the scaled aluminium and reinforced concrete piles. As illustrated in **Figure 5-7**, at an applied load of 10 N for both the piles, the bending moments were for all practical purposes the same. However, as the magnitude of the applied load increased to 30 N, a change in the bending moment experienced by the scaled reinforced concrete pile was observed towards the bottom of the pile in comparison to that of the scaled aluminium pile, with lower moments developing in the section of the reinforced concrete pile that was deeper below the surface level. At these loads, it was assumed that the reinforced concrete section was still uncracked, thus the difference could potentially only be due to the change in the pile-soil rigidity, which is also a function of the Young's modulus of the soil, that is affected by the load history. The small differences can also be attributed to the formation of micro-cracks in the concrete.

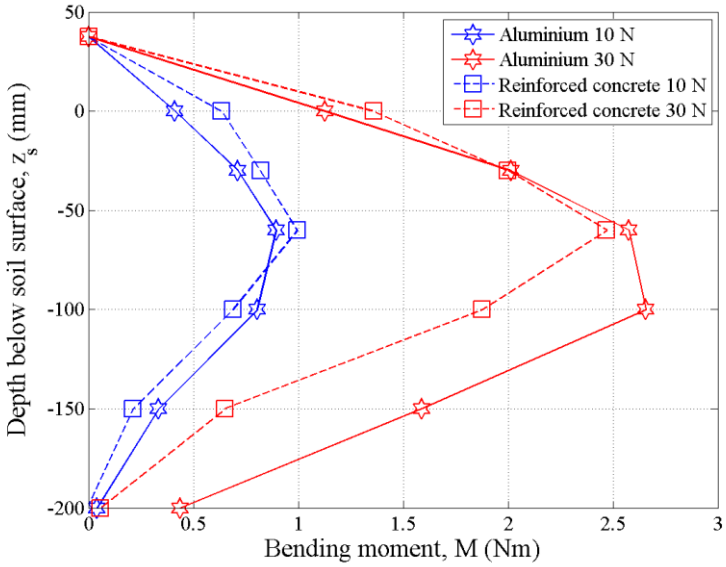

Figure 5-7: Bending moment with depth - first load cycle

After establishing the bending moments in the pile, the lateral displacement of the pile was also plotted, as indicated in **Figure 5-8** for both the scaled aluminium and reinforced concrete pile. As expected, the displacements of the scaled aluminium pile were much higher than that observed for the scaled reinforced concrete pile for an applied load of 10 N and 30 N respectively. This was expected as displacement calculations are concerned with the flexural rigidity of a section, and the flexural rigidity of the scaled aluminium pile was smaller than that of the scaled uncracked reinforced concrete pile.

Based on the observed behaviour for the strain, bending moment and lateral displacement information mentioned above, even at low loads under elastic pile properties, a difference

between the results from the scaled aluminium and reinforced concrete pile was observed. This was an indication that the behaviour of the scaled reinforced concrete pile could not be matched with a scaled aluminium pile, even on the first load cycle at low loads in the same soil having no prior load history. Thus, care should be taken when using hollow aluminium piles for modelling reinforced concrete structures at model scale.

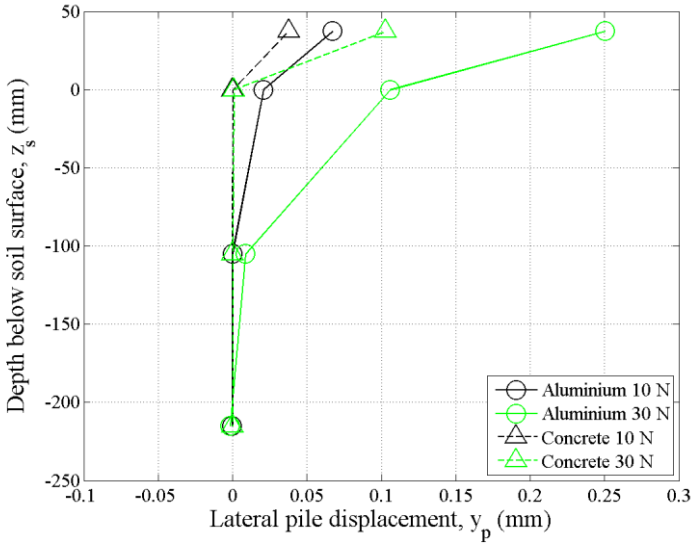

Figure 5-8: Lateral displacement of the pile with depth - first load cycle

5.6 CYCLIC RESPONSE OF THE SCALED ALUMINIUM PILE

As with the monotonic test, a cyclic lateral load was applied to the top of the same scaled aluminium pile to observe the response of both the soil and the pile to repeated applied loads. By loading the pile cyclically, the long-term behaviour of the aluminium pile to repeated loading could be determined. The cyclic lateral load test on the aluminium pile was also conducted to a maximum load magnitude of about 100 N (Winterkorn & Fang, 1975), corresponding to 15% of the ultimate capacity of the aluminium pile of 695 N. In this way, the response of the pile to cyclic loading could be investigated and compared to that of the monotonic test results. Furthermore, for this test, the focus was on lateral load-displacement and bending moment response of the pile, as well as the absolute and secant stiffness of the soil-pile system, observing the behaviour of the aluminium pile to both an increase in load magnitude and the number of load cycles.

5.6.1 Applied load cycles

During the cyclic load test of the aluminium pile, the pile was subjected to three different load magnitudes, applying these loads for a number of cycles to the top of the pile. A small number

of load cycles were applied at a relative low load magnitude, followed by much larger number of load cycles at higher load magnitudes to observe long-term cyclic effects. **Table 5-3** indicates the average horizontal force (lateral load) that was applied to the pile cap, and the number of load cycles for which the pile experienced that force. It should be noted that the entire test was conducted on a single model in the centrifuge with the pile being loaded successively to each load magnitude.

Table 5-3: Average horizontal load and number of cycles – aluminium

Average horizontal load (N)	Number of cycles, *N*
50	300
90	1000
110	1000

5.6.2 Load-displacement response

Figure 5-9 indicates the load-displacement response of the aluminium pile for the entire cyclic lateral load test, with the lateral load (H) plotted on the y-axis and pile head displacement (y_h) on the x-axis. The load-displacement response of the aluminium pile for the monotonic test is also shown in the same figure to compare the behaviour of the pile under both monotonic and cyclic loading conditions. From **Figure 5-9** it can be seen that the only difference between load-displacement curves of the two tests were the permanent displacement experienced by the pile, where the permanent displacement of the cyclic test was much higher than that of the monotonic test.

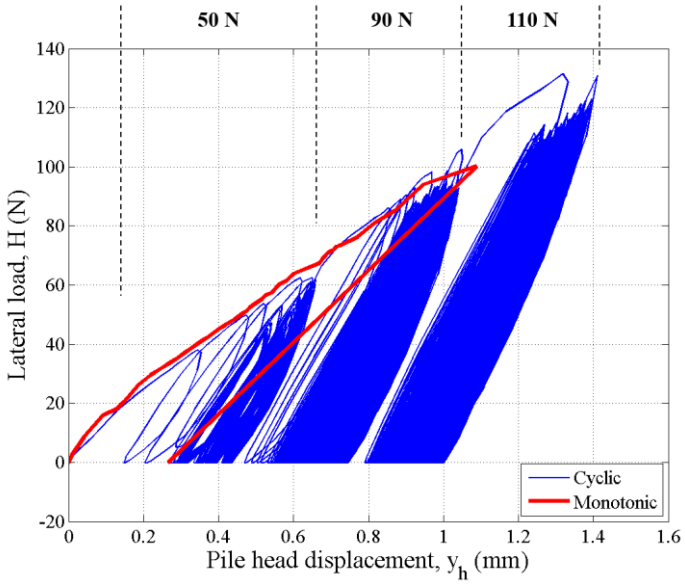

Figure 5-9: Load-displacement response – cyclic aluminium test

Furthermore, the slope of the loading curve for the monotonic test matched well with the slope generated by the cyclic lateral loading, as the magnitude of the applied load increased. This illustrated that the maximum displacement of the pile is only affected by the magnitude of the applied load, and not by the number of load cycles at a particular load. Thus, the only difference between the two tests was the permanent displacement of the pile after load removal. Lastly, these results also confirm that the trends observed from centrifuge testing are repeatable

As mentioned previously, the pile was loaded successively with the three load magnitudes and is shown in **Figure 5-9**, with perfect load control not being possible. By considering the cyclic results only, it can be seen that, as the magnitude of the lateral load increased, the displacement of the pile head also increased, as expected, with the permanent displacement also increasing with both load magnitude and number of load cycles. The cyclic response indicates large permanent displacement in the first few cycles at each load, becoming resilient after about 10 cycles. This is similar to what was observed by Werkmeister *et al.* (2004) within the plastic shakedown range (range A).

5.6.3 Bending moment response

It is important to consider the behaviour and response of the pile itself to cyclic lateral loading. Therefore, the effect of load magnitude and number of cycles on the bending moment response of the pile was investigated. However, before considering the effect of cycles on the bending moment behaviour of the pile, it was important to first consider the difference between the bending moments, at a particular lateral load magnitude, under both monotonic and cyclic loading conditions, as mentioned by Poulos (1982). **Figure 5-10** indicates the bending moment (M) development along the length of the pile under both monotonic and cyclic loading conditions.

These bending moments experienced by the pile was as a result of the applied lateral load (H) at the top of the pile. Similar to the monotonic test, the bending moments were plotted against depth below the soil surface (z_s) to better visualise the response in terms of depth into the soil. **Figure 5-10 (a)** and **(b)** indicates the response of the pile for both the monotonic and cyclic lateral load tests at 50 N and 90 N, respectively. Loads to 110 N could not be compared, due to the fact that, for the monotonic test, the pile was only loaded to 100 N. As illustrated in **Figure 5-10**, the results from the monotonic and cyclic tests at the same load magnitudes showed similar responses. The maximum measured bending moment under both the monotonic and cyclic loading conditions occurred at 100 mm below the soil surface and was unaffected by the number of load cycles that was applied to the pile. By considering the peak bending moment, which occurred some location between the measured bending moments, peak moment moves deeper with an increasing number of load cycles. It should however be noted that the loads

compared in **Figure 5-10** were significantly lower than the ultimate load capacity of the pile (within 15% of the estimated ultimate load capacity).

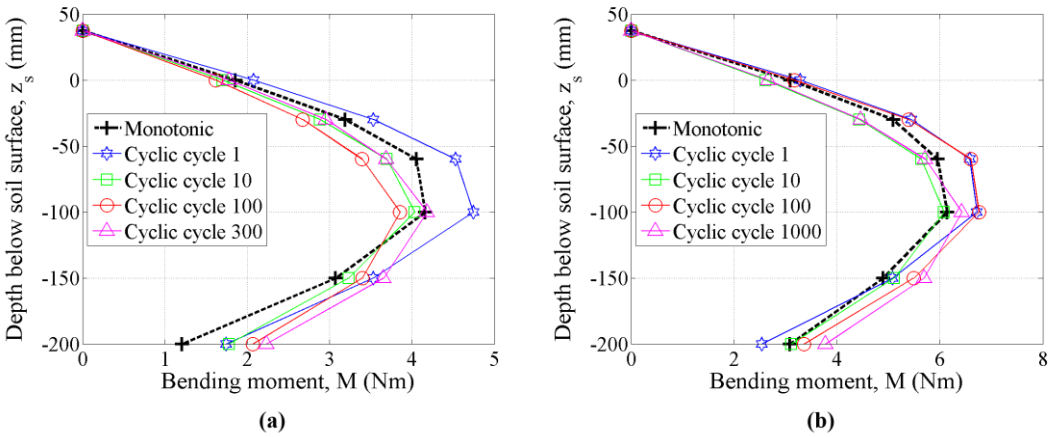

Figure 5-10: Comparison between monotonic and cyclic bending behaviour: (a) 50 N, (b) 90 N – aluminium

Figure 5-11 indicates the bending moment development along the length of the pile under cyclic conditions only. The bending moments were also plotted against depth below the soil surface. **Figure 5-11 (a)**, **(b)** and **(c)** indicates the response of the pile for cyclic lateral loads with magnitudes of 50 N, 90 N and 110 N, respectively. For each of the load magnitudes, only a few of the load cycles were indicated for discussion purposes. To determine the effect of the number of load cycles on the bending moment response, the bending moments for each of the load magnitudes were normalised by the bending moment experienced at the soil surface (M_h) as indicated in **Figure 5-11**. The bending moment at the soil surface was taken as the bending moment measured by the strain gauges at that location.

It can be seen in **Figure 5-11** that, as the magnitude of the applied lateral load increased, the bending moment response of the pile also increased, similar to the monotonic test. The maximum measured bending moment occurred approximately five pile diameters below the soil surface (100 mm). By observing the normalised bending moment diagrams, it can be seen that an increase in number of load cycles had minimal influence on the bending moment response towards the top of the pile when the lateral load was applied. However, at and below approximately five pile diameters the influence is more significant, which differs from what Kirkwood & Haigh (2014) observed.

Kirkwood & Haigh (2014) indicated that the development of permanent bending moments (M_{per}), or locked-in moments in the pile should be considered as it explains certain behaviours

of the pile under cyclic loading. These moments are permanent bending moments that remained in the pile after the lateral load is removed (H = 0 N) and is indicated in **Figure 5-12**.

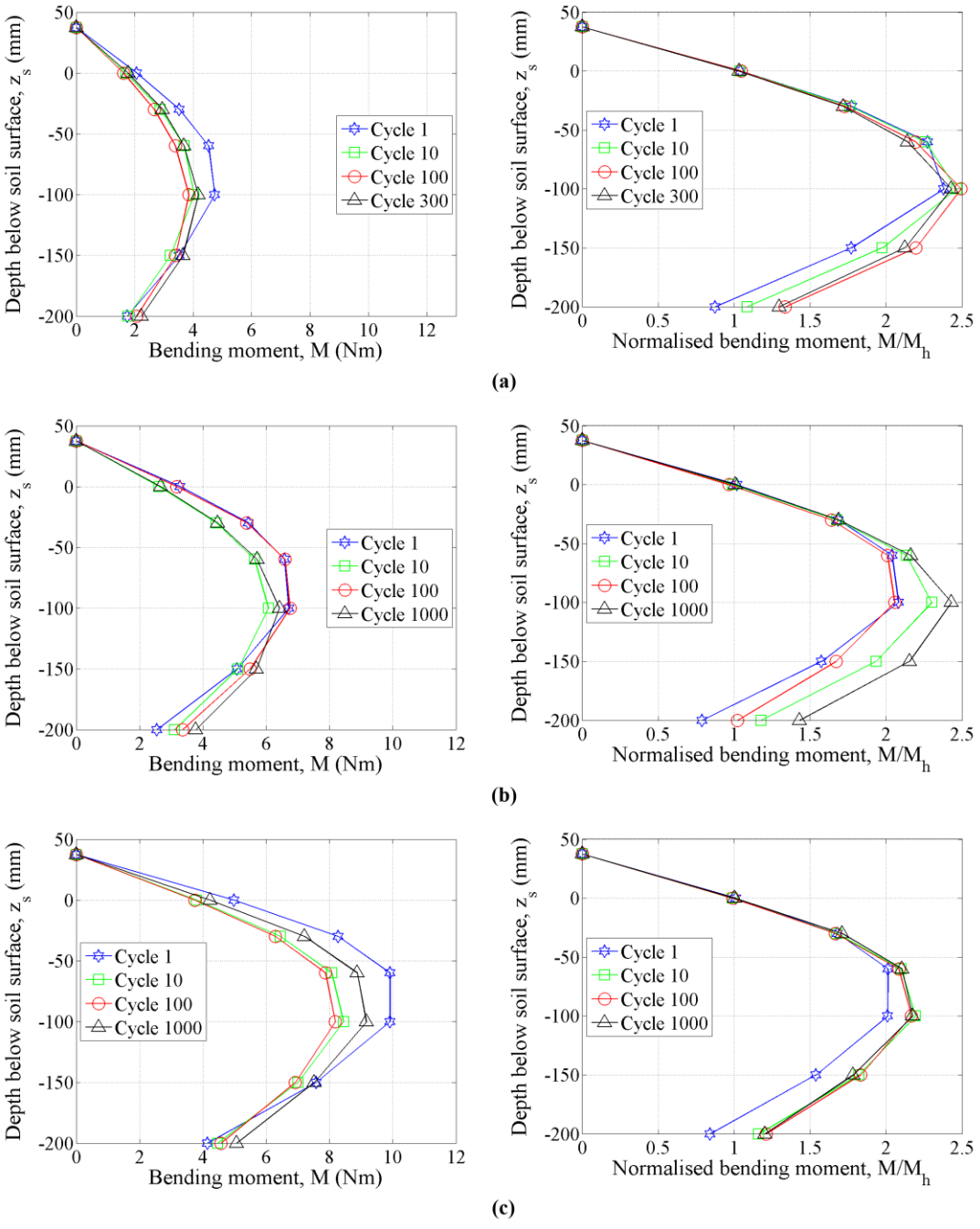

Figure 5-11: Bending moment and normalised bending moment with depth: (a) 50 N, (b) 90 N, (c) 110 N – aluminium

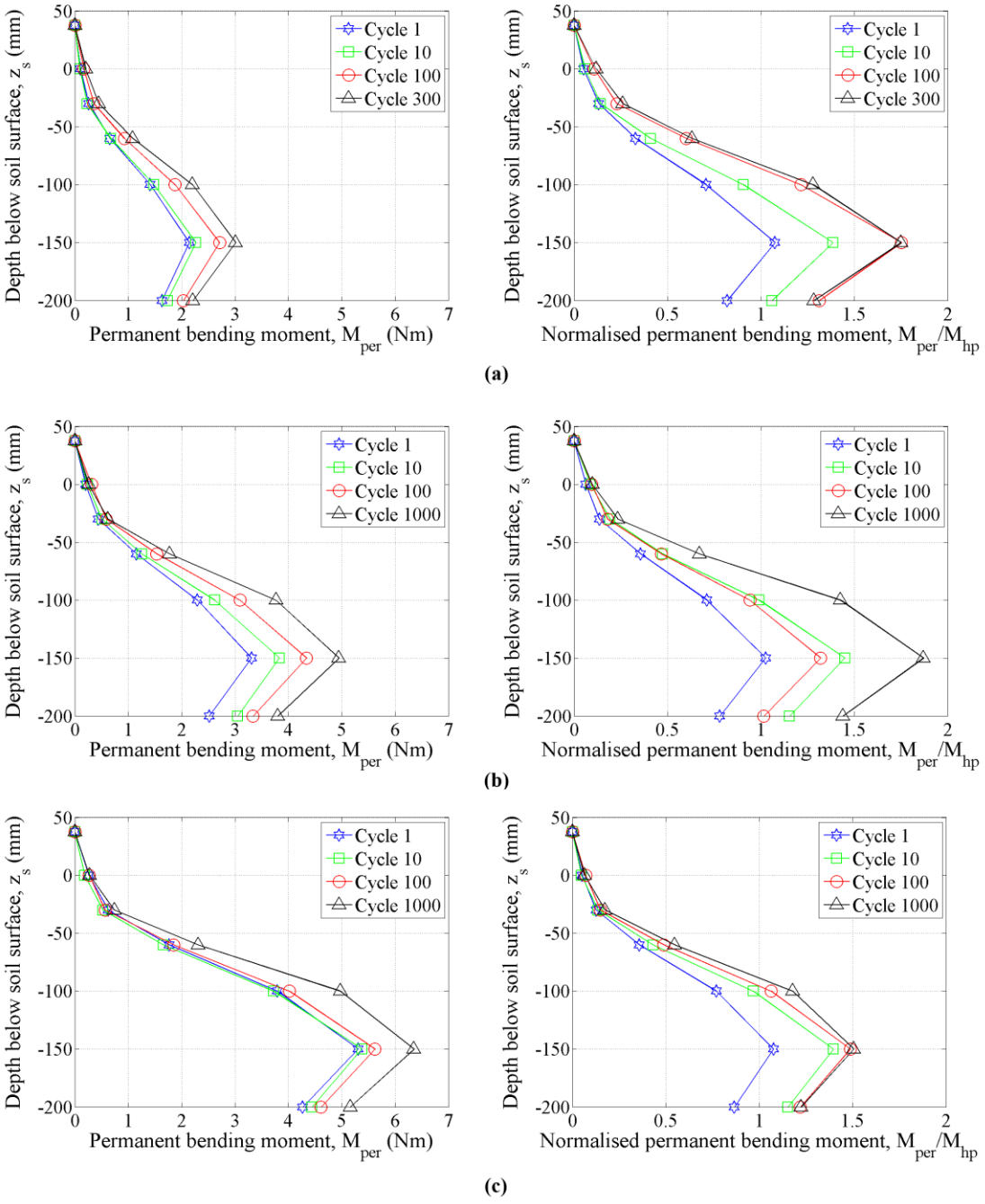

Figure 5-12: Permanent bending moment and normalised bending moment with depth: (a) 50 N, (b) 90 N, (c) 110 N – aluminium

The permanent bending moments were plotted against depth below the soil surface, similar to the bending moments above. **Figure 5-12 (a)**, **(b)** and **(c)** indicates this permanent response of the pile after the cyclic lateral loads, with magnitudes, 50 N, 90 N and 110 N, respectively, have been removed. Only the results of a few of the load cycles were presented for each of the load magnitudes for discussion purposes. To determine and better visualise the effect of number of

load cycles on the permanent bending moment response, the permanent bending moments for each of the load magnitudes were normalised with the bending moment at the soil surface (M_{hp}) from the previous load cycle when the load was applied, and is also indicated in **Figure 5-12**. The bending moment at the soil surface was taken as the bending moment measured by the strain gauges at that location from the previous load cycle.

It can be seen in **Figure 5-12** that, as the magnitude of the applied lateral load increased, the permanent bending moment response of the pile increased. Furthermore, it should be mentioned that the permanent bending moments recorded after the 90 N and 110 N load cycles also included the permanent moments from the previous load cycles and load magnitudes. Regardless of that, the trend between locked-in moments and number of load cycles can be observed. The maximum locked-in moments occurred approximately seven pile diameters below the soil surface (150 mm). Looking at the normalised bending moment diagrams for the locked-in moments, it can be seen that as the number of load cycles increased at the same load magnitude, the permanent bending moments also increased, which is similar to what Kirkwood & Haigh (2014) observed. These locked-in moments were as a result of the changing soil conditions surrounding the pile creating locked-in soil stresses in response to the applied cyclic lateral loads.

Figure 5-13 illustrates the combined bending and permanent bending moment distributions along the length of the pile compiled from **Figure 5-11** and **Figure 5-12**, respectively, for the different load magnitudes. This shows the magnitude of the permanent bending moments that were left in the pile after the load had been removed. **Figure 5-13 (a)**, **(b)** and **(c)** indicates both the bending moment and permanent bending moment response of the pile under load magnitudes of 50 N, 90 N and 110 N, respectively. It should be noted that the maximum measured bending moment occurred at 100 mm below the surface of the soil and the maximum measured permanent bending moment at 150 mm below the surface of the soil. Large differences between the bending moment and permanent bending moment existed towards the top of the pile, whereas the difference reduced below 100 mm. The permanent bending moment at 150 mm below the soil surface was about 50% of the bending moment experienced by the pile at that same location under load application. This response was observed for all the load magnitudes. Considering the moments at 200 mm below the soil surface, insignificant differences between the permanent bending moment and the bending moment under load application existed. This was due to the changing soil conditions along the length of the pile caused by cyclic loading, resulting in locked-in soil stresses towards the bottom of the pile.

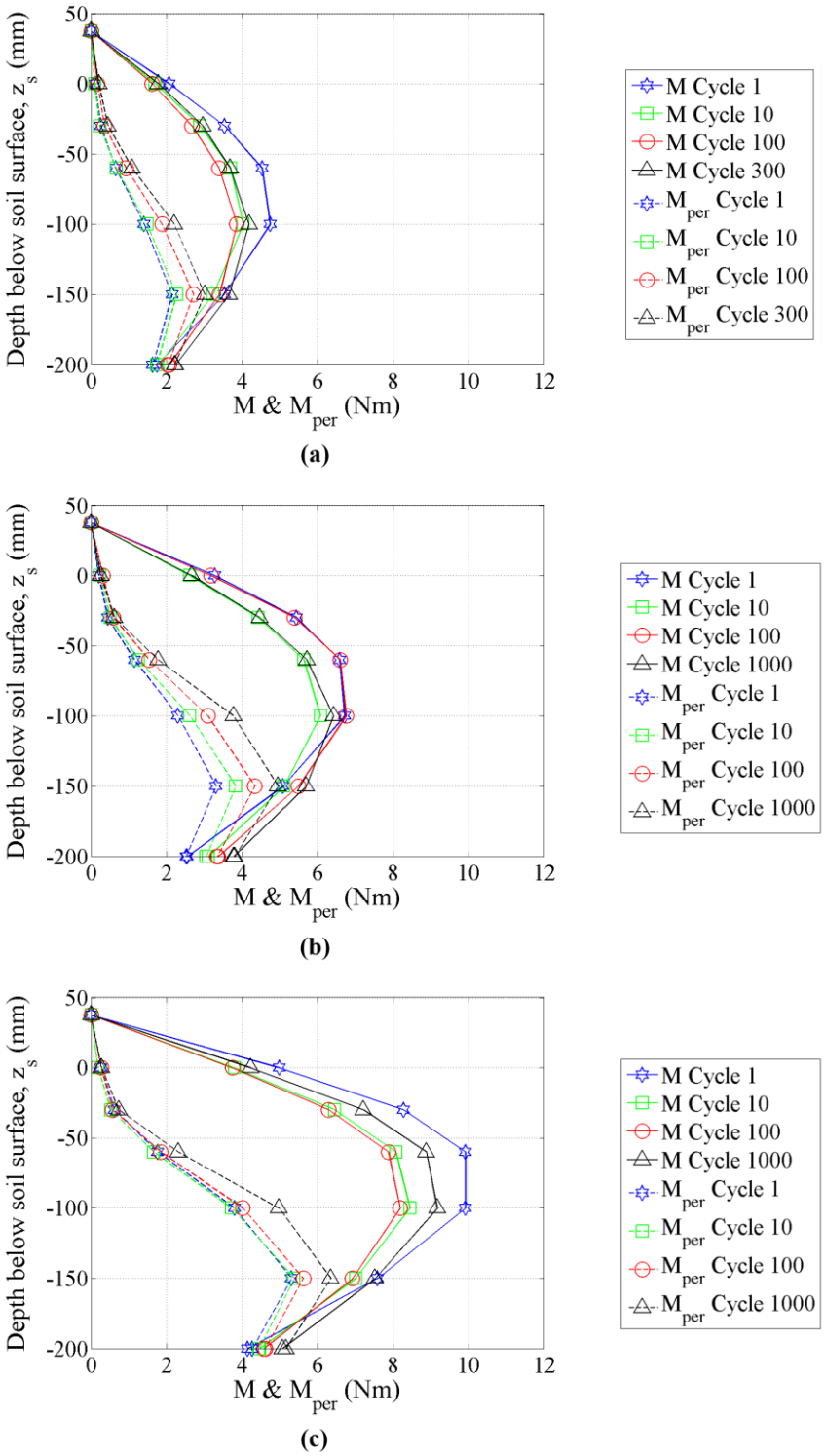

Figure 5-13: Combined bending moment and permanent bending moment with depth: (a) 50 N, (b) 90 N, (c) 110 N – aluminium

5.6.4 Lateral pile displacement

Apart from the bending moment response of the pile to cyclic loading, the lateral displacement of the pile should also be considered under these conditions. This aided in explaining some of

the behavioural trends observed above that could not be explained by the bending moments alone. The effect of load magnitude and number of load cycles on the lateral displacement response were investigated and is discussed here. **Figure 5-14** indicates the lateral pile displacement (y_p) along the length of the pile as a result of the applied cyclic lateral load (H) at the top of the pile. The lateral displacements were plotted against depth below the soil surface (z_s). **Figure 5-14 (a)**, **(b)** and **(c)** indicates the lateral displacement response of the pile to cyclic lateral loads with magnitudes of 50 N, 90 N and 110 N, respectively. For each of the load magnitudes, only a few of the load cycles were indicated, similar to the bending moments above.

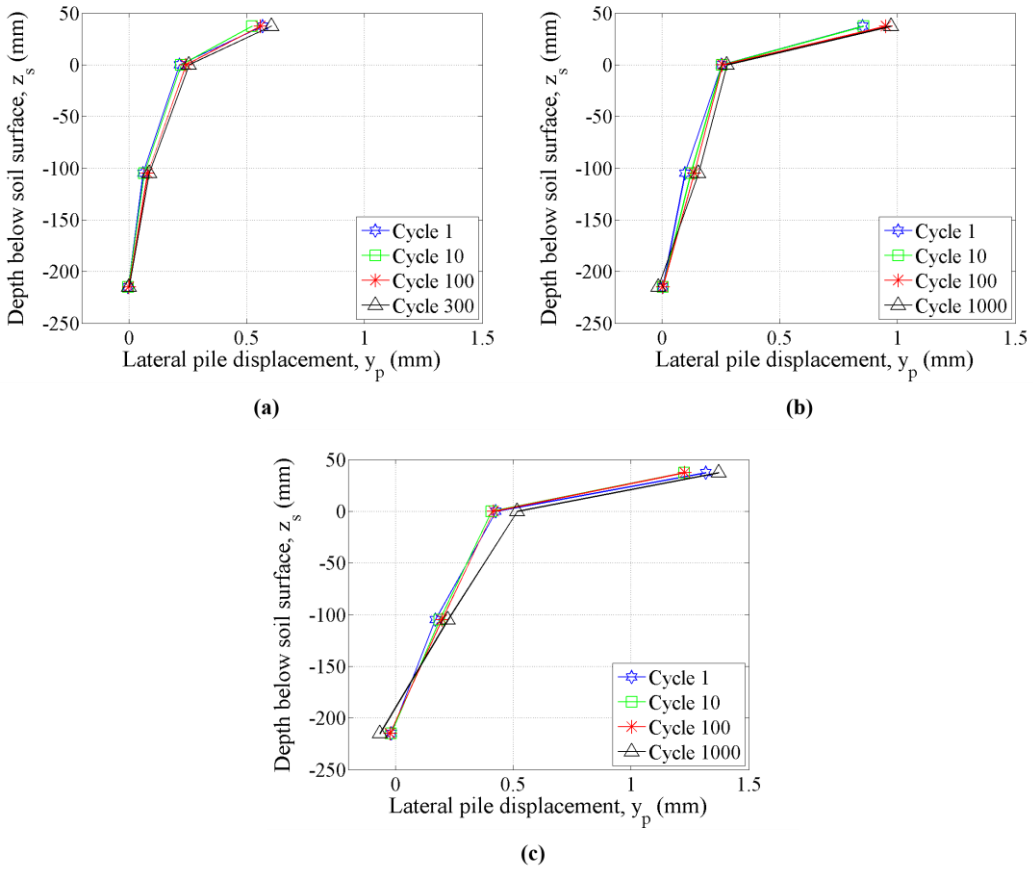

Figure 5-14: Lateral pile displacement with depth: (a) 50 N, (b) 90 N, (c) 110 N – aluminium

It can be seen in **Figure 5-14** that, as the magnitude of the applied lateral load increased, the displacement of the pile also increased, similar to the monotonic test. As expected, the maximum displacement occurred at the point of load application (z_s = 37.5 mm). As the number of load cycles at a particular load increased, the lateral displacement of the pile increased minimally, as illustrated. This supports the observation mentioned earlier that only the magnitude of the applied load had an influence on the maximum displacement of the pile and

not the number of load cycles at that particular load. This indicates that the applied loads were small enough that cyclic loading resulted in resilient soil behaviour (Werkmeister *et al.*, 2004).

Furthermore, this behaviour can be observed by plotting the maximum pile head displacement (y_h) and permanent pile head displacement (y_{hper}) against the number of load cycles (N) for each load magnitude, as illustrated in **Figure 5-15**. The maximum pile head displacement is the displacement as a result of the applied lateral load (H), where the permanent pile head displacement is the displacement remaining after the lateral load has been removed (H = 0 N). It can be seen that as the magnitude of the applied load and the number of load cycles increased, both the maximum pile head displacement and permanent pile head displacement increased. The difference between the maximum pile head displacement and the permanent pile head displacement increased with an increase in the magnitude of the applied load. But more significantly, the difference reduced with number of load cycles (densification with number of load cycles).

The permanent pile head displacement explains the observed locked-in moments in the pile mentioned in the previous section, as well as the difference in the load-displacement behaviour between monotonic and cyclic loaded test. Movement of the soil surrounding the pile occurred due to repetitive loading, resulting in permanent displacement of the pile, creating locked-in stresses in the soil and locked-in moments in the pile.

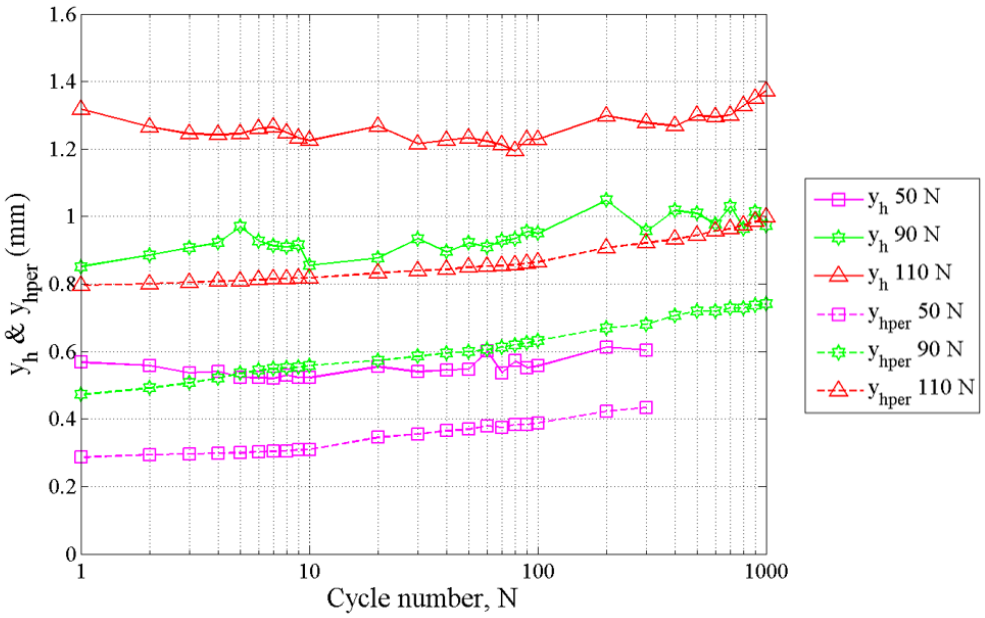

Figure 5-15: Pile head displacement and permanent pile head displacement with number of cycles – aluminium

It should be mentioned that the permanent pile head displacement for the 90 N and 110 N applied loads also included the permanent displacement from the previous load cycles and load magnitudes. Regardless of that, the trend between the permanent lateral displacement of the pile head and number of load cycles could be observed. It is interesting to note the change in the permanent pile head displacement over the number of load cycles. For both 90 N and 110 N lateral loads, 1000 load cycles were applied to the pile. The change in permanent pile head displacement at 90 N was more than that experienced at 110 N, 0.3 mm opposed to 0.2 mm, indicating possible stiffening and densification of the soil that took place due to repeated loading and unloading of the soil, influencing the permanent pile head displacement.

5.6.5 Absolute and secant pile stiffness

As mentioned in Section 2.4.2, the response of the soil-pile system to cyclic loading can be observed by considering the absolute and secant pile stiffnesses respectively, enabling the effect of load magnitude and number of load cycles to be investigated. The pile absolute stiffness (K_N) relates the soil state at cycle N to the initial state for a particular lateral load magnitude. This describes the evolution of the interaction between the pile and the surrounding soil and is defined as the ratio between the applied load and the absolute deflection of the pile at that load (Abadie & Byrne, 2014), and is dependent on the amount of permanent deformation that has taken place at a particular load. For the cyclic test on the aluminium pile in the centrifuge, the test was conducted on a single model, with the same pile being loaded cyclically at various load magnitudes. Thus, due to the magnitude of the lateral cyclic loads not remaining constant for the duration of the test, the initial state of the soil changed for each load magnitude. This was due to the gradual densification of the sand caused by the previous load cycles that had to be taken into account for calculating the absolute stiffness of the soil-pile system. Alternatively, the secant pile stiffness (k_N) relates the state of the soil-pile interaction after N cycles. This behaviour is critical and drives the change in natural frequency of the structure with cycle number (Abadie & Byrne, 2014). Both these concepts are better described by considering **Figure 5-16**, with K_0 being the slope of the first cycle of the load-displacement curves at each new load magnitude. **Figure 5-16 (a)**, **(b)** and **(c)** represent the load-displacement response of the aluminium pile subjected to cyclic lateral loads with magnitudes of 50 N, 90 N and 110 N, respectively. These graphs indicate the first and last cycle for each of the respective loads, demonstrating how the absolute and secant pile stiffnesses were calculated based on the dashed slope lines.

The first cycle of the load-displacement curves, for each load magnitude, exhibited non-linear behaviour of the soil. This is demonstrated by considering the gradient of the load-unload curves. The gradient of the load-unload curves (secant pile stiffness) increased with an increase

in lateral displacement, whereas the absolute pile stiffness decreased. Lastly, for each load magnitude in **Figure 5-16**, the horizontal pile head displacement was not zeroed. Thus, at higher loads, the displacement just before the first load cycle at that load is the permanent displacement caused by the previous loads and load cycles. As seen in **Figure 5-16**, the absolute and secant pile stiffness were calculated from the measured displacement of the pile at the position of load application, keeping in mind that, if the pile displacement was taken at other locations the stiffness response would be different. However, as indicated in the literature (Section 2.4.2), the effect of cyclic loading is largely concerned with the change in stiffness, rather than the stiffness itself.

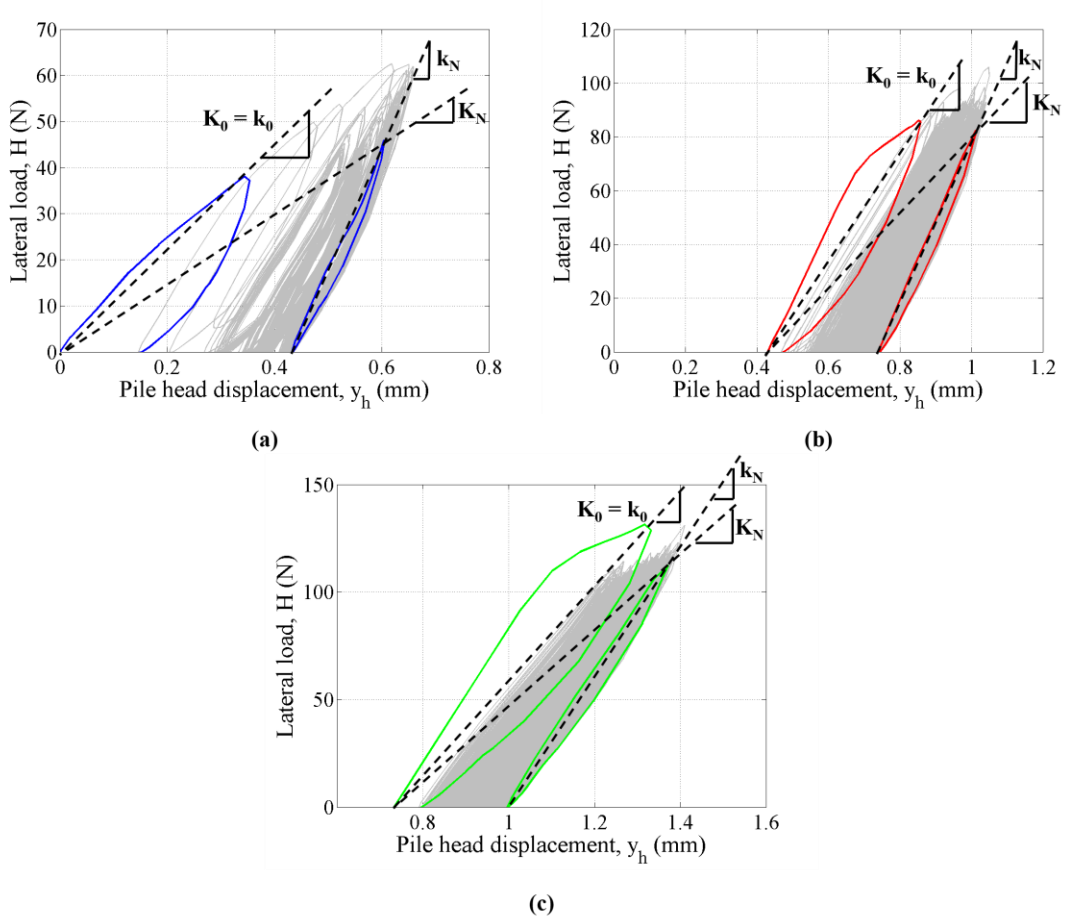

Figure 5-16: Load-displacement response – absolute and secant pile stiffness: (a) 50 N, (b) 90 N, (c) 110 N – aluminium

By considering the absolute pile stiffness as illustrated in **Figure 5-17,** an increase in the initial absolute pile stiffness occurred for each increase in load magnitude. The highest initial stiffness was experienced with the 110 N applied load and the lowest initial stiffness experienced with the 50 N applied load (see initial gradients, K_0, for each load magnitude in **Figure 5-16**). This was due to the gradual densification of the sand, caused by the previous load cycles, increasing

the initial density of the soil prior to the next load magnitude (successive loading of the same pile). It can also be seen that, for each load magnitude, the absolute pile stiffness decreased logarithmically with an increase in number of load cycles, which was expected, as the pile experienced accumulating permanent displacement with an increase in the number of load cycles. This was similar to what Little & Briaud (1988) observed.

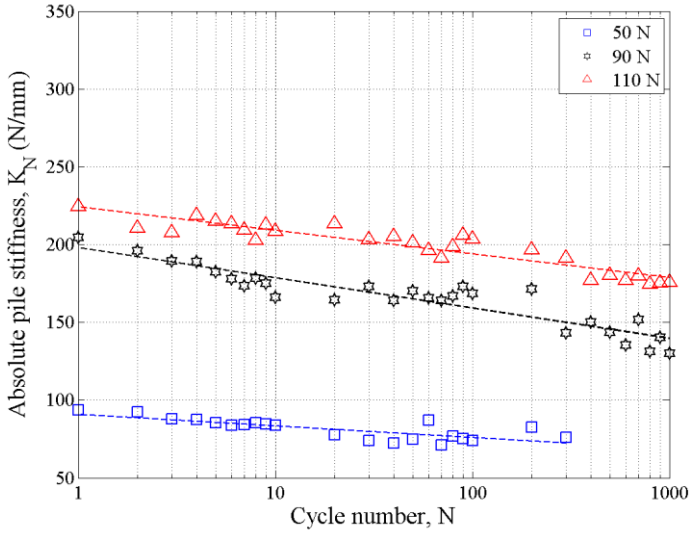

Figure 5-17: Absolute pile stiffness – aluminium

Verdure *et al.* (2003) indicated that to better visualise the effect of number of cycles on pile stiffnesses, the results should be normalised with the stiffness value from the second load cycle (K_1) for a particular load magnitude. This was to remove the non-linear behaviour of the soil during the first load cycle (K_0) at each load increase, as indicated above. By doing this, it can be seen in **Figure 5-18**, that the decrease in absolute pile stiffness was more prominent for lower load magnitudes than for higher load magnitudes. This was due to the higher initial density of the soil at higher loads, caused by the gradual densification of the soil at lower loads, resulting in the rate of increase in permanent displacement of the pile to cycle numbers, decreasing, which explains the behaviour observed from the permanent pile head displacement above.

The secant pile stiffness, as indicated in **Figure 5-19** decrease for each increase in load magnitude, with the highest initial stiffness, k_0, being experienced with the 110 N applied load and the lowest stiffness experienced with the 50 N applied load. This was due to the non-linear behaviour of the soil during the first cycle at each load increase, causing the secant pile stiffness to decrease initially with each new load magnitude. The secant stiffness at 110 N was higher than that at 50 N due to the change in initial density of the soil.

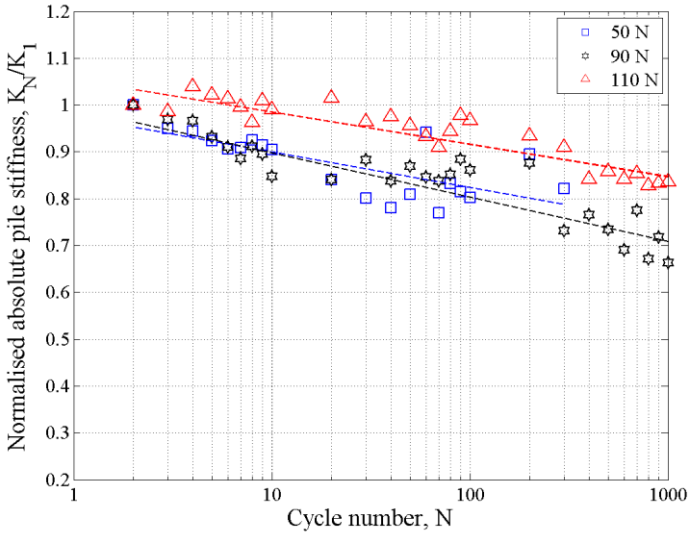

Figure 5-18: Normalised absolute pile stiffness – aluminium

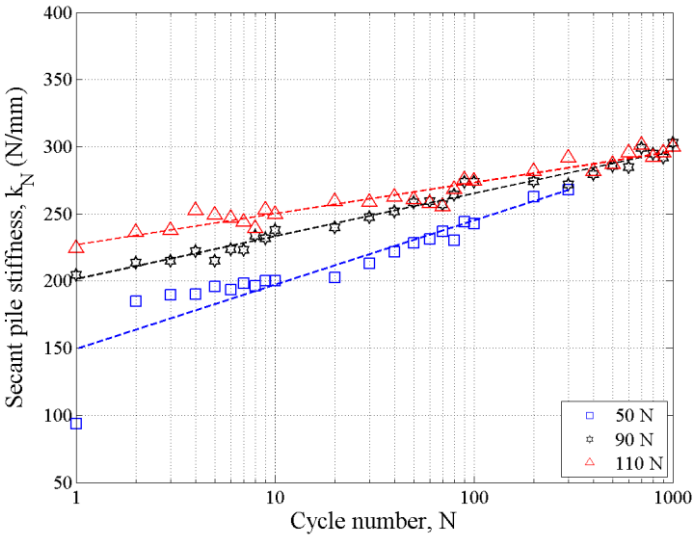

Figure 5-19: Secant pile stiffness – aluminium

For each load magnitude, the secant pile stiffness increased logarithmically with an increase in number of load cycles, which was expected. Densification of the soil in front of the pile occurred as a result of the number of load cycles, increasing the soil stiffness, resulting in the secant pile stiffness increasing, converging to a value of approximately 300 N/mm after 1000 cycles at 90 N and 110 N, respectively. For the 50 N load magnitude, there was a dramatic increase between the first and second load cycle. This was due to the non-linear behaviour of the virgin soil, after which the secant pile stiffness increased slightly. This was not the case at 90 N and 110 N, even though non-linearity of the soil was still experienced. The non-linearity

of the loading curves for the first cycles at these loads were no longer evident due to the soil densification induced by the previous load cycles.

To reduce the influence of the non-linear behaviour of the soil during the first load cycle (k_0), the secant pile stiffness was normalised with the stiffness value from the second load cycle (k_1). As illustrated in **Figure 5-20**, an increase in the normalised secant stiffness occurred with an increase in number of load cycles, similar to what Little & Briaud (1988), Leblanc *et al.* (2010), Li *et al.* (2010) and Abadie & Byrne (2014) observed. The rate at which the secant pile stiffness increased, decreased at higher load magnitudes. This was due to the densification of the soil caused by the load cycles at lower loads. Densification and particle re-orientation of the soil in front of the pile occurred, resulting in the stiffness of the soil increasing to withstand the applied stresses, affecting the relative rigidity of the soil-pile system. Due to the increase in the stiffness of the soil, the relative rigidity of the soil-pile system decreased, resulting in the pile behaving more flexible, affecting the distribution of moments as well as the deflection of the pile.

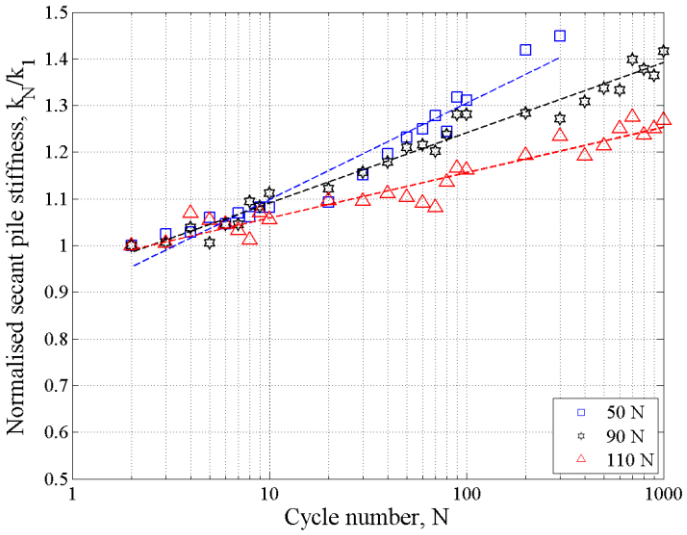

Figure 5-20: Normalised secant pile stiffness – aluminium

5.6.6 Comparison to load-displacement techniques

In order to determine the validity of the results obtained from the cyclic test on the scaled aluminium pile in the centrifuge, the results were also compared to that predicted by the LPILE program. Similar procedures for obtaining the predicted values from the LPILE program for the monotonic test was followed but for this analysis, the effect of cyclic loading was also incorporated. As all tests were conducted in soil of constant relative density, for simplicity, the stiffness was kept the same. Thus, for this analysis the coefficient of subgrade reaction of 2.4 MN/m^3 was used.

To aid in comparing predicted to measured values, the results from the centrifuge model had to be converted to full-scale values by applying the appropriate scaling laws. **Figure 5-21** indicates the comparison between the measured and predicted bending moments of the pile.

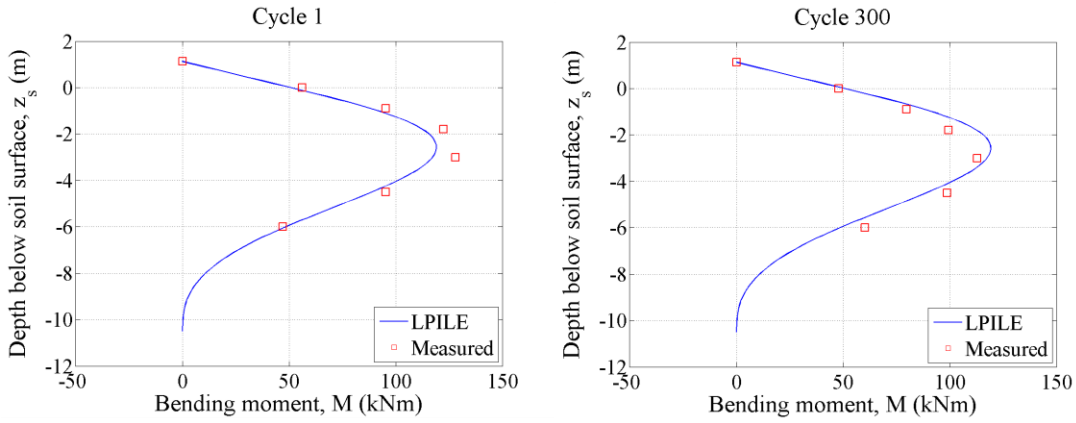

(a)

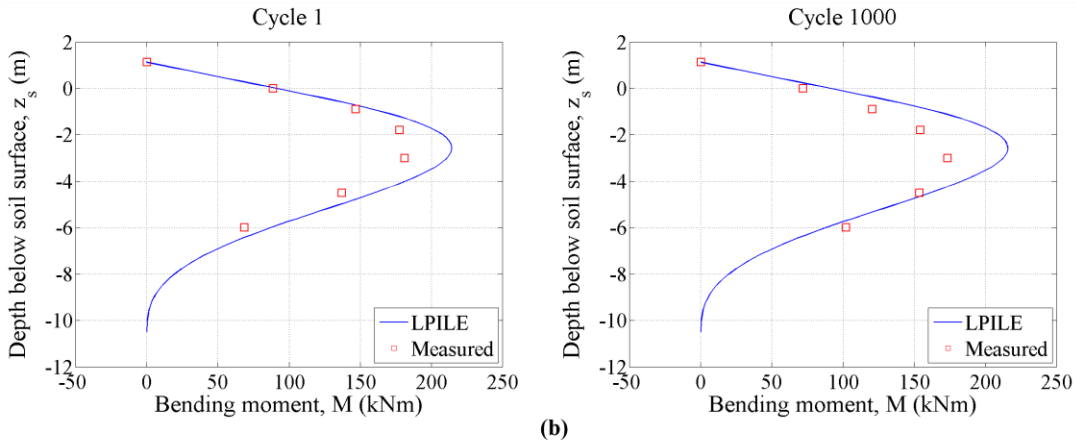

(b)

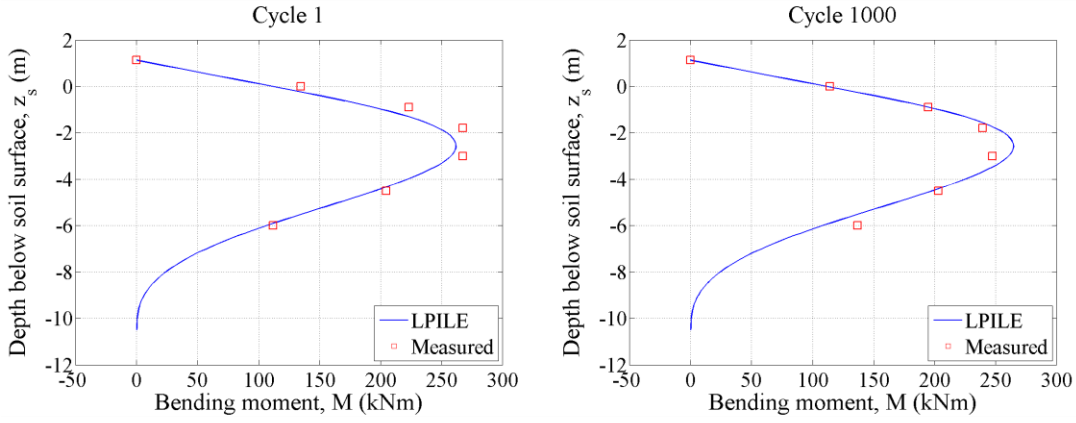

(c)

Figure 5-21: LPILE comparison with bending moment results at full-scale from cyclic test: (a) 50 N, (b) 90 N, (c) 110 N – aluminium

Figure 5-21 (a), **(b)** and **(c)** indicates the measured bending moment results from the centrifuge test at full-scale, as well as the predicated results using the LPILE program, for cyclic load magnitudes of 50 N, 90 N and 110 N, respectively. For each load magnitude, only two cycles

were indicated. From **Figure 5-21** it can be seen that a reasonable correlation exists between the measured and predicted bending moment values for the selected coefficient of subgrade reaction. Furthermore, **Figure 5-22** indicates the comparison between the measured and predicted lateral displacements of the pile.

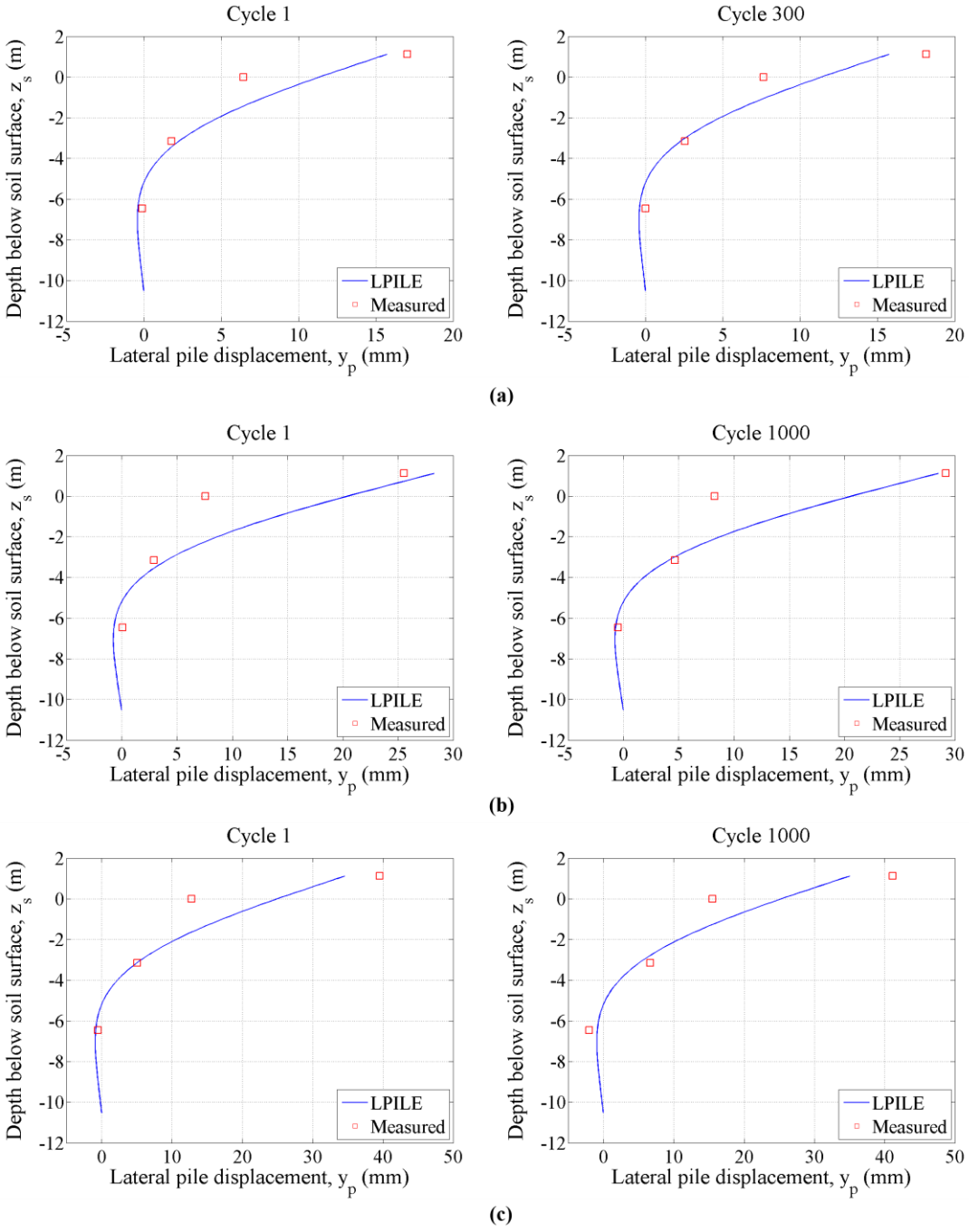

Figure 5-22: LPILE comparison with lateral pile displacement results at full-scale from cyclic test: (a) 50 N, (b) 90 N, (c) 110 N – aluminium

Figure 5-22 (a), **(b)** and **(c)** indicates the measured lateral displacement results from the centrifuge test at full-scale, as well as the predicated results using the LPILE program, for cyclic

load magnitudes of 50 N, 90 N and 110 N, respectively. Similar to the bending moments, only two cycles are indicated for each load magnitude. From **Figure 5-22** it can be seen that a good correlation between the measured and predicted lateral displacement values were obtained for the selected coefficient of subgrade reaction. However, the measured lateral displacement at the soil surface did not seem to be in agreement with the predicted shape. The readings obtained from this LVDT seems to be incorrect. Overall, the slight change in the predicted and measured bending moment and lateral displacement could be attributed to the selection for simplicity, a single coefficient of subgrade reaction was selected, which is not necessarily true, as the Young's modulus of the soil changes.

5.6.7 Summary

Results based on the observed behaviour of the scaled aluminium pile under cyclic loading conditions were as follows:

- As the magnitude of the applied load increased the bending moment and the lateral displacement of the pile also increased.
- The maximum measured bending moment occurred at five pile diameters below the surface of the soil, while the maximum lateral displacement of the pile occurred at the point of load application, similar to the monotonic test on the scaled aluminium pile.
- The number of load cycles did not influence the maximum displacement of the pile but did, however, influence the permanent displacement of the pile. For the cyclic load test the pile experienced more permanent displacement than for the monotonic test.
- Permanent locked-in moments occurred in the pile after load removal during the cyclic load test due to the repeated loading and unloading of the pile. The maximum locked-in moments occurred seven pile diameters below the surface of the soil, opposed to the five pile diameters where the maximum bending moment occurred under loading. Furthermore, at depths deeper than five pile diameters below the soil surface more than 50% of the bending moments were retained in the pile as permanent bending moments. This was due to changing soil conditions surrounding the pile, creating locked-in soil and pile stresses in response to the applied cyclic lateral loads.
- The permanent pile displacement, after load removal, increased with an increase in the number of load cycles and load magnitude, which probably caused the permanent locked-in moments that occurred in the pile.
- The difference between the lateral displacement of the pile upon load application and the permanent displacement of the pile after load removal increased as the magnitude of the applied load increased.

- The rate at which the permanent displacement of the pile increased was influenced by the densification the soil surrounding the pile.
- The first load cycle at each load magnitude caused the most damage to the soil-pile system.
- Regardless of the load magnitude, the absolute pile stiffness decreased logarithmically with an increase in number of load cycles. The rate of decease was influenced by the densification of the soil caused by cyclic loading.
- The secant pile stiffness increased logarithmically with an increase in number of load cycles, regardless of the magnitude of the applied load. Densification and particle re-orientation of the soil surrounding the pile occurred due to repeated loading, resulting in the secant pile stiffness increasing also affecting the rate of increase.
- The measured bending moment and lateral displacement results from the centrifuge test was in good agreement with the predicted values from the LPILE software package.

5.7 CYCLIC RESPONSE OF THE SCALED REINFORCED CONCRETE PILE

Similar to the cyclic aluminium test, a cyclic lateral load was applied to the top of the scaled reinforced concrete pile to observe the response of both the soil and the pile to the applied load. For this test the pile was only loaded cyclically to a maximum load magnitude of about 100 N (Winterkorn & Fang, 1975), exceeding the 77 N lateral capacity of the reinforced concrete pile. This was to determine the long-term response (uncracked, cracked and yielding) of the scaled reinforced concrete pile to repeated loading, allowing for comparisons between the scaled aluminium and reinforced concrete piles to be drawn. Furthermore, for this test, the focus was on the lateral load-displacement and bending moment response of the pile, as well as the absolute and secant stiffness of the soil-pile system, observing the behaviour of the scaled reinforced concrete pile to both an increase in load magnitude and number of load cycles.

5.7.1 Applied load cycles

During the cyclic load test of the scaled reinforced concrete pile, the pile was subjected to three different load magnitudes, applying these loads for a number of load cycles to the top of the pile. A small number of cycles were applied at a relative low load magnitude, followed by much higher number of load cycles at larger load magnitudes to observe long-term cyclic effects. The aim was to replicate the cycles and loads applied to the scaled aluminium pile to the scaled reinforced concrete pile. **Table 5-4** indicates the average horizontal force (lateral load) that was applied to the pile cap and the associated number of load cycles. This was not the same as for the aluminium pile but is fairly close such that behavioural trends could still be compared. The magnitude of the horizontal loads were chosen such that the concrete pile would not crack during the first two sets of cyclic loading, while a significant risk of cracking existed when a

100 N load was applied repeatedly (S/N curves in Chapter 2). Similar to the cyclic aluminium test, it should be noted that the entire test on the scaled reinforced concrete pile was conducted on a single model in the centrifuge with the pile being loaded successively for each load magnitude.

Table 5-4: Average horizontal load and number of cycles – reinforced concrete

Average horizontal load (N)	Number of cycles, *N*
30	150
65	1000
100	1000

5.7.2 Load-displacement response

Figure 5-23 indicates the load-displacement response of the scaled reinforced concrete pile for the entire cyclic lateral load test, with the lateral load (*H*) plotted on the y-axis and pile head displacement (y_h) on the x-axis.

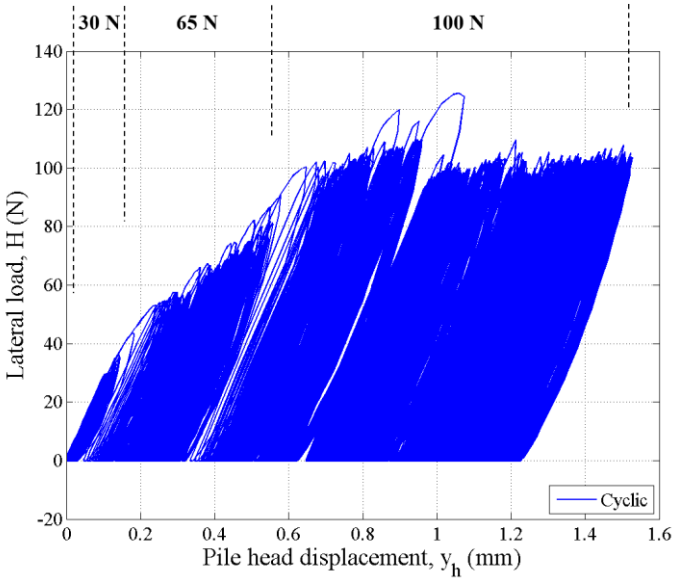

Figure 5-23: Load-displacement response – cyclic reinforced concrete test

As mentioned previously, the scaled reinforced concrete pile was also loaded successively with the three load magnitudes as shown in **Figure 5-23**, with perfect load control not being possible. It can be observed that, as the lateral load increased, the displacement of the pile head increased, as expected, with the permanent displacement also increasing with both load magnitude and number of load cycles. The load-displacement response was similar to that observed by Lin & Liao (2006) for a pile with a changing flexural rigidity caused by the concrete pile cracking and exhibiting highly non-linear behaviour as opposed to the scaled aluminium pile. The reduction in flexural rigidity can be seen by the large permanent displacements that occurred during the

load cycles at an applied load of 100 N. It is worth noting that even at low loads no resilient behaviour was observed for the scaled reinforced concrete pile (Werkmeister *et al.*, 2004), which differs significantly from the scaled aluminium pile. A discussion on the reduction of the flexural rigidity of the scaled reinforced concrete pile and the corresponding behaviour is discussed in the sections to follow.

5.7.3 Bending moment response

In order to determine the bending moment response of the scaled reinforced concrete pile, it was necessary to consider the strain developing within the pile. This was necessary due to concrete having a low tensile capacity, resulting in the formation of cracks in the section at the locations where the tensile capacity is exceeded, something that is typically not a problem when dealing with metal sections (aluminium pile). Usually, once this point is reached, the uncracked elastic sectional properties no longer applies. Thus, by monitoring the strain development in the pile, the formation and position of cracks could be determined in order to apply the appropriate sectional properties when obtaining the corresponding bending moment in the pile. Based on the theoretical calculations in Chapter 4 with regard to the cracking moment, the concrete section should crack when 88 micro-strain in the pile is exceeded.

Figure 5-24 indicates the bending strain (ε_b) along the length of the pile under cyclic loading conditions for both the tension and compression side of the pile. These strains experienced by the pile were as a result of the applied cyclic lateral load (H) at the top of the pile. The bending strains were plotted against the depth below the soil surface (z_s). **Figure 5-24 (a)**, **(b)** and **(c)** indicates the response of the pile for cyclic lateral loads with magnitudes of 30 N, 65 N and 100 N, respectively. The strain on the tension side of the pile is indicated by ‘T’, whereas the strain on the compression side of the pile is indicated by ‘C’ in **Figure 5-24**. For each of the load magnitudes, only a few of the load cycles were indicated for discussion purposes. This aided in determining whether a crack had formed in the pile where the tensile capacity of the scaled concrete was exceeded. For the 150 load cycles at 30 N applied load, it can be seen that the pile behaved symmetrically, with the response of the pile being almost the same on both the tension and compression side. At 65 N applied load, the first 100 load cycles also exhibited symmetrical behaviour. However, as indicated by cycle 1000, a crack had formed in the concrete section at about 100 mm below the soil surface. This was indicated by the reduction in the strain measured on the tension side of the pile by the strain gauge at the location of 100 mm below the soil surface, and an increase in the strain measured on the compression side of the pile at that same location. Further investigation into this matter showed that the crack formed after 500 load cycles at an applied load of 65 N at about 145 micro-strain, which was

significantly higher than the theoretically predicted strain. The presence of the crack could also be observed by considering the strain development in the pile at 100 N applied load.

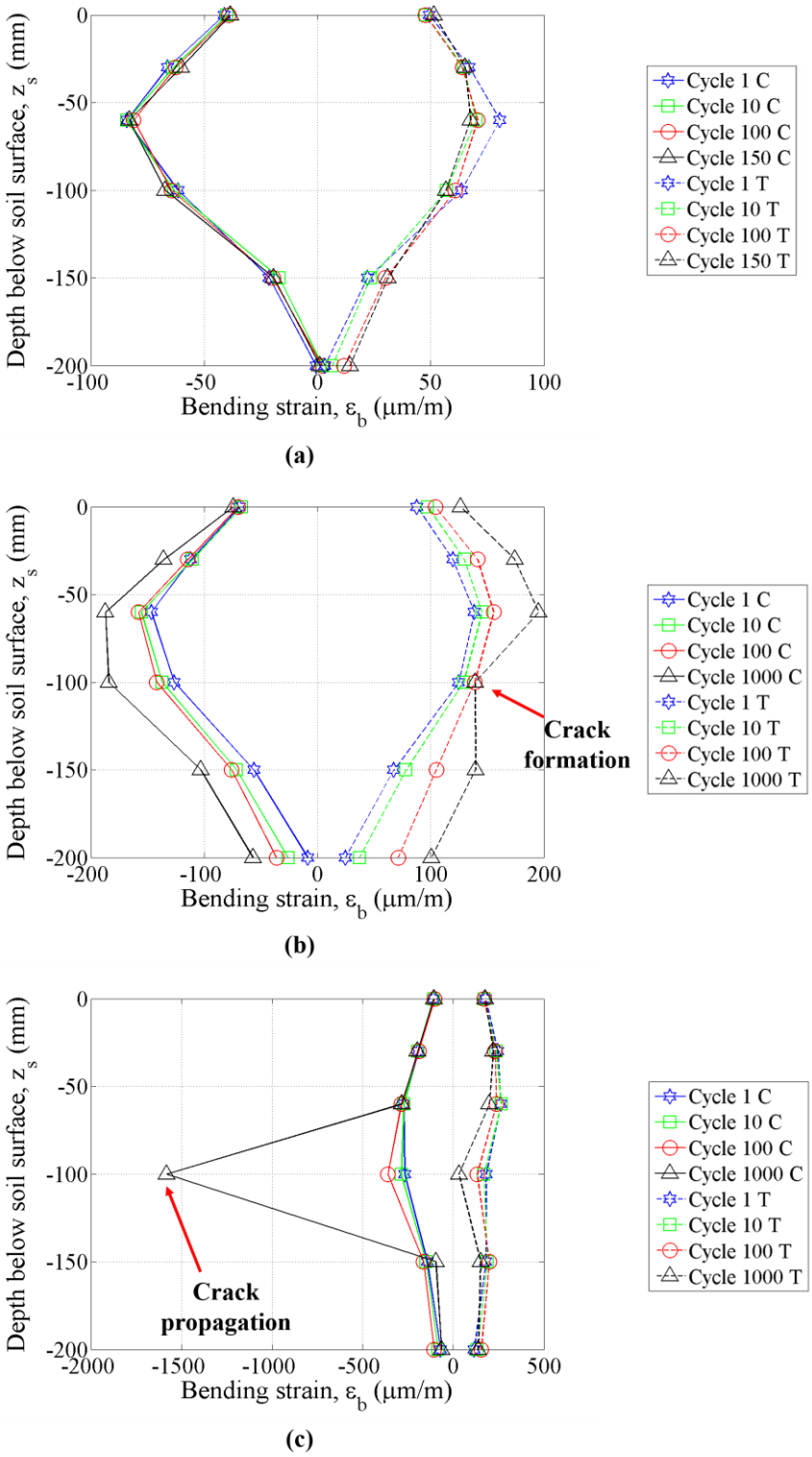

Figure 5-24: Strain development: (a) 30 N, (b) 65 N, (c) 100 N – reinforced concrete

As the number of load cycles increased at 100 N, the strain measured on the tension side of the pile at 100 mm below the soil surface continued to reduce, resulting in the strain on the compression side to increase. This was indicative of a plastic hinge that had formed in the concrete section, with the top part of the pile, above the crack, rotating about this point increasing the compression strain. For the first 100 load cycles at 100 N, the crack was small. However, at cycle 1000, the crack had propagated significantly, as indicated by the large strain on the compression side at 100 mm below the soil surface.

Figure 5-25 indicates the position of the crack that formed in the scaled reinforced concrete pile section. The size of the crack was approximately 0.5 mm and was measured with a TECHGEAR Eaglescope Digital Microscope after the tests were conducted in the centrifuge.

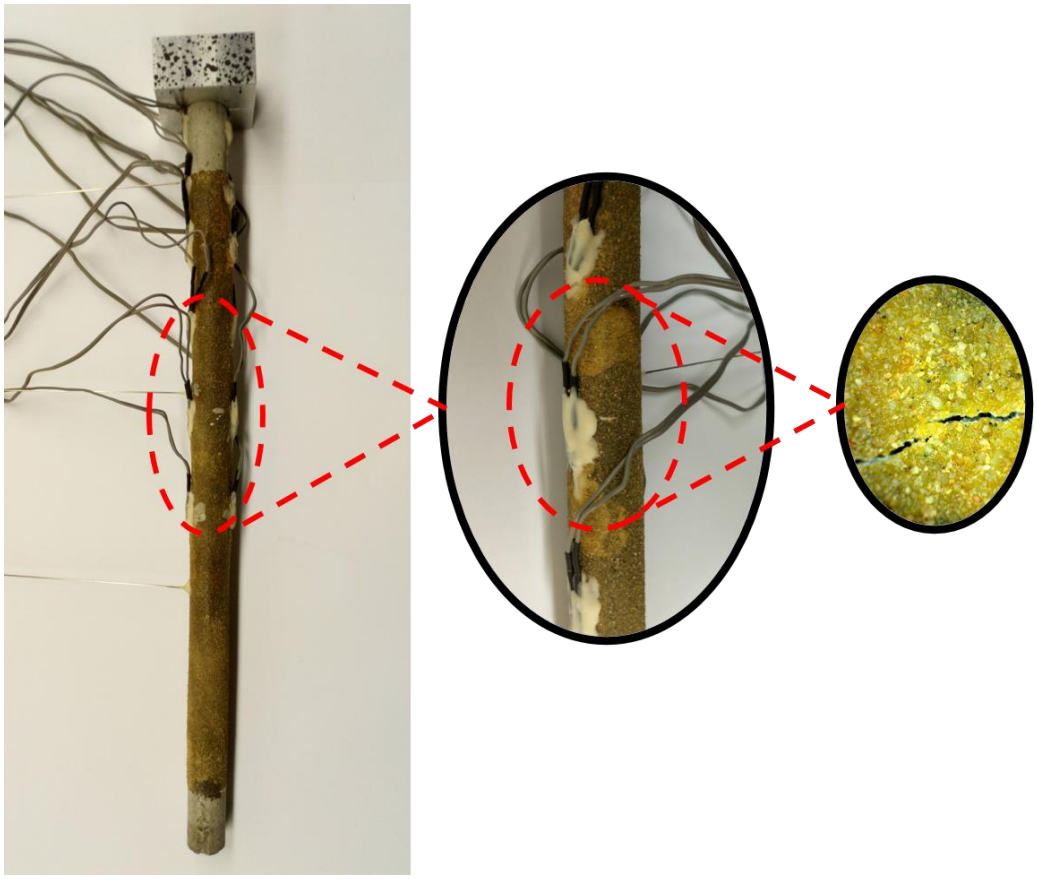

Figure 5-25: Crack formation in the scaled reinforced concrete pile

After considering the strain development in the pile, the bending moment experienced by the pile was calculated, incorporating the appropriate changes in flexural rigidity after the pile section had cracked (Section 4.5). **Figure 5-26** indicates the bending moment (M) development along the length of the pile under cyclic conditions. The bending moments were plotted against the depth below the soil surface (z_s), similar to the strain above. **Figure 5-26 (a)**, **(b)** and **(c)** indicates the response of the pile for cyclic lateral loads under magnitudes of 30 N, 65 N and

100 N, respectively. For each of the load magnitudes, only a few of the load cycles were indicated for discussion purposes. To determine the effect of number of load cycles on the bending moment response, the bending moments for each of the load magnitudes were normalised with the bending moment at the soil surface (M_h) and is also indicated in **Figure 5-26**. The bending moment at the soil surface was taken as the bending moment measured by the strain gauges at that location.

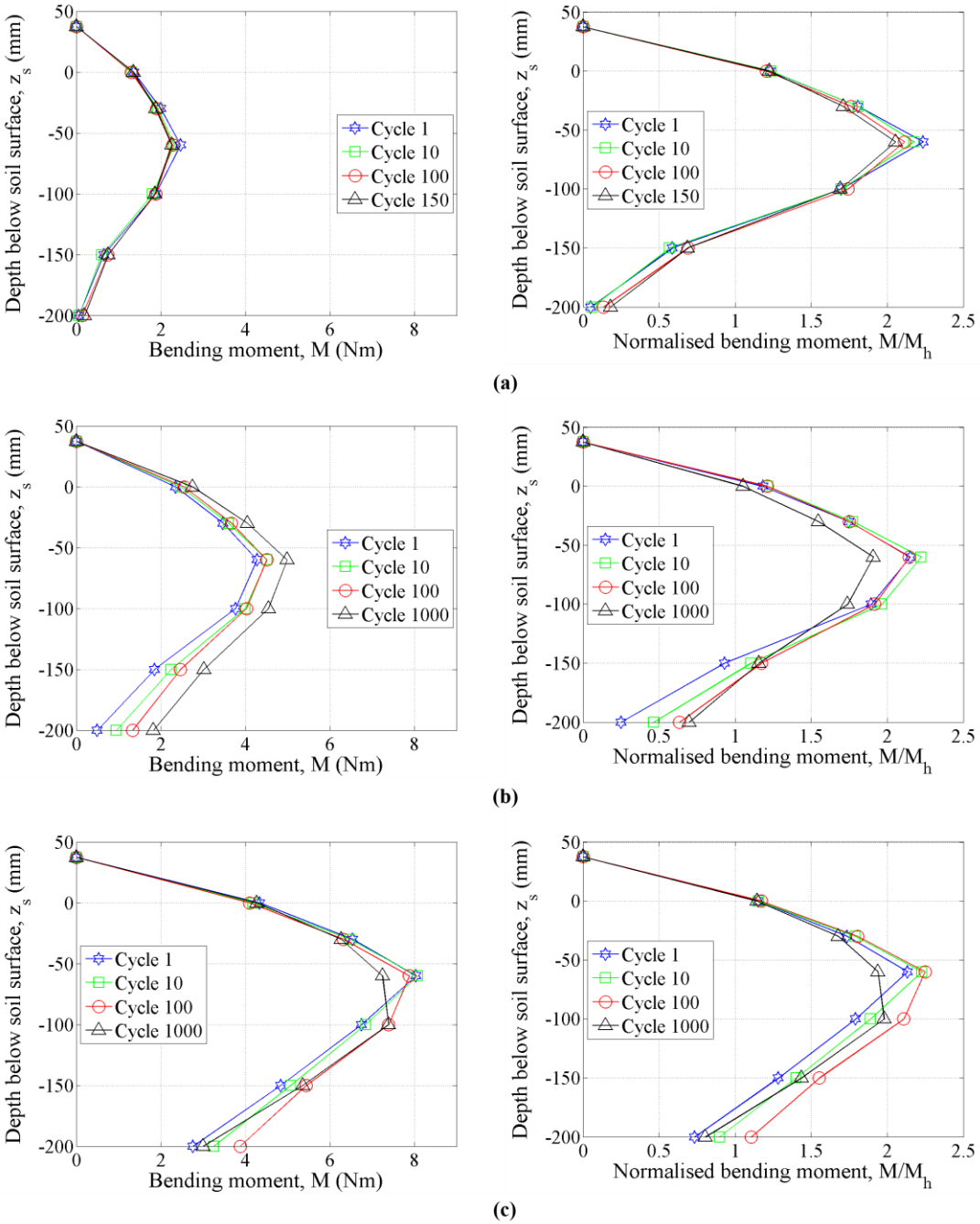

Figure 5-26: Bending moment and normalised bending moment with depth: (a) 30 N, (b) 65 N, (c) 100 N – reinforced concrete

It can be seen in **Figure 5-26** that, as the magnitude of the applied lateral load increased, the bending moment response of the pile also increased, similar to the aluminium pile test. The maximum measured bending moment occurred approximately three pile diameters below the soil surface (60 mm), which is different to that experienced by the aluminium pile (five pile diameters). By considering the normalised bending moment diagrams, it can be seen that the increase in number of load cycles had an influence on the bending moment response below the position where the maximum bending moment occurred, which differs from what Kirkwood & Haigh (2014) observed. It should be pointed out that theoretically the concrete section should crack at all locations where the moment exceeds 2.7 Nm, after which the elastic sectional properties of the pile no longer applies. Based on the observed strain data at some of the locations, which seemed fairly symmetrical (no cracking) at moments exceeding the cracking moment, elastic sectional properties were still applied to these strains.

Kirkwood & Haigh (2014) indicated that the development of permanent bending moments (M_{per}), or locked-in moments in the pile should be considered. These moments were permanent bending moments that remained in the pile after the lateral load is removed (H = 0 N). Similar to the aluminium pile test, these moments were plotted as indicated in **Figure 5-27**. The permanent bending moments were plotted against the depth below the soil surface. **Figure 5-27 (a)**, **(b)** and **(c)** indicates the permanent response of the pile after the cyclic lateral loads, with magnitudes of 30 N, 65 N and 100 N, respectively, have been removed. To determine and better visualise the effect of number of cycles on the permanent bending moment response, the permanent bending moments for each of the load magnitudes, were normalised with the bending moment at the soil surface (M_{hp}) from the previous load cycle when the load was applied, and this is also indicated in **Figure 5-27**. The bending moment at the soil surface was taken as the bending moment measured by the strain gauges at the soil surface from the previous load cycle.

It can be seen in **Figure 5-27** that, as the magnitude of the applied lateral loaded increased, the permanent bending moment response of the pile also increased. It should be mentioned that the permanent bending moments experienced after loading to 65 N and 100 N also includes the permanent moments from the previous load cycles and load magnitudes. Regardless of that, the trend between locked-in moments and number of load cycles can be observed. As with the scaled aluminium pile, the maximum locked-in moment occurred approximately seven pile diameters below the soil surface (150 mm). Looking at the normalised bending moment diagrams for the locked-in moments, it can be seen that as the number of load cycles increased at the same load magnitude, the permanent bending moments also increased, which is similar to what Kirkwood & Haigh (2014) observed and what was observed for the scaled aluminium pile. These locked-in moments were as a result of the densification of the soil surrounding the

pile creating locked-in soil stresses in response to the applied cyclic lateral loads. A slight reduction in the permanent bending moment with increasing number of cycles seems to indicate crack growth.

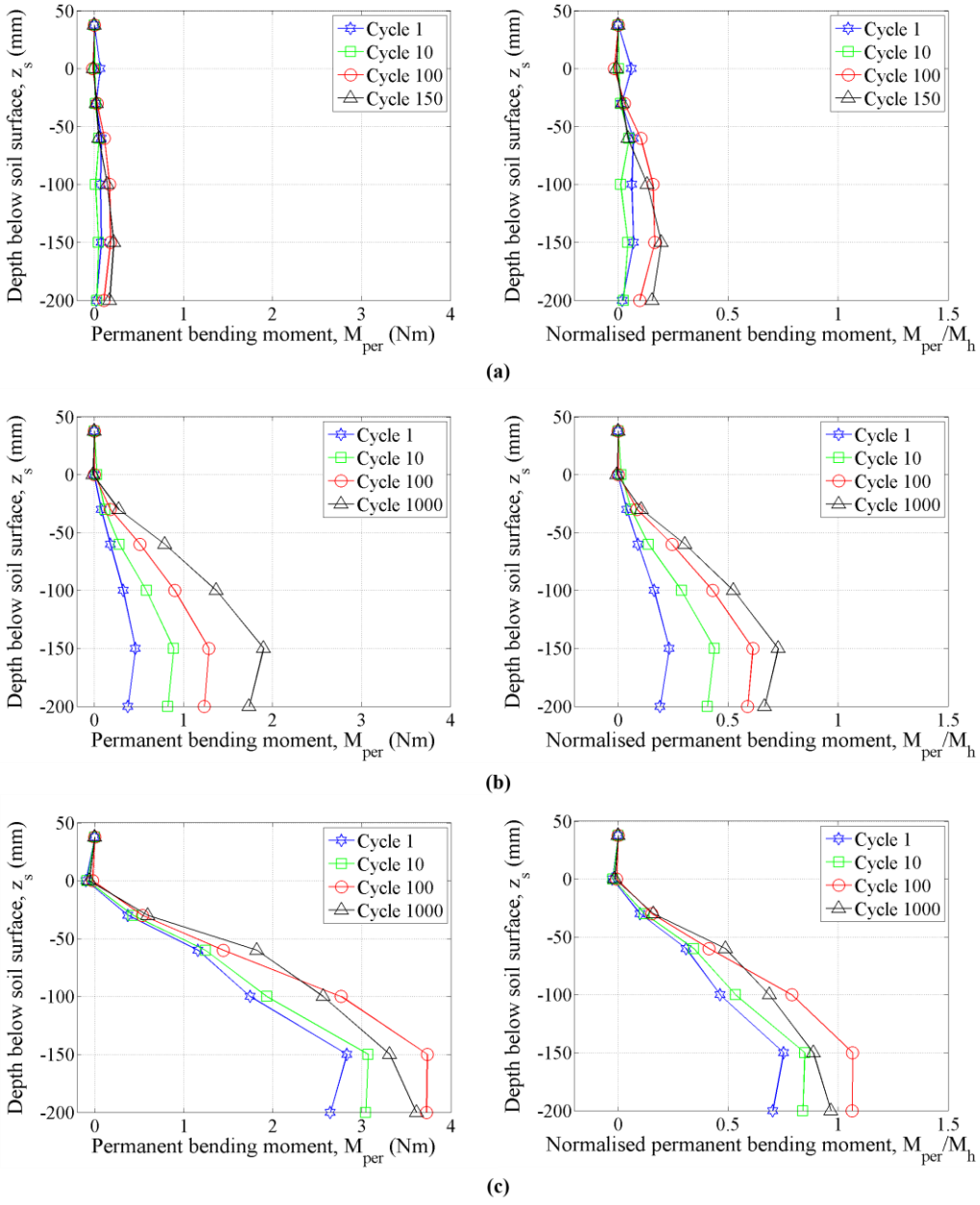

Figure 5-27: Permanent bending moment and normalised bending moment with depth: (a) 30 N, (b) 65 N, (c) 100 N – reinforced concrete

Figure 5-28 (a), **(b)** and **(c)** indicates both the bending moment and permanent bending moment response of the pile after the cyclic lateral loads, with magnitudes of 30 N, 65 N and 100 N, respectively. It should be noted that the maximum measured bending moment occurred at 60 mm below the surface of the soil and the maximum measured permanent bending moment

at 150 mm below the surface of the soil. Similar to the scaled aluminium pile test, large differences between the bending moment and permanent bending moment existed towards the top of the pile, whereas the difference reduced for depths exceeding 150 mm.

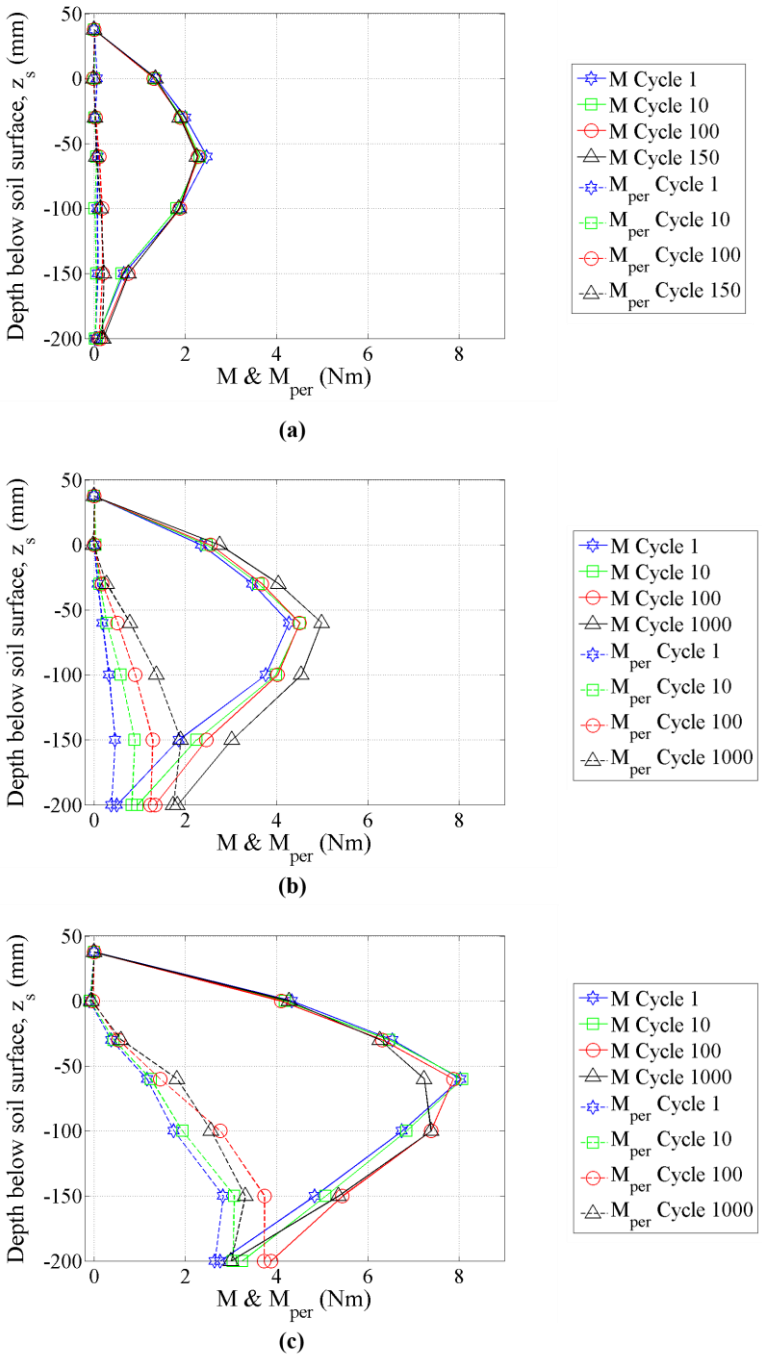

Figure 5-28: Combined bending moment and permanent bending moment with depth: (a) 30 N, (b) 65 N, (c) 100 N – reinforced concrete

The permanent bending moment at 150 mm below the soil surface was also about 50% of the bending moment experienced by the pile at that location under load application. This response

was observed at all the load magnitudes. This was due to the changing soil conditions along the length of the pile, as a result of cyclic loading, causing locked-in soil stresses towards the bottom of the pile. Considering the moments at 200 mm below the soil surface, insignificant differences between the permanent bending moment and the bending moment under load application existed.

5.7.4 Lateral pile displacement

Apart from the bending moment response of the pile to cyclic loading, the lateral displacement of the pile should also be considered under these conditions. The effect of load magnitude and number of load cycles on the lateral displacement response was investigated and is discussed here. **Figure 5-29** indicates the lateral pile displacement (y_p) along the length of the pile as a result of the applied cyclic lateral load (H) at the top of the pile. Similar to the aluminium cyclic pile test, the lateral displacements were also plotted against the depth below the soil surface (z_s). **Figure 5-29 (a)**, **(b)** and **(c)** indicates the response of the pile to cyclic lateral loads with magnitudes of 30 N, 65 N and 100 N, respectively. For each of the load magnitudes, only a few of the load cycles were indicated for discussion purposes.

It can be seen in **Figure 5-29** that, as the magnitude of the applied lateral load increased, the displacement of the pile also increased, similar to the cyclic aluminium test. As expected, the maximum displacement occurred at the point of load application (z_s = 37.5 mm). At small loads, the scaled reinforced pile experienced small movements in the soil, with all the movement primarily occurring above the soil surface. It is also worthwhile mentioning that the scaled reinforced concrete pile exhibited lower displacements than that of the aluminium pile at lower loads. This is indicative of the scaled reinforced concrete pile having a higher flexural stiffness than that of the scaled aluminium pile. As the magnitude of the applied load increased, more of the soil was mobilized to resist the applied loads, resulting in the displacement of the pile increasing. However, the large increase in the lateral displacement at the top of the pile at 100 N applied load was not only due to the magnitude of the applied load. It was also due to the formation and propagation of a crack in the concrete at approximately 500 load cycles of an applied load with a magnitude of 65 N, as indicated with the bending moment response in the previous section. The crack created a point of rotation in the pile, resulting in the pile to rotate about this point upon load application, increasing the displacement above this crack significantly. The effective embedment length of the pile reduced, with the part of the pile above the crack having to work harder to resist the applied load causing higher displacements.

Furthermore, with regard to cycle number, at small loads (H = 30 N), the lateral displacement of the pile showed similar behaviour to that of the scaled aluminium pile, with the number of load cycles at a particular load having minimal effect on the maximum displacement of the pile.

This was due to the pile still being uncracked. However, at higher applied loads (65 N and 100 N), the pile cracked, resulting in the number of load cycles having a significant effect on the maximum displacement of the pile above the crack, differing from the behaviour observed with the aluminium pile.

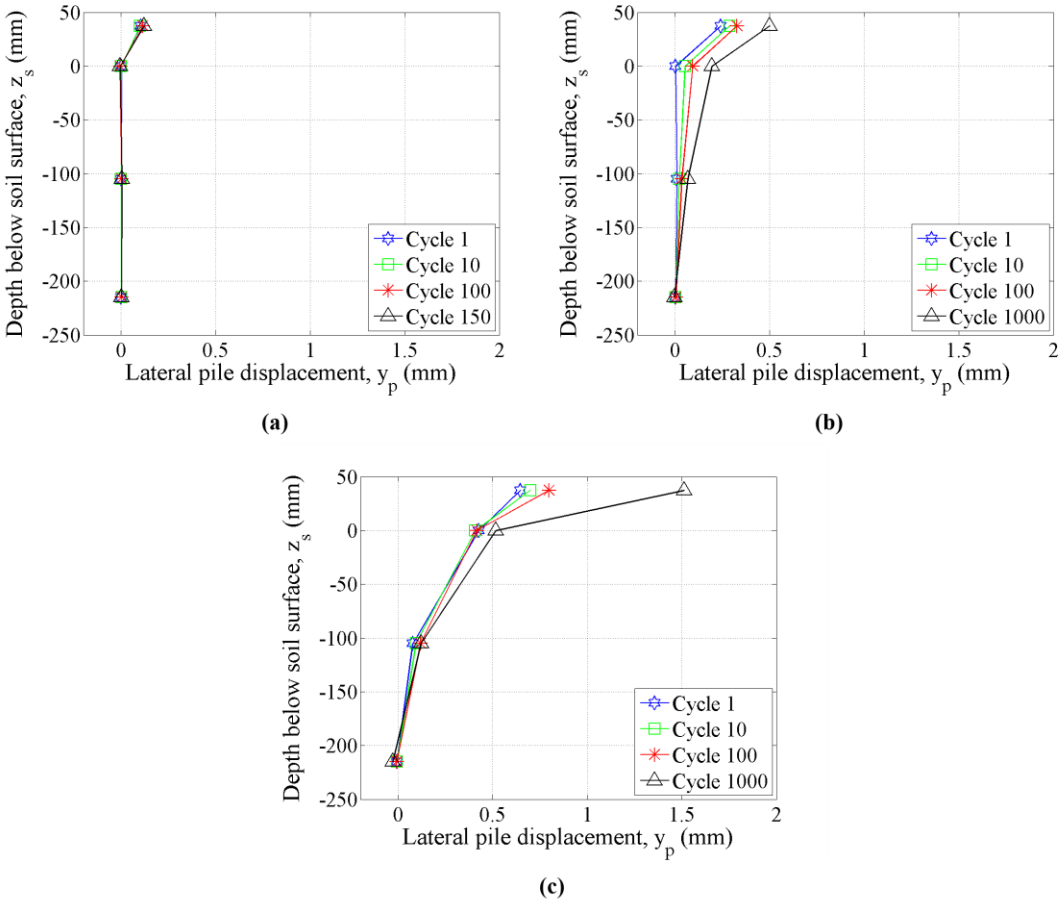

Figure 5-29: Lateral pile displacement with depth: (a) 30 N, (b) 65 N, (c) 100 N – reinforced concrete

As mentioned, both the magnitude of the lateral load and the number of load cycles had a significant effect on the horizontal pile movement, especially at higher applied loads once the reinforced concrete pile had cracked. This behaviour can be observed by plotting the maximum pile head displacement (y_h) and permanent pile head displacement (y_{hper}) against the number of load cycles (**Figure 5-30**). It can be seen that as the load magnitudes and number of load cycles increased, there was an increase in the pile displacement. At 30 N no significant increase in the lateral pile head displacement was observed with cycle numbers due to the reinforced concrete section still being uncracked. However, the displacement of the pile head significantly increased after the formation of a crack in the section. This can be seen when considering the graph for an applied load of 100 N, where the crack propagated, resulting in large

displacements. Similar to the scaled aluminium pile it can be seen that as the magnitude of the applied load increased, the difference between the pile head displacement and the permanent pile head displacement increased. But more significantly, the difference also reduced with number of load cycles (densification with number of load cycles).

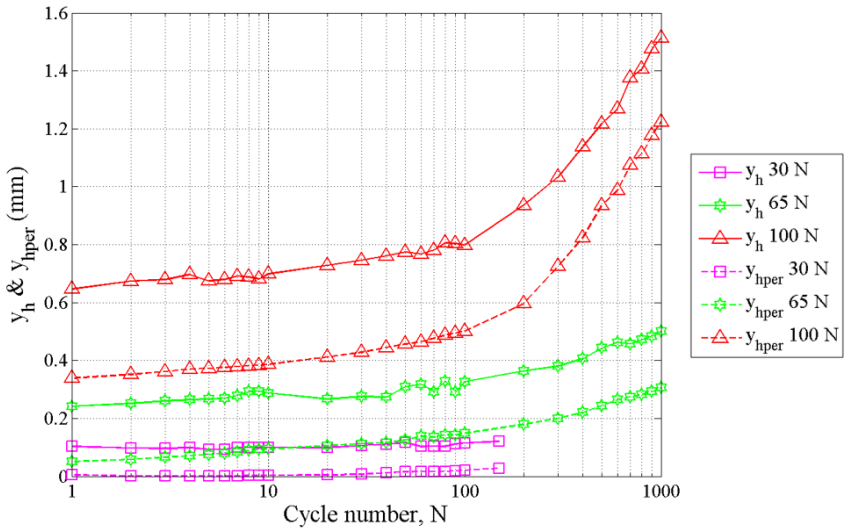

Figure 5-30: Pile head displacement and permanent pile head displacement with number of cycles – scaled reinforced concrete

The permanent pile head displacement explains the observed locked-in moments in the pile mentioned in the previous section. Movement of the soil surrounding the pile occurred due to repetitive loading, resulting in permanent displacement of the pile, creating locked-in stresses in the soil and locked-in moments in the pile. It should be mentioned that the permanent pile head displacement for the 65 N and 100 N applied loads also included the permanent displacement from the previous load cycles and load magnitudes. Regardless of that, the trend between the permanent lateral displacement of the pile head and number of load cycles could be observed.

It is interesting to note the change in the permanent pile head displacement over the number of load cycles for the duration of the test. Different from what was observed from the scaled aluminium pile, the rate of increase in permanent displacement of the scaled reinforced concrete pile with load cycle numbers was largely influenced by the non-linear behaviour of the concrete and the formation of a crack in the section, rather than a change in the stiffness of the soil caused by the previous load cycles on the soil. This can be explained by considering **Figure 5-30**. A significant increase in the permanent displacement of the pile took place after about 300 load cycles at 100 N, opposed to the permanent displacement that occurred at lower loads. The large change in permanent pile head displacement was not observed for the aluminium pile that

remained uncracked. Furthermore, this behaviour regarding the permanent displacement of the pile was similar to what was observed by Werkmeister *et al.* (2004). It seemed that the pile exhibited behaviour within incremental plastic deformation range (range C) as proposed by Werkmeister *et al.* (2004), with progressive plastic deformation and strains occurring for each load cycle at the same load level.

5.7.5 Absolute and secant pile stiffness

As mentioned in Section 2.4.2, the response of the soil-pile system to cyclic loading can be observed by considering the absolute and secant pile stiffnesses, respectively, enabling the effect of load magnitude and number of load cycles to be investigated. Procedures for calculating the absolute pile stiffness (K_N) and secant pile stiffness (k_N) were applied to the results from the scaled reinforced concrete pile. For the cyclic test on the scaled reinforced concrete pile in the centrifuge, the test was also conducted on a single model, with the same pile being loaded cyclically at various load magnitudes. Thus, due to the lateral cyclic loads not remaining constant for the duration of the test, the initial density of the soil (K_0) changed for each load magnitude. This was due to the gradual densification of the sand caused by the previous load cycles and had to be taken into account for calculating the absolute and secant pile stiffnesses, respectively. Both these concepts were illustrated for the scaled reinforced concrete pile in **Figure 5-31**, with K_0 changing to the slope of the first cycle of the load-displacement curves at each new load magnitude as indicated. **Figure 5-31 (a)**, **(b)** and **(c)** represent the load-displacement response of the scaled reinforced concrete pile subjected to cyclic lateral loads with magnitudes of 30 N, 65 N and 100 N, respectively.

These graphs indicate the first and last cycle for each of the respective loads, demonstrating how the absolute and secant pile stiffnesses were calculated based on the dashed slope lines. From **Figure 5-31** it can be noted that the initial density of the soil changed for each load magnitude due to the densification of the soil caused by the previous load cycles. The first cycle of the load-displacement curves, for each load magnitude, exhibited non-linear behaviour of the soil, but to a lesser extent at lower loads, where the pile was still uncracked. This was not the case with the scaled aluminium pile that had a lower flexural rigidity (E_mI_m). This non-linear behaviour can be described by considering the gradient of the load-unload curves. The gradient of the load-unload curves (secant pile stiffness) increased with an increase in lateral displacement, whereas the absolute pile stiffness decreased. Lastly, similar to the aluminium pile, for each load magnitude in **Figure 5-31**, the horizontal pile head displacement was not zeroed. Thus, at higher loads, the displacement just before the first load cycle at that load is the permanent displacement caused by the previous loads and load cycles.

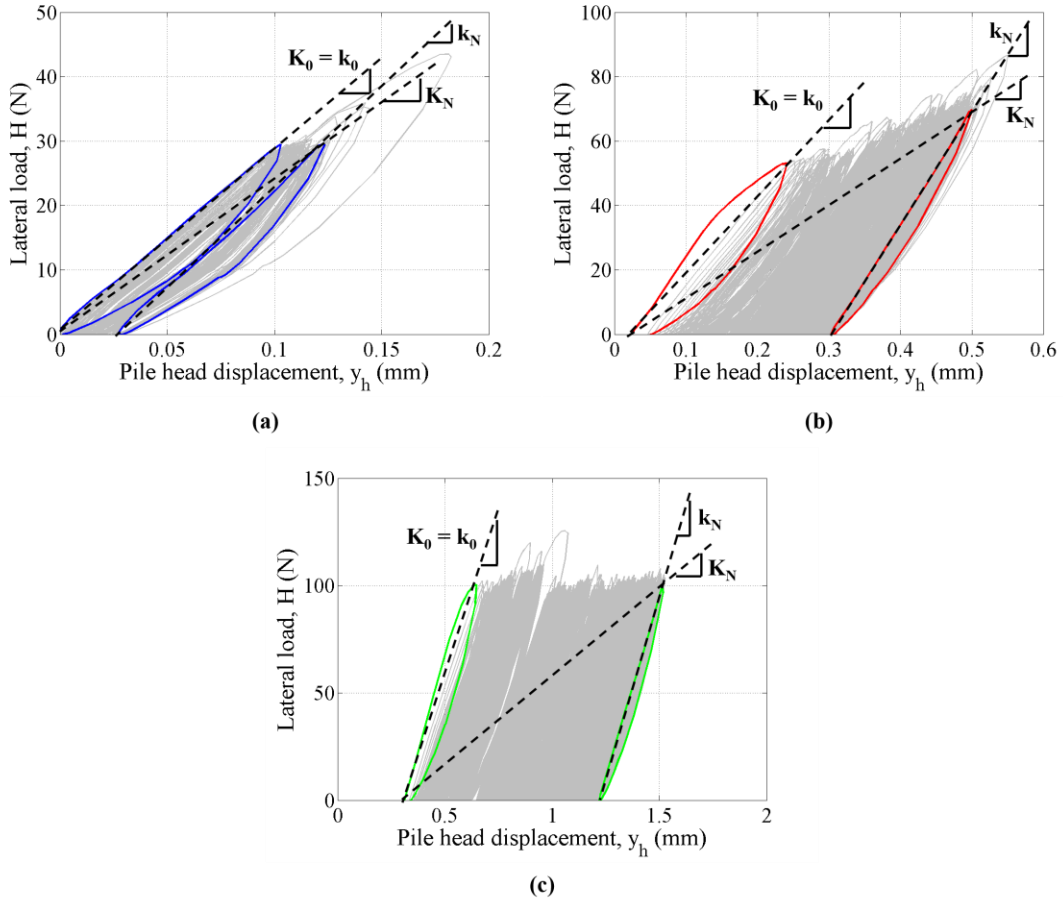

Figure 5-31: Load-displacement response – absolute and secant pile stiffness: (a) 30 N, (b) 65 N, (c) 100 N

As seen in **Figure 5-31**, the absolute and secant pile stiffness for the scaled reinforced concrete pile were also calculated from the measured displacement of the pile at the position of load application. Considering the absolute pile stiffness, as illustrated in **Figure 5-32**, an increase in the initial absolute pile stiffness occurred for each increase in load magnitude, with the highest initial stiffness experienced with the 100 N applied load. This was due to the densification of the soil, caused by the previous load cycles, increasing the initial density of the soil prior to the next load magnitude (successive loading of the same pile). However, this was not the case with the initial stiffness experienced with the 65 N applied load, as it exhibited the lowest initial stiffness. Furthermore, for each load magnitude, the absolute pile stiffness decreased logarithmically with an increase in number of load cycles, which was expected, as the pile experienced accumulating permanent displacement with an increase in the number of load cycles. This was similar to what Little & Briaud (1988) observed.

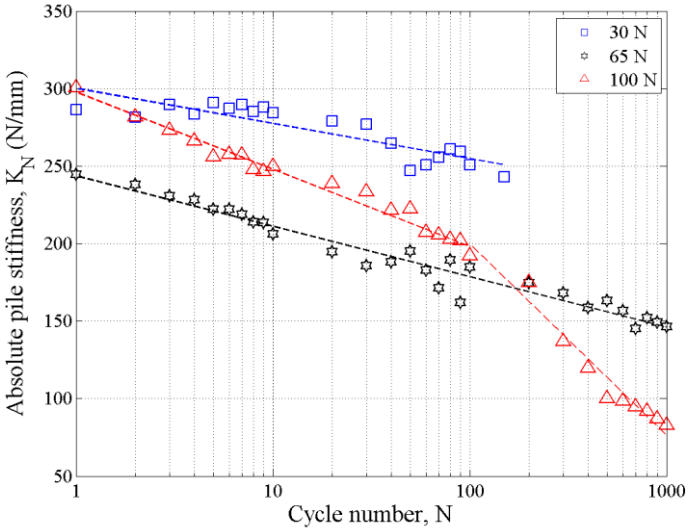

Figure 5-32: Absolute pile stiffness – reinforced concrete

To better visualise the effect of number of cycles on pile stiffnesses, the results were normalised with the stiffness value from the second load cycle (K_1) for a particular load magnitude. This was to remove the non-linear behaviour of the soil during the first load cycle (K_0) at each load increase, as indicated above. By doing this, it can be seen in **Figure 5-33**, that the rate of decrease in the absolute pile stiffness was more prominent for higher load magnitudes than for lower load magnitudes, which is opposite to what was observed with the scaled aluminium pile.

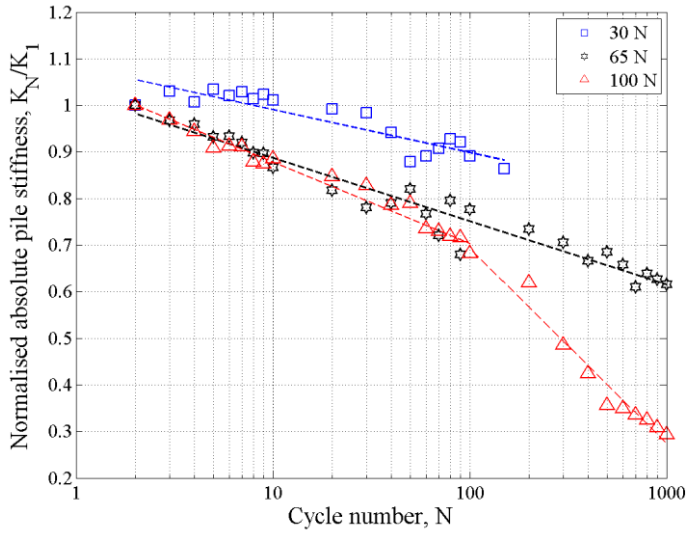

Figure 5-33: Normalised absolute pile stiffness – reinforced concrete

This was caused by the changing sectional properties of the pile, with the formation of a crack. The crack increased the rate of permanent displacement of the pile to cycle numbers as indicated

above. This significant change in lateral displacement of the pile, caused by the propagation of the crack, resulted in the absolute pile stiffness decreasing rapidly, which was not observed with the aluminium pile. This is indicated by the change in the slope of the logarithmic trendline at 100 N in **Figure 5-32** and **Figure 5-33**, respectively, and was also mentioned by Little & Briaud (1988).

Moving on to the secant pile stiffness, from **Figure 5-34** it can be seen that there was a decrease in the secant pile stiffness for each increase in load magnitude, with the highest initial stiffness still being experienced with the 100 N applied load. This was due to the non-linear behaviour of the soil during the first cycle at each load increase, causing the secant pile stiffness to decrease initially. The secant stiffness at 100 N was higher than that at 50 N. This was due to the change in the initial density of the soil, as mentioned above with the absolute pile stiffness. It can also be seen that, for each load magnitude, the secant pile stiffness increased logarithmically with an increase in number of load cycles, which was expected, similar to the aluminium pile, converging to a value of approximately 350 N/mm after 1000 cycles at 65 N and 100 N, respectively. Densification of the soil in front of the pile occurred as a result of the number of load cycles, increasing the soil stiffness, resulting in the secant pile stiffness increasing.

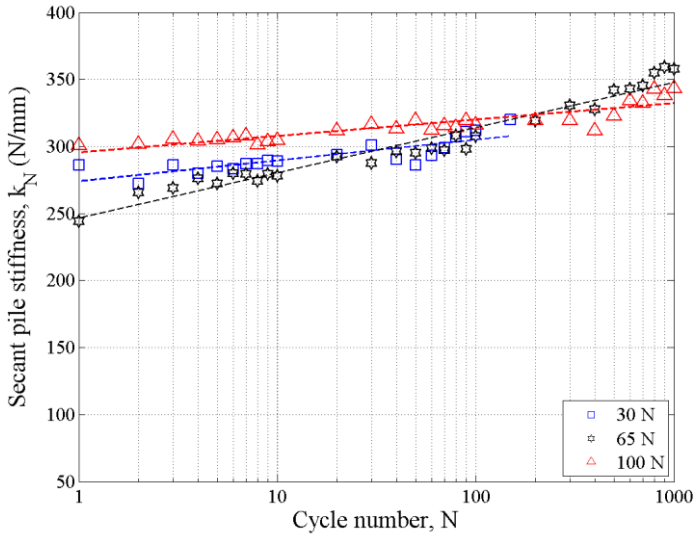

Figure 5-34: Secant pile stiffness – reinforced concrete

To minimise the non-linear behaviour of the soil during the first load cycle (k_0), the secant pile stiffness was normalised with the stiffness value from the second load cycle (k_1). From **Figure 5-35** it can be seen that there is an increase in the secant stiffness with an increase in number of load cycles, similar to what Little & Briaud (1988), Leblanc *et al.* (2010), Li *et al.* (2010) and

Abadie & Byrne (2014) observed. As with the aluminium pile, the rate at which the secant modulus increases, decreases at higher load magnitudes. This was due to the densification of the soil caused by the load cycles at lower loads. Densification and particle re-orientation of the soil in front of the pile occurred, resulting in the stiffness of the soil increasing to withstand the applied stresses, also affecting the relative rigidity of the soil-pile system, similar to the aluminium pile. Due to the increase in the stiffness of the soil, the relative rigidity of the soil-pile system decreased, resulting in the pile behaving in a more flexible manner, affecting the distribution of moments as well as the deflection of the pile.

Lastly, from **Figure 5-34** and **Figure 5-35** it can be concluded that the change in sectional properties of the reinforced concrete pile had almost no effect on the observed pile secant stiffness response, but does however affect the relative rigidity significantly.

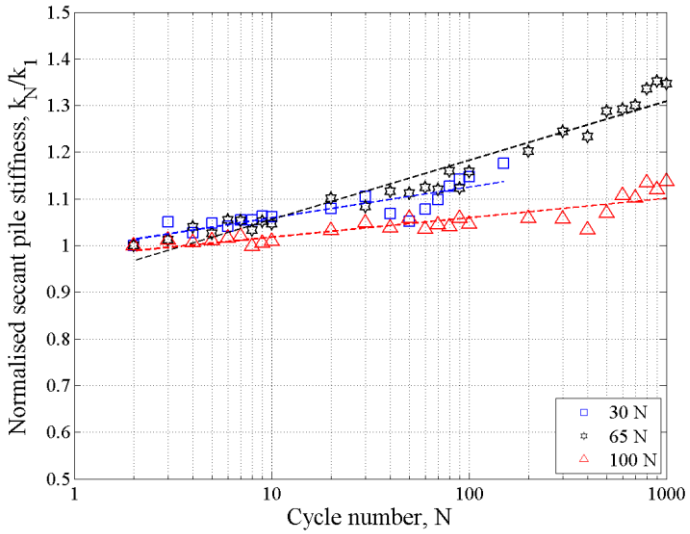

Figure 5-35: Normalised secant pile stiffness – reinforced concrete

5.7.6 Comparison to load-displacement technique

In order to determine the validity of the results obtained from the cyclic test on the scaled reinforced concrete pile in the centrifuge, the results were also compared to that predicted by the LPILE program. Similar procedures were followed than for the scaled aluminium pile, using the same soil properties but different pile properties. For this analysis, the effect of cyclic loading was also incorporated. The scaled reinforced concrete pile was assumed to remain uncracked for the duration of the analysis, as the student version of LPILE does not allow for non-linear pile effects to be incorporated. As all tests were conducted in soil of constant relative density, for simplicity, the stiffness was kept the same. Thus, for this analysis a coefficient of subgrade reaction of 2.4 MN/m^3 was used.

To aid in comparing the predicted values to the measured values, the results from the centrifuge scale model had to be converted to full-scale values by applying the appropriate scaling laws. **Figure 5-36** indicates the comparison between the measured and predicted bending moments of the pile. **Figure 5-36 (a)**, **(b)** and **(c)** indicates results for a cyclic load magnitude of 30 N, 65 N and 100 N, respectively. For each load magnitude, only two cycles were indicated.

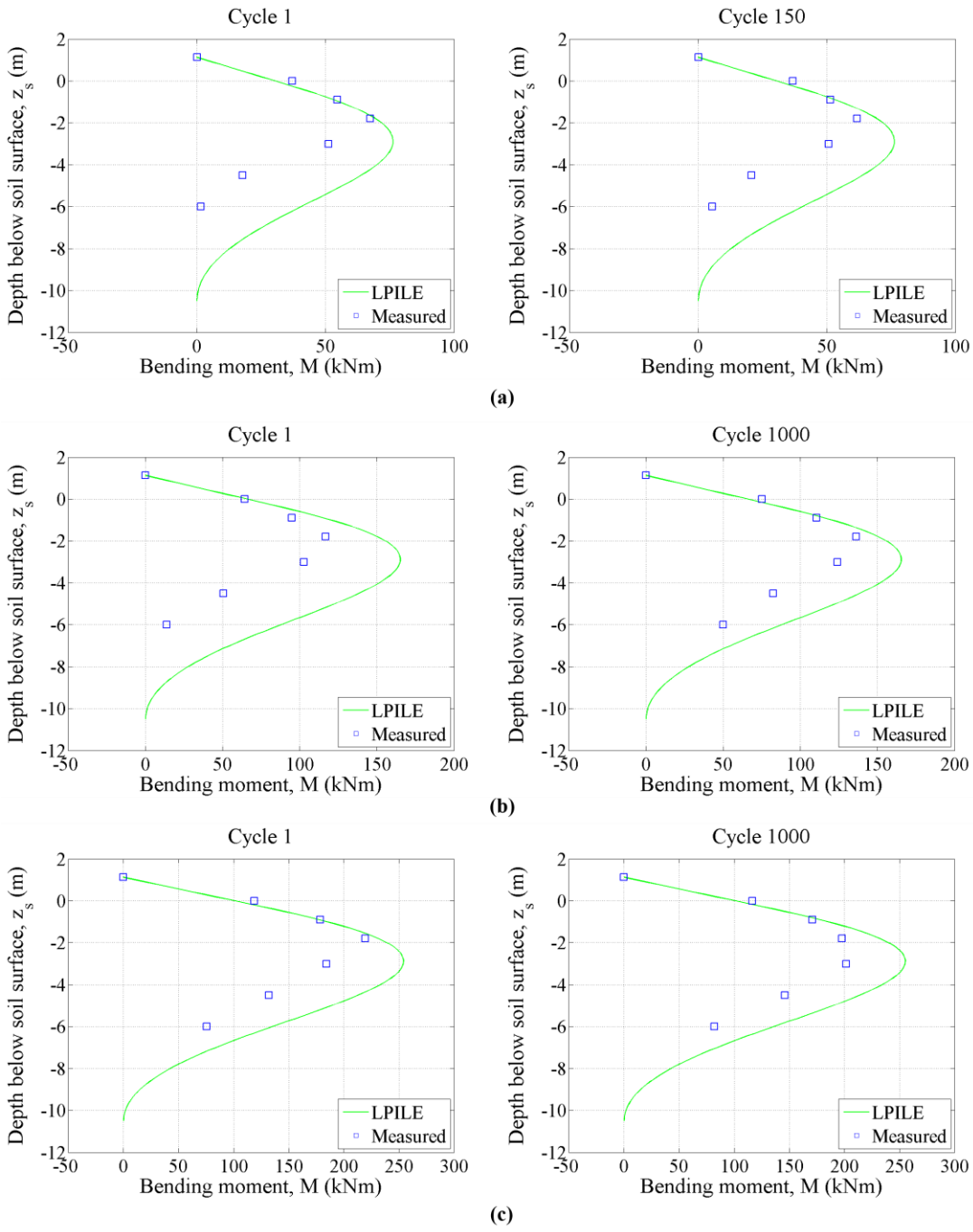

Figure 5-36: LPILE comparison with bending moment results at full-scale from cyclic test: (a) 30 N, (b) 65 N, (c) 100 N – scaled reinforced concrete

From **Figure 5-36** it can be seen that a good correlation between the measured and predicted bending moment values were obtained for the top part of the pile. However, deeper than 2 m below the soil surface, the predicted bending moment overestimated the measured behaviour significantly. Furthermore, **Figure 5-37** indicates the comparison between the measured and predicted lateral displacements of the pile.

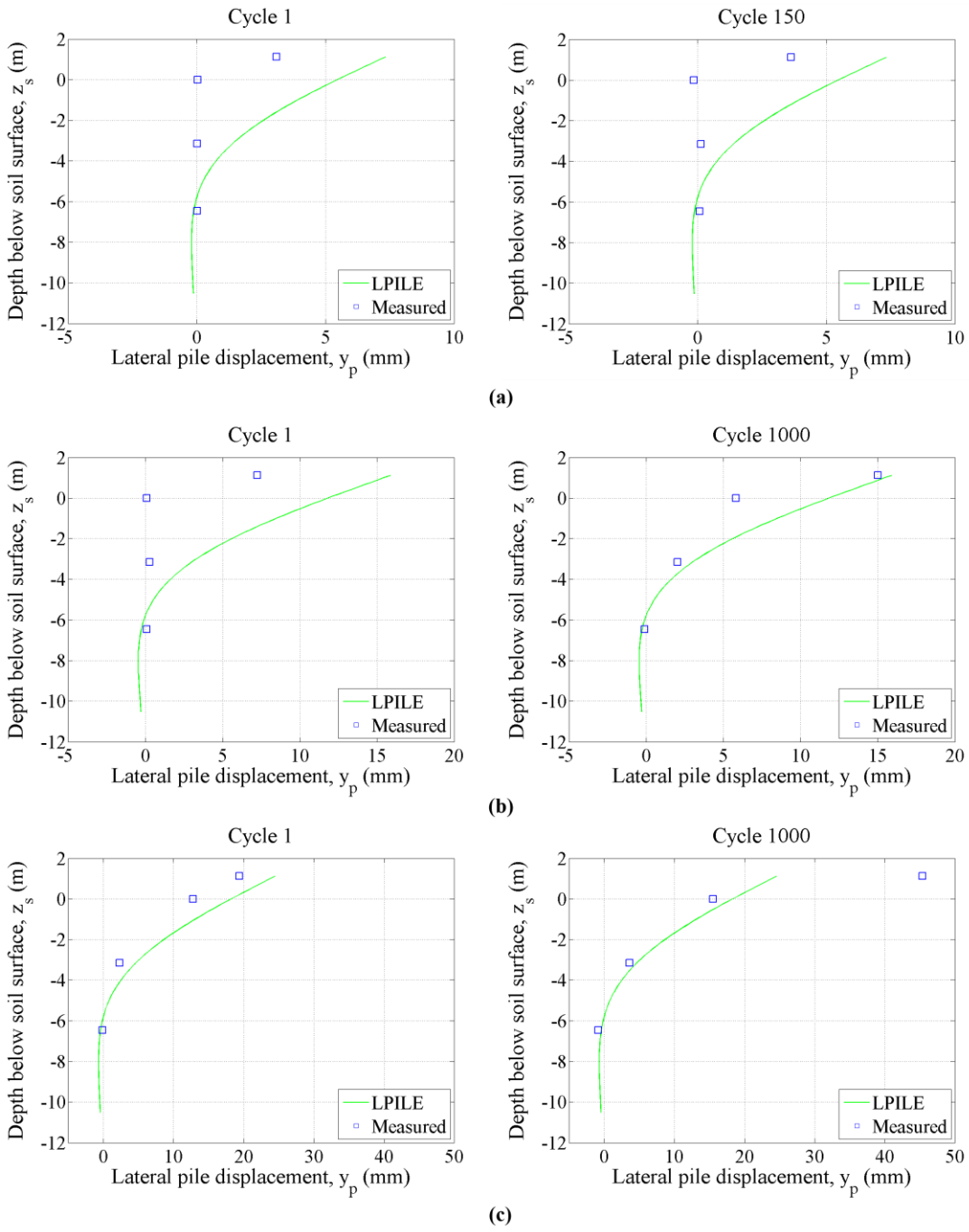

Figure 5-37: LPILE comparison with lateral pile displacement results at full-scale from cyclic test: (a) 30 N, (b) 65 N, (c) 100 N - scaled reinforced concrete

Figure 5-37 (a), **(b)** and **(c)** indicates results for a cyclic load magnitude of 30 N, 65 N and 110 N, respectively. Similar to the bending moments, for each load magnitude, only two cycles are indicated. In **Figure 5-37** it can be seen that the predicated lateral displacement overestimated the measured behaviour. The measured displacement after 1000 load cycles of 65 N, and 1 load cycle and 1000 load cycles of 100 N, only showed a good correlation to the predicted values due to the formation of a crack that occurred in the reinforced concrete pile during the centrifuge test.

5.7.7 Summary

Results based on the observed behaviour of the scaled reinforced concrete pile under cyclic loading conditions include the following:

- As the magnitude of the applied load increased, the bending moment and lateral displacement of the pile increased.
- The maximum measured bending moment occurred at three pile diameters below the soil surface, differing from what was observed from the scaled aluminium pile. The maximum lateral displacement of the pile occurred at the point of load application.
- Before the concrete cracked, behaviour similar to that of the aluminium pile was observed for the concrete pile. Only the load magnitude had an influence on the bending moment and lateral displacement of the pile, being unaffected by the number of load cycles.
- Significant lateral displacement of the pile occurred after a crack had formed in the concrete section, which was influenced by both the load magnitude and the number of load cycles.
- Non-linear behaviour of the concrete was evident, as indicated by the strain measurements. A plastic hinge formed in the concrete section after the formation of a crack, resulting in the part above the crack rotating about this point.
- The formation of a crack had minimal effect on the bending moment response of the pile.
- Permanent locked-in moments occurred in the pile after load removal during the cyclic load test, increasing with both load magnitude and number of load cycles. However, a slight decrease in the permanent moment was observed as the crack propagated.
- Similar to the scaled aluminium pile, the maximum locked-in moments occurred seven pile diameters below the surface of the soil, as opposed to the three pile diameters where the maximum bending moment occurred under loading. As with the scaled aluminium pile, 50% of the bending moments remained in the pile as permanent bending moments at depths deeper than five pile diameters below the soil surface. This was due to changing soil conditions surrounding the pile, creating locked-in soil and pile stresses in response to applied cyclic lateral loads.

- At low loads, when the concrete was still uncracked, the number of load cycles did not influence the maximum displacement of the pile. However, at higher applied loads, the pile cracked, resulting in the number of load cycles having a significant effect on the maximum displacement of the pile above the crack.
- Permanent displacement of the pile after load removal increased with an increase in the number of load cycles and load magnitude, which probably caused the locked-in moments occurring in the pile.
- The difference between the displacement of the pile under loading and the permanent displacement of the pile increased as the magnitude of the applied load increased.
- The first load cycle at each load magnitude caused the most damage to the soil-pile system.
- Regardless of the magnitude of the applied load, the absolute pile stiffness decreased logarithmically with an increase in number of load cycles, as the pile experienced accumulating permanent displacement. The rate of decrease was influenced significantly by the change in the behaviour of the pile after cracking.
- The secant pile stiffness increased logarithmically with an increase in number of load cycles, regardless of the load magnitude. The rate of increase was also influenced by the densification of the soil caused by cyclic loading. The changing sectional properties of the pile after cracking did not have an effect on the pile secant stiffness response.
- The measured bending moment from the centrifuge test was in good agreement with the predicted values from the LPILE software package towards the top of the pile. However, at more than five pile diameters below the soil surface, the bending moments were overestimated and were unable to accurately model the bending moment. Furthermore, the lateral displacement results from the centrifuge test was not in good agreement with the predicted values from the LPILE software package.

5.8 CONCLUSION

In this chapter, the data recorded from all the centrifuge tests was presented and discussed. For the monotonic test on the aluminium pile, trends similar to that observed from literature was obtained. The measured results also matched the results obtained from the software package, LPILE, that was originally developed and calibrated using full-scale metal piles.

The cyclic test on the aluminium pile also showed trends similar to that observed in literature. Repeated loading of the pile resulted in densification of the soil in front of the pile, changing the stiffness and response of the soil. Permanent displacement of the pile was also observed with cyclic loading, causing locked-in moments and stresses in the pile and the surrounding soil.

During the cyclic test on the reinforced concrete pile, similar behavioural trends were observed for the uncracked concrete section than for the aluminium pile. However, after the formation of a crack in the concrete section, highly non-linear behaviour of the reinforced concrete pile occurred, which was not observed for the aluminium pile. This resulted in large permanent displacements of the reinforced concrete pile, which greatly influenced the response of the soil-pile system. A significant change in the relative rigidity of the reinforced concrete pile was observed after the formation of cracks in the section, raising the question of whether, when modelling reinforced concrete piles, cracked or uncracked sections should be modelled.

A comparison between the measured results for the aluminium and reinforced concrete piles as presented in this chapter is provided in Chapter 6. The similarities and differences in the measured behavioural trends were studied, to aid in answering the research question and objectives in Chapter 1.

6 RESULTS AND DISCUSSIONS: COMPARISON

6.1 INTRODUCTION

This chapter contains a comparison between the response observed from the scaled aluminium and reinforced concrete piles in the centrifuge tests, based on selected results from Chapter 5. By comparing the behaviour of the two piles, similarities and differences can be highlighted, establishing whether the research question and the objectives in the beginning of the dissertations were addressed.

The first part of the chapter focusses on the comparison between the monotonic response of the scaled aluminium and reinforced concrete piles, investigating the first load cycle under low loads, with the soil having no prior load history. This is followed by a discussion and comparison of the cyclic response of the two piles, which allowed conclusions to be drawn.

6.2 MONOTONIC RESPONSE COMPARISON

For comparing the monotonic response of the two piles, the strain development and lateral displacement data were considered. This was based on the results from the first load cycle from each of the cyclic load tests on the scaled aluminium and reinforced concrete piles respectively, under the condition that both the pile and the surrounding soil had no prior load history. Thus, the load response experienced by the piles can be considered monotonic.

Due to the flexural rigidity of the two piles not being the same, the pile behaviour could not be compared directly. The flexural stiffness of the concrete pile was 1.63 times that of the aluminium pile. By using the factor (relative stiffness), the measured strain and deflection results from the reinforced concrete pile were adjusted, allowing for comparison with the aluminium pile results.

Figure 6-1 indicates the bending strain (ε_b) development along the length of the pile for the aluminium and adjusted reinforced concrete pile results when exposed to the first load cycle. The strains for both the tension (T) and compression (C) sides of the piles are shown. Results are presented for an applied lateral load of 10 N and 30 N, respectively, which for the aluminium pile corresponded to 1.5% and 4% of the ultimate capacity of the aluminium pile calculated in Section 4.6.6. For the reinforced concrete pile, these loads corresponded 13% and 40% of the ultimate capacity of the reinforced concrete pile (Section 4.6.6). From **Figure 6-1** it can be seen that, for all practical purposes, after adjusting the reinforced concrete results to take the difference in flexural stiffness into account, the aluminium and reinforced concrete piles showed the same results with depth for a 10 N load. However, as the magnitude of the applied

load increased to 30 N, a significant difference between the measured data was observed at depths exceeding 50 mm below the soil surface, with the strain in the reinforced concrete pile being only half of that in the aluminium pile at a depth of 150 mm below the soil surface. The strain measured for both piles above 50 mm below the surface of the soil, at 30 N, was still in good agreement with each other. This is an indication that, even at low loads under monotonic load conditions, a difference between the behaviour of the aluminium and reinforced concrete pile was observed.

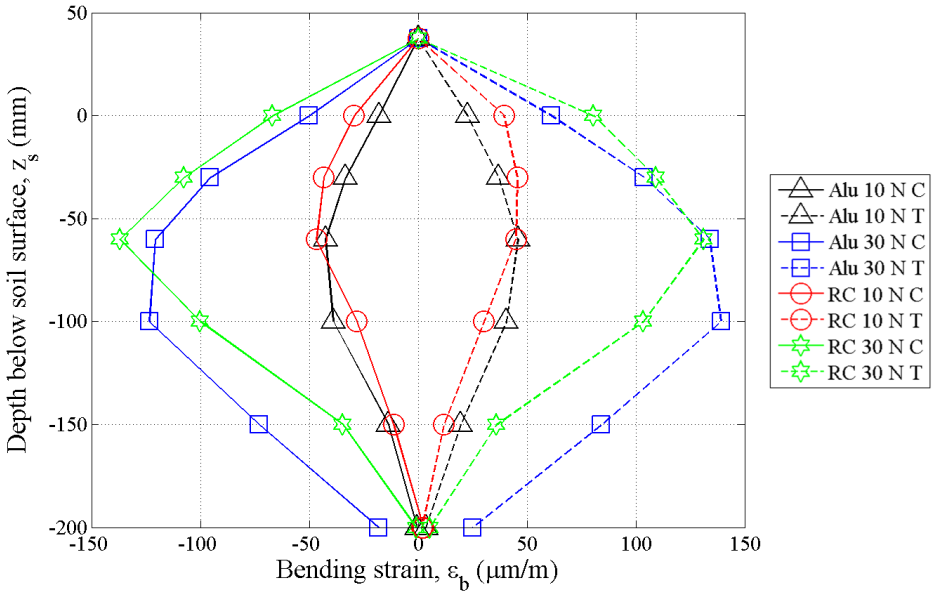

Figure 6-1: Adjusted strain development – monotonic

The measured pile displacements for the aluminium and reinforced concrete piles were compared to the predicted results obtained from the LPILE program. In order to compare the results, the scaled results had to be converted to full-scale values using appropriate scaling laws. The coefficient of subgrade reaction of 2.4 MN/m^3 selected for the sand in Chapter 5 was also used for this analysis. **Figure 6-2 (a)** and **(b)** show the measured and predicted values for the lateral displacement of the aluminium and reinforced concrete piles, respectively, for an applied monotonic load of 10 N and 30 N. It should be noted that a poor representation of the results was obtained from the LPILE program for both the piles, with the response of the reinforced concrete pile being completely overestimated. The slight difference between the measured and predicted results for the aluminium pile is possibly due to the small magnitude of the applied load, resulting in the response of the soil still being stiffer (small strain stiffness). The coefficient of subgrade reaction of 2.4 MN/m^3 for the sand was originally obtained and selected for an applied lateral load of 50 N in Chapter 5, which is larger than these loads. Thus, for loads

smaller than 50 N, the stiffness of the soil should be higher, resulting in smaller lateral displacements.

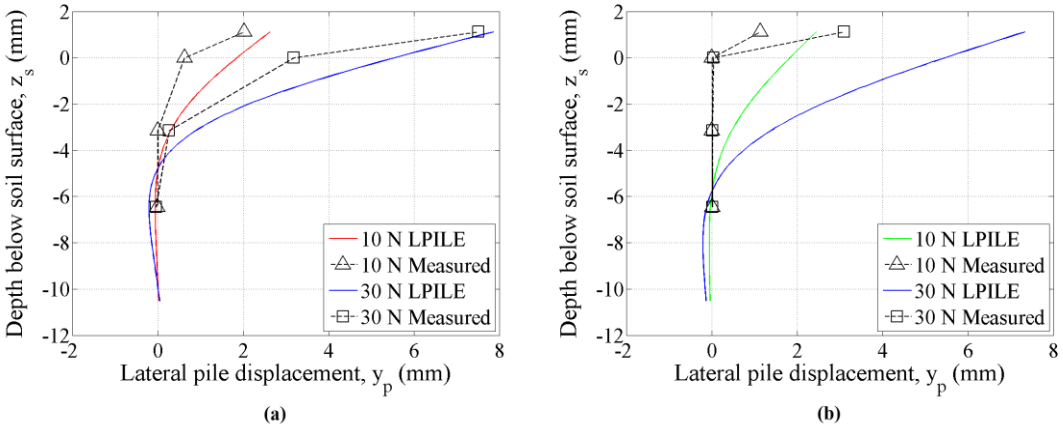

Figure 6-2: LPILE comparison with lateral pile displacement results at full-scale: (a) aluminium, (b) reinforced concrete – monotonic

Figure 6-3 presents the lateral displacement (y_p) along the length of the pile for the aluminium and reinforced concrete pile results, applying the relative stiffness ratio to the reinforced concrete pile. Results are presented for an applied lateral load of 10 N and 30 N, respectively. It can be seen that at an applied load of 10 N, the lateral displacement of the piles differed slightly, which ties into the behaviour observed with the strains. However, as the load magnitude increased, the difference between the displacement of the aluminium and reinforced concrete pile increased.

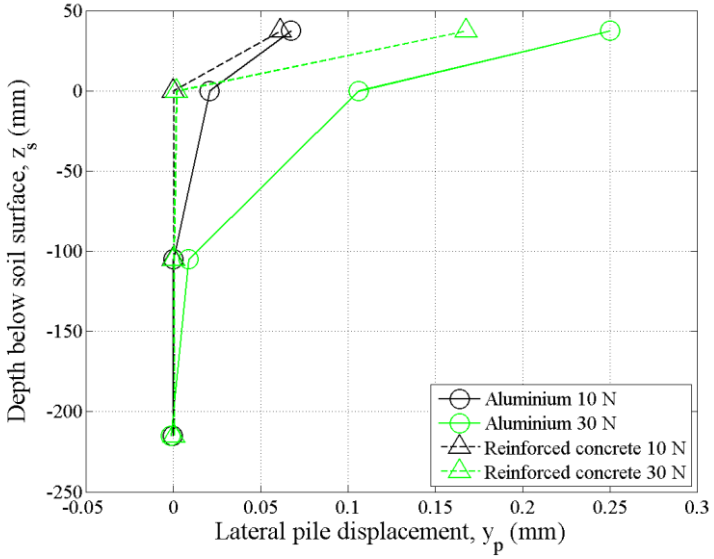

Figure 6-3: Adjusted lateral displacement of the pile with depth – monotonic

The difference might link to the contribution of shear to the overall displacement of piles. As indicated in Chapter 4, the axial rigidity (which influences the shear capacity) of the reinforced concrete pile was significantly larger than that of the aluminium pile. Duncan *et al.* (1994) and Long & Vanneste (1994) indicated the influenced of both bending (*EI*) and shear (*EA*) on the displacement of the pile. However, due to a lack of information, their equations could not be applied to determine whether the difference is linked to the axial rigidity. By observing the curvature of the deflected profiles for the aluminium and reinforced concrete piles, it is evident that the majority of the movement of the reinforced concrete pile occurred above the soil surface, whereas the movement of the aluminium pile distributed deeper into the soil (even at loads as small as 4% of the ultimate capacity). As deflection (displacement) is proportional to the second integral of the bending moment (strain), this explains the difference observed between the strains of the two piles deeper into the soil. This again emphasises the importance of considering the behaviour of concrete, and how it is different than the behaviour of aluminium, even at low loads.

6.3 CYCLIC RESPONSE COMPARISON

Based on the results obtained from the entire cyclic load test on the two piles, the cyclic response of the scaled aluminium and reinforced concrete piles can be compared by considering the load-displacement and soil stiffness changes with cycles and permanent displacement.

Figure 6-4 and **Figure 6-5** indicates the cyclic load-displacement response for the aluminium and reinforced concrete pile, respectively. In each figure, cycle 1 (blue), cycle 100 (red) and cycle 1000 (black) is highlighted for each load magnitude, with the rest of the cycles shown in grey. From both these figures it can be seen that the first load cycle at each load magnitude caused the most deformation to the surrounding soil, with the large hysteresis loop that is present. After this, the hysteresis loop width decreases with number of load cycles for both the aluminium and reinforced concrete pile.

However, when considering and comparing the overall load-displacement response of the two piles at the different load magnitudes it can be seen that, for the aluminium pile, the soil-pile response suffered large deformation during the first few cycles at each load, becoming resilient with an increase in the number of load cycles (range B) (Werkmeister *et al.*, 2004). During range B, resilient behaviour of the soil is observed, with permanent displacements/strains gradually increasing with an increase in number of load cycles. The reinforced concrete pile showed completely different behaviour, regardless of the magnitude of the applied load. Initially, at 30 N, the response of the soil-pile system was completely resilient, with nearly no permanent displacement increase as the number of load cycles increased (range A) (Werkmeister *et al.*, 2004). However, at 65 N and 100 N significant permanent deformation

occurred at lower loads than that of the aluminium, largely due to the formation of cracks in the concrete section that was not present with the aluminium pile. Large displacements/strains occurred for each additional load application at 100 N (range C) (Werkmeister *et al.*, 2004).

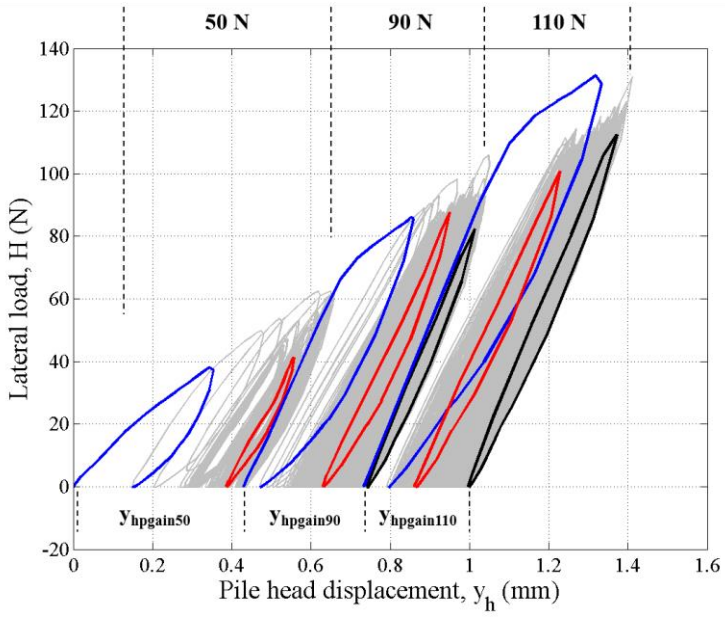

Figure 6-4: Load-displacement response - cyclic aluminium

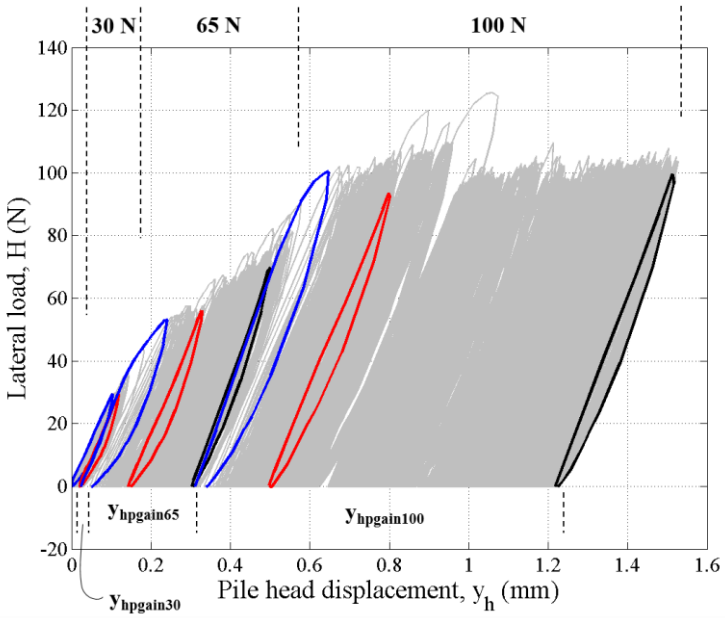

Figure 6-5: Load-displacement response - cyclic reinforced concrete

In order to compare the load-displacement results for the two piles, envelopes to the load-displacement response graphs above, were plotted. **Figure 6-6** presents the envelopes for the aluminium and reinforced concrete pile results after applying the relative stiffness ratio to the

displacement results of the reinforced concrete pile, thus making it possible to compare the two piles. From the start of the curve, even for an uncracked concrete section, the reinforced concrete pile exhibited non-linear behaviour in comparison to that of the aluminium pile that showed a fairly linear response.

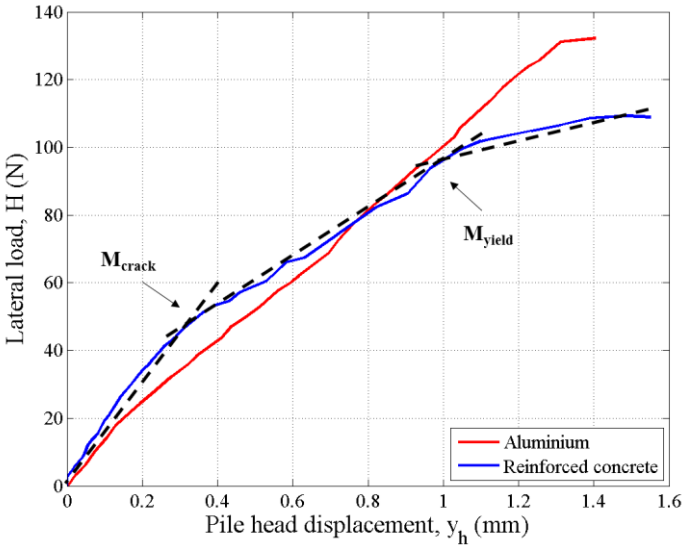

Figure 6-6: Static failure curves

After considering the relative stiffness between the two piles, at low loads, the reinforced concrete pile had a stiffer response than the aluminium pile. The non-linear response of the concrete was further influenced by the formation of cracks in the section, and a change in the stiffness of the pile, at a load of approximately 50 N, which corresponded to the predicted cracking load (H_{crack}) in Chapter 4. The reinforced concrete pile yielded at a load of about 90 N, which was slightly higher than the predicted value in Chapter 4. Large differences between the two piles existed past this point of yielding. This is due to the formation and propagation of cracks in the reinforced concrete pile, which was not the case for the aluminium pile.

To investigate and compare the response of the soil to cyclic loading of the aluminium and reinforced concrete piles, the secant pile stiffness of the soil-pile system, and how it was influenced by the load magnitude and the number of load cycles were considered. From **Figure 6-4** for the aluminium pile, cycle 1000 (black cycle) for load magnitudes 90 N and 110 N, respectively, was extracted. Similar for the reinforced concrete pile, cycle 1000 (black cycle) was extracted from **Figure 6-5**, for load magnitudes 65 N and 100 N, respectively. These cycles are plotted in **Figure 6-7 (a)** and **(b)** for the aluminium and reinforced concrete piles, respectively. As illustrated for both piles, considering the slope of the line connecting the peak of the loading curve and the origin (secant pile stiffness), the stiffness converged to a constant

value for each pile as the number of cycles increased. The secant pile stiffness (slope of the line) for the aluminium pile was calculated as 300 N/mm, where the slope for the reinforced concrete pile was slightly steeper, calculated as 350 N/mm. Thus, based on this it appears that, regardless of the magnitude of the load, the secant pile stiffness will eventually converge to a constant value after a certain number of load cycles. Lastly, it should also be mentioned that cycle 1000 at 100 N for the reinforced concrete pile included the formation of the crack in the concrete section. Based on the observed behaviour it seems that the formation of a crack did not influence the secant stiffness response, and that the secant pile stiffness is mainly affected by the resilient modulus of the soil.

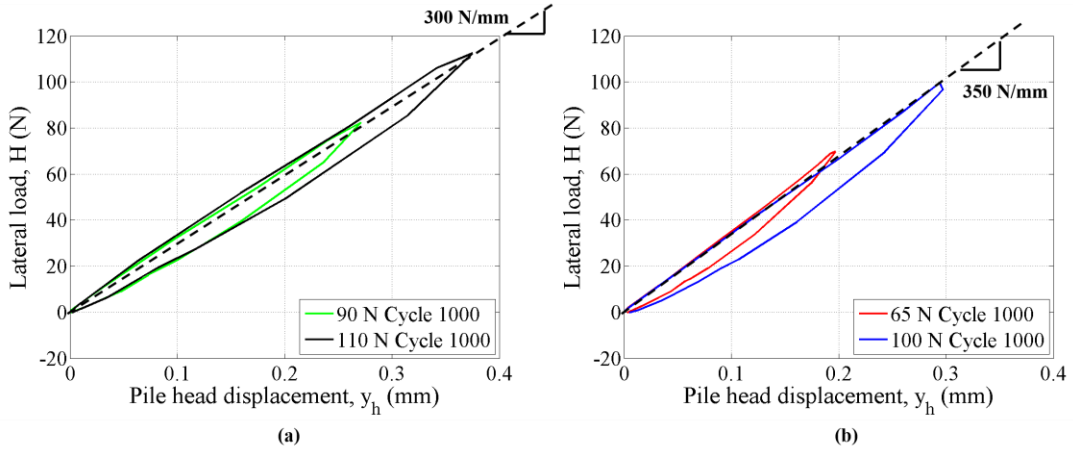

Figure 6-7: Secant stiffness cycles: (a) aluminium, (b) reinforced concrete

Furthermore, to demonstrate the secant pile stiffness for the aluminium and reinforced concrete piles converging, the secant pile stiffnesses as shown previously in Section 5.6.5 and Section 5.7.5 are combined on a single plot (see **Figure 6-8**). As mentioned above, it can be seen that as the number of load cycles for both piles increased (at any load magnitude), the secant pile stiffness converged to a constant value, with the stiffness unaffected by the formation of a crack. Densification of the soil in front of the piles were observed for both piles.

Lastly, by considering the permanent displacement of the pile, interesting differences between the aluminium and reinforced concrete pile was observed. From **Figure 6-4** and **Figure 6-5**, the permanent pile head displacement gain (y_{hpgain}) can be calculated for each pile, as indicated on the x-axis in both these figures. The permanent pile head displacement gain is the difference between the permanent displacement after the last load cycle and the permanent displacement at the first load cycle for each lateral load magnitude. The permanent displacement of the pile is largely influenced by the magnitude of the applied load and the number of load cycles. Thus, even though the cyclic tests on the aluminium and reinforced concrete piles was not conducted

at the same load magnitudes and number of load cycles, a trend can be observed from the data calculated from each test.

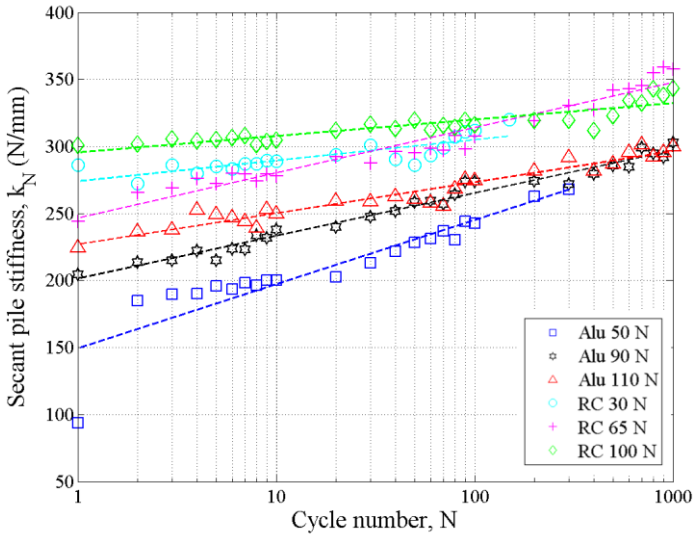

Figure 6-8: Combined secant stiffness

Figure 6-9 shows the permanent pile head displacement gain against the magnitude of the applied load for both piles after *N* cycles at each load. The permanent pile head displacement gain for the 50 N load on the aluminium pile and the 30 N load on the reinforced concrete pile was shown as unshaded markers. This is to highlight that only 300 and 150 load cycles were applied to the aluminium and reinforced concrete pile at those loads respectively, as opposed to the 1000 load cycles at higher loads (solid markers).

It is worth noting that, for the scaled aluminium pile, a decrease in the permanent pile head displacement gain occurred as the magnitude of the applied load increased. This differs from what was observed with the reinforced concrete pile, where the permanent pile head displacement increased with an increase in the load magnitude. The rate of increase for the reinforced concrete pile was higher than the rate of decrease for the aluminium pile. This is largely due to the formation of cracks in the concrete section, resulting in a steep increase in the permanent pile head displacement after 65 N. This was also observed from the absolute pile stiffness in Section 5.6.5 and Section 5.7.5 in Chapter 5, which is dependent on the amount of permanent deformation generated at each load magnitude. A significant change in the absolute pile stiffness occurred after the formation of a crack in the concrete section, which was not observed with the aluminium pile. This behaviour confirms the observations made by Little & Briaud (1988) namely that a change in flexural stiffness (cracking) of the pile caused greater degradation to the soil-pile system.

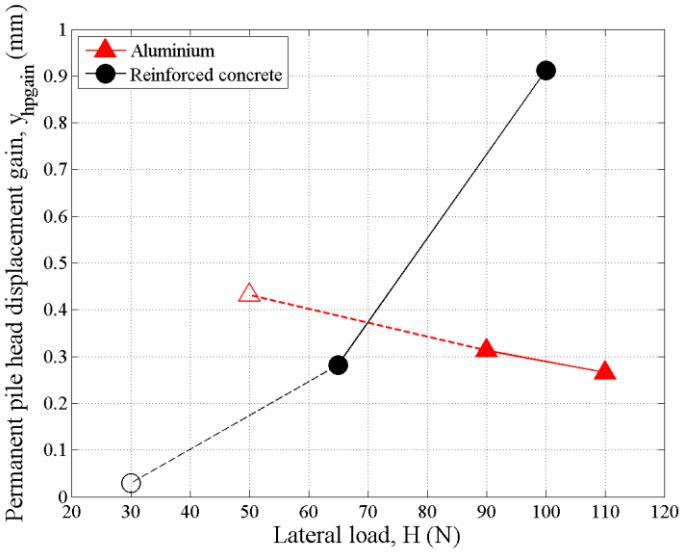

Figure 6-9: Comparison permanent pile head displacement gain

Thus, besides the secant pile stiffness for both the aluminium and reinforced concrete piles that showed similar trends with cyclic loading, the overall response of the reinforced concrete pile could not be matched with an aluminium pile.

6.4 SUMMARY

In this chapter, a comparison between the behaviour of the aluminium and reinforced concrete piles were presented and discussed, considering both the monotonic and cyclic response of the two piles.

At low lateral loads, under monotonic loading conditions, it was already evident from the strain and displacement data that the response of the reinforced concrete pile was not replicated by the aluminium pile. At a load of 30 N, 40% of the ultimate capacity of the reinforced concrete pile was used, compared to only 4% of the aluminium pile. This is due to the aluminium pile having a much larger yield strength than the reinforced concrete pile, which cracked at low loads (non-linear material behaviour).

Furthermore, comparing the responses of the piles under cyclic loading conditions significant differences were also observed. When considering the static failure curve, it was noticeable from the start that the response of the reinforced concrete pile was non-linear, in comparison to the fairly linear response of the aluminium pile. The non-linear behaviour of the reinforced concrete pile was further influenced by the cracking and yielding moment that occurred in the pile as the magnitude of the applied load increased.

The overall load-displacement response of both piles to cyclic loading indicated a densification of the soil in front of the pile with an increase in number of load cycles (secant pile stiffness), converging to a constant value, regardless of the magnitude of the applied load and the number of load cycles. Furthermore, the formation of cracks did not seem to have an influence on the secant pile stiffness response. The secant pile stiffness (k_N) seems to be a function of soil stiffness and the effect of pile stiffness seems to be limited.

Significant permanent deformation was observed for the reinforced concrete pile after the formation of a crack in the section, which was not the case with the aluminium pile. The permanent deformation associated with a given number of load cycles increased for the reinforced concrete pile and decreased for the aluminium pile as the magnitude of the applied load increased. The absolute pile stiffness (K_N) seems to be significantly affected by the pile stiffness.

Thus, based on the observed results, care should be taken when modelling reinforced concrete piles with aluminium. Significant differences which cannot be avoided, occurred, that contributed to a difference in the observed behaviour between the two piles.

7 CONCLUSIONS AND RECOMMENDATIONS

7.1 INTRODUCTION

This chapter summarises the main conclusions reached based on the results obtained from the various centrifuge test. Conclusions are followed by recommendations based on the findings of the study and aspects that can be considered for future research.

7.2 CONCLUSIONS

The aim of the research was to establish whether metal pile sections in a centrifuge could be used to realistically and with sufficient accuracy model the monotonic and cyclic response of reinforced concrete piles subjected to lateral loading. Many design assumptions and methods with regard to pile foundations are based on the principles observed from metal piles, which raises the question of the validity of these assumptions and methods for the use of analysing and designing reinforced concrete piles.

After considering literature, tests were conducted in the centrifuge on a scaled aluminium and reinforced concrete pile in sand at constant relative density, subjected to both monotonic and cyclic loading conditions. The magnitude of the applied lateral loads corresponded to that suggested by literature for reinforced concrete piles for respectively uncracked and cracked, or yielding response, of the concrete section. The soil-pile interaction mechanisms were observed and discussed, as this primarily affected not only the pile bending and displacement behaviour under lateral loads, but also the behaviour of the soil surrounding the pile.

It is normal practice to use scaling laws when designing a centrifuge experiment. As flexural behaviour was studied, the flexural stiffness of the piles was taken into account. This does however not take into account the limiting effect of the relatively low cracking and yield strength of the concrete pile. Analysis of the pile capacities revealed that a scaled hollow aluminium pile would be able to resist a load up to 100 times larger than the failure load of a scaled reinforced concrete pile with similar flexural stiffness.

The monotonic lateral load test on the scaled aluminium pile showed similar trends to that observed from literature regarding bending moments and lateral displacement. The results obtained also matched well with that predicted by the software package, LPILE, that has been widely used, and was originally calibrated from tests on steel piles.

Regardless of the difference in flexural rigidity between the aluminium and reinforced concrete piles, after adjusting the results for the reinforced concrete pile to take this difference into

account, significant differences between the pile behaviour was observed, even at low applied loads, during the first load cycle when the concrete was still uncracked. The strains measured in the aluminium and reinforced concrete piles near the soil surface were in good agreement, however, deeper into the soil a significant difference between the measured strains was observed, with the reinforced concrete pile experiencing about 50% less strain.

By considering the scaled aluminium and reinforced concrete piles under cyclic loading conditions, similar trends to that observed from literature was obtained. This proved that both piles modelled the concept of laterally loaded piles under cyclic loading quite well regarding bending and lateral displacement. Locked-in moments was also observed in both piles, due to repetitive loading, caused by permanent displacement and deformation of the pile. The static failure curves for the piles, forming an envelope over the measured results from the cyclic tests, indicated the noticeable non-linear response of the uncracked reinforced concrete pile in comparison to the aluminium pile that exhibited a fairly linear response at the same loads. The non-linear behaviour of the reinforced concrete pile was further influenced by the cracking and yielding moment that occurred in the pile. Changes in the properties of the soil (soil densification) occurred due to repetitive loading of the pile, which was observed for both the aluminium and reinforced concrete piles. This densification will also result in a change of the relative rigidity of the pile, with the pile response moving more towards that of a flexible pile. The response of the aluminium pile was in reasonable agreement with the predicted values from the LPILE program, while the predicted values obtained for the response of the scaled reinforced concrete pile overestimated the values measured.

The formation of a crack in the reinforced concrete section resulted in highly non-linear response of the reinforced concrete pile due to the low tensile strength of the concrete. This had a significant effect on displacement of the pile under loading and the permanent displacement of the pile when the load was removed. The rate at which the permanent displacement increased after cracking was influenced by the magnitude of the load and the number of load cycles, affecting the absolute pile stiffness significantly. This suggested that the absolute pile stiffness is primarily a function of the stiffness of the pile. Furthermore, the overall load-displacement response of the reinforced concrete pile indicated that, similar to the aluminium pile, densification of the soil in front of the pile occurred due to repetitive loading (secant pile stiffness), converging to a constant value regardless of the magnitude of the applied load. The formation of cracks did not seem to have an influence on the secant pile stiffness response, possibly indicating that secant pile stiffness is a function of the soil stiffness and not the pile stiffness. Lastly, the formation of cracks in the reinforced concrete section had a significant effect on the relative rigidity of the soil-pile system, which was not the case for the aluminium

pile. The significant reduction in pile flexural stiffness caused a decrease in the pile-flexibility factor, resulting in the reinforced concrete pile behaving as a flexible pile.

Thus, based on the results obtained from this dissertation, care should be taken when using aluminium sections for modelling reinforced concrete piles at model scale. Apart from the secant pile stiffness for both the aluminium and reinforced concrete piles that showed similar results in terms of cyclic loading, the overall monotonic and cyclic response of the reinforced concrete pile, including the true material behaviour and failure mechanisms, could not be matched with the aluminium pile. Significant differences that cannot be avoided between the two piles, existed, especially considering the change in the relative rigidity that occurs for the reinforced concrete pile after the formation of cracks in the section, raising the question of whether, when modelling reinforced concrete piles, cracked or uncracked sections should be modelled.

7.3 RECOMMENDATIONS

Due to the low tensile strength of concrete it is recommended that scaled reinforced concrete piles should be used when modelling full-scale reinforced concrete piles in physical models. Not only the flexural rigidity should be matched, but prototype load capacity should be taken into account when designing a centrifuge model for testing piles.

Based on results obtained during this project some recommendations for future research include the following:

- Investigating the effect of different relative densities of the soil on the soil-pile response for single scaled aluminium and reinforced concrete piles subjected to lateral loading, as the interaction between the stiffnesses seems to govern the response of the soil-pile system.
- Testing the influence of pile diameter on the response of single piles subjected to lateral loading using scaled reinforced concrete piles.
- Investigating the response of laterally loaded piles for various embedment lengths.
- Establishing the effect of pile head conditions (fixed or free) and soil-pile interaction roughness on the response of a laterally loaded pile.
- Determine the influence of vertical loads on the behaviour and response of laterally loaded scaled reinforced concrete piles.
- Use finite element modelling to model laterally loaded piles, observing the soil-structure interaction problem by modelling the soil as a continuum, also observing the effect of non-linear pile behaviour on the response of the soil-pile system.
- Establishing the effect of an additional pile(s) in the soil, observing the distribution of forces and stresses between the piles.

- Locked-in pile and soil stresses should be studied.

8 REFERENCES

Abadie, C.N. & Byrne, B.W. 2014. Cyclic loading response of monopile foundations in cohesionless soils. In Vol. 2 of *Proceedings of the 8th International Conference on Physical Modelling in Geotechnics.* Edited by C. Gaudin & D. White. CRC Press, Boca Raton, Florida, pp 779-784.

Ashour, M. & Norris, G. 2000. Modeling lateral soil-pile response based on soil-pile interaction. *Journal of Geotechnical and Geoenvironmental Engineering*, Vol 126, No 5, pp 420-428.

ASTM International. C192/C192M – 18 *Standard Practice for Making and Curing Concrete Test Specimens in the Laboratory*. West Conshohocken, PA; ASTM International, 2018. doi: https://doi.org/10.1520/C0192_C0192M-18.

ASTM International. C511 – 19 *Standard Specification for Mixing Rooms, Moist Cabinets, Moist Rooms, and Water Storage Tanks Used in the Testing of Hydraulic Cements and Concretes*. West Conshohocken, PA; ASTM International, 2019. doi: https://doi.org/10.1520/C0511-19.

ASTM International. D2487-11 *Standard Practice for Classification of Soils for Engineering Purposes (Unified Soil Classification System).* West Conshohocken, PA; ASTM International, 2011. doi: https://doi.org/10.1520/D2487-11.

ASTM International. D4253 – 16 *Standard Test Methods for Maximum Index Density and Unit Weight of Soils Using a Vibratory Table*. West Conshohocken, PA; ASTM International, 2016. doi: https://doi.org/10.1520/D4253-16.

ASTM International. D4254 – 16 *Standard Test Methods for Minimum Index Density and Unit Weight of Soils and Calculation of Relative Density*. West Conshohocken, PA; ASTM International, 2016. doi: https://doi.org/10.1520/D4254-16.

ASTM International. D4546 – 14e1 *Standard Test Methods for One-Dimensional Swell or Collapse Soils*. West Conshohocken, PA; ASTM International, 2014. doi: https://doi.org/10.1520/D4546-14E01.

ASTM International. D7181 – 11 *Standard Test Method for Consolidation Drained Triaxial Compression Test for Soils*. West Conshohocken, PA; ASTM International, 2011. doi: https://doi.org/10.1520/D7181-11.

Barton, Y.O. 1982. Laterally loaded model piles in sand: centrifuge testing and finite element analyses. PhD thesis. University of Cambridge, UK.

Bogard, D. & Matlock, H. 1980. Simplified calculation of p-y curves for laterally loaded piles in sand. *Unpublished Report, The Earth Technology Corporations, Inc.*, Houston, Texas.

British Standards Institution. (2009). BS EN 12390-3:2009 *Testing Hardened Concrete. Compressive Strength of Test Specimens*. London, England: BSI.

British Standards Institution. (2000). BS EN 12390-6:2000 *Testing Hardened Concrete. Tensile Splitting Strength of Test Specimens.* London, England: BSI.

British Standards Institution. (2013). BS EN 12390-13:2013 *Testing Hardened Concrete. Determination of Secant Modulus of Elasticity in Compression*. London, England: BSI.

British Standards Institution. (2014). BS EN 1992-1-1:2004 + A1:2014 *Eurocode 2: Design of Concrete Structures - General Rules and Rules for Buildings.* London, England: BSI.

Broms, B.B. 1964b. Lateral resistance of piles in cohesionless soils. *Journal of the Soil Mechanics and Foundations Division: Proceedings of the American Society of Civil Engineers (ASCE),* Vol 90, No SM3, pp 123-156.

Brown, D.A., Reese, L.C. & O'Neill, M.W. 1987. Cyclic lateral loading of a large-scale pile group. *Journal of Geotechnical Engineering*, Vol 113, No 11, pp 1326-1343.

Byrne, G. & Berry, A.D. 2008. *A Guide to Practical Geotechnical Engineering in Southern Africa.* 4th ed. FRANKI.

Domone, P. & Illston, J. 2010. *Construction Materials: Their Nature and Behaviour.* 4th ed. Spon Press, Abingdon, Oxon.

Duncan, J.M., Evans Jr, L.T. & Ooi, P.S.K. 1994. Lateral load analysis of single piles and drilled shafts. *Journal of Geotechnical Engineering*, Vol 120, No 6, pp 1018-1033.

Dyson, G.J. & Randolph, M.F. 2001. Monotonic lateral loading of piles in calcareous sand. *Journal of Geotechnical and Geoenvironmental Engineering*, Vol 127, No 4, pp 346-352.

EI Naggar, M.H. & Heidari, M. 2018. Geo-structural nonlinear analysis of piles for performance-based design. *Proceedings of the International Conference on Geotechnical Research and Engineering (ICGRE18)*, Budapest, Hungary.

Fleming, K., Weltman, A., Randolph, M. & Elson, K. 2008. *Piling Engineering*. 3rd ed. CRC Press.

Gere, J.M. & Goodno, B.J. 2013. *Mechanics of Materials*. 8th ed. CENGAGE Learning.

Georgiadis, M., Anagnostopoulos, C. & Saflekou, S. 1992. Centrifugal testing of laterally loaded piles in sand. *Canadian Geotechnical Journal*, Vol 29, pp 208-216.

Jacobsz, S.W., Kearsley, E.P. & Kock, J.H.L. 2014. The geotechnical centrifuge facility at the University of Pretoria. In Vol. 1 of *Proceedings of the 8th International Conference on Physical Modelling in Geotechnics.* Edited by C. Gaudin & D. White. CRC Press, Boca Raton, Florida, pp 169-174.

Jagodnik, V. & Arbanas, Z. 2015. Testing of laterally loaded piles in natural sandy gravels. *International Journal of Physical Modelling in Geotechnics*, Vol 15, No 4, pp 191-208.

Johnson, K.L. 1986. Plastic flow, residual stresses and shakedown in rolling contacts. *Proceedings of the 2nd International Conference on Contact Mechanics and Wear of Rail/Wheel Systems*. Edited by G.M.L. Gladwell, H. Ghonem & J. Kalousek, University of Waterloo Press, Waterloo, Canada.

Kirkwood, P.B. & Haigh, S.K. 2014. Centrifuge testing of monopiles subject to cyclic lateral loading. In Vol. 2 of *Proceedings of the 8th International Conference on Physical Modelling in Geotechnics.* Edited by C. Gaudin & D. White. CRC Press, Boca Raton, Florida, pp 827-831.

Klar, A., Vorster, T.E.B., Soga, K. & Mair, R.J. 2005. Soil-pipe interaction due to tunnelling: comparison between winkler and elastic continuum solutions. *Geotechnique*, Vol 55, No 6, pp 461-466.

Knappett, J.A., Brown, M.J., Shields, L., Al-Defae, A.H. & Loli, M. 2018. Variability of small-scale model reinforced concrete and implications for geotechnical centrifuge testing. In Vol. 2 of *Proceedings of the 9th International Conference on Physical Modelling in Geotechnics.* Edited by A. McNamara, S. Divall, R. Goodey, N. Taylor, S. Stallebrass & J. Panchal. CRC Press, Taylor & Francis Group, pp 241-246.

Knappett, J.A. & Craig, R.F. 2012. *Craig's Soil Mechanics.* 8th ed. Spon Press, Abingdon, Oxon, New York.

Knappett, J.A., O'Reilly, K., Gilhooley, P., Reid, C. & Skeffington, K. 2010. Modelling precast concrete piling for use in a geotechnical centrifuge. In Vol. 1 of *Proceedings of the 7th International Conference on Physical Modelling in Geotechnics.* Edited by S. Springman, J. Laue & L. Seward. CRC Press, Taylor & Francis Group, pp 141-146.

Knappett, J.A., Reid, C., Kinmond, S. & O'Reilly, K. 2011. Small-scale modelling of reinforced concrete structural elements for use in a geotechnical centrifuge. *Journal of Structural Engineering*, Vol 137, No 11, pp 1263-1271.

Leblanc, C., Houlsby, G.T. & Byrne, B.W. 2010. Response of stiff piles in sand to long-term cyclic lateral loading. *Geotechnique*, Vol 60, No 2, pp 79-90.

Lee, M.K. & Barr, B.I.G. 2004. An overview of the fatigue behaviour of plain and fibre reinforced concrete. *Cement and Concrete Composites*, Vol 26, pp 299-305.

Li, W., Igoe, D. & Gavin, K. 2015. Field tests to investigate the cyclic response of monopiles in sand. *Geotechnical Engineering: Proceedings of the Institution of Civil Engineers (ICE)*, Vol 168, No GE5, pp 407-421.

Li, W., Zhu, B. & Yang, M. 2017. Static response of monopile to lateral load in overconsolidated dense sand. *Journal of Geotechnical and Geoenvironmental Engineering*, Vol 143, No 7, pp 04017026.

Li, Z., Haigh, S.K. & Bolton, M.D. 2010. Centrifuge modelling of mono-pile under cyclic lateral loads. In Vol. 2 of *Proceedings of the 7th International Conference on Physical Modelling in Geotechnics*. Edited by S. Springman, J. Laue & L. Seward. CRC Press, Taylor & Francis Group, pp 965-970.

Lin, H., Ni, L., Suleiman, M.T. & Raich, A. 2015. Interaction between laterally loaded pile and surrounding soil. *Journal of Geotechnical and Geoenvironmental Engineering*, Vol 141, No 4, pp 04014119.

Lin, S.S. & Liao, J.C. 1999. Permanent strains of piles in sand due to cyclic lateral loads. *Journal of Geotechnical and Geoenvironmental Engineering*, Vol 125, No 9, pp 798-802.

Lin, S.S. & Liao, J.C. 2006. Lateral response evaluation of single piles using inclinometer data. *Journal of Geotechnical and Geoenvironmental Engineering*, Vol 132, No 12, pp 1566-1573.

Little. R.L. & Briaud, J.L. 1988. *Full scale cyclic lateral load tests on six single piles in sand* (No. TAMU-RR-5640). Texas A&M University College Station Department of Civil Engineering.

Long, J.H. & Vanneste, G. 1994. Effects of cyclic lateral loads on piles in sand. *Journal of Geotechnical Engineering*, Vol 120, No 1, pp 225-244.

Lyndon, A. & Pearson, R.A. 1988. Skin friction effects on laterally loaded large diameter piles in sand. *Centrifuge*, Vol 88, pp 363-370.

Madabhushi, G. 2015. *Centrifuge Modelling for Civil Engineers.* 1st ed. CRC Press Taylor and Francis Group, Boca Raton Florida.

Matlock, H. & Reese, L.C. 1961. Foundation analysis of offshore pile supported structures. *Proceedings of the 5th International Conference on Soil Mechanics and Foundation Engineering (SMFE)*, pp 91-97.

McClelland, B. & Focht, J.A. 1958. Soil modulus for laterally loaded piles. *Journal of the Soil Mechanics and Foundations Division, ASCE*, Vol 123, pp 1049.

Mosley, B., Bungey, J. & Hulse, R. 2012. *Reinforced Concrete Design to Eurocode 2.* 7th ed. Palgrave Macmillan, London, UK.

Murchison, J.M. & O'Neill, M.W. 1984. Evaluation of p-y relationship in cohesionless soils. *Analysis and Design of Pile Foundations*, pp 174-191. ASCE.

Nip, D.C.N. & Ng, C.W.W. 2005. Back-analysis of laterally loaded bored piles. *Geotechnical Engineering: Proceedings of the Institute of Civil Engineers (ICE)*, Vol 158, No GE2, pp 63-73.

Noor, F.A. & Boswell, L.F. 1992. *Small scale modelling of concrete structures*. Elsevier Applied Science, London, New York.

O'Neill, M.W. & Murchison, J.M. 1983. An evaluation of p-y relationships in sands. *Research Report No GT-DF02-83*, University of Houston, Texas.

Ovesen, N.K. 1979. The scaling law relationship – panel discussion. *Proceedings of the 7th European Conference on Soil Mechanics and Foundation Engineering*, pp 319-323.

Parker, F. & Reese, L.C. 1970. Experimental and analytical studies of behavior of single piles in sand under lateral and axial loading. *Research Report No 117-2*, Center for Highway Research, The University of Texas, Austin, Texas.

Palmer, L.A. & Thompson, J.B. 1948. The earth pressure and deflection along the embedded lengths of piles subjected to lateral thrusts. *Proceedings of the 2nd International Conference on Soil Mechanics and Foundation Engineering (SMFE)*, pp 156-161.

Peck, R.B., Hanson, W.E. & Thornburn, T.H. 1974. *Foundation Engineering*, John Wiley.

Pinto, P.L., Anderson, B. & Townsend, F.C. 1999. Comparison of horizontal load transfer curves for laterally loaded piles from strain gauges and slope inclinometer: a case study. *Field Instrumentation for Soil and Rock, ASTM International.*

Poulos, H.G. 1982. Single pile response to cyclic lateral load. *Journal of Geotechnical and Geoenvironmental Engineering*, Vol 108, GT3, pp 355-375.

Poulos, H.G. & Davis, E.H. 1974. *Elastic Solutions for Soil and Rock Mechanics.* 1st ed. John Wiley & Sons, Sydney, Australia.

Poulos, H.G. & Davis, E.H. 1980. *Pile Foundation Analysis and Design.* John Wiley & Sons, Toronto, Canada.

Poulos, H.G. & Hull, T. 1989. The role of analytical geomechanics in foundation engineering. *Foundation Engineering: Current Principles and Practices, ASCE, Reston, 2*, pp 1578-1606.

Reese, L.C. 1977. Laterally loaded piles: program documentation. *Journal of Geotechnical and Geoenvironmental Engineering*, Vol 103, No GT4, pp 287-305.

Reese, L.C. 1985. Documentation of the computer program LPILE1. *Ensoft Inc.*, Austin, Texas.

Reese, L.C., Cooley, L.A. & Radhakrishnan, N. 1984. *Laterally loaded piles and computer program COM624G.* University of Texas, Austin, Texas.

Reese, L.C., Cox, W.R. & Koop, F.D. 1974. Analysis of laterally loaded piles in sand. *Proceedings of the 6th Annual Offshore Technology Conference*, pp 473-483.

Reese, L.C., Cox, W.R. & Koop, F.D. 1975. Field testing and analysis of laterally loaded piles in stiff clay. *Proceedings of the 7th Offshore Technology Conference*, pp 671-690.

Reese, L.C. & Matlock, H. 1956. Non-dimensional solutions for laterally loaded piles with soil modulus assumed proportional to depth. *Proceedings of the 8th Texas Conference on SMFE*, University of Texas, Austin, Texas.

Reese, L.C. & Welch, R.C. 1975. Lateral loading of deep foundations in stiff clay. *Journal of Geotechnical and Geoenvironmental Engineering*, Vol 101, No 7, pp 633-649.

Ruesta, P.F. & Townsend, F.C. 1997. Evaluation of laterally loaded pile group at roosevelt bridge. *Journal of Geotechnical and Geoenvironmental Engineering*, Vol 123, No 12, pp 1153-1161.

Russo, G. 2016. A method to compute the non-linear behaviour of piles under horizontal loading. *Soils and Foundations*, Vol 56, No 1, pp 33-43.

Sabnis, G.M., Harris, H.G., White, R.N. & Saeed Mirza, M. 1983. *Structural Modeling and Experimental Techniques.* Prentice-Hall, Englewood Cliffs, New Jersey, USA.

Soutsos, M. & Domone, P. 2017. *Construction Materials: Their Nature and Behaviour*. 5th ed. CRC Press Taylor and Francis Group, Abingdon, Oxon.

Schofield, A.H. 1980. Cambridge geotechnical centrifuge operations. *Geotechnique*, Vol 30, No 3, pp 227-268.

Scott, R.F. 1980. Analysis of centrifuge pile tests: simulation of pile driving. *Research Report*, American Petroleum Institute OSAPR Project 13, California Institute of Technology, Pasadena, California.

Smith, I. 2014. *Smith's Elements of Soil Mechanics*. 9th ed. John Wiley & Sons Limited.

Smith, T.D. 1987. Pile horizontal modulus values. *Journal of Geotechnical Engineering*, Vol 113, No 9, pp 1040-1044.

Swain, C.W. 1979. The behaviour of piled foundations supporting a model offshore structure. PhD thesis, University of Cambridge, UK.

Tak Kim, B., Kim, N.K., Jin Lee, W. & Su Kim, Y. 2004. Experimental load-transfer curves of laterally loaded piles in nak-dong river sand. *Journal of Geotechnical and Geoenvironmental Engineering*, Vol 130, No 4, pp 416-425.

Taylor, R.N. 1995. *Geotechnical centrifuge technology*. 1st ed. Blackie Academic & Professional, Glasgow.

Terzaghi, K. 1955. Evaluation of coefficients of subgrade reaction. *Geotechnique*, Vol 5, No 4, pp 297-326.

Terzaghi, K., Peck, R.B. & Mesri, G. 1996. *Soil Mechanics in Engineering Practice.* 3rd ed. John Wiley & Sons.

Tomlinson, M.J. 1980. *Foundation Design and Construction.* 4th ed. Pitman Books Limited.

Verdure, L., Garnier, J. & Levacher, D. 2003. Lateral cyclic loading of single piles in sand. *International Journal of Physical Modelling in Geotechnics*, Vol 3, No 3, pp 17-28.

Westergaard, H.M. 1926. Stresses in concrete pavements computed by theoretical analysis. *Public roads.*

Werkmeister, S., Dawson, A.R. & Wellner, F. 2001. Permanent deformation behavior of unbound granular materials and the shakedown theory. *Transport Research Record*, Vol 1757, No 1, pp 75-81.

Werkmeister, S., Dawson, A.R. & Wellner, F. 2004. Pavement design model for unbound granular materials. *Journal of Transportation Engineering*, Vol 130, No 5, pp 665-674.

Winterkorn, H.F. & Fang, H.Y. 1975. *Foundation Engineering Handbook.* Van Nostrand Reinhold Company International.

Yan, L. & Byrne, P.M. 1992. Lateral pile response to monotonic pile head loading. *Canadian Geotechnical Journal*, Vol 29, pp 955-970.

Yuan, B., Chen, R., Deng, G., Peng, T., Luo, Q. & Yang, X. 2016. Accuracy of interpretation methods for deriving p-y curves from model pile tests in layered soils. *Journal of Testing and Evaluation*, Vol 45, No 4, pp 1238-1246.

Zhang, L. 2009. Nonlinear analysis of laterally loaded rigid piles in cohesionless soil. *Computers and Geotechnics*, Vol 36, pp 718-724.

Zhu, B., Li, T., Xiong, G. & Lui, J.C. 2016. Centrifuge model tests on laterally loaded piles in sand. *International Journal of Physical Modelling in Geotechnics*, Vol 16, No 4, pp 160-172.

APPENDIX A: PARAMETRIC STUDY (MULTI-VARIABLE ANALYSIS)

This appendix accompanies the results and discussions of the parametric study conducted in Chapter 3 using the subgrade reaction analysis approach to determine the response and behaviour of the soil-pile system to variations in the properties of the pile and the soil.

E_p = 10 GPa
n_h = 1.0 MN/m³

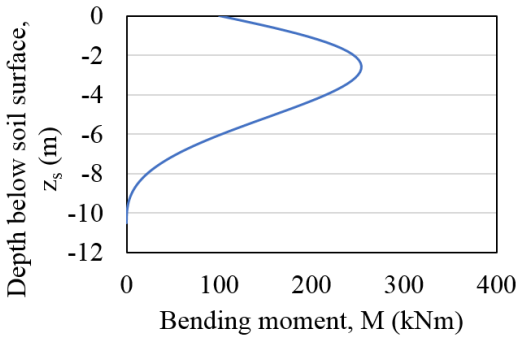

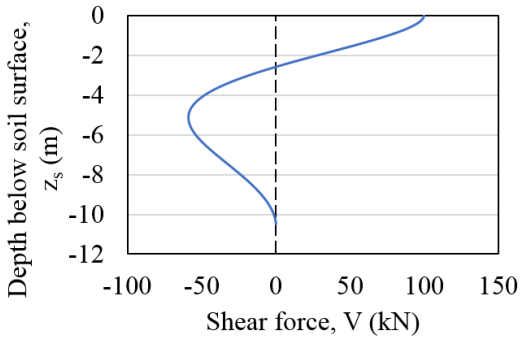

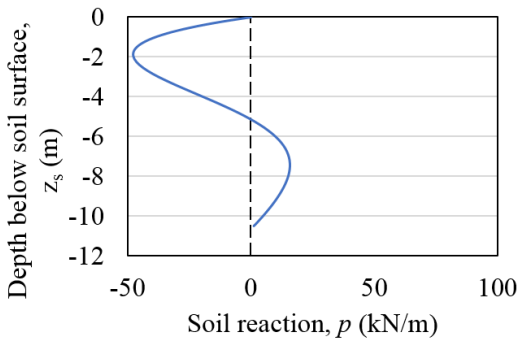

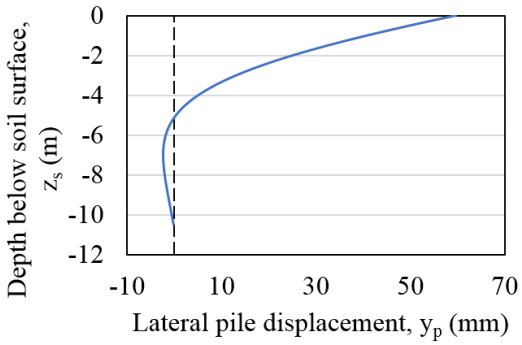

E_p = 25 GPa
n_h = 1.0 MN/m³

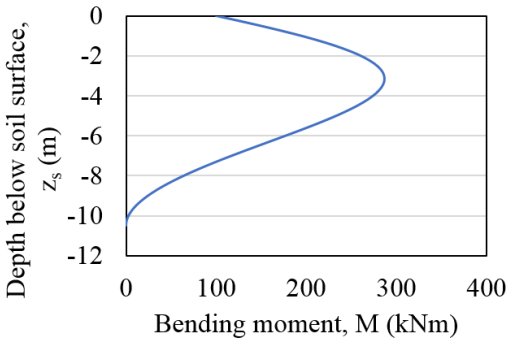

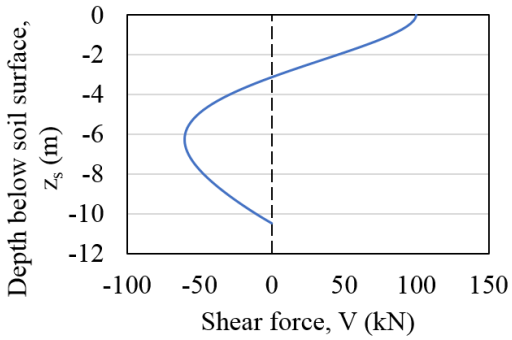

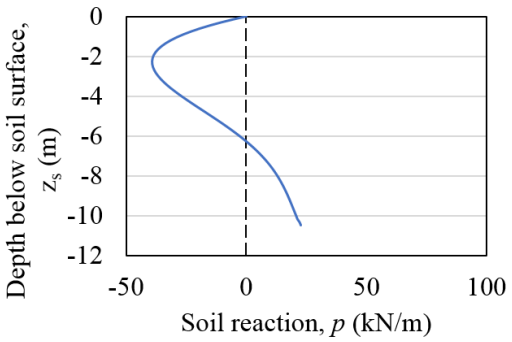

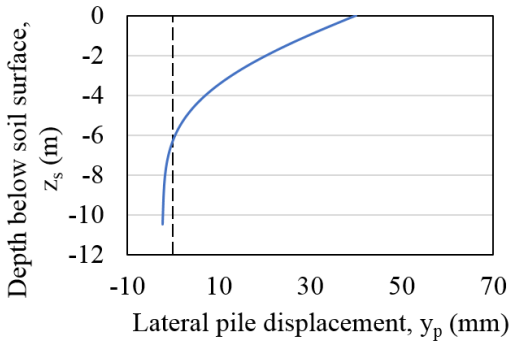

E_p = 50 GPa
n_h = 1.0 MN/m³

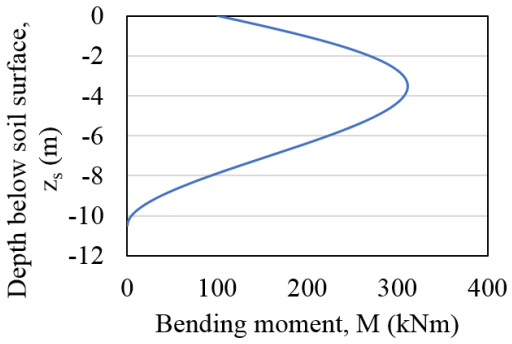

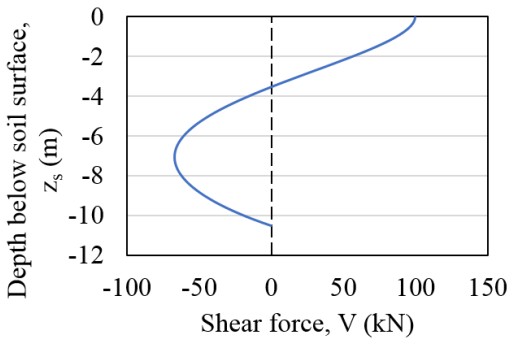

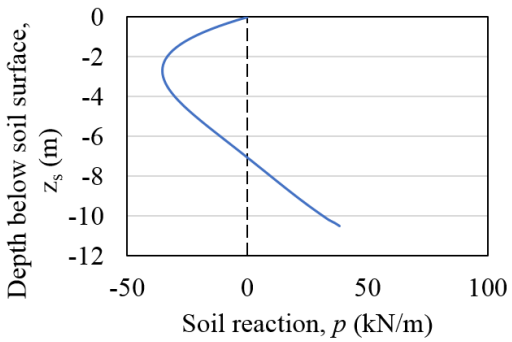

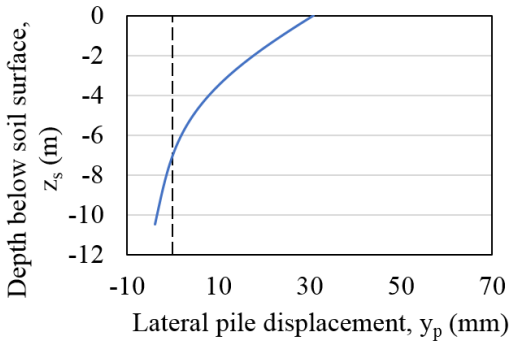

E_p = 100 GPa
n_h = 1.0 MN/m³

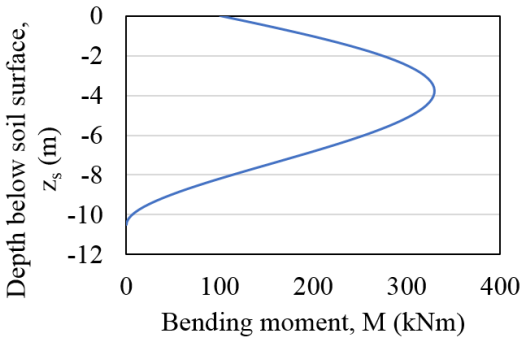

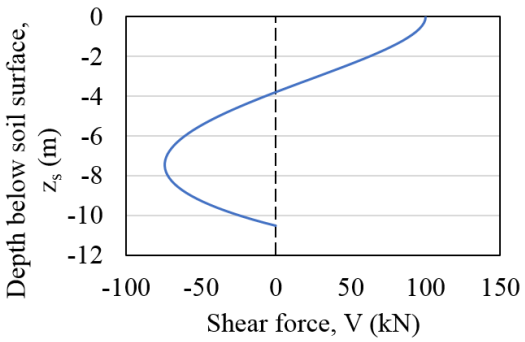

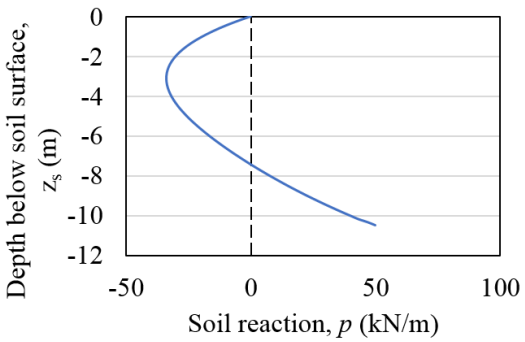

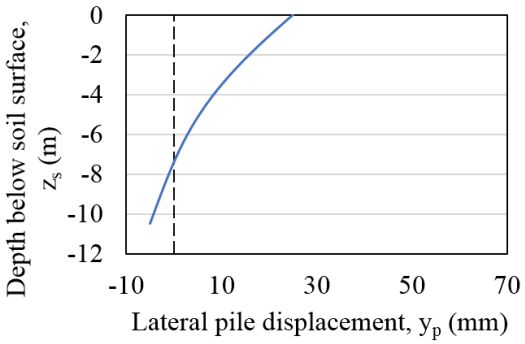

E_p = 150 GPa
n_h = 1.0 MN/m³

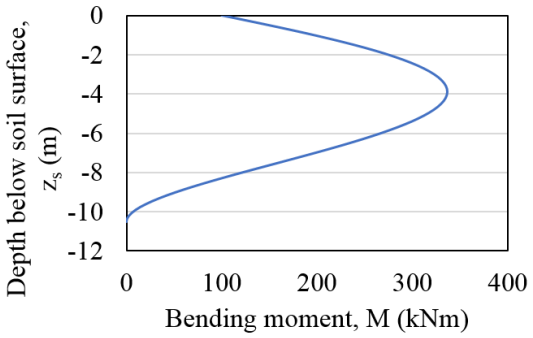

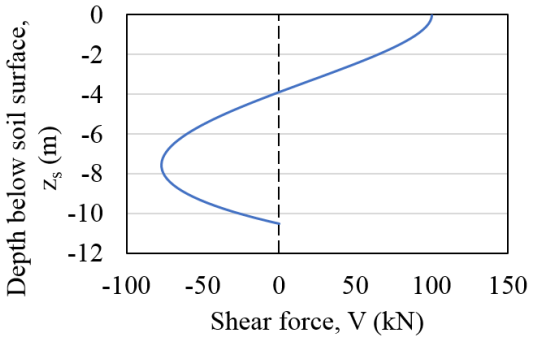

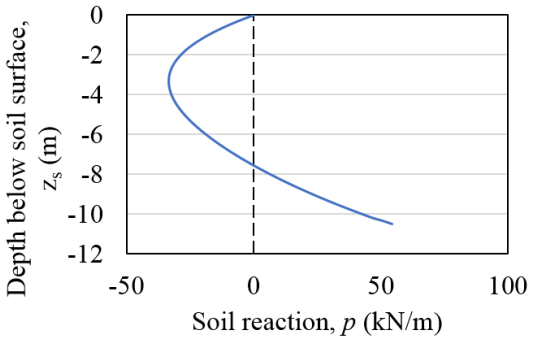

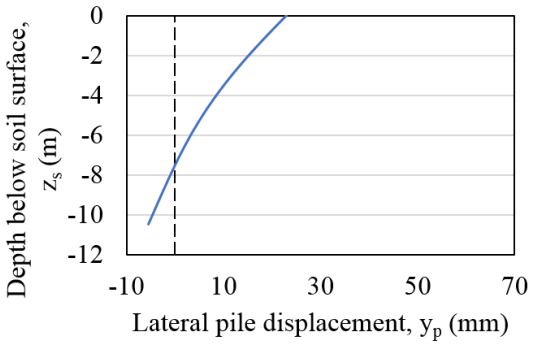

E_p = 200 GPa
n_h = 1.0 MN/m³

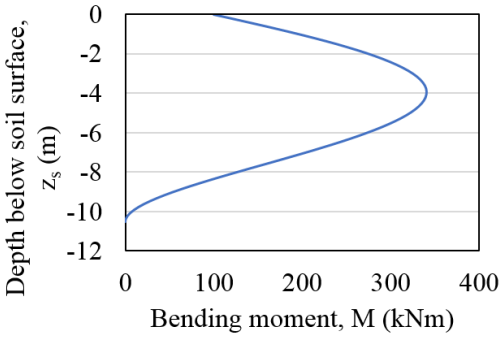

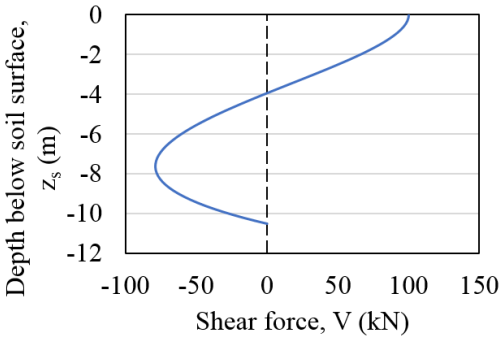

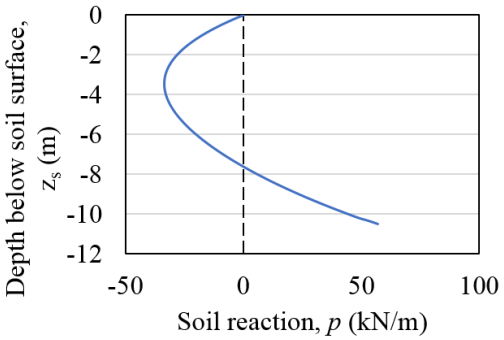

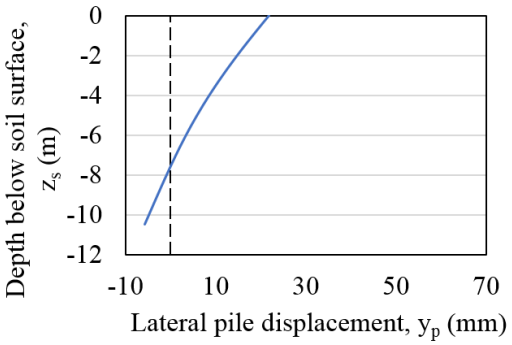

E_p = 10 GPa
n_h = 2.2 MN/m³

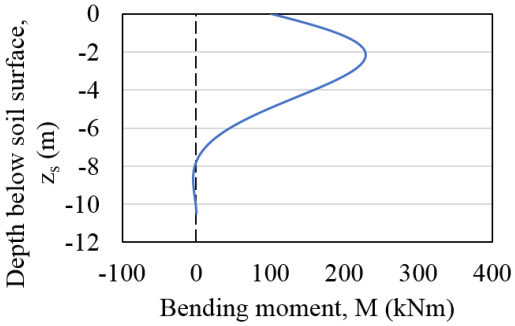

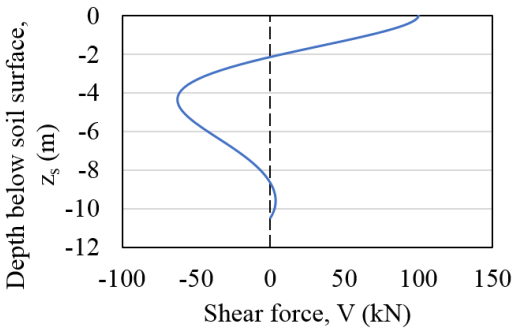

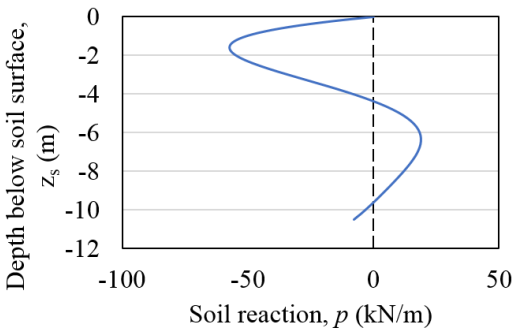

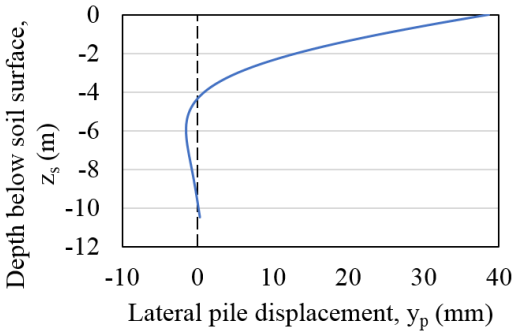

E_p = 25 GPa
n_h = 2.2 MN/m³

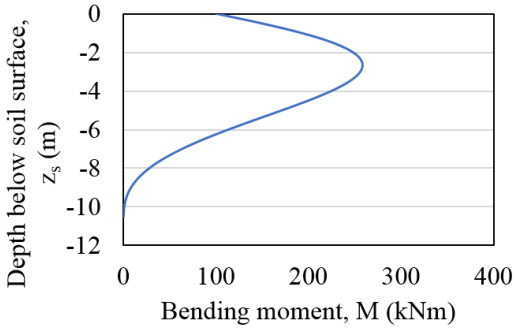

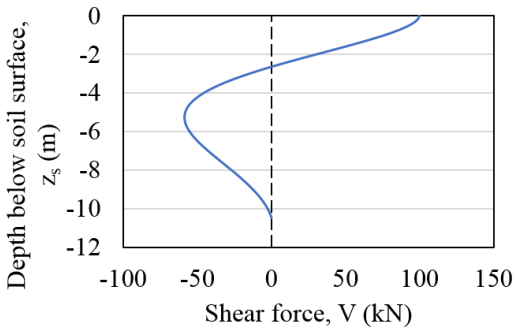

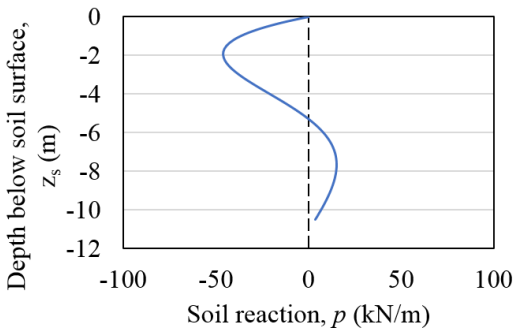

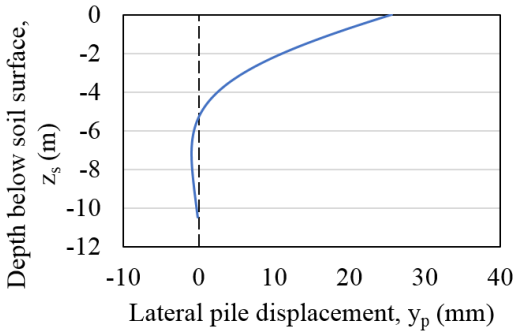

E_p = 50 GPa
n_h = 2.2 MN/m³

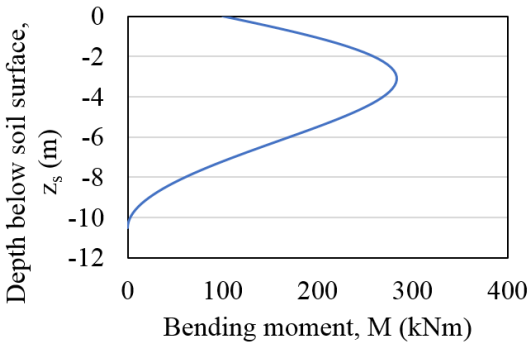

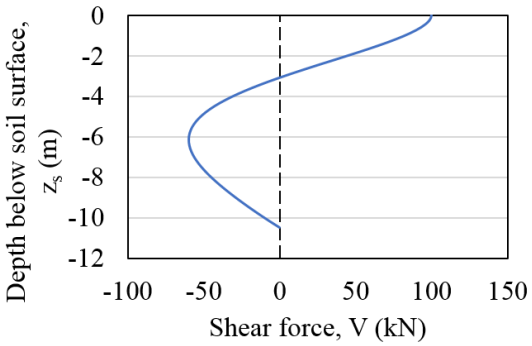

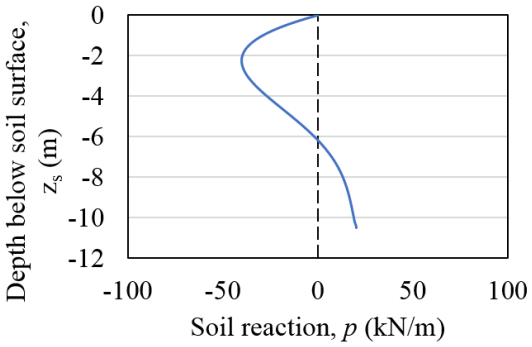

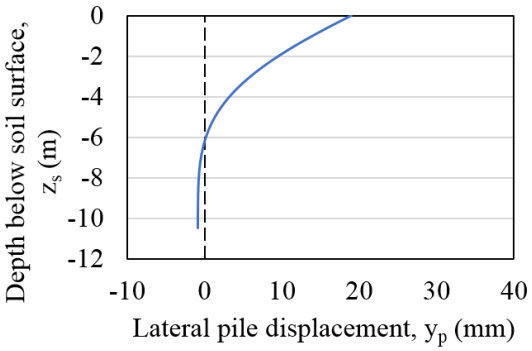

E_p = 100 GPa
n_h = 2.2 MN/m³

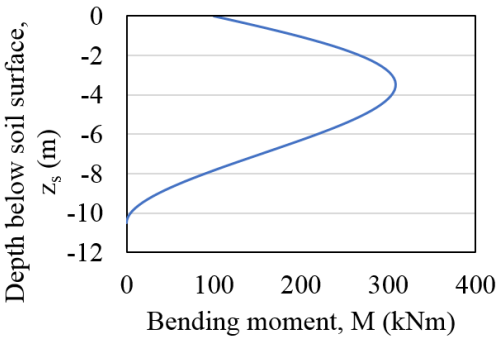

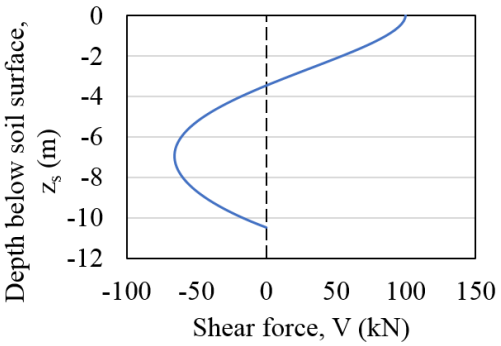

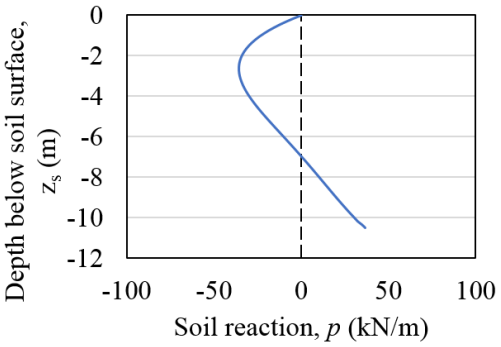

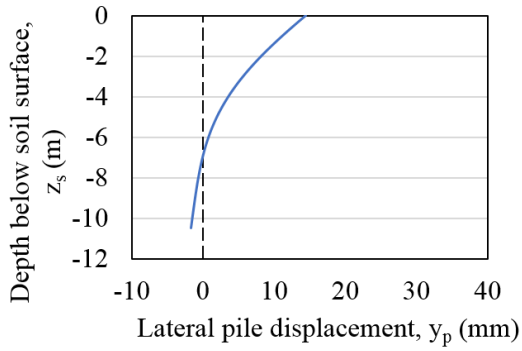

E_p = 150 GPa
n_h = 2.2 MN/m³

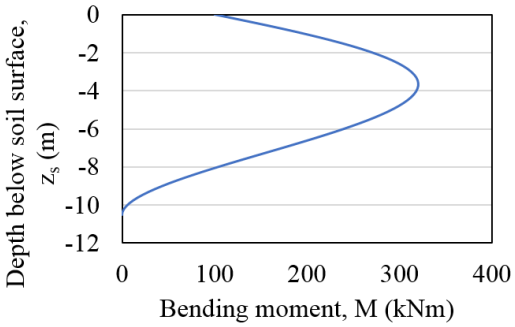

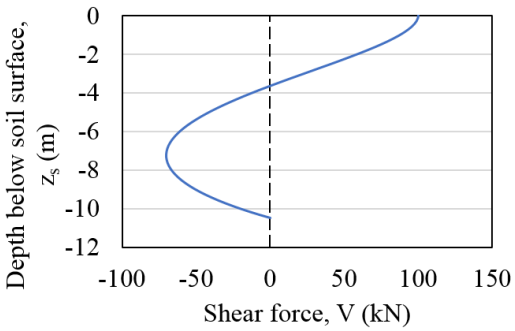

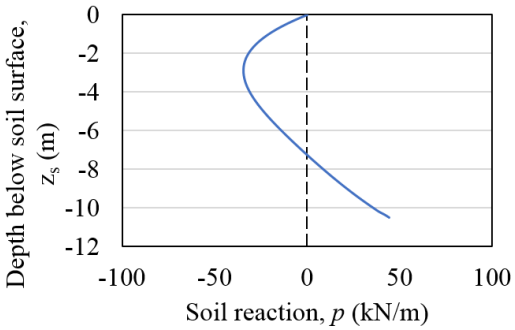

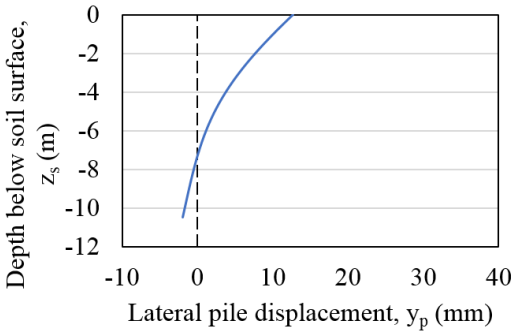

E_p = 200 GPa
n_h = 2.2 MN/m³

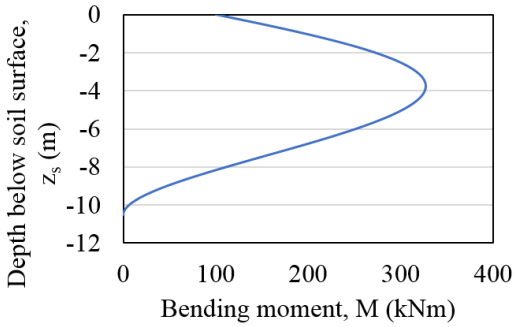

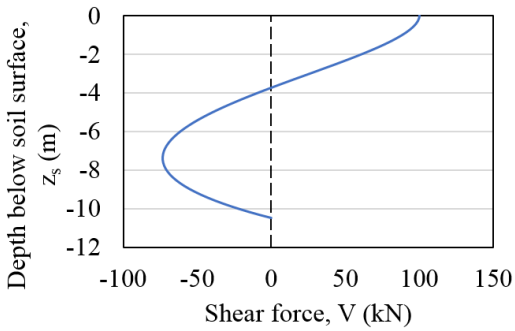

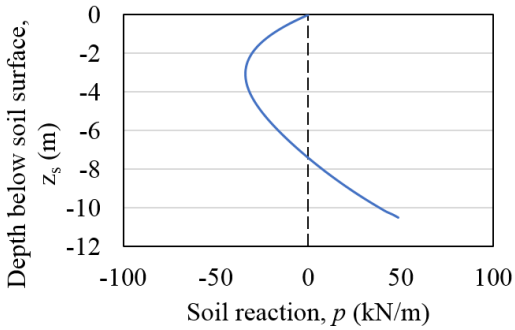

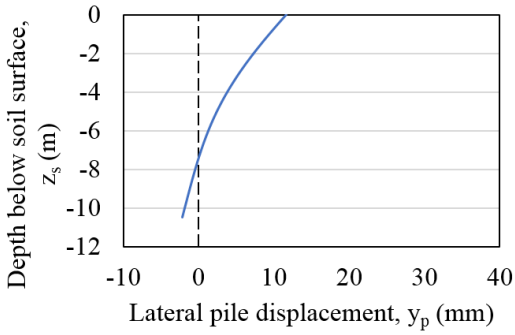

E_p = 10 GPa
n_h = 6.6 MN/m³

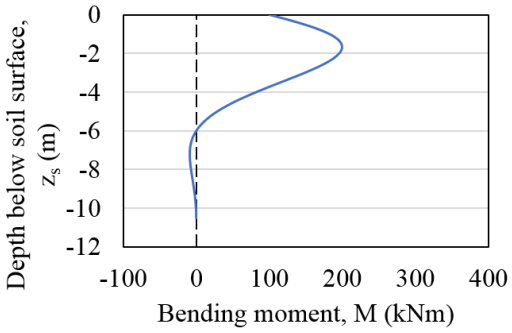

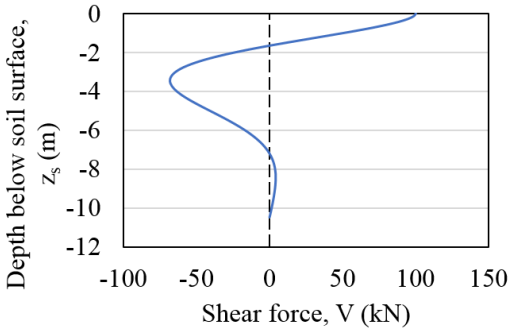

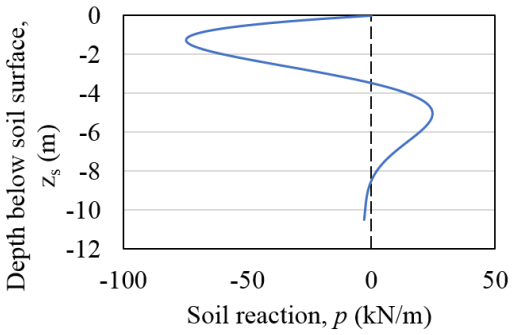

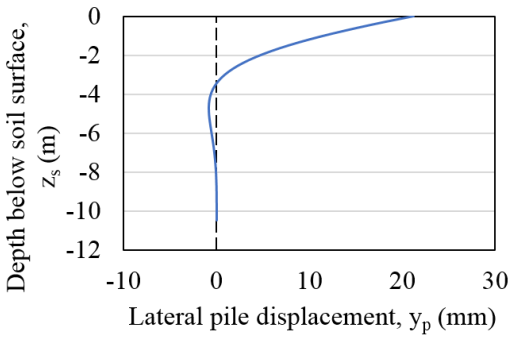

E_p = 25 GPa
n_h = 6.6 MN/m³

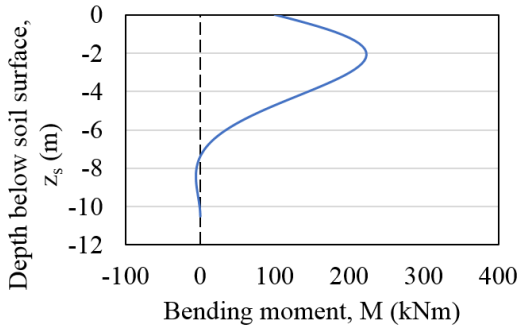

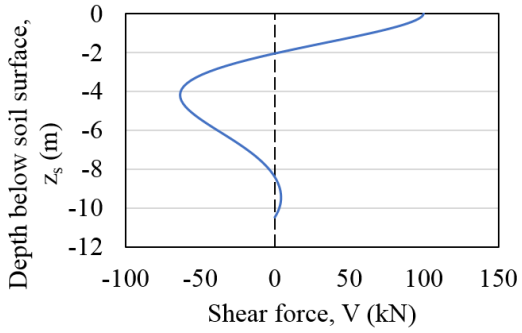

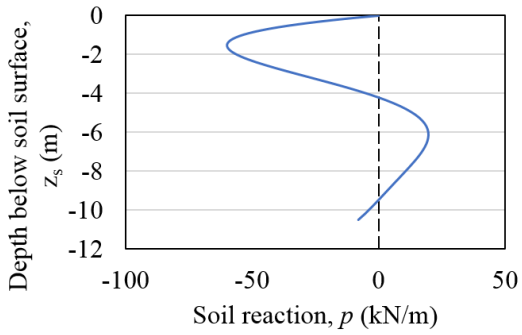

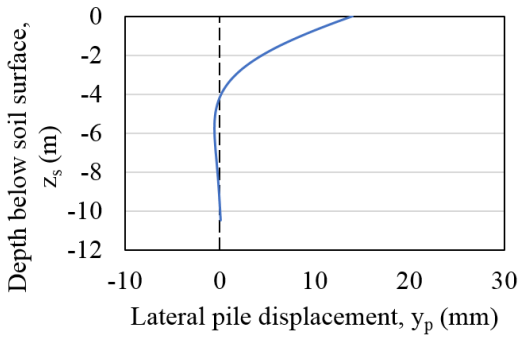

E_p = 50 GPa
n_h = 6.6 MN/m³

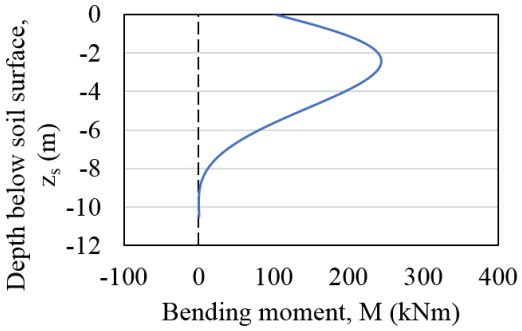

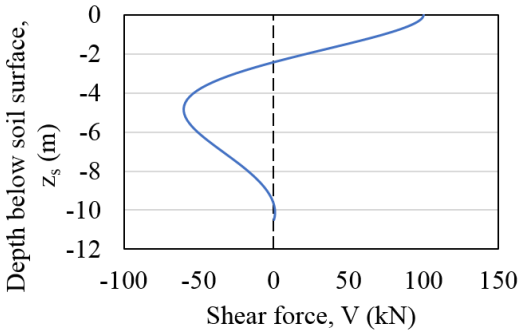

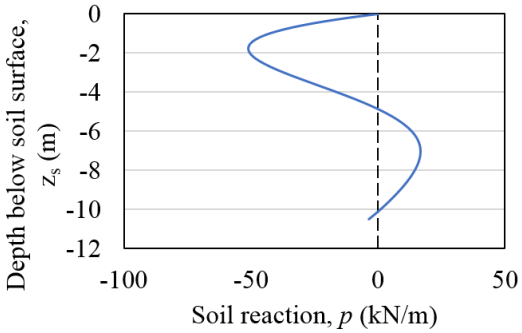

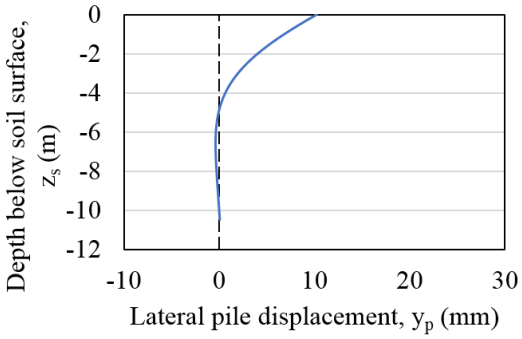

E_p = 100 GPa
n_h = 6.6 MN/m³

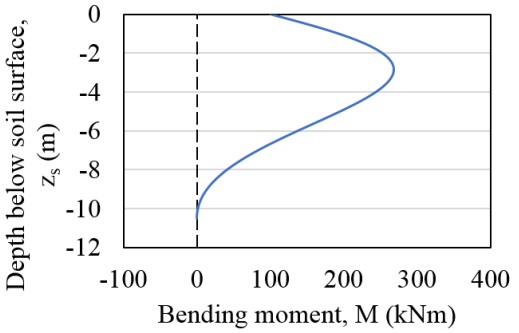

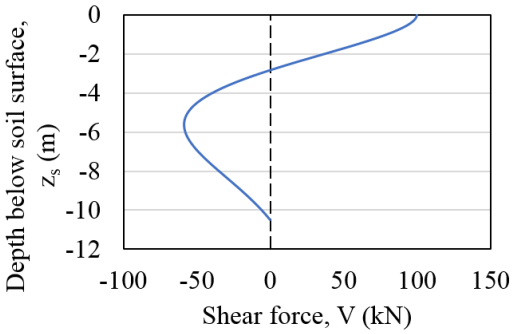

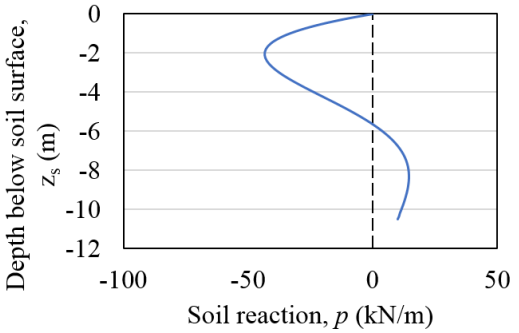

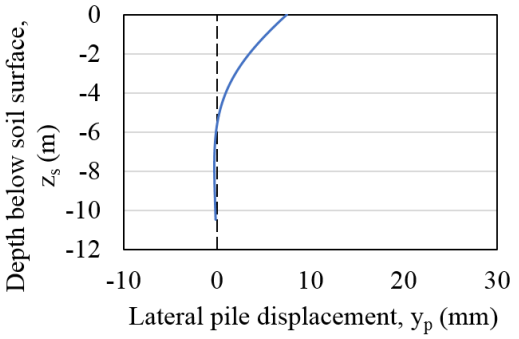

E_p = 150 GPa
n_h = 6.6 MN/m³

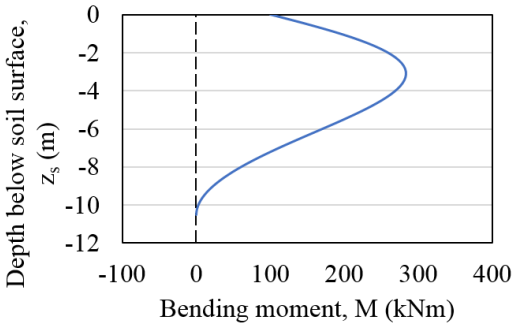

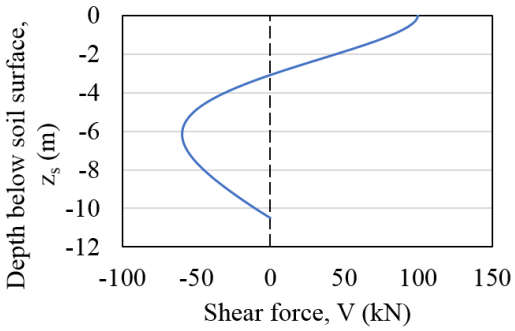

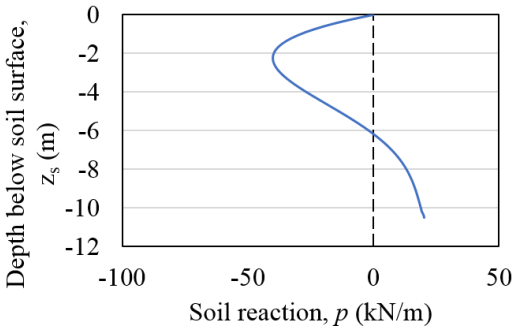

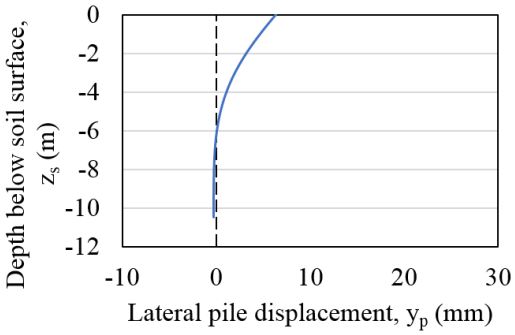

E_p = 200 GPa
n_h = 6.6 MN/m³

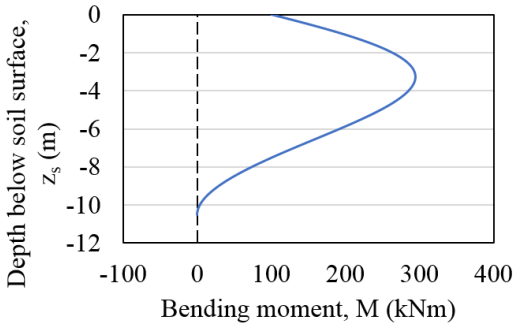

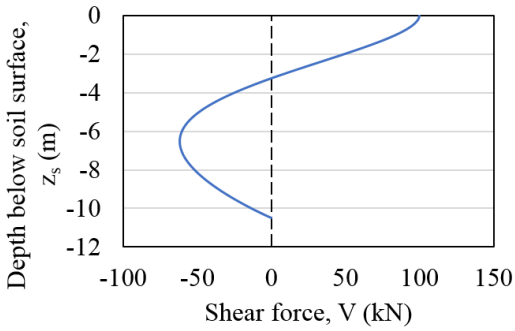

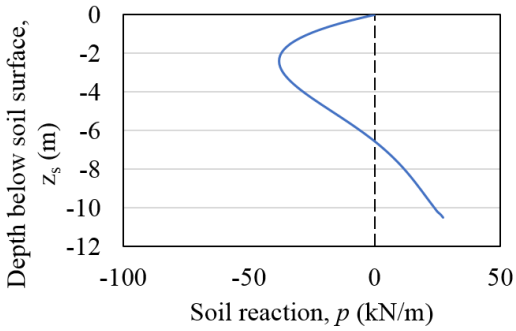

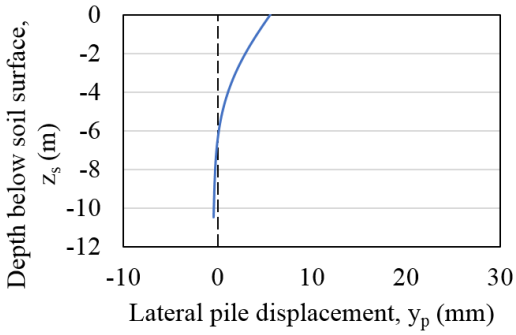

E_p = 10 GPa
n_h = 17.6 MN/m³

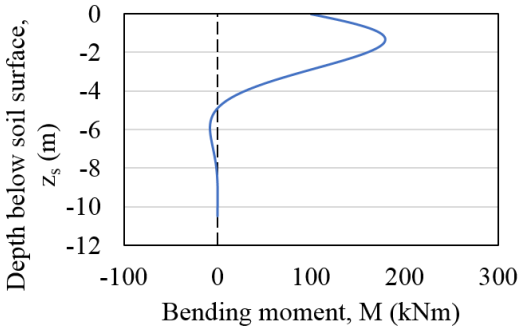

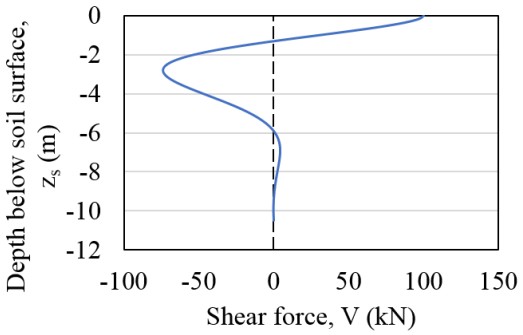

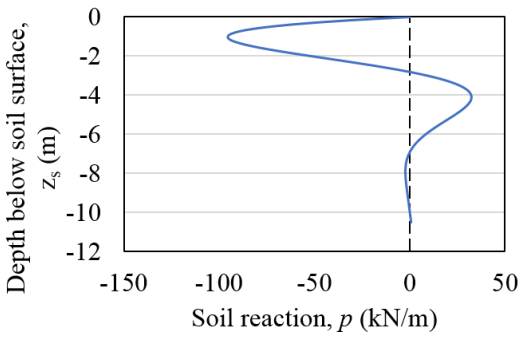

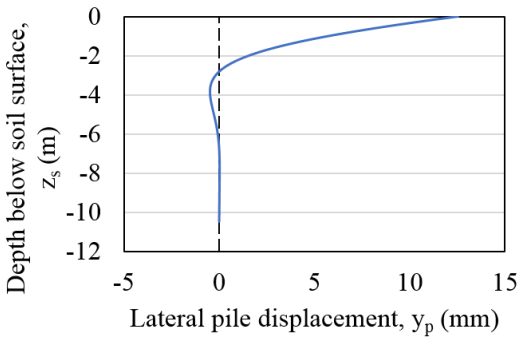

E_p = 25 GPa
n_h = 17.6 MN/m³

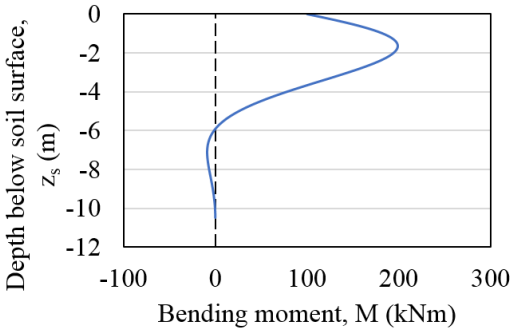

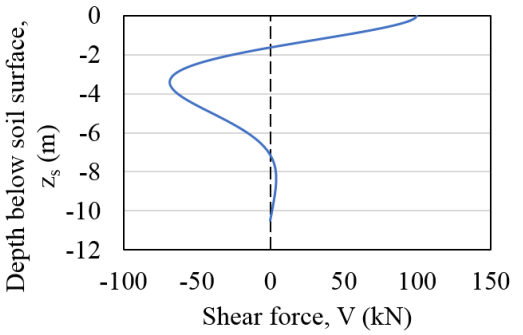

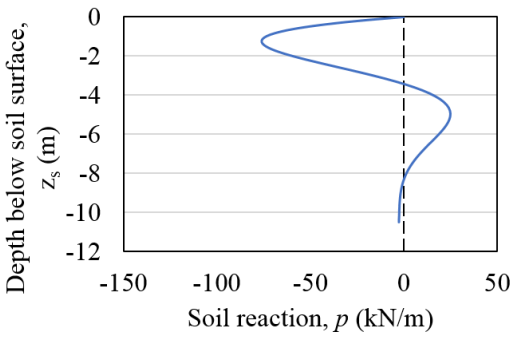

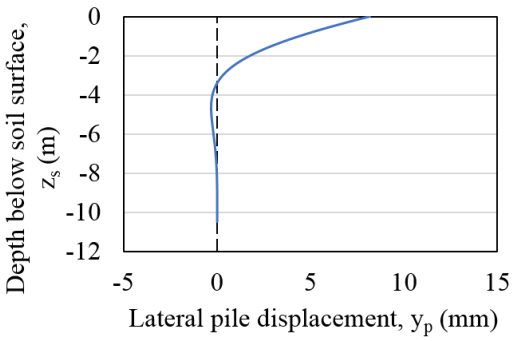

E_p = 50 GPa
n_h = 17.6 MN/m³

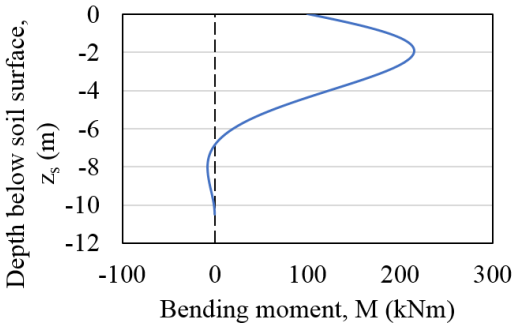

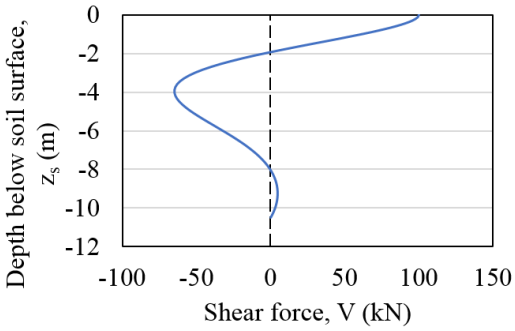

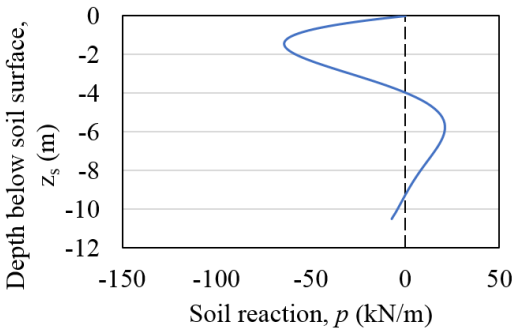

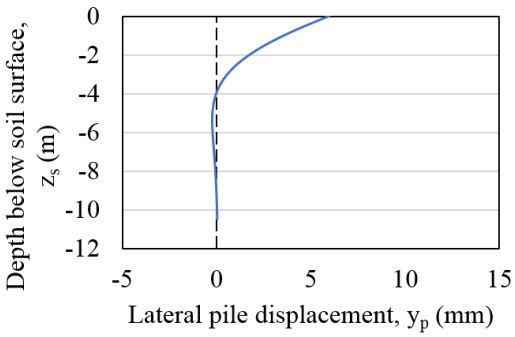

E_p = 100 GPa
n_h = 17.6 MN/m³

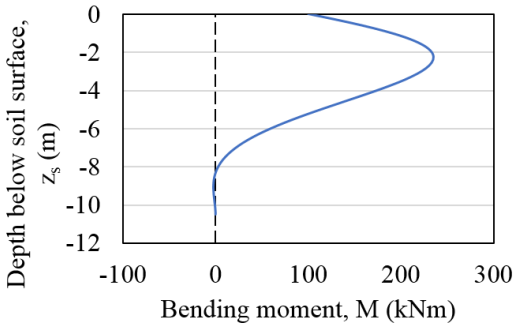

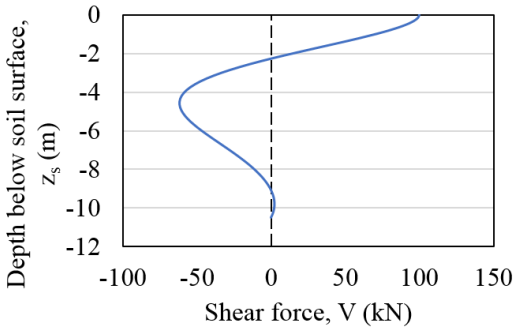

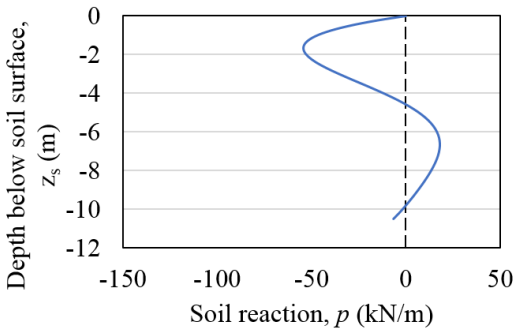

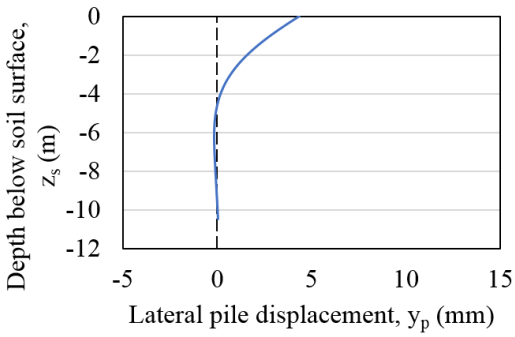

E_p = 150 GPa
n_h = 17.6 MN/m³

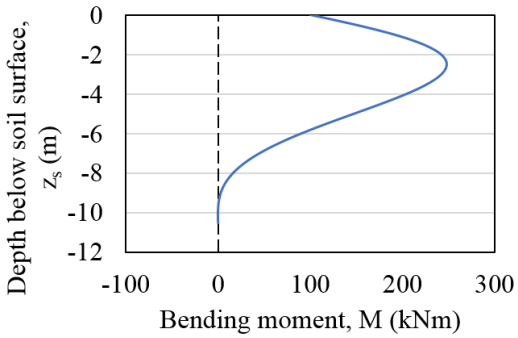

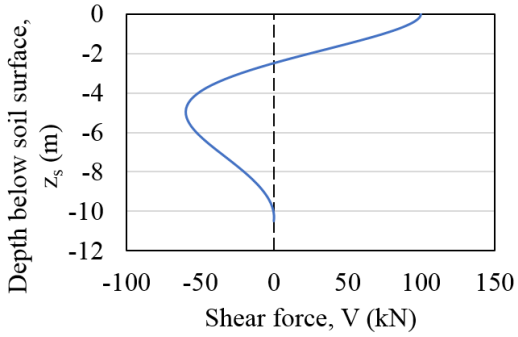

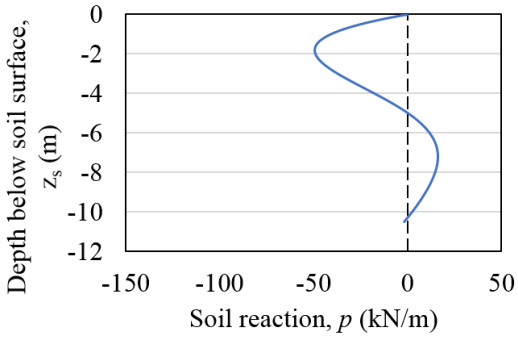

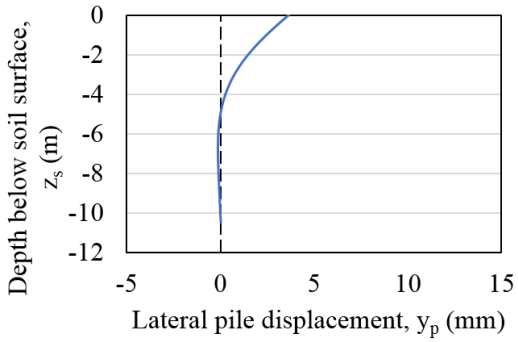

E_p = 200 GPa
n_h = 17.6 MN/m³

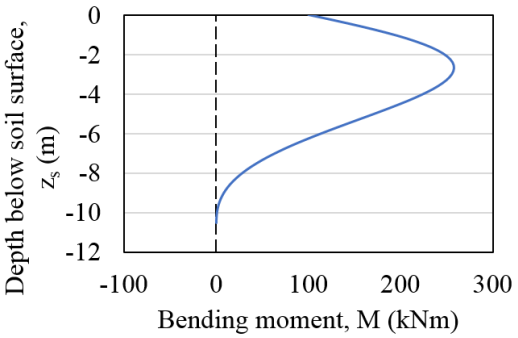

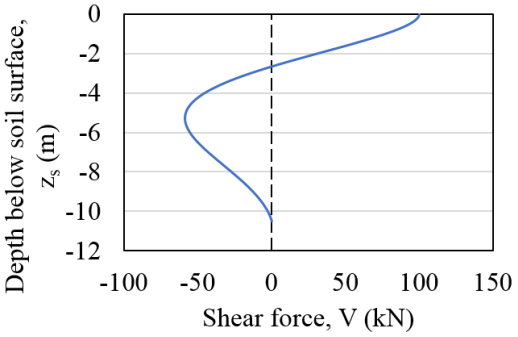

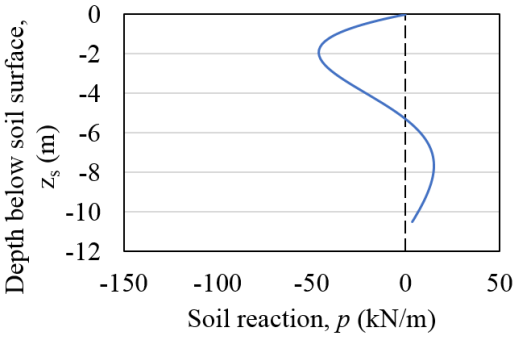

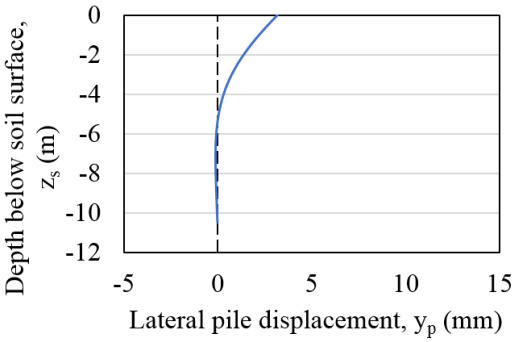

E_p = 10 GPa
n_h = 25.0 MN/m³

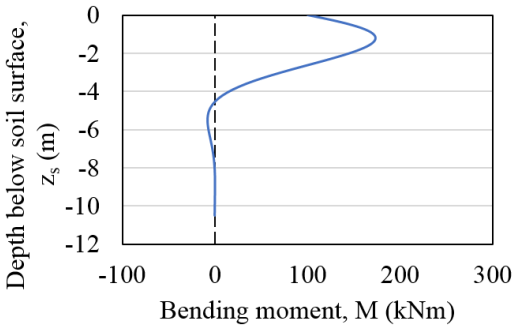

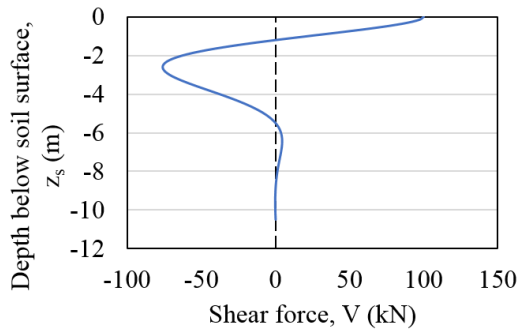

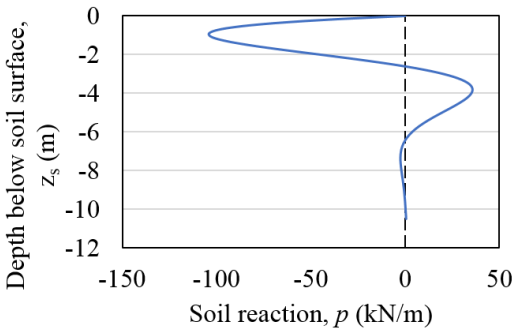

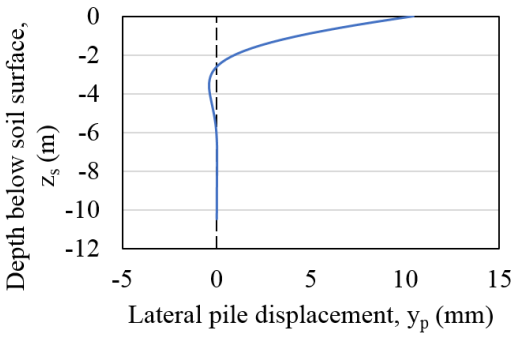

E_p = 25 GPa
n_h = 25.0 MN/m³

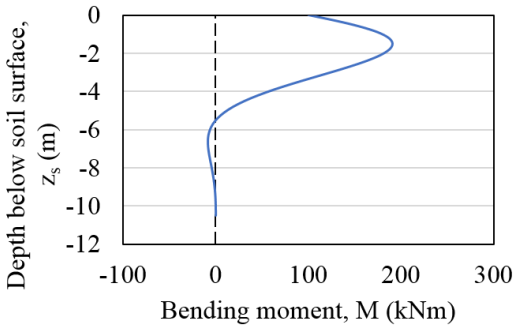

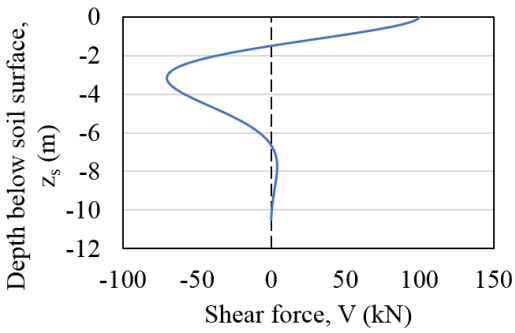

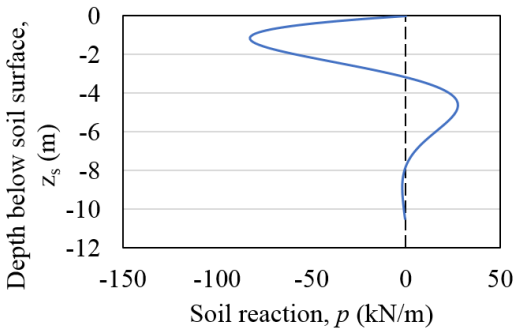

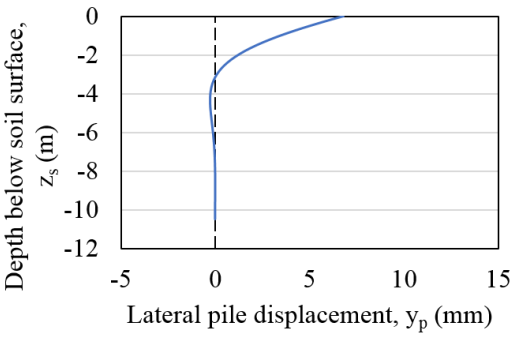

E_p = 50 GPa
n_h = 25.0 MN/m³

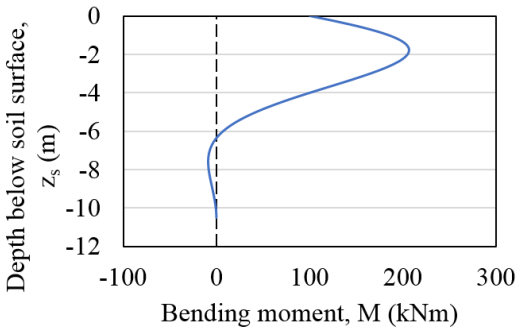

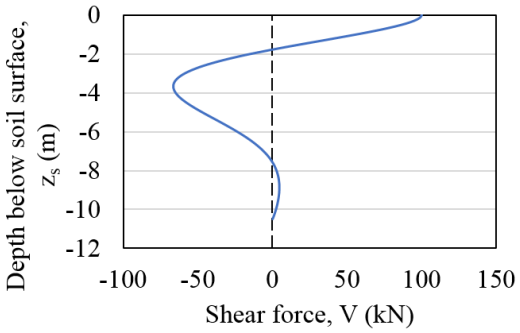

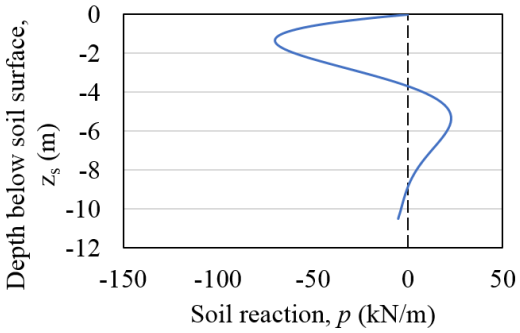

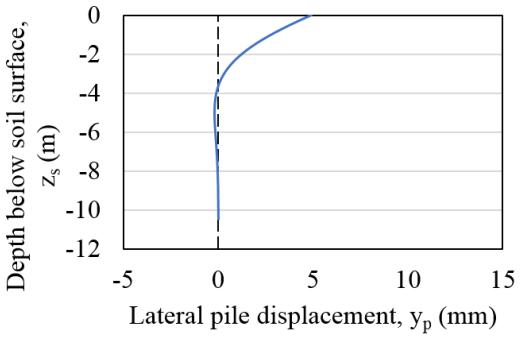

E_p = 100 GPa
n_h = 25.0 MN/m³

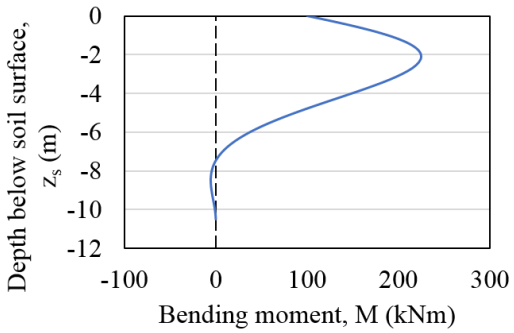

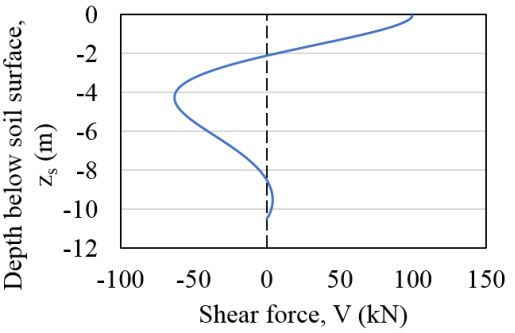

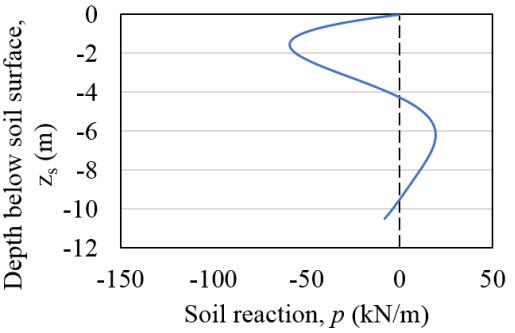

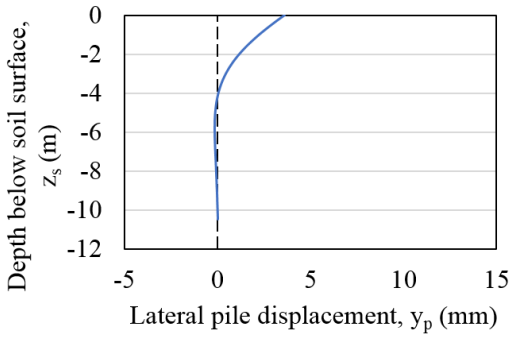

E_p = 150 GPa
n_h = 25.0 MN/m³

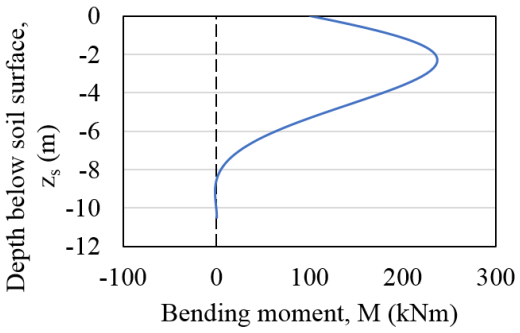

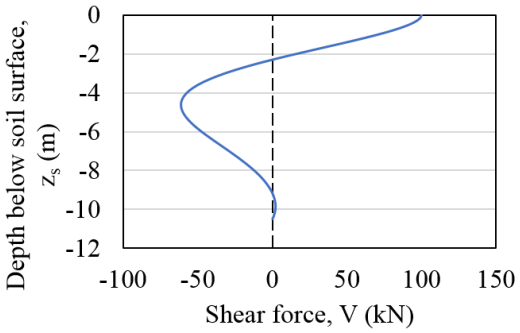

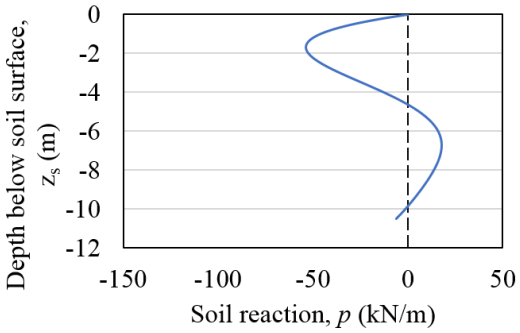

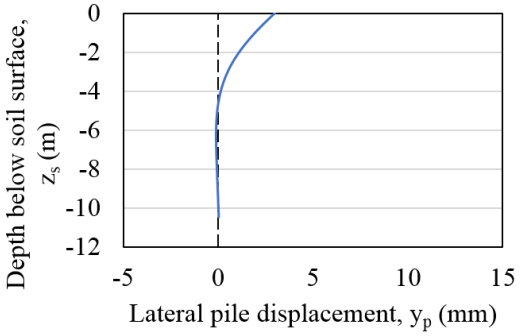

E_p = 200 GPa
n_h = 25.0 MN/m³

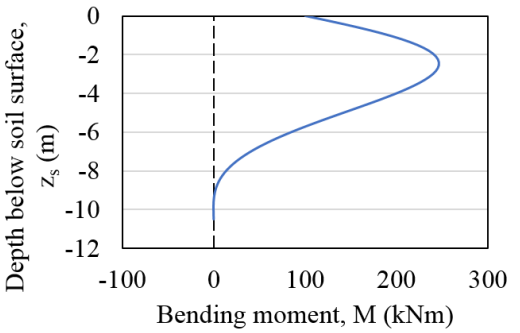

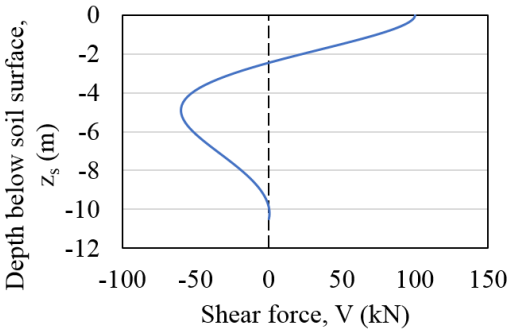

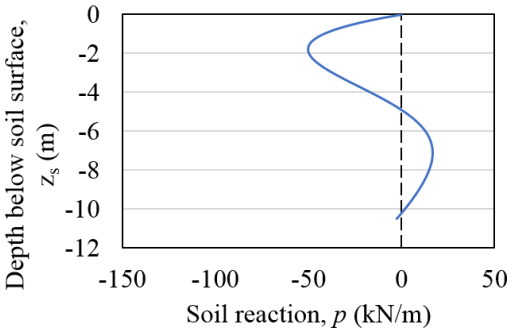

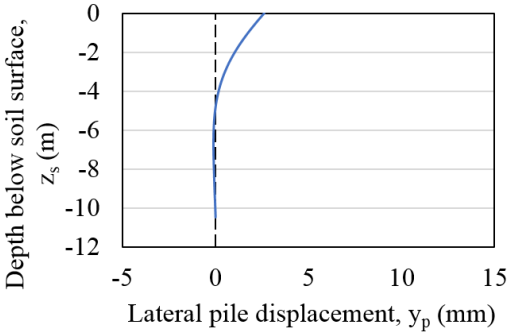

E_p = 10 GPa
n_h = 50.0 MN/m³

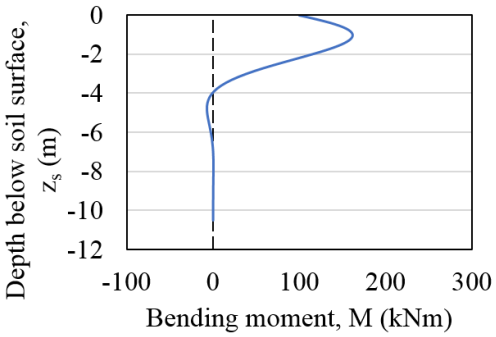

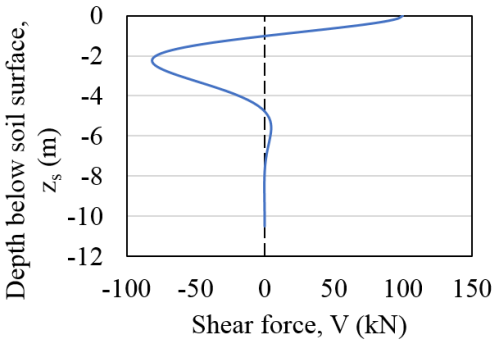

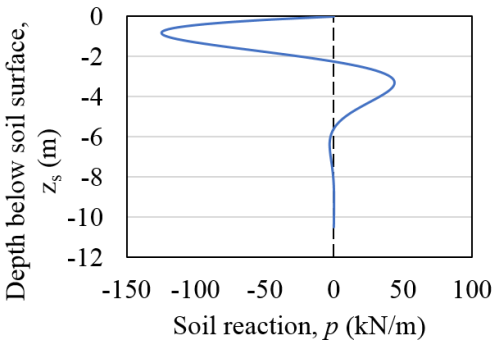

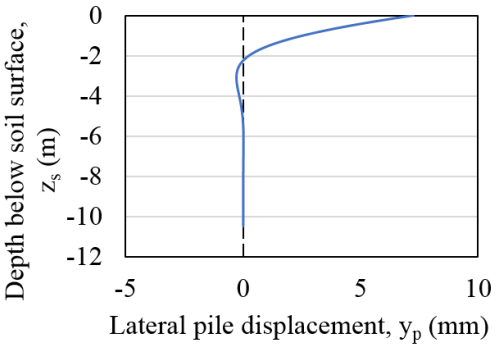

E_p = 25 GPa
n_h = 50.0 MN/m³

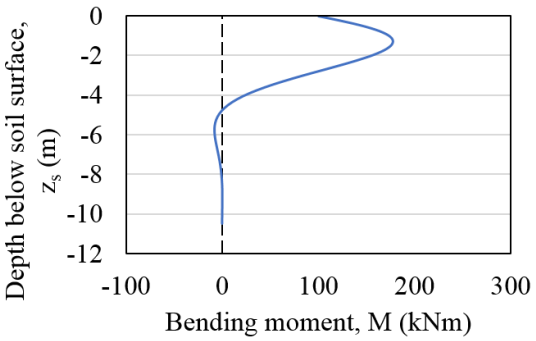

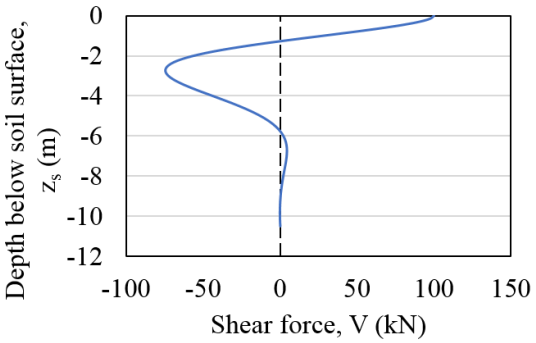

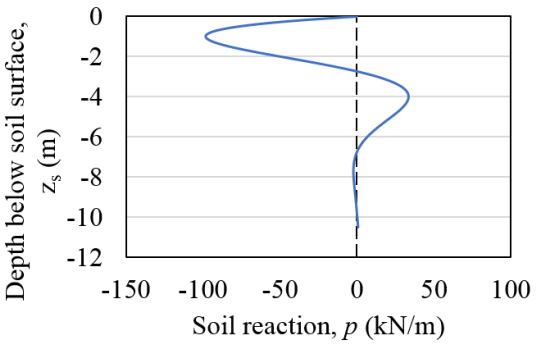

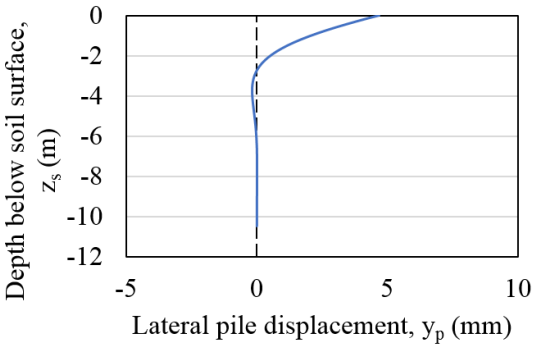

E_p = 50 GPa
n_h = 50.0 MN/m³

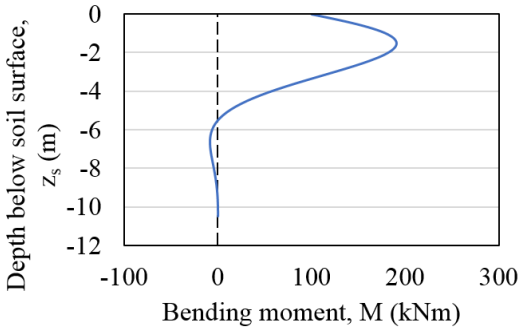

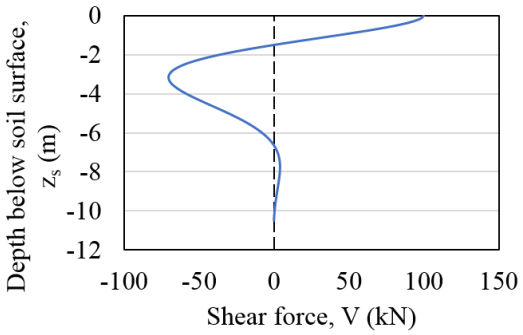

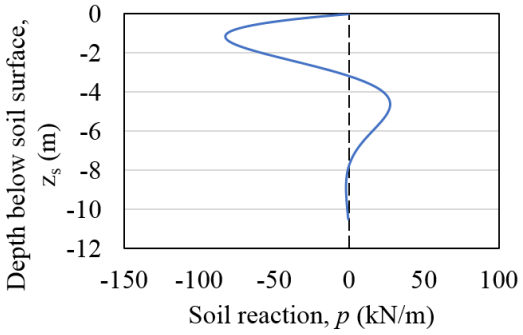

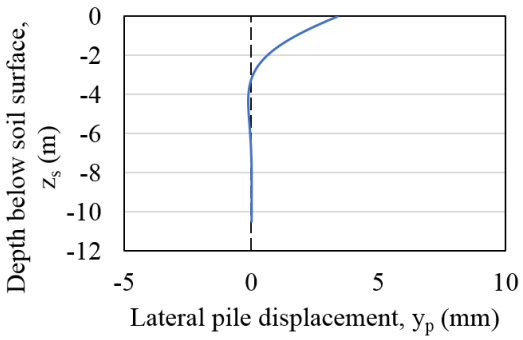

E_p = 100 GPa
n_h = 50.0 MN/m³

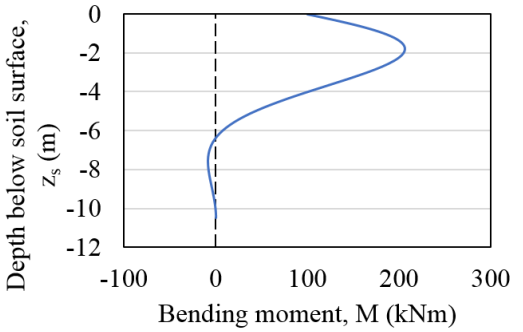

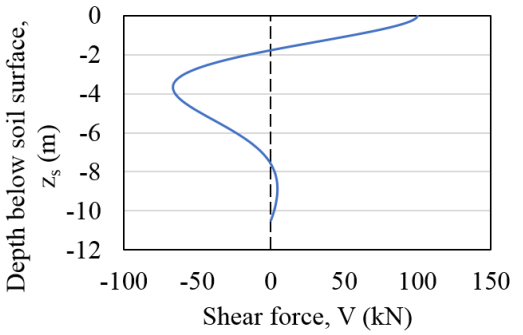

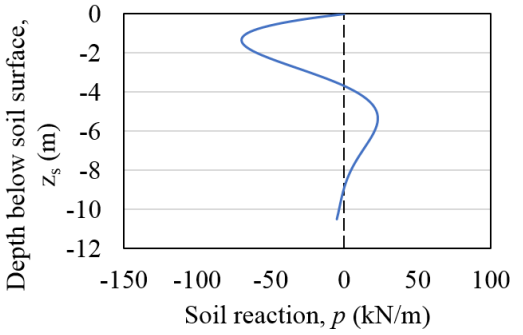

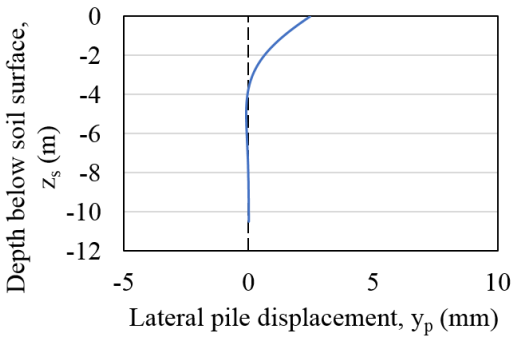

E_p = 150 GPa
n_h = 50.0 MN/m³

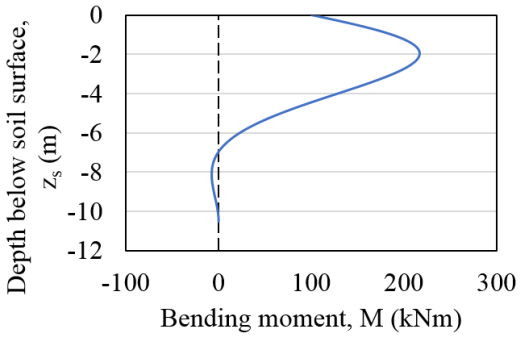

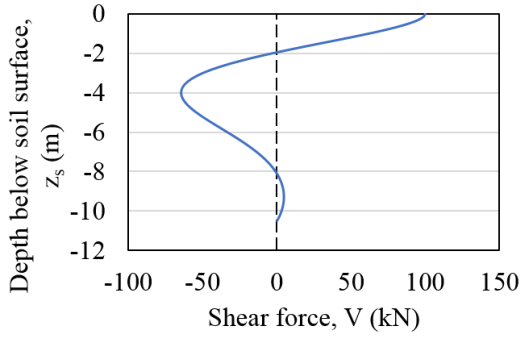

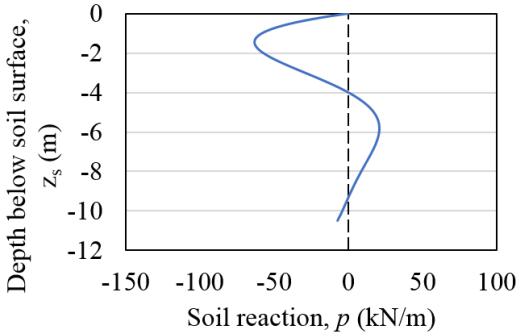

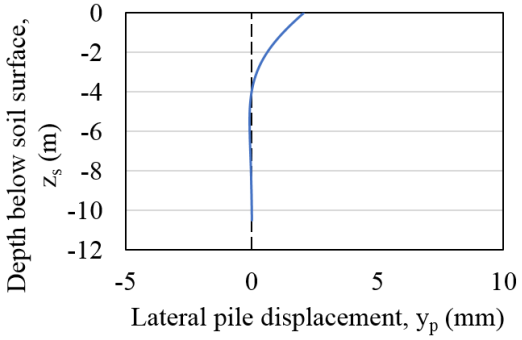

E_p = 200 GPa
n_h = 50.0 MN/m³